

Ph.D. by Published Work



**Development and Application of *In Vitro* 3D Liver Models for
more Physiologically Relevant Hazard Assessment of Engineered
Nanomaterials**

Submitted to Swansea University in fulfilment of the requirements for the
degree of Ph.D. by Published Works.

2021

Samantha Victoria Llewellyn



Professor Shareen H. Doak

Dedication

I would like to dedicate this thesis to my two wonderful grandparents, Bee Baddock and Gareth Llewellyn, who's strength and love for life I admire so greatly and who wished for me to become a doctor, before it even crossed my mind.

Secondly, I would like to dedicate this thesis to my future self for when you are faced with the challenges in life that make you question your strength, your self-worth and threaten your confidence in your ability. If you can complete a PhD in a Global Pandemic, with limited human contact and no form of escape from it all, then you can achieve anything.

'Self-doubt kills more dreams than failure ever will!'

- Suzy Kassem -



Declaration

I, **Samantha Victoria Llewellyn**, declare that:

This thesis has not been previously accepted in substance for any degree and is not being concurrently submitted in candidature for any degree.

Signed (Candidate) ... on 28/06/2021

Statement 1

This thesis is the result of my own independent investigations, except where otherwise stated and that other sources are acknowledged by footnotes giving explicit references and a detailed bibliography appended.

Signed (Candidate) ... on 28/06/2021

Statement 2

I hereby give consent for my thesis, if accepted, to be available online in the University's Open Access Repository and for inter-library loan after expiry of the bar on access, and for the title and summary to be made available to outside organisations.

Signed (Candidate) ..... on 28/06/2021

Acknowledgments

First and foremost, I would like to thank my supervisor Prof. Shareen Doak for all of her guidance, continued support and belief in me over these past few years. I would also like to thank Dr Gillian Conway, Dr Kirsty Meldrum, Dr. Martin Clift, and the PATROLS Consortium for all the assistance and valuable advice they have given me, and Swansea University Medical School for financially supporting my research project.

In addition, completing this PhD would not have been possible without my immediate family, Mum, Dad and Megan, and my partner, Alexei Payne, for all the reassurance, encouragement and support they have given me throughout. I thank each of you for your unwavering belief in me and for the motivation to keep going, even when I thought I had nothing left to give. For this, I am eternally grateful.

Lastly, I would like to thank all my friends both near and far, with a special mention to Chelsea Ambrose, Demi Pritchard, Rhiannon Beadman, Tom Ormsby, Qiellor Haxhiraj and Swansea City Hockey Club for giving me the chance to escape, stay true to myself and for the motivation to continue.

Abstract

Due to the expanding use of nanotechnology in consumer applications, human and environmental exposure to engineered nanomaterials (ENM) is inevitable. Hepatic toxicology is important when considering ENM exposure, as the liver is the major site of ENM secondary deposition and accumulation post exposure, as well as being vital in metabolic homeostasis and detoxification. The vast range of ENMs available deems it untenable to rely on *in vivo* based methods to elucidate the immediate and lasting effects of ENM exposure. Therefore, this research project aimed to develop an advanced 3D *in vitro* liver model with enhanced physiological relevance to better understand the human health hazards, specifically genotoxicity, associated with ENM exposure. The *in vitro* model developed was a HepG2 3D liver spheroid model with 14-day viability and liver-like functionality, as well as proliferating capabilities required to support the evaluation of fixed DNA damage endpoints. Utilising this model, the next objective was to evaluate several toxicological endpoints (*e.g.* liver function, (pro-)inflammatory response, cytotoxicity and genotoxicity) for a variety of ENMs (TiO₂, ZnO, Ag, BaSO₄ and CeO₂) under different exposure regimes designed to better mimic human exposure routes. To achieve this, the ENM were 1) pre-treated in a series of biological simulant fluids to mimic inhalation and ingestion exposure routes, and 2) applied to the 3D liver model for both short- (24hr) and prolonged (120hr) single-bolus, and repeated-fractionated daily ENM exposure regimes, prior to hazard characterisation. The effects of material biotransformation upon reactivity, cytotoxicity, (pro-)inflammatory and genotoxic potential of Ag and TiO₂ was demonstrated, and illustrated that the necessity of ENM pre-treatment prior to *in vitro* hazard assessment should be reserved for ENM that exhibit high degrees of physico-chemical transformation and reactivity (*i.e.* a tiered testing strategy). When comparing dosing durations, no cytotoxicity or significant reduction in liver-like functionality was observed across either acute, prolonged or repeated exposure regimes. Acute exposure to all ENMs induced a significant increase ($p \leq 0.05$) in genotoxicity, albeit not dose-dependently. ZnO, which rapidly dissolves into ions, was the only material to exhibit genotoxicity at both an acute and prolonged exposure. For the materials selected in this study, there was no significant difference between prolonged, bolus or repeated exposure regimes, indicating that the added complexity of fractionated dosing was not necessary. In conclusion, 3D *in vitro* hepatic spheroid models have the capacity to be utilised for evaluating more realistic ENM exposures, thereby providing a future approach to better support *in vitro* ENM hazard assessment in a routine and easily accessible manner.

Table of Contents

1.0 Summary of Published Work	1
1.1 Author Contribution Declaration	5
2.0 Abbreviations List	10
3.0 Figures and Tables List	13
3.1 Figures	13
3.2 Tables	14
4.0 Publications	15
4.1 Publication I	16
4.2 Publication II	36
4.3 Publication III.....	47
4.4 Publication IV	59
4.5 Publication V.....	82
5.0 Critical Review	113
5.1 <i>In Vitro</i> 3D HepG2 Liver Model Development	116
5.2 ENM Exposure Scheme Design	119
5.2.1 Inhalation Simulant Fluids.....	121
5.2.2 Oral Ingestion Simulant Fluids.....	123
5.3 ENM Exposure Regimes	129
5.4 Secondary Genotoxicity and <i>In Vitro</i> 3D Liver Coculture Model Development	131
5.4.1 <i>In Vitro</i> 3D Liver Coculture Model Characterisation.....	138
5.4.2 <i>In Vitro</i> 3D Liver Coculture Model ENM Exposures	141
5.5 Future Outlooks.....	148
5.6 Conclusion.....	150
6.0 References	151
7.0 Evidence of Publication	157
8.0 Appendices	160

1.0 Summary of Published Work

I. *In Vitro* Three-Dimensional Liver Models for Nanomaterial DNA Damage Assessment

First Author

A literature review of current 3D *in vitro* liver models available to support engineered nanomaterial (ENM) associated hazard assessment, with a specific focus on genotoxicity and DNA damage. This research highlights where advancements could be made to the existing models to enhance the physiological relevance and predictivity of the *in vitro* test systems.

Submitted: Small Journal, 28th September 2020

Published: 15th January 2021

Llewellyn, S.V., Niemeijer, M., Nymark, P., Moné, M.J., van de Water, B., Conway, G.E., Jenkins, G.J.S. and Doak, S.H. (2021). *In Vitro* Three-Dimensional Liver Models for Nanomaterial DNA Damage Assessment. *Small*, 2006055. doi: 10.1002/sml.202006055

II. Advanced 3D Liver Models for Genotoxicity Testing *In Vitro* Following Long-Term Nanomaterial Exposure.

First Author

Methods paper describing the production of the advanced 3D *in vitro* liver model developed by Samantha Llewellyn at Swansea University and its utilisation for genotoxicity testing. The paper highlights that the 3D liver model is suitable for use with engineered nanomaterials (ENMs) and can be utilised to evaluate genotoxicity post ENM exposure using the ‘gold standard’ *in vitro* micronucleus assay.

Submitted: JoVE Journal, 20th December 2019

Published: 6th May 2020

Llewellyn, S. V., Conway, G. E., Shah, U. K., Evans, S. J., Jenkins, G. J. S., Clift, M. J. D., Doak, S. H. (2020). Advanced 3D Liver Models for *In vitro* Genotoxicity Testing Following Long-Term Nanomaterial Exposure. *J. Vis. Exp.* (160), e61141, doi:10.3791/61141

III. Adaptation of the *in vitro* micronucleus assay for genotoxicity testing using 3D liver models supporting longer-term exposure durations.

Third Author

Publication III describes the development and optimisation of the 3D HepG2 liver spheroid model to support longer-term ENM exposure and the *in vitro* micronucleus assay for ENM associated genotoxicity assessment. Samantha contributed to this data paper by generating a large proportion of the optimisation and characterisation data produced in the development of the 3D *in vitro* HepG2 liver spheroid model described in publication II. Samantha contributed data to produce two out of the four figures in the paper and additionally provided data for all of the data tables (two) in the manuscript. Furthermore, Samantha contributed text to the methods and results sections of the paper, in addition to providing text for some aspects of the discussion.

Submitted: Mutagenesis Journal, 15th May 2020

Published: 1st July 2020

Conway, G.E., Shah, U.-K., Llewellyn, S., Cervena, T., Evans, S.J., Al Ali, A.S., Jenkins, G.J., Clift, M.J.D., and Doak, S.H. (2020) Adaptation of the *in vitro* micronucleus assay for genotoxicity testing using 3D liver models supporting longer-term exposure durations. *Mutagenesis*, Volume 35, Issue 4, Pages 319–330. doi: 10.1093/mutage/geaa018

IV. Simulating Nanomaterial Transformation in Cascaded Biological Compartments to enhance the Physiological Relevance of *In Vitro* Dosing Regimes: Optional or Required?

First Author

Publication IV assessed the impact of enhancing ENM exposure regimes to emulate more realistic human exposure scenarios, relevant to the human liver. The primary focus of the publication is on the physico-chemical transformation that ENM may undergo following oral exposure, prior to those materials reaching the liver; and the consequence that has on toxicological outcome. Gastric, intestinal and blood simulant fluids were used to pre-treat the test ENMs (Titanium Dioxide and Silver) prior to *in vitro* liver model exposures. The subsequent impact of the pre-treated ENM as compared to pristine materials was then evaluated using a range of relevant hazard endpoint assays.

Submitted: Small Journal, 30th July 2020

Published: 21st January 2021

Llewellyn, S.V., Kämpfer, A., Keller, J.G., Vilsmeier, K., Büttner, V., Ag Seleci, D., Schins, R.P.F., Doak, S.H. and Wohlleben, W. (2021). Simulating Nanomaterial Transformation in Cascaded Biological Compartments to Enhance the Physiological Relevance of In Vitro Dosing Regimes: Optional or Required? *Small*, 2004630. doi: 10.1002/smll.202004630.

V. Understanding the Impact of More Realistic Low-dose, Prolonged Engineered Nanomaterial Exposure on Genotoxicity using 3D Models of the Human Liver.

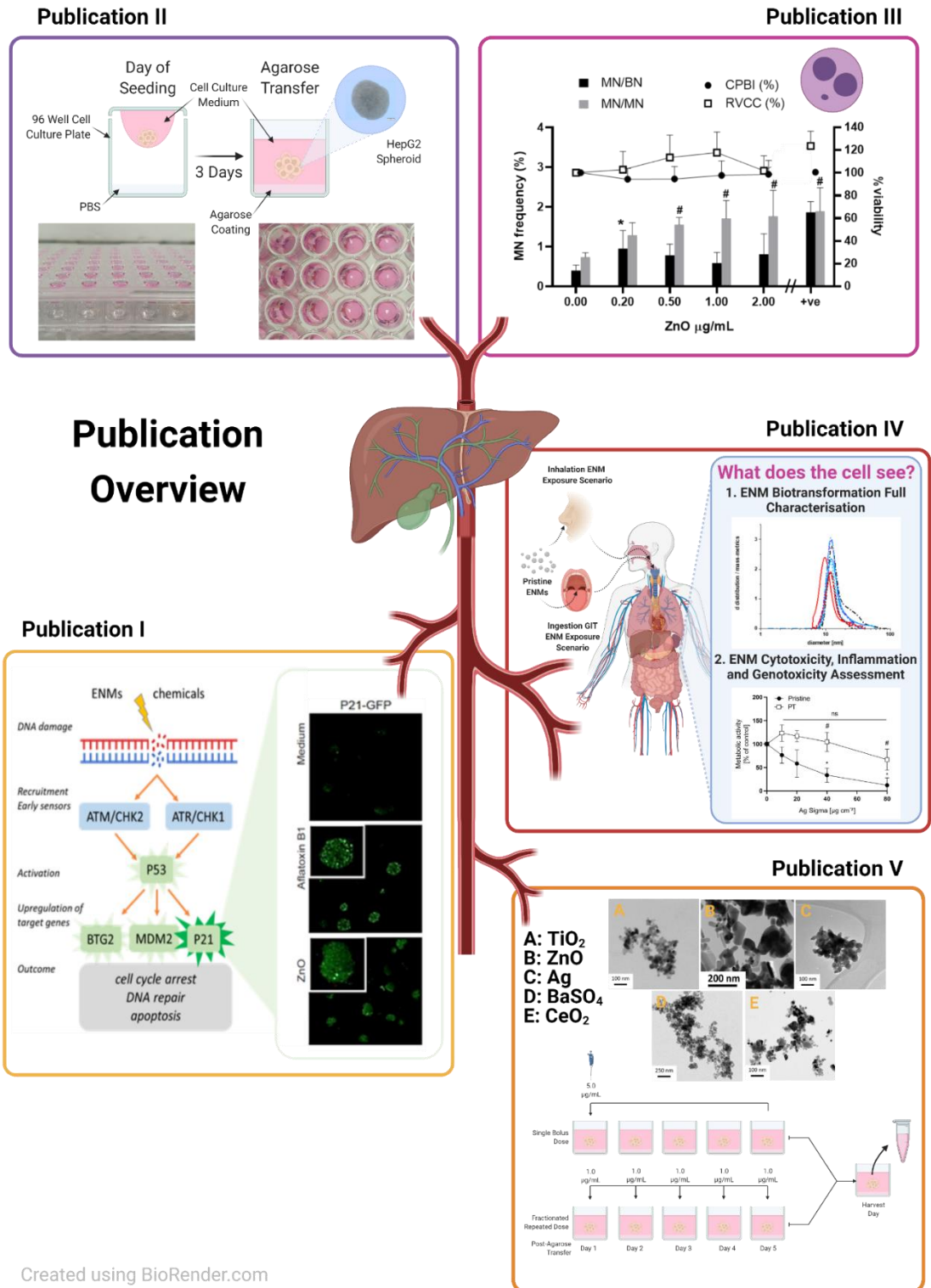
First Author

This publication looks to build upon the previous four publications, by applying the 3D HepG2 spheroid model developed in publications II & III, for *in vitro* ENM hazard assessment. A variety of ENMs (Titanium Dioxide, Zinc Oxide, Silver, Barium Sulfate and Cerium Dioxide) and toxicity endpoints were used to evaluate the potential adverse outcomes associated with exposure to these ENMs on the human 3D liver model. In line with maintaining realistic low-dose ENM exposure regimes, an acute (24 h) and, a single, bolus and a repeated, fractionated prolonged (5-day) ENM exposure were performed to determine if a significantly different toxicological outcome would be observed between the exposure regimes. Extensive physico-chemical ENM data was also undertaken to support the toxicological responses observed.

Submitted: Journal of Nanobiotechnology, 22nd March 2021

Published: 13th June 2021

Llewellyn, S.V., Conway, G.E., Zanoni, I., Jørgensen, A.K., Shah, U-K., Ag Seleci, D., Keller, J.G., Kim, J-W., Wohlleben, W., Jensen, K.A., Costa, A., Jenkins, G.J.S., Clift, M.J.D. and Doak, S.H. (2021). Understanding the Impact of More Realistic Low-dose, Prolonged Engineered Nanomaterial Exposure on Genotoxicity using 3D Models of the Human Liver. *J. Nanobiotechnol*, 19(193). doi: 10.1186/s12951-021-00938-w.


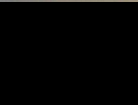















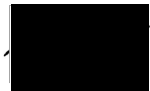
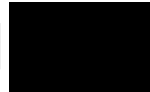


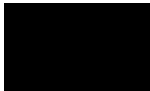







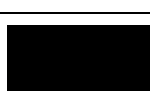

Created using BioRender.com


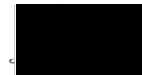



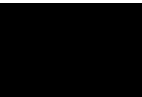









Figure 1: Schematic overview highlighting the key themes discussed in each of the five publications submitted alongside this PhD project.




1.1 Author Contribution Declaration

The following people and institutions, listed in the table below, contributed to the publication of work undertaken as part of this thesis. Therefore, we the undersigned agree with the below stated “proportion of work undertaken” for each of the above published peer-reviewed manuscripts contributing to this thesis.

Author Number:	Author Name:	Author Institute:	Author Contribution:	Proportion of Contribution (%)	Author Signature:
Publication I - <i>In Vitro</i> Three-Dimensional Liver Models for Nanomaterial DNA Damage Assessment					
1	Samantha V. Llewellyn	Swansea University	SVL formulated the research plan, conducted the literature search, created Figures 1 - 4 and Table 2, and wrote 75% of the manuscript.	50.0	
2	Marije Niemeijer	Leiden University	MN co-wrote some sections of the manuscript, created Figure 5 and contributed Table 2, as well as approved and reviewed the final manuscript.	15.0	
3	Penny Nymark	Institute of Environmental Medicine Karolinska Institute and Misvik Biology	PN contributed the AOP research for the introduction of the manuscript, reviewed and approved the final manuscript.	5.0	
4	Martijn J. Moné	Leiden University	MM reviewed and approved the final manuscript.	2.0	
5	Bob van de Water	Leiden University	BW approved the final manuscript.	2.0	
6	Gillian E. Conway	Swansea University	GC helped to structure the review, co-wrote and reviewed the manuscript.	9.0	
7	Gareth J.S. Jenkins	Swansea University	GJ reviewed and approved the final manuscript.	2.0	
8	Shareen H. Doak	Swansea University	SHD conceived the project and research themes of the manuscript, as well as reviewed the manuscript throughout.	15.0	
Publication II - Adaptation of the <i>in vitro</i> micronucleus assay for genotoxicity testing using 3D liver models supporting longer-term exposure durations.					
1	Gillian E. Conway	Swansea University	GC performed some of the experiments, collected and analysed the data. GC co-wrote the paper and reviewed the manuscript.	30.0	
2	Ume-Kulsoom Shah	Swansea University	UKS performed the experiment for Figure 4, and collected and analysed the data. UKS co-wrote the paper and reviewed the final manuscript.	15.0	
3	Samantha V. Llewellyn	Swansea University	SVL performed the experiments for Figures 2 and 3a, 3c, 5, 6 and Table 1, collected and analysed the data. SVL co-wrote the paper and reviewed the manuscript.	25.0	
4	Teresa Cervena	Institute of Experimental Medicine of the CAS	TC performed experiments for Figure 6, collected and analysed the data.	3.0	
5	Stephen J. Evans	Swansea University	SJE performed experiments for Figure 3b, collected and analysed the data.	3.0	
6	Abdullah S. Al Ali	Swansea University	AA assisted with the experiments for Fig 3c.	2.0	

7	Gareth J.S. Jenkins	Swansea University	GJ contributed to study design, reviewed and approved the manuscript.	5.0	
8	Martin J.D. Clift	Swansea University	MJDC reviewed and approved the manuscript.	2.0	
9	Shareen H. Doak	Swansea University	SHD conceived the project and designed the experiments. SHD co-wrote the paper, reviewed and approved the manuscript.	15.0	
Publication III - Advanced 3D Liver Models for Genotoxicity Testing <i>In Vitro</i> Following Long-Term Nanomaterial Exposure.					
1	Samantha V. Llewellyn	Swansea University	SVL performed the experiments for all the figures, collected and analysed the data. SVL filmed the protocol, co-wrote the paper and reviewed the manuscript.	55.0	
2	Gillian E. Conway	Swansea University	GC assisted with filming the protocol, co-wrote the paper and reviewed the manuscript.	20.0	
3	Ume-Kulsoom Shah	Swansea University	UKS performed experiments for Figure 7, collected and analysed the data.	4.0	
4	Stephen J. Evans	Swansea University	SJE reviewed and approved the manuscript.	2.0	
5	Gareth J.S. Jenkins	Swansea University	GJSJ reviewed and approved the manuscript.	2.0	
6	Martin J.D. Clift	Swansea University	MJDC reviewed and approved the manuscript.	2.0	
7	Shareen H. Doak	Swansea University	SHD conceived the project and designed the experiments. SHD co-wrote the paper, reviewed and approved the manuscript.	15.0	
Publication IV - Simulating Nanomaterial Transformation in Cascaded Biological Compartments to enhance the Physiological Relevance of <i>In Vitro</i> Dosing Regimes: Optional or Required?					
1	Samantha V. Llewellyn	Swansea University	SVL performed the experiments and data analysis for Figures 7 and S4, collected and analysed the data. SVL designed the graphical abstract, co-wrote and consolidated the manuscript.	20.0	
2	Angela A. Kämpfer	IUF - Leibniz Research Institute for Environmental Medicine	AAK performed the experiments and data analysis for Figure 5, 6 and S3, produced Tables S7 and S8, and co-wrote the manuscript.	15.0	
3	Johannes G. Keller	BASF SE	JGK performed the experiments and data analysis for Figures 2, 3, S1 & S2 and produced Tables S1 - S6.	15.0	
4	Klaus Vilsmeier	BASF SE	KV designed Figure 1 and assisted with the experiments for Figures 2, 3, S1 & S2 and Tables S1 - S6.	5.0	
5	Veronika Büttner	IUF - Leibniz Research Institute for Environmental Medicine	VB performed the experiments for Figure 5, 6 and S3.	5.0	

6	Didem Ag Seleci	BASF SE	DAS performed experiments for Figure 4.	5.0	
7	Roel P.F. Schins	IUF - Leibniz Research Institute for Environmental Medicine	RPFS reviewed and approved the manuscript.	5.0	
8	Shareen H. Doak	Swansea University	SHD conceived the research idea, co-wrote the paper, reviewed and approved the manuscript.	15.0	
9	Wendel Wohleben	BASF SE	WW conceived the research idea, co-wrote the paper, reviewed and approved the manuscript.	15.0	
Publication V: Understanding the Impact of More Realistic Low-dose, Prolonged Engineered Nanomaterial Exposure on Genotoxicity using 3D Models of the Human Liver.					
1	Samantha V. Llewellyn	Swansea University	SVL produced and analysed the data for all ENM exposures on the 3D liver models, as well as generating Figures 2-6 and Table 1, 3-5, and wrote the manuscript itself.	45.0	
2	Gillian E. Conway	Swansea University	GC generated the data for the two different dosing regime experiments and reviewed the final manuscript.	5.0	
3	Ilaria Zanoni	CNR-ISTEC-National Research Council of Italy	IZ is responsible for the DLS data generated in Table 2, provided the results description for this Table and contributed towards data in Table 1.	5.0	
4	Amalie K. Jorgensen	National Research Centre for the Working Environment	AKJ generated the oxygen reactivity and dissolution data in Figure 1.	5.0	
5	Ume-Kulsoom Shah	Swansea University	UKS assisted with the experiments required for Figure 3a and 3b.	2.0	
6	Didem Ag Seleci	BASF SE	DAG performed the experiments and data analysis for Table 1.	5.0	
7	Johannes G. Keller	BASF SE	JGK performed the experiments and data analysis for Table 1.	2.0	
8	Jeong Won Kim	Korea Research Institute of Standards and Science	JWK generated the XPS data in Table 1 and Figure S3.	2.0	
9	Wendel Wohleben	BASF SE	WW provided the data in Table 1 and Figure S2. WW reviewed and approved the manuscript.	3.0	
10	Keld A. Jensen	National Research Centre for the Working Environment	KAJ provided the physico-chemical discussion relating to the oxygen reactivity and dissolution data in Figure 1, reviewed and approved the manuscript.	5.0	
11	Anna Costa	CNR-ISTEC-National Research Council of Italy	AC reviewed and approved the final manuscript.	2.0	

12	Gareth J.S. Jenkins	Swansea University	GJSJ reviewed and approved the final manuscript.	2.0	
13	Martin J.D. Clift	Swansea University	MJDC reviewed and approved the final manuscript.	2.0	
14	Shareen H. Doak	Swansea University	SHD provided the study design and supervision on the written manuscript.	15.0	

2.0 Abbreviations List

2D	Two Dimensional
3D	Three Dimensional
AFB1	Aflatoxin B1
Ag	Silver
AOPs	Adverse Outcome Pathways
ATCC	American Type Culture Collection
AUC	Analytical Ultracentrifugation
BAC	Bacterial Artificial Chromosome
B[a]P	benzo[a]pyrene
BaSO₄	Barium Sulfate
BCG	Bromocresol Green Albumin
BET	Brunauer-Emmett-Teller
BN	Binucleated
BSA	Bovine Serum Albumin
CAS	Chemical Abstracts Service
CBMN	Cytokinesis-block Micronucleus
CEN	European Committee for Standardization
CeO₂	Cerium Dioxide
CI	Confidence Intervals
CO₂	Carbon Dioxide
CPBI	Cytokinesis-block Proliferation Index
CPH	1-hydroxy-3-carboxy-pyrrolidine
Cyto B	Cytochalasin B
DAPI	4',6-diamidino-2-phenylindole
ddH₂O	Double Distilled Water
DILI	Drug-induced Liver Injury
DMEM	Dulbecco's Modified Eagle Medium
DMETs	Drug-Metabolizing Enzymes and Transporters
DMPO	5,5-Dimethyl-1-pyrroline-N-oxide
DMSO	Dimethyl Sulfoxide
DNA	Deoxyribonucleic Acid
DQ12	Dörentruper Quartz sample, Grinding n.12 (respirable crystalline silica)
ECACC	European Culture of Authenticated Cell Cultures
ECM	Extracellular Matrix
EDTA	Ethylenediaminetetraacetic acid
ELISA	Enzyme-Linked Immunosorbent Assay
ENM	Engineered Nanomaterial
EPR	Electron Paramagnetic Resonance
FBS	Foetal Bovine Serum
FCS	Foetal Calf Serum
fpg	formamidopyrimidine DNA glycosylase
FRAS	Ferric Reduction Ability of Serum
GFP	Green Fluorescent Protein

GIT	Gastro-Intestinal Tract
HBS	Human Blood Serum
ICP-MS	Inductively Coupled Plasma Mass Spectrometry
IFN-γ	Interferon Gamma
IL-6	Interleukin 6
IL-8	Interleukin 8
ISDD	In Vitro Sedimentation, Diffusion and Dosimetry
ISO	International Organization for Standardization
IUF_G	Gastric Simulant Fluid
IUF_I	Intestinal Simulant Fluid
IWGT	International Workshop on Genotoxicity Testing
JOVE	Journal of Visualized Experiments
JRC	Joint Research Centre
KET	Key Enabling Technology
LOAEL	Lowest Observed Adverse Effect Level
LSECs	Liver Sinusoidal Endothelial Cells
LSF	Lung Simulant Fluid
MMS	Methanesulfonate
MN	Micronucleus
MOA	Mode of Action
MWCNT	Multi-Walled Carbon Nanotube
NF-$\kappa\beta$	Nuclear Factor Kappa β
NP	Nanoparticle
O₂	Oxygen
OECD	The Organisation for Economic Co-operation and Development
PBS	Phosphate Buffered Saline
PHH	Primary Human Hepatocytes
PhIP	2-amino-1-methyl-6-phenylimidazo(4,5-b) pyri-dine
PMA	Phorbol 12-myristate 13-acetate
PSF	Phagolysosomal Simulant Fluid
PT	Pre-Treated
PVP	Polyvinylpyrrolidone
REACH	Registration, Evaluation, Authorization and Restriction of Chemicals
RICC	Relative Increase in Cell Count
RNA	Ribonucleic Acid
RNS	Reactive Nitrogen Species
ROS	Reactive Oxygen Species
RPD	Relative Population Doubling
RSMN	Reconstructed Skin Micronucleus
RT	Room Temperature
RVCC	Relative Viable Cell Count
SD	Standard Deviation
SDS	Safety Data Sheets
SDS	Standard Deviation
SEM	Standard Error of the Mean
SI	Supplementary Information

SiO₂	Silicon Dioxide
SOP	Standard Operating Procedure
TB	Trypan Blue
TBS	Tris-buffered Saline
TEM	Transmission Electron Microscopy
TG	Test Guideline
TGA	Thermogravimetric Analysis
TiO₂	Titanium Dioxide
TNF-α	Tumor Necrosis Factor Alpha
UV	Ultraviolet
XPS	X-Ray Photoelectron Spectroscopy
XRD	X-Ray Diffraction
XRF	X-Ray Fluorescence
ZnO	Zinc Oxide

3.0 Figures and Tables List

3.1 Figures

Figure 1	Representative images of the hanging drop spheroid model set-up and process used to form the HepG2 spheroids.	118
Figure 2	Schematic illustration of the sequential incubations required for simulating the translocation of ENMs to the liver, following both oral and inhalation exposure routes.	121
Figure 3	Comparison of IL-8 and TNF- α pro-inflammatory response post-acute and longer-term exposure to both pristine and pre-treated TiO ₂ and Ag ENMs.	127
Figure 4	Cytotoxicity and genotoxicity response in HepG2 spheroids following acute and longer-term exposure to both pristine and pre-treated TiO ₂ and Ag ENMs.	128
Figure 5	Albumin expression in HepG2/Kupffer cell co-culture liver spheroids over a 10 day period.	134
Figure 6	Baseline concentration of TNF- α in HepG2/Kupffer cell co-culture liver spheroids over a 10 day period.	135
Figure 7	Confocal microscopy image of a HepG2/Kupffer cell co-culture spheroid on Day 1.	136
Figure 8	Confocal microscopy Z-stack image of two different HepG2/Kupffer cell co-culture spheroids on Day 1.	137
Figure 9	Average cell viability (%), concentration of albumin and urea per HepG2/Kupffer cell coculture spheroid during 14 days in culture.	139
Figure 10	Baseline IL-8 (pro-)inflammatory mediator release from 80 pooled HepG2/Kupffer cell coculture spheroids over 14 days in culture.	141
Figure 11	Average concentration of albumin and urea produced by HepG2/KC coculture spheroids following acute and prolonged exposure to Ag and TiO ₂ ENMs.	142
Figure 12	Baseline IL-8 release from HepG2/KC coculture spheroids following acute and prolonged exposure to Ag and TiO ₂ ENMs.	144
Figure 13	Cytokinesis-Block Proliferation Index and Micronuclei Frequency (%) induced in HepG2/KC coculture spheroids following acute exposure to Ag and TiO ₂ ENMs.	146

3.2 Tables

Table 1	Compositional breakdown of potential simulant fluids devised as a more physiological representative alternative to human lung surfactant.	122
Table 2	Description of the composition and physiochemical properties of the selected simulant lung fluid proposed for ENM pre-treatment schemes.	123
Table 3	Composition of the gastric and intestinal simulant fluids used in the pre-treatment of the ENMs used in publication IV.	124

4.0 Publications

4.1 Publication I

In Vitro Three-Dimensional Liver Models for Nanomaterial DNA Damage Assessment

Samantha V. Llewellyn, Marije Niemeijer, Penny Nymark, Martijn J. Moné, Bob van de Water, Gillian E. Conway, Gareth J. S. Jenkins, and Shareen H. Doak*

Whilst the liver possesses the ability to repair and restore sections of damaged tissue following acute injury, prolonged exposure to engineered nanomaterials (ENM) may induce repetitive injury leading to chronic liver disease. Screening ENM cytotoxicity using 3D liver models has recently been performed, but a significant challenge has been the application of such in vitro models for evaluating ENM associated genotoxicity; a vital component of regulatory human health risk assessment. This review considers the benefits, limitations, and adaptations of specific in vitro approaches to assess DNA damage in the liver, whilst identifying critical advancements required to support a multitude of biochemical endpoints, focusing on nano(genoto)xicology (e.g., secondary genotoxicity, DNA damage, and repair following prolonged or repeated exposures).

1. Introduction

Throughout the years an increasing demand for smaller, lighter, faster, more adaptable, and durable technologies has led to the widespread adoption of engineered nanomaterials (ENMs) in a variety of industries such as food, cosmetics, textiles,


S. V. Llewellyn, Dr. G. E. Conway, Prof. G. J. S. Jenkins, Prof. S. H. Doak
In vitro Toxicology Group, Institute of Life Science, Swansea University
Medical School

Swansea University
Singleton Park, Swansea, Wales SA2 8PP, UK
E-mail: S.H.Doak@swansea.ac.uk

M. Niemeijer, Dr. M. J. Moné, Prof. Dr. B. van de Water
Division of Drug Discovery and Safety
Leiden Academic Centre for Drug Research
Leiden University
Einsteinweg 55, Leiden 2333 CC, The Netherlands

P. Nymark
Division of Toxicology
Misvik Biology
Karjakatu 35 B, Turku FI-20520, Finland

P. Nymark
Institute of Environmental Medicine
Karolinska Institute
Nobels väg 13, Stockholm 17 177, Sweden

 The ORCID identification number(s) for the author(s) of this article can be found under <https://doi.org/10.1002/smll.202006055>.

© 2021 The Authors. Small published by Wiley-VCH GmbH. This is an open access article under the terms of the Creative Commons Attribution License, which permits use, distribution and reproduction in any medium, provided the original work is properly cited.

DOI: 10.1002/smll.202006055

manufacturing, electronics, energy, and the biomedical field. Nanotechnology had an estimated global market worth \$48.9 billion in 2017 and is projected to reach \$75.8 billion by the end of 2020; with the latter three industries (electronics, energy, and biomedicine) sharing over 70% of the global nanotechnology market.^[1] Nanomaterials are defined as a natural, incidental, or manufactured materials containing particles in an unbound, monodispersed state, or as an aggregate/agglomerate where 50% or more of the particles possess one or more external dimensions in the size range 1–100 nm.^[2] Nanotechnology is based on utilizing materials with pre-existing beneficial properties

in bulk (>500 nm) and enhancing their physico-chemical properties via an increase in surface area to volume ratio by manufacturing these materials into particles of 1–100 nm in size.^[3–5] However, the novel size specific physico-chemical properties (e.g., shape, size, crystal structure, composition, and surface charge) that enable ENMs to be associated with their advantageous applications are concomitantly causing heightened concerns regarding their potential adverse and unpredictable effects upon the environment and human health.^[3,6] With the continued manufacturing, integration, and extensive application of ENMs, the risk of release into the environment and human exposure increases. Human ENM exposure occurs through four primary routes; dermal, inhalation, ingestion, or injection. Once ENMs have entered the body, they can undergo systemic translocation if they are able to traverse the biological barriers and enter circulation. This often results in multiple sites of deposition affecting various, secondary organ systems such as the liver, kidneys, and spleen.^[7–12]

After inhalation, ingestion, and systemic administration through injection, it has been shown that ENMs deposit and can accumulate in the liver.^[13–18] Hepatic toxicology is key when considering both chemical and ENM exposure, as the liver is vital for maintaining metabolic homeostasis and detoxification of both endogenous and exogenous substances.^[19] For example, the liver possesses a higher mononucleated phagocytic system than that found in most other tissues or even the blood. This was illustrated when almost all of the administered dose of radiolabeled [48V] titanium dioxide (TiO₂) ENMs injected intravenously to healthy, female Wistar–Kyoto rats was directed straight to the liver for clearance.^[20] However, the alveolar–blood-barrier and gut barrier act to reduce the rate of translocation into

systemic circulation, with only 4.3% and 0.6% of the administered ENM dose entering the blood stream after 1 h. Although, the aim is to reduce the ENM load on surrounding tissues, this incidentally causes greater retention of the ENMs over extended periods of time.^[20] It is becoming more apparent that translocation to secondary organs following inhalation or ingestion is low with <1% of the insoluble ENMs reaching secondary organs. The liver has been identified as a secondary organ that is highly susceptible to accumulation of ENMs and may result in liver damage and disease upon prolonged exposure.^[20–22] Recently, Modrzynska et al. illustrated this by exposing 324 young adult female mice (C57BL/6) to 3.24 mg mL⁻¹ of 10 nm TiO₂, 13 nm cerium dioxide (CeO₂), and 14 nm carbon black via three different exposure regimes; intratracheal instillation, intravenous injection, and oral gavage.^[23] All three ENMs were found to translocate to the liver, primarily detected in the hepatic capillaries (e.g., sinusoids) and appeared to have been phagocytized by the liver resident macrophages, known as Kupffer cells. Even 180 days after exposure these ENMs remained within the liver tissue. The frequency and size of the ENM aggregates found in the liver tissue varied depending on the exposure method, suggesting not all the material is cleared easily from the liver.^[23] Miller et al. also demonstrated this element of bio-persistence in 14 healthy, human males, whereby 3.8 nm gold (Au) ENMs inhaled over a 2 h period remained within the blood stream 3 months later, even after being detected in the blood of some volunteers as early as 15 min after exposure.^[24] These findings suggested that ENM translocation into systemic circulation occurs rapidly and with no evidence of a time-dependent increase in Au ENMs present in the blood, indicating that the rate of translocation may be balanced by the rate of clearance.^[24] However, slow incremental accumulation and bio-persistence in systemic tissues poses a potential threat to human health and the environment in the long-term. Evidence for this was demonstrated by the significant increase in DNA strand breaks and hepatic genotoxicity detected, only at later time points (28 and 180 days), following inhalation exposure to carbon black.^[23]

Experimental toxicology has focused on supporting “The 3 Rs” directive to reduce, replace, and refine in vivo animal-based experiments with the aim to develop and utilize advanced in vitro-based systems as more ethical, cost effective, high-throughput alternatives for hazard characterization and risk assessment of chemicals and drugs. Regulations introduced by the EU Registration, Evaluation, Authorization and Restriction of Chemicals stress the need for standardized,^[25] next generation in vitro tests systems that can be trusted to provide predictive and reliable results. Since multiple studies have shown that ENMs are able to accumulate in the liver and can lead to hepatotoxicity upon long-term exposure, there is a need to enhance the longevity and realism of current in vitro liver models to accurately assess the hepatotoxic potential of nanomaterials. Ideally, these in vitro models need to emulate the physiological environment of the human liver, as well as remain functionally stable over longer periods of time to be able to support more realistic exposure scenarios (e.g., long-term single or repeated, low-dose exposures, sequential incubations in physiologically relevant simulants fluids, and the addition of multiple cell types). In addition, to fully reflect the in vivo situation, advanced multicellular 3D in vitro models are needed to

recapitulate the complex, intricate organ structure and active metabolic function. This ensures a better understanding of the underlying mechanisms leading to liver injury in a natural exposure scenario. ENM exposure in the liver has been linked to the induction of lysosomal disruption, as well as mitochondrial disruption. The latter can lead to an imbalance in oxidative homeostasis, an inflammatory response involving the release of cytokines, recruitment of immune cells, and subsequent oxidative stress. All of which can result in reduced liver functionality, DNA damage, and cell viability.^[26]

There are a wide range of 3D in vitro liver models available on the market to support chemical and drug toxicity screening, all with benefits and limitations as extensively reviewed by Lauschke et al., 2019 and van Grunsven, 2017. Based on these reviews, a number of these model test systems are designed in a manner that could deem them unsuitable for ENM associated DNA damage assessment in vitro. For example, the addition of matrices or scaffolds creates a barrier that ENMs may not be able to traverse, thereby preventing appropriate exposure of the test material to the target cells. This has the potential to result in dosimetry inaccuracies and uncertainty concerning the actual ENM concentrations applied to the culture. Another limitation is that current in vitro 3D liver models are often formed from static, fully differentiated cells (i.e., non-dividing cell models) which limits genotoxicity assessment; for example, it deems them unsuitable for use with the gold-standard cytokinesis-block micronucleus (CBMN) assay (OECD TG487), where actively dividing cells are a necessity. Furthermore, there is a distinct lack of 3D in vitro liver models with the capability to evaluate secondary genotoxicity mechanisms induced by a chronic inflammatory response, which is recognized as a key mechanism underlying DNA damage induction associated with ENM exposure in vivo.^[27–29] The standard in vitro 2D and 3D monoculture test systems for genotoxicity evaluation are only capable of detecting primary genotoxicity, thereby overlooking a key DNA damage mechanism associated with ENM exposure that occurs in vivo. Therefore, in this review we focus our discussion on the evaluation of currently available in vitro liver models and their suitability for ENM-induced DNA damage screening.

2. Liver Anatomy, Physiology, and Adverse Outcome Pathways Associated with Hepatic Engineered Nanomaterial Exposure

The liver consists mostly of hepatocytes (60%), and other non-parenchymal cell types, that influence the response toward ENM accumulation in the liver. Non-parenchymal cells include Kupffer cells (phagocytes), stellate cells (lipocytes), and liver sinusoidal endothelial cells (LSECs) which form the walls of the sinusoids (50–180 nm wide blood vessels) that carry blood throughout the liver.^[30,31] These cells are organized into a hexagonal shaped liver lobule with the central vein in the middle, and the sinusoids radiating out to the vertices where the portal triad (including the portal vein, hepatic artery, and bile duct) is located, as indicated in **Figure 1**. Liver lobules are structured with a vast sinusoidal network to allow for the free transfer of oxygen, nutrients, and waste products between the hepatocytes

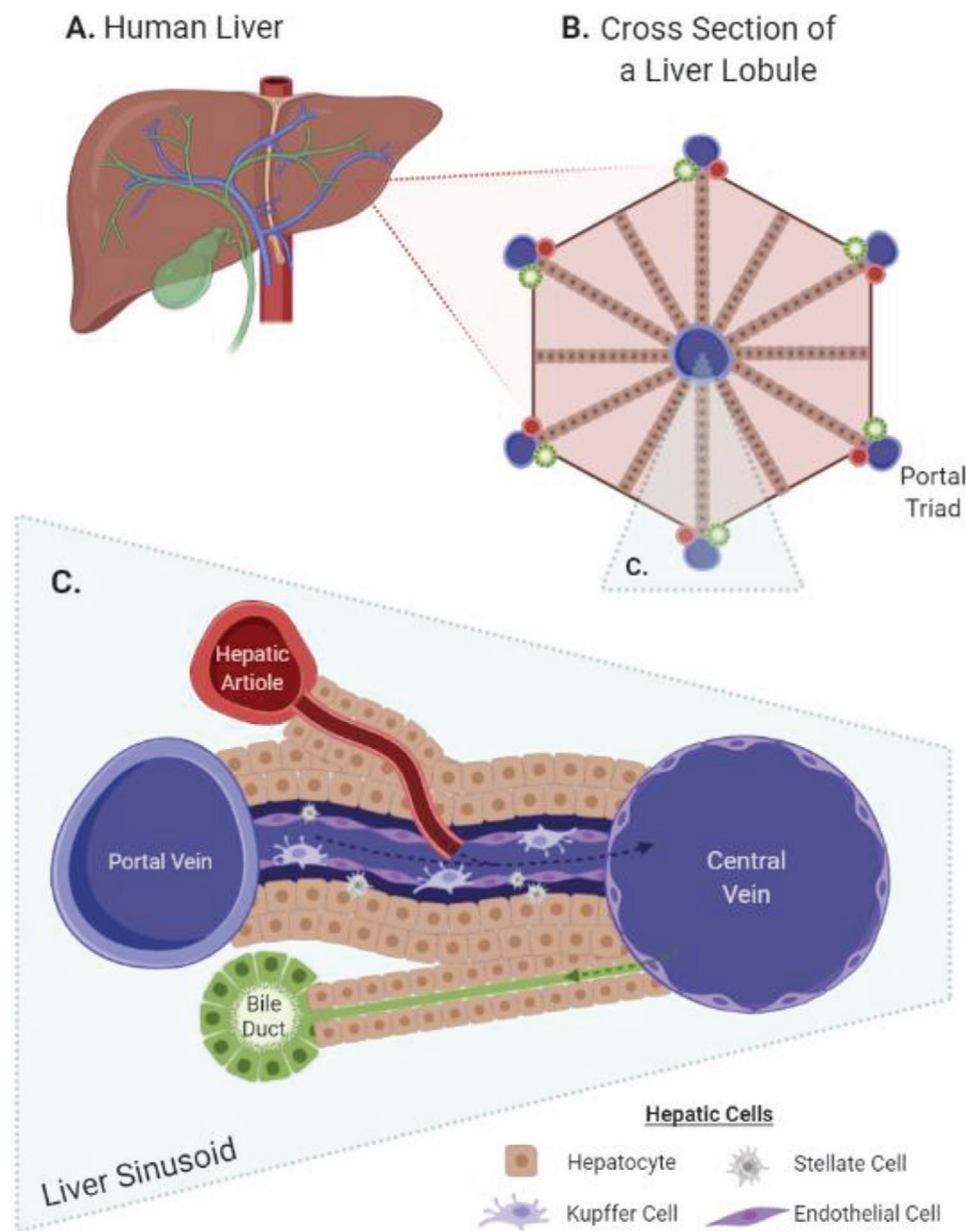


Figure 1. Diagrammatic representation of human liver physiology broken down from A) the liver itself to B) the hepatic lobules consisting of C) multiple liver sinusoids arranged in a hexagonal format. Created with BioRender.com.

and blood traversing along the sinusoid. This results in location dependent partitioning of cellular functionalization, known as “metabolic zonation”.^[31] As a result, the diverse cell populations and specific anatomical organization are crucial to maintaining a viable organ system and hepatic functionality.

The liver possesses the ability to repair and restore sections of damaged tissue following acute injury. However, prolonged exposure to ENMs may induce repetitive injury leading to chronic liver disease, whereby the regenerative capabilities are impaired, and the hepatocytes begin to undergo cell death as a result of inflammation.^[19,32] There are four main adverse outcomes associated with hepatic injury (**Figure 2**), with liver inflammation, fibrosis, and cancer identified as adverse outcomes relevant to chemical and ENM toxicological risk

assessment, and thus are key focal points when developing hepatic models in vitro. In 2012, the Organisation for Economic Co-operation and Development (OECD) launched a new initiative to develop a framework to assess these adverse outcomes and the key events leading up to them. Adverse outcome pathways (AOPs) are substance-agnostic and strictly describe the sequence of biological events connecting an exposure to an adverse outcome. In other words, AOPs do not describe the mode of action of a specific substance, even if a substance is linked to AOPs by their ability to provoke the molecular initiating events. A specific substance may also be used to provide empirical evidence for the existence of an AOP; for example, two AOPs describing liver pathologies have been linked to ENM as stressors.^[33] AOPs have the potential to support systematic

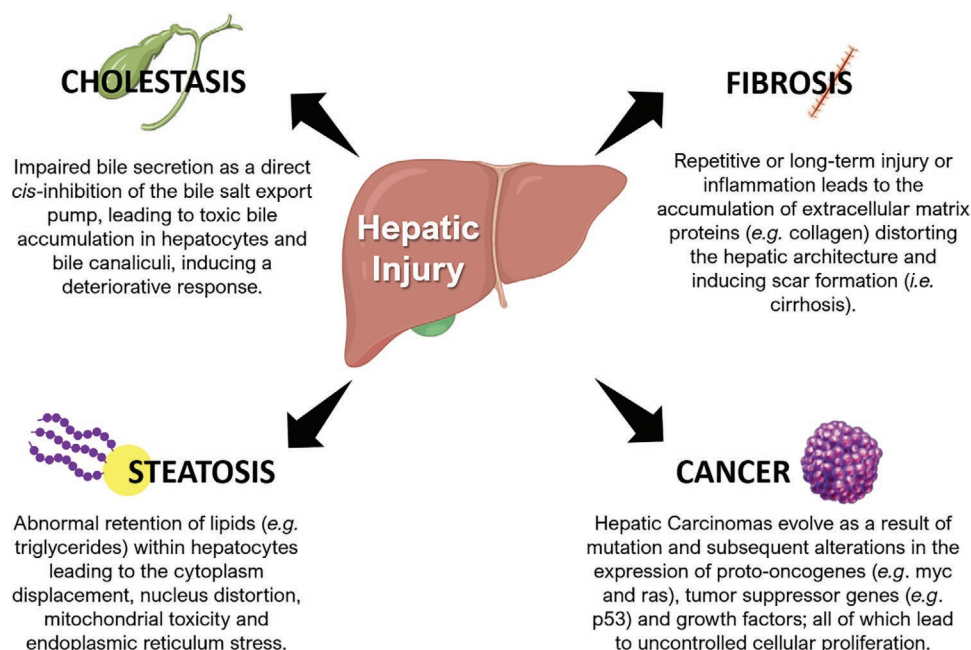


Figure 2. An overview of the four main AOPs associated with hepatic injury. Created with BioRender.com.

review and integration of highly diverse data types, including information from novel *in silico* and *in vitro* assays, which are generally not employed by risk assessors.^[34] There are currently 20 AOPs describing diverse liver pathologies in the AOP-Wiki, 17 of which are focused on liver pathologies in humans, including hepatotoxicity (two AOPs), liver injury (two AOPs), non-alcoholic steatohepatitis (one AOP), steatosis (five AOPs), cholestasis (one AOP), fibrosis (two AOPs), and cancer (four AOPs). One of the AOPs (AOP: 38 for liver fibrosis) has been endorsed by the OECD (indicating high quality) and is one of the most well-developed AOPs to date.^[33] In addition, three AOPs for liver cancer are under review by the OECD (AOP: 41, 46, and 220) and four are in development under the OECD work plan (AOP: 27 [cholestasis], 37 [cancer], 130 [hepatotoxicity], and 144 [fibrosis]). AOPs provide a useful tool for predicting specific mechanisms behind hepatotoxicity and should be considered as flexible constructs open to continual development and refinement as more relevant data is released.^[35]

2.1. Liver Fibrosis

Prolonged incidence of hepatic apoptosis and/or necrosis often leads to the formation of hard scar tissue in place of healthy soft liver tissue; a process more commonly known as liver fibrosis. Liver fibrosis is mediated by a plethora of growth factors and cytokines released by damaged or dying hepatocytes. This leads to the activation of integrated signaling cascades, which are responsible for the phenotypic transformation of quiescent vitamin-A storing hepatic stellate cells into contractile, proliferative, and fibrogenic myofibroblast-like cells.^[32,36] Thus, the majority of *in vitro* liver fibrosis models are found to comprise of hepatic epithelial cells cocultured independently with hepatic stellate cells or with the addition of other non-parenchymal cell

types (e.g., human Kupffer cells and LSECs). Multiple models have been developed in an attempt to recreate a pro-fibrotic environment using the introduction of hepatic stellate cells, which have been acknowledged as the leading scar forming cell type in most liver injuries.^[32,37] It has been frequently found that the greater presence of hepatic stellate cells is commonly linked to the proliferation of hepatoma cells and enhanced tumor metastasis.^[38,39]

2.2. Liver Inflammation

In the liver, host defense and innate immune response is mediated by the resident macrophages, Kupffer cells.^[40,41] Kupffer cells are localized within the hepatic sinusoid and account for 15% of the total hepatic cell population, resulting in a 1 to 4 ratio of Kupffer cells to hepatocytes. They are active members of the mononuclear phagocytic system, that serve a vital role in the mediation of inflammatory response, immune-mediated hepatotoxicity, liver injury, regeneration, and prevention of liver disease.^[42] Kupffer cells function primarily in the ingestion and degradation of both endogenous and exogenous xenobiotics as well as senescent cells, cell debris, and other particulate matter present in the portal blood.^[42] Furthermore, they are known to phagocytose pathogens, recruit neutrophils, and release both (pro-)inflammatory (e.g., IL-1 β , IL-6, and TNF- α) cytokines and (pro-)fibrotic markers (e.g., TGF- β).^[42,43] Kupffer cells are replete with toll-like receptors (i.e., TLR4, TLR2, TLR3, and TLR9) and have been shown to release inflammatory cytokines, such as TNF- α , IL-1 β , IL-6, IL-12, IL-18, and IL-10 on activation with lipopolysaccharide.^[41,44,45] The release of these factors influence and regulate the phenotypes of neighboring hepatocytes and other non-parenchymal cells (e.g., stellate cells and endothelial cells), by triggering signaling pathways that regulate

cell proliferation, viability, and cell death as well as functional cell changes (e.g., hepatocyte drug-metabolizing enzyme activities).^[42,46,47] The presence of Kupffer cells is known to be a key determinant of liver fibrosis, as there is a finely balanced autoregulation between the release of (pro-)inflammatory and inflammatory mediators which in certain cases can exacerbate the initial damage.^[45] Subsequently, Kupffer cells can facilitate chronic inflammation and liver fibrosis as a result of oxidative stress induced by cytokine release; a known adverse outcome of ENM exposure.

ENMs can act as exogenous reactive oxygen species (ROS)/reactive nitrogen species (RNS) inducers that can influence intracellular calcium concentrations, activate (pro-)inflammatory transcription factors (e.g., nuclear factor kappa β [NF- κ B]) and modulate cytokine production via the production of free radicals contributing to an imbalance in the redox homeostasis of the cell.^[48,49] It has been hypothesized that the increased surface area and presence of pro-oxidant functional groups on the ENM surface are responsible for their enhanced ability to produce ROS.^[49,50] ENM-related oxidative stress has been reported to incite a series of pathological events from inflammation and fibrosis to genotoxicity (i.e., chromosomal aberrations including single and double strand breakages and loss/gain of whole chromosomes, point mutations, and epigenetic changes) and carcinogenesis.^[5,48,51] It is widely accepted that ENMs can both directly and indirectly affect intracellular ROS and/or antioxidant (e.g., glutathione and *N*-acetyl-cysteine) levels which are often linked with a (pro-)inflammatory response.^[52–54]

Consequently, not only do these resident macrophages play an important anti-inflammatory role, but their presence within an advanced in vitro model allows for secondary genotoxicity to be assessed. Therefore, models which include multiple cell types, specifically Kupffer cells, in a 3D environment would be more beneficial to accurately assess the comprehensive effect of ENM exposure, accumulation within liver, and the progression toward hepatic adverse outcomes. In addition, it has been shown that hepatic metabolism, such as glutamine and albumin synthesis, cytochrome p450 enzyme activation, xenobiotic metabolism, and urea synthesis are often enhanced when cultured with macrophages.^[55] Kostadinova et al. further illustrated this when culturing hepatocytes with non-parenchymal cells (i.e., Kupffer cells, endothelial cells, and stellates cells) which not only displayed increased albumin synthesis, but also increased transferrin, fibrinogen, and urea production. Furthermore, the macrophage coculture alone had increased CYP450 inducibility, and was more responsive to inflammatory stimuli and hepatotoxins when compared to the monoculture model.^[56] This not only indicates that the inclusion of non-parenchymal cells may more realistically recapitulate liver structure, function, and response to toxins, but may also provide the necessary improvement in the predictive value of in vitro liver models.

2.3. Liver Cancer

Commonly, the etiology of multiple liver pathologies stems from liver fibrosis impeding liver functionality via the distortion of hepatic architecture and blood flow.^[32] Later stages of

liver fibrosis are often associated with the development of cirrhosis and hepatocellular carcinoma; the second leading cause of cancer-related deaths globally, with a 55% increase in liver cancer mortality rates in the UK alone over the last decade.^[32,57–59] Liver cancers are categorized as a heterogeneous group of malignant tumors with different histological features. Tumor progression can be subdivided into different “modes of action” (MOA) with chemicals being defined as having a non-mutagenic or mutagenic MOA. Aflatoxin B1 for example, is a highly potent hepatic carcinogen, found as a contaminant of food, and is known to adopt a mutagenic MOA (AOP 46, AOP-Wiki). Metabolism of aflatoxin B1 results in the formation of the metabolite aflatoxin B1-8,9-epoxide, that can induce pro-mutagenic adducts believed to cause a mutation in the p53 tumor suppressor gene; a gene responsible for cell cycle regulation, initiation of DNA repair and apoptosis.^[60,61] Alterations in the p53 gene, as well as B-catenin gene are also commonly reported in hepatocellular carcinoma.^[62] Although each MOA may be toxin specific, there are common key events highlighted, for instance the disruption of hepatic homeostasis favoring reduced apoptotic activity paired with enhanced cell proliferation resulting in preneoplastic foci and hyperplasia. These key events can be further advanced by a few factors including chronic inflammation, oxidative stress, NF- κ B activation, and inhibition of gap junction intercellular communication.^[35]

Hepatocellular carcinoma is the most common form of primary liver cancer and originates in mature hepatocytes. Under normal “healthy” conditions, differentiated hepatocytes are quiescent and only proliferate upon hepatic injury; so much so they can replicate more than 50 times. It is paramount that current in vitro hepatic models are able to sustain long-term culture to be able to fully assess the initial toxicological insult, as well as the regenerative ability of the hepatocytes to modulate and ameliorate the adverse reactions associated with injury over time. This is particularly pertinent when evaluating the impact of a chemical or ENM exposure on genomic integrity and stability, as DNA damage can be repaired during cell division. Therefore, what may appear to induce genotoxicity following acute (24 h) exposure may no longer have the same effect following prolonged exposure. Prolonged exposure to a chemical or ENM could even result in bioaccumulation leading to metabolic saturation and a “tipping point” of toxicity.^[63,64] As a result, ENMs or chemicals originally categorized as non-genotoxic following acute exposure, may actually have unforeseen, long-term adverse outcomes.

3. Human Derived Hepatocytes for In Vitro Liver Models

With the liver being an essential organ undertaking a vital role in metabolic homeostasis and the detoxification of a plethora of endogenous and exogenous substances. It is imperative that robust and physiologically relevant in vitro model systems are established to support hepatic toxicological hazard assessment following both acute and long-term exposure regimes.^[19] A number of in vitro liver models have been developed and utilized to mimic the in vivo microenvironment including; human liver microsomes, human cell lines, primary human

hepatocytes (PHHs), human liver slices, and isolated perfused livers.^[65,66] Regarded as a “gold standard” technique, often 2D PHHs are used to study hepatotoxicity of chemicals *in vitro*. However, the hepatic phenotype rapidly declines over time showing fast dedifferentiation and so they are deemed unfit for long-term exposure studies in a 2D setup. Even with additional features (e.g., an extracellular matrix [ECM] protein sandwich culture) to enhance the physiological relevance of the 2D *in vitro* microenvironment, PHH cultures lose their hepatic functionality after 14 days in culture, with evidence of reduced albumin and urea production.^[67] Similarly, 2D systems developed with human hepatic cancer cell lines like HepaRG or HepG2, were found to exhibit reduced hepatic characteristics and metabolic activity, specifically cytochrome P450 (CYP450) enzymes (e.g., CYP1A2 and CYP3A4).^[68–70] Reduced expression of phase I enzymes, such as CYP1A2 and CYP2E1, and the subsequent decline in metabolic activity has resulted in some pro-mutagenic compounds (e.g., styrene, aromatic amines, and 2,4-diaminotoulene) being difficult to detect with 2D systems alone.^[71–73] Overall, 2D liver models allow for rapid low-cost, high-throughput screening of chemicals or ENMs and are suitable for the evaluation of acute toxicity. However, 2D systems generally show decreased hepatic phenotype, a reduced metabolic capability, both of which diminish further over extended culture periods, and do not emulate the complex intricacies of the 3D organ system (e.g., intracellular interactions and bile canaliculi). These factors alone have the potential to limit their predictivity for identifying hepatotoxicants. With the longevity of 2D hepatocyte models restricted to less than two weeks, they do not allow for long-term, repeated exposure scenarios to be conducted thereby missing the evolution of toxicity during chronic conditions. To study the hepatotoxic effects of ENM exposure *in vitro*, a robust 3D model that has demonstrated long-term stability, liver functionality, and allows for both acute, chronic, and repeated exposure regimes is required.

It is widely accepted that 3D *in vitro* liver models better mimic the *in vivo* complexities and intricate multicellular interactions than their 2D counterparts.^[19,67,74,75] These features improve the longevity of *in vitro* hepatic models allowing for long-term and repeated exposure regimes to be investigated. In addition, these features have enabled enhanced physiological, organo-typic features like bile canaliculi, active transporter processes, and CYP450 drug-metabolizing capabilities to develop. As a result, the physiological relevance and thereby the predictivity of the models has improved. In a 3D setup, PHHs remain the “gold standard” for hepatic hazard assessment and are considered the most sensitive cell type compared to other *in vitro* liver cell models; HepG2, HepaRG, and Upcyte hepatocytes.^[65,76,77] PHHs are considered to possess the closest representation of active hepatic metabolism (e.g., expression of phase I and phase II enzymes, transporters, and nuclear factors) similar to that found *in vivo*, with CYP450 activity much greater than that observed in hepatic cell lines. However, PHH models exhibit interindividual donor variation and are known to undergo significant de-differentiation during long-term culture.^[77] Interlaboratory comparisons were conducted using HepG2, HepaRG, Upcyte, and PHH models to determine if the different *in vitro* hepatic models could correctly identify the nine drug-induced liver injury (DILI)-implicated compounds

from the four non-DILI-implicated compounds. Sison-Young et al., found that PHHs positively identified eight out of the nine DILI compounds, yet this was closely followed by HepG2 cells which correctly identified six out of the nine (>66%) chemical compounds.^[77] Due to the expensive, complex, and variable nature of the PHH models, demand for research and further development of hepatocyte-derived cell line models has been established.

Immortalized human cell lines are sourced from one donor and are often genetically modified or transformed in a manner that ensures they maintain an element of their original phenotype.^[68] These cultures tend to be readily proliferating, amenable to subculture, resistant to de-differentiation, and are far less sensitive to environmental changes than the PHHs. These characteristics, in line with being relatively inexpensive and easily accessible, highlight cell line-derived 3D models as valuable tools for early-stage drug, chemical, and ENM toxicity screening *in vitro*. A number of human immortalized cell lines, like HepG2, HepaRG, and Huh7, have been successfully utilized across a variety of 3D platforms and have displayed more liver-like functionality and phenotypic consistency than their previous 2D counterparts.

More recently, both HepaRG and HepG2 cell lines appear to be the most frequently studied cell lines and have been readily used in a range of systems, from spheroids in the hanging drop format and ultralow adhesion plates through to scaffold-based (e.g., hydrogels, Matrigel) or bioreactor systems that offer more structural support to the 3D culture.^[68,69,78–81] HepaRG cells originate from hepatic-differentiated, grade-one Edmonson hepatocarcinoma and have been shown to retain their bipotent hepatic progenitor-like characteristics, with a high level of differentiation and expression of typical hepatic functions, including CYP-dependent metabolism, CYP induction, and drug transporter expression.^[68,82] Furthermore, HepaRG possess expression of a major organic anion transporter (MRP-2) involved in bile excretion, together with the ability to form tight junctions, both of which provide the basis for the formation of functional canicular structures allowing for the passage of bile.^[68] It has been suggested that these HepaRG 3D systems exhibit enhanced metabolic functions as a result of both selective hepatocyte differentiation and accelerated maturation induced by limited cellular proliferation. Evaluation of these HepaRG cells for drug and chemical toxicity testing showed a similar response to PHH cultures when assessing the effect of acetaminophen; with a high activation of genes related to liver damage as compared to HepG2 cells, indicating this cell line could serve as a surrogate for PHHs. Gunness et al., demonstrated this further when HepaRG spheroids exposed to 0.5–80 mmol L⁻¹ of acetaminophen for 24 h exhibited a similar dose-dependent response with an EC₅₀ value of 2.7 mM which reflects the concentration observed *in vivo*. This is suggested to be directly correlated to the high levels of CYP2E1 activity producing *N*-acetyl-*p*-benzoquinone imine in abundance.^[78] Although several HepaRG-based 3D models have been reported to better mimic *in vivo*-like microenvironments they do not parallel the metabolic competence and biological relevance of that found in the PHH models, lacking a stable genetic background and the ability to proliferate. Conway et al., demonstrated this with an average binucleate frequency of less

than 10.0% regardless of the concentration and exposure time to the actin polymerization inhibitor, cytochalasin B. This was deemed unsuitable in accordance with OECD Test Guideline 487 for the CBMN regulatory standard genotoxicity assessment *in vitro*.^[83,84]

HepG2 cells, when cultured in an advanced setup may also represent a suitable alternative to PHHs for *in vitro* high-throughput toxicological screening. HepG2 cells have been shown to parallel if not outperform HepaRG cells in the detection of hepatotoxicants. Research has shown that HepG2 cells have a sensitivity of 80% to hepatotoxins and can correctly identify 66.7% of DILI-implicated compounds.^[77,85] HepG2 cells are non-tumorigenic, epithelial-like hepatocytes derived from a hepatocellular carcinoma and can biotransform numerous xenobiotic compounds. This cell line has been well characterized and, contrary to previous literature, found to share similar gene expression profiles as PHH cultures for drug-metabolizing enzymes and transporters (DMETs) when cultured in a 3D format.^[77,86] HepG2 cells are easily accessible, cost-effective, and offer limited intercellular variation whilst retaining a high level of proliferation and phenotypic stability. They are able to secrete typical liver plasma proteins including albumin, fibrinogen, and transferrin, but often lack sufficient gene expression of some essential phase I and II biotransformation enzymes, critical for certain CYP450 enzymes. Guo et al., demonstrated this when they assessed the expression of 251 DMETs including 84 phase I genes, 83 phase II genes, and 84 phase III genes in four cell lines (HepG2, Hep3B, SK-Hep1, and Huh7). In PHH, 69 out of the 84 phase I genes were detected in RNA preparations whilst only 44 phase I genes were expressed highly enough by HepG2 cells resulting in a reduced capability to catalyze oxidation, reduction, hydrolysis, cyclization, and decyclization reactions.^[65] However, the transition from culturing HepG2 cells in a 2D format compared to a 3D format has enhanced their hepatic phenotype significantly. Shah et al. illustrated this enhanced metabolic capacity of HepG2 cells, when cultured in a 3D environment, with a 6-fold increase in CYP1A1 activity and a 30-fold increase in CYP1A2 compared to the equivalent 2D format.^[70] Furthermore, the enhanced activity of the phase I enzymes resulted in greater sensitivity to metabolically activated genotoxicants. Whereby, no genotoxicity was observed in 2D following 24 h exposure to 5 μM of amino-1-methyl-6-phenylimidazo(4,5-b)pyridine, yet in 3D a significant increase in fixed DNA damage was observed.^[70] This highlights that it is critically important to not solely consider the building blocks of the model (i.e., the cell line and culture supplements) but also the architecture of the system (i.e., 3D cellular arrangement) and how this may enhance the primary features of the original foundations (e.g., cellular polarization, intercellular interactions, and canicular structures).

4. Three-Dimensional In Vitro Liver Model Systems

The variety of liver cell lines described in Section 3 can be adapted to suit multiple 3D platforms. Some examples of such advanced culture systems include the formation of stem-cell derived hepatic organoids, hepatic spheroids, bioreactor

systems, microchips (e.g., organ-on-a-chip), bioprinted organ systems, and microfluidic flow models. All of which improve the longevity and differentiation of the cell lines into enhanced, fully functional hepatocytes within a more physiologically relevant setup. However, the majority of these novel approaches lack a robust, economical, and simple design. They often involve laborious assembly, limited accessibility to specific resources necessary for model construction, demonstrate increased variation, and require expensive equipment and skilled expertise. These challenges represent barriers for the use of such 3D model systems in high-throughput and/or screening approaches to facilitate predictive toxicology, and many of these models are not able to support genotoxicity assessment.^[69]

One method that appears to overcome many of the challenges faced in 3D model design for hepatocyte systems is the development of liver spheroids, also known as microtissues. Hepatic 3D spheroid models are generated when monodispersed cells self-assemble into compact spherical structures. They are used frequently *in vitro* hepatic toxicology as the technique is simple by design, highly adaptable, and is shown to recapitulate the liver microenvironment well.^[76,87] One simple technique to develop 3D liver spheroids is through the use of gravity in the hanging drop method as illustrated in **Figure 3**, or the use of ultralow attachment plates which are a less laborious, but more expensive alternative. Spheroids produced via these techniques often form extensive intracellular interactions and produce their own ECM. Another approach to generate 3D structures in culture is by plating cells within an ECM using a scaffold, such as Matrigel.^[88] With this scaffold-based method, multiple spheroids can be generated within one well, but they often vary more in size, shape, and number compared to the scaffold-free methods. However, a low-acyl gellan gum functional polymer matrix has been found to produce uniform spheres of $115.5 \pm 1.7 \mu\text{m}$ in diameter, which can also be used with human induced pluripotent stem cells.^[89] In addition, for some cell types including HepG2 cells, a scaffold can help to improve the hepatic phenotype and arrest proliferation, thereby enabling long-term stability.^[90] Nonetheless, using a scaffold can add additional complexity to harvesting the cells for biochemical endpoint analysis as well as hinder the uptake and penetrance of ENMs in particular when compared to scaffold-free methods.

The versatility of these basic 3D model systems offers the potential for further advancements to emulate true *in vivo* conditions. Examples of this have been seen in the introduction of fluidic-based systems to recapitulate blood flow,^[91,92] or the addition of non-parenchymal cell types to mimic the complex interplay of immunity, cell signaling pathways, and feedback loops.^[32,93] Yet, it is worth noting that the greater human resemblance and complexity the *in vitro* models possess, often makes it more difficult to culture, manipulate, and apply in a hazard characterization setting. Furthermore, these modifications do not fully resolve a major limitation of the current *in vitro* 3D systems; the lack of complex vascular structures crucial to efficient oxygenation, transport of nutrients, and waste removal from hepatic tissues, which occur *in vivo*. In an attempt to counteract this, cells grown in 3D culture perform these functions by diffusion or zonation alone. As a result, the

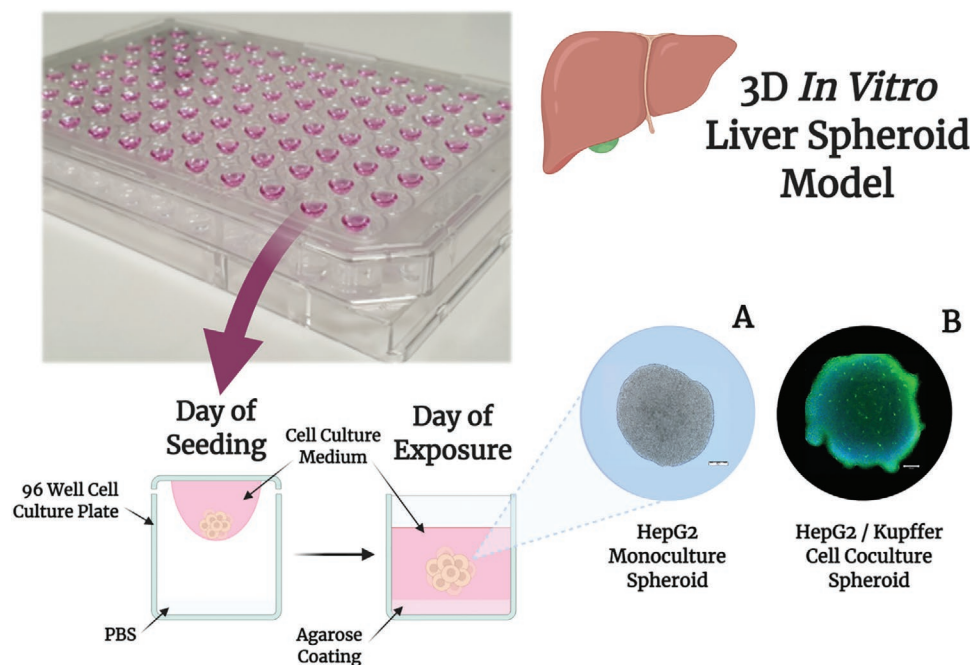


Figure 3. Illustration of a 3D in vitro liver spheroid model developed by Llewellyn et al., 2020, and formed via the hanging drop technique prior to transfer into the well plate for ENM exposure. Microscopy images of A) HepG2 monoculture spheroid and B) HepG2/Human Kupffer cell coculture spheroid taken 4 days after seeding (i.e., the day of ENM or chemical exposure) using a 10× objective with a light microscope and fluorescent confocal microscope, respectively. Green fluorescence represents the CD68 (ab222914, Abcam, UK) positive staining for the human Kupffer cells, whilst the blue fluorescence signifies the DAPI nuclear staining. The scale bars represent 100 μm. Created with BioRender.com.

longevity of these in vitro 3D model systems is often limited by cell viability as the restricted oxygen and nutrient diffusion in conjunction with an accumulation of waste at the core of the microtissue, as shown in **Figure 4**, causes a necrotic core to develop. The limit of this diffusion is thought to be ≈100–150 μm of tissue.^[94,95] Based on this, a number of in vitro

3D models have been developed to be much smaller in order to limit cellular proliferation, the progression of necrosis, and extend the longevity of the cultures. Extending the longevity of the 3D model systems is an important factor when considering these in vitro liver models for use in ENM toxicity testing and hazard assessment. The continuous inclusion of ENMs into everyday applications assures that humans will be exposed to low doses of these materials on a regular, repeated basis over long durations of time. Therefore, there is a greater need for in vitro models to remain viable over extended periods of culture. A feature that a number of 3D liver models do not have without reducing the proliferative capacity of the model or increasing the complexity and subsequent production costs of that model.

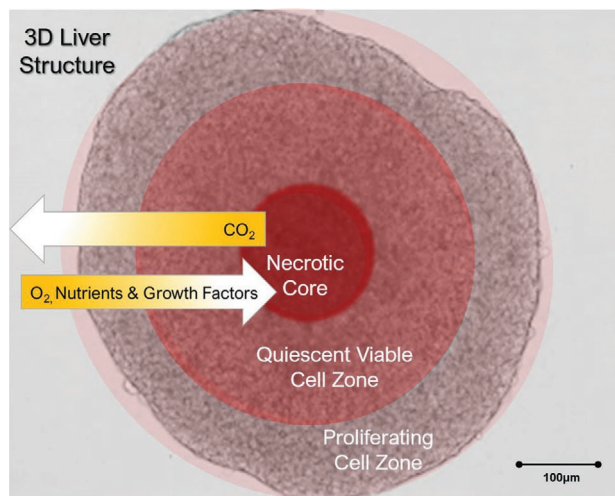


Figure 4. Diagrammatic representation of the nutrient gradient exhibited within 3D liver structure. Cellular zonation illustrated by the darkening shades of red toward the center of the 3D structure, indicating a reduction in cell viability as a result of reduced oxygen (O₂), nutrients, and growth factors and elevated carbon dioxide (CO₂) concentrations indicated by the graduated yellow arrows.

5. In Vitro Liver Model Systems for Engineered Nanomaterial Hazard Assessment

Some of the 3D liver in vitro systems described in Section 4 have already been applied for the evaluation of ENM-induced hepatotoxicity as shown in **Table 1**. However, many of the advanced 3D test systems have been designed on the basis of testing chemicals alone and do not take into consideration the challenges associated with testing ENMs. For example, a particular challenge is the variable sedimentation and diffusion rates associated with different ENMs (e.g., size, shape, and density) and variability based on the individual test system (e.g., exposure medium, scaffold material, and construction variabilities in establishing 3D models). This often results in an unequal distribution of ENMs across the test system or on

Table 1. 2D, 3D, and advanced in vitro liver models utilized for ENM toxicity screening.

In vitro model		Suitability for ENM toxicity screening		Reference ENM studies	Cell type used	Exposure time	ENMs tested
		Pros	Cons				
2D	Monolayer	+ high-throughput + simple	– short-term only – monoculture	(Yang et al., 2019)	HL-7702	Single (24 h)	Silica NPs
				(Lorscheidt et al., 2019)	HepG2	Single (24 h)	SiO ₂
				(Chen et al., 2019)	HepG2	Single (24 h)	ZnO
				(Cornu et al., 2018)	PHH, PRH	Repeated (until 3 days)	PLGA, Silica NPs
				(Brown et al., 2019)	mESC reporter, HepG2, Caco-2	Single (24 h)	TiO ₂ , DQ12, carbon
				(Gao et al., 2020)	hiPSC-HLCs	Single (24 h)	Ag
	PHH sandwich	+ bile canaliculi network + high-throughput	– short-term only – possible hindrance by overlay – monoculture				
	Micro-patterned co-culture	+ long-term + high-throughput + multi cell type	– lacks 3D cell-cell structure				
3D	Spheroids <i>Hanging-drop</i>	+ long-term + equal spheroid size + multi cell type	– More labor intensive – One spheroid/well	(Fledderman et al., 2019)	HepG2	Single (24h) Repeated (until 7 days)	SiO ₂
				(Conway et al., 2020)	HepG2, HepaRG	Repeated (until 5 days)	ZnO
				(Elje et al., 2020)	HepG2	Single (24h)	TiO ₂ , Ag, ZnO
	<i>Ultra-low attachment plates</i>	+ long-term + high-throughput + multi cell type + equal spheroid size	– One spheroid/well	(Kermanizadeh et al., 2019)	PHH, PHH-non-parenchymal cells co-culture	Single (24h) Repeated (until 7 days)	Ag, MWCNT, TiO ₂ , ZnO
				(Senyavina et al., 2016)	HepaRG	Single (6h, 24h)	Ag
	<i>Micromold</i>	+ long-term + multiple spheroids + multi cell type + equal spheroid size	– More labor intensive				
	<i>Bioreactors</i>	+ long-term + large scale	– heterogenous spheroid size – low-throughput				
	<i>Scaffold-based</i>	+ long-term + multiple spheroids + high-throughput + multi cell type	– possible hindrance by scaffold for ENM exposure – heterogenous spheroid size	(Dubiak-Szepietowska et al., 2016)	HepG2	Single (24h, 72h)	Ag, SiO ₂ , ZnO
				(Lee et al., 2009)	HepG2	Single (until 24h)	CTAB-Au, citrate-Au, CdTe
	Liver organoids	+ self-organizing + expansion	– short-term only – low-throughput				
	Liver-on-a-chip	+ long-term + microfluidics + zonation possibilities + multi cell type	– low-throughput	(Li et al., 2019)	PRH	Repeated (3 and 7 days)	SPION
(Esch et al., 2014)				HepG2-C3A co-culture	Single (24h)	Carboxylated polystyrene NPs	
Bioprinted	+ 3D architecture	– low-throughput					

the cell surface of the 3D liver model, which has the potential to cause dosimetry inaccuracies and uncertainty concerning the actual ENM concentrations applied to the culture. This limitation can be overcome theoretically using the *in vitro* sedimentation, diffusion, and dosimetry model, or its more recent derivatives (e.g., ISD3) often referred to with ENM suspension exposures.^[96,97] A further complication with ENM hazard assessment, is the changeable nature in the physico-chemical characteristics of the materials themselves alongside their tendency to aggregate or agglomerate, as this makes predicting biological interactions and cellular uptake difficult. With these challenges in mind, it is not surprising that, unlike chemicals, ENMs do not translocate and permeate the inner cell layers of the 3D structures as efficiently. Albeit, not without its limitations, technological advancements in *in vitro* 3D model ENM hazard assessment techniques provide potential alternatives to reduce the reliance on animal-based testing methods.

Dubiak-Szepietowska et al. showed the applicability of 3D HepG2 cells for ENM toxicity studies. Here, HepG2 cells were plated in three different hydrogels (Matrigel, collagen type 1, and gelatin) resulting in the formation of 3D spheroids with improved hepatic phenotype and function, as demonstrated by an increase in albumin and urea production after 10 days of culture compared to the 2D system.^[88] However, these spheroids displayed a decreased sensitivity toward ENM exposures for both 24 and 72 h compared to conventional 2D culture. This could be explained by improved cell-to-cell interactions and intercellular signaling in 3D culture, which not only encourages the cells to differentiate into more complex structures but alters the signaling (and possibly repair) activities in a cell. More importantly however, the hindered diffusion of ENMs in the hydrogels are likely to result in lower cellular ENM uptake during the acute phase.^[88] Hence, the use of 3D models formed with scaffolds or matrices may not be suitable to study the effects of ENM exposure.

Nonetheless, 3D human liver microtissue models are shown to identify adverse reactions after repeated long-term exposure to a range of ENMs.^[74,93] A study by Kermanizadeh et al. (2014) showed that scaffold-free primary human 3D liver microtissues, consisting of both PHHs and non-parenchymal cells, were able to identify hepatotoxic effects of ENMs during a 15-day, repeated exposure regime. Here, predominantly, cytotoxicity was seen after prolonged or repeated exposure scenarios and not with single exposures alone, highlighting the importance of having a long-term stable *in vitro* liver model to recognize ENM-induced hepatotoxicity. A more recent study, by Kermanizadeh et al. (2019), evaluated the recovery capabilities of liver spheroid microtissues after 7- or 14-day repeated ENM exposure to zinc oxide (ZnO), TiO₂, and CeO₂ and the positive control quartz containing ≈87% crystalline silica (DQ12). During the recovery periods, a reduction in cytokine production was observed, suggesting the microtissues could recover and emulate an element of liver regeneration as found *in vivo*. Interestingly, darkfield imaging highlighted that the ENMs could translocate through the outer surface cell layers of the spheroid and even penetrate the core, providing evidence to support that ENM exposure on 3D model systems can be comprehensive.^[74] However, after two weeks of culture a decline in the viability of the untreated control suggests the 3D model system was not as stable as first

thought and should be used no longer than 14 days for long-term ENM exposure screening.

Although this study highlights the suitability of this PHH 3D liver model for longer-term ENM hazard assessment, Llewellyn et al. also demonstrated that HepG2 cells could be cultured in a hanging drop format for up to 14 days without the need for specialized equipment or scaffolds.^[80] The liver spheroids were ≈500 μm in diameter and able to support both acute (24 h) and longer-term (5 days) ENM exposure regimes without a significant reduction in cell viability in the untreated controls. Furthermore, HepG2 spheroids seeded at 4000 cells per spheroid, were found to retain sufficient proliferative capabilities to be able to support the CBMN assay for genotoxicity assessment following both chemical (aflatoxin B1) and ENM (TiO₂ and Ag) exposure;^[80,83] a feature that other *in vitro* 3D hepatocyte models are currently unable to offer. Interestingly, another HepG2-based spheroid model was utilized to compare the cytotoxicity and genotoxicity using the comet assay, of Ag, ZnO, and TiO₂ ENMs following acute 24 h exposure.^[98] In both 2D and 3D cultures the relative cell viability decreased in a concentration-dependent manner after exposure to Ag and ZnO ENMs, whilst TiO₂ had no effect. For ZnO ENMs, the calculated EC₅₀ values were in the same range for 2D and 3D cultures: 10.1 and 16.2 μg cm⁻², respectively. Yet, the induced cytotoxicity of Ag ENMs was higher in 2D cultures compared to 3D cultures, with EC₅₀ values of 3.8 and >30.0 μg cm⁻², respectively.^[98] This could be attributed to the high levels of agglomeration observed with the increased hydrodynamic diameter of Ag ENMs from 373 ± 0.04 to 508.8 ± 29.5 nm further reducing the penetrative capabilities of the Ag ENMs into the compact, 3D spheroid structure.

Despite the advantages of using 3D models, their compact intricate structure can result in the uneven distribution and hindered penetration of ENM across the 3D structures.^[99–102] A recent study by Fledderman et al. (2019) showed that SiO₂ nanoparticles could only penetrate 20 μm, corresponding to three cell layers, into the HepG2 spheroids created via the hanging drop method. In concordance, a study by Huang et al. demonstrated that Au nanoparticles showed size dependent penetration into tumor tissue or spheroids, where nanoparticles of 15 nm or larger were unable to penetrate the tissue.^[101] As highlighted by these two studies and the aforementioned PHH study undertaken by Kermanizadeh et al. (2019), the translocation capabilities and localization of ENMs can vary considerably from model to model and so should be characterized for each model independently to ensure an accurate representation of ENM distribution is carried out as seen *in vivo*.

Whilst screening ENM cytotoxicity using *in vitro* models has been performed routinely, not many have been able to adapt and utilize the 3D liver models for ENM associated genotoxicity. Most ENM associated hepatic genotoxicity studies have been assessed *in vivo* or with 2D hepatic, monoculture systems *in vitro*. When performing a literature search using the terms “3D *in vitro* liver model nanomaterial genotoxicity,” only 9 publications were identified in PubMed, whilst “3D *in vitro* liver model nanomaterial toxicity” retrieved 19 relevant publications and “3D *in vitro* liver model toxicity” returned 189 publications. This highlights the novelty of 3D *in vitro* liver models being utilized for ENM genotoxicity hazard assessment and a

clear knowledge gap for further research and development to be undertaken.

6. In Vitro Engineered Nanomaterial Associated Genotoxicity Assessment

Genotoxicity arises as a result of DNA damage induced by an exogenous agent which is subsequently fixed as permanent mutations to the genetic information within a cell. These mutations may lead to the incorrect transcription of DNA to mRNA required for protein translation. When a mutation alters the genetic coding for a protein, it can affect the assembly and subsequent function of that protein. Erroneous alterations to proteins that play a critical role in the body can disrupt normal development or cause malignancies, and other pathogenic effects via mechanisms like uncontrolled proliferation, mitochondrial dysfunction, or defective metabolism.^[103] Multiple *in vivo* and *in vitro* studies have reported that some ENMs exhibit clear cytotoxic, (pro-)inflammatory, and sometimes genotoxic effects, thus raising concerns as to the long-term implications on human health.^[104,105] Exposure to ENMs can induce genotoxicity via primary and/or secondary mechanisms. Primary mechanisms dominate *in vitro* ENM associated genotoxicity testing, whilst secondary genotoxicity is recognized as the main genotoxic mechanism *in vivo*.^[28,29] Primary mechanisms can be classified into direct or indirect genotoxicity:

- Direct mechanisms of genotoxicity involve DNA damage caused by the direct, physical interaction of ENMs with the chromosomes or DNA molecule itself.^[27,28]
- Indirect mechanisms of genotoxicity arise from ENM mediated induction of ROS/RNS or the release of toxic ions from soluble ENMs (e.g., zero-valent metals, like silver) that can interfere with DNA complexes or cell cycle proteins (e.g., spindle apparatus and centrioles) that can hinder cellular replication, DNA repair, and division.^[27,28]

Genotoxicity is extensively linked to elevated ROS and an imbalance in oxidative homeostasis following ENM exposure. ROS can interact directly with DNA, disrupt DNA complexes, and cause DNA strand breaks, chromosomal aberrations, and alterations; all of which can induce mutations.^[5,48,51,63] Secondary genotoxicity arises *in vivo* as a result of chronic inflammation caused by the recruitment and activation of immune cells (e.g., macrophages and neutrophils). This cascade results in the continued release of inflammatory mediators and excessive ROS produced during phagocytosis, both of which subsequently induce DNA damage in the surrounding epithelial tissue.^[27,106]

ENM associated genotoxicity can differ between *in vitro* and *in vivo* settings, as the latter is reliant on biokinetic patterns and often involves interaction between multiple cell types. However, DNA damage and associated genotoxicity can be assessed *in vitro* using a range of assays that test particular biochemical endpoints or target specific DNA damage mechanisms, allowing for a more controlled and targeted approach. Magdolenova et al. found that only 2.58% of articles on “NP toxicity” describe genotoxicity studies; of the 112 articles found, 94 were *in vitro*-based

genotoxicity studies whilst 22 were *in vivo* studies.^[106] The comet assay, CBMN assay, γ -H2AX, Green Fluorescent Protein (GFP)-gene reporters, and transcriptomic screening are a few examples of common techniques utilized to assess gene activation/deactivation, DNA damage, and genotoxicity *in vitro*. The *in vitro* mammalian cell gene mutation tests using the HPRT and XPRT Genes (TG476) and the *in vitro* mammalian cell micronucleus test (TG487) have undergone rigorous validation and have recognized OECD test guidelines. As described in Table 2, not all of the genotoxicity assays available are acceptable for regulatory purposes and are, therefore, only deemed suitable for research purposes in order to provide an insight into the underlying mechanisms behind ENM associated genotoxicity. Table 1 further highlights the benefits and limitations to the current assays available to assess DNA damage and genotoxicity *in vitro* that have the potential to be adapted for use with 3D hepatic model systems.

7. Adapting Three-Dimensional In Vitro Liver Models to Support Genotoxicity Assessment

Genotoxicity can be assessed using a number of techniques, as highlighted in Table 2 of Section 6. Each technique has specific applications and genotoxicity targeted endpoints (e.g., chromosome aberrations or fixed DNA damage foci), but not many have been adapted for use with 3D *in vitro* liver models, let alone been tailored to support ENM exposures, as shown by the limited publications in the scientific literature to date. Of the genotoxicity assessments performed, there are principally three techniques which have been successfully adapted to support ENM associated genotoxicity in 3D liver models: the CBMN assay, the comet assay, and bacterial artificial chromosome (BAC)-GFP reporter cell line systems.

The CBMN assay is a reliable and multifaceted technique that measures gross chromosomal damage illustrated by the frequency of micronuclei present.^[107] It is a “gold standard” technique for assessing *in vitro* DNA damage and genotoxicity and is described by the OECD Test Guideline 487.^[84,108] The CBMN assay can readily detect both aneugenic and clastogenic acting compounds alluding to potential DNA damage mechanisms. Aneugenic compounds result in the loss or addition of whole chromosomes, whilst clastogenic compounds induce gene mutations and structural aberrations, including fragmentation and rearrangement of a chromosome.^[109] Furthermore, the cytostatic status of the cell can be determined using the ratio of mononucleated, binucleated, and multinucleated cells to calculate the cytokinesis-block proliferation index.^[84,110,111] Although a popular and reliable method for assessing genotoxicity, the CBMN assay is rarely used with 3D *in vitro* hepatic models as many are static models based on primary or differentiated hepatocytes (e.g., HepaRG) which do not have the capability to actively proliferate. As fixed DNA damage is only visible after the cells have undergone one cell cycle (i.e., undergone division), with a low binucleate frequency, the CBMN assay cannot be used to accurately predict genotoxicity. Conway et al. highlighted this when assessing

Table 2. Current, available assays used to assess DNA damage and genotoxicity in vitro that have the potential to be adapted for use with 3D hepatic model systems.

In Vitro Test	Description of Assay	Genotoxicity Endpoints Assessed	Advantages	Disadvantages	Adapted to support 3D Liver Cultures	Regulatory Approval
Micronucleus Assay	Mutagenicity test system used for the detection of small membrane-bound DNA fragments, known as micronuclei, originating from the loss of a whole chromosome or fragments of a chromosome (lacking a centromere). Number of micronuclei visible in the cytoplasm of interphase cells is scored. (OECD, 2016)	Fixed DNA Damage; Clastogenicity/ Aneugenicity; Cytostasis	Multiple Endpoints Assessed; Allows for DNA repair; Evaluation and Quantification of both structural and numerical chromosomal damage; High Sensitivity when coupled with Fluorescent In Situ Hybridization; Supports both short and long-term exposure schemes	Time Consuming; Experienced scoring expertise required	Yes	OECD Approved Test Guideline for Assessing Genotoxicity In Vitro – Guideline 487 (OECD, 2016)
Chromosome Aberration Assay	In vitro test system used to identify substances that cause structural chromosome aberrations, including changes to chromosome number and/or chromosomal deletions, inversions and translocations. (OECD, 2016)	Fixed DNA Damage; Chromosome Mutations including Numerical and Structural Aberrations; Clastogenicity/ Aneugenicity	Accurate Identification and Discrimination of Chromatid and Chromosome type Aberrations; Possible co-detection of Mitotic Indices	Laborious; Requires Highly Skilled Personnel; Cost Intensive; Scoring Subjectivity	No	OECD Approved Test Guideline for Assessing Genotoxicity In Vitro – Guideline 473 (OECD, 2016)
Point Mutation Assays (e.g., Mouse Lymphoma Assay and HPRT/XPRT Gene Mutation Assay)	Gene mutation tests identify substances that induce point mutations on the X chromosome, which subsequently inactivates or modifies the function of the gene product via base pair substitutions or frameshift mutations. Evidence of this mutation can be seen in the absence of the functional gene product (protein) that affects the growth of mutant cell colonies in selective media. (OECD, 2015)	Fixed DNA Damage; Point (Gene) Mutation; Clastogenicity	Detects Point and Chromosomal mutation; Adapted for High-throughput screening	Laborious; Time Consuming Assay (Duration: 6 Weeks); Open to Human Subjectivity in Scoring Procedure; Only specific (male) cell types are suitable for detection of gene mutations	No	OECD Approved Test Guideline for Assessing Genotoxicity In Vitro – Guideline 490/476 (OECD, 2016)
Comet Assay	Alkaline (>pH 13) single-cell gel electrophoresis based assay used to identify substances that induce DNA damage, including both single and double stranded breaks in eukaryotic cells.	DNA Strand Breaks; Alkali Labile Sites; Oxidized and Alkylated Base Regions	Detects DNA damage; Fast; Cost Effective; High-throughput screening	Does not measure fixed DNA damage lesions as the damage it detects has the potential to be repaired; High variability due to lack of standardized protocol	Yes	There is no standardized method for the in vitro comet assay, but there is an OECD Approved Test Guideline for the In Vivo version of the Alkaline Comet Assay only – Guideline 489 (OECD, 2016)
Transcriptomics	Techniques, using microarray, qRT-PCR or RNA-seq, analyze the quantity of messenger (m)RNA molecules present, which reflects the genes that are being actively expressed as protein products at a given time.	Upregulation and Downregulation of Gene Transcription	Entire Genome assessed; Elucidation of DNA damage mechanisms; High-throughput screening	Expensive; Time Point sensitive	Yes, albeit limited by RNA yield from 3D culture system	No
GFP-Reporter Systems	These systems are based on a Green fluorescent protein (GFP) hybridized gene reporter used to identify the expression of specifically targeted genes (e.g., p53, γ -H2AX), which fluoresce green if the gene is actively expressed in individual eukaryotic cells.	Gene Transfer and Expression	High-throughput; Can be coupled with Live Imaging	Requires Transgenic Cell Lines; Often cultured with a Scaffold/Matrice limiting ENM Applicability	Yes	No

the suitability of HepaRG and HepG2 cell lines to support the CBMN assay, whereby HepaRG, regardless of cytochalasin B concentration and exposure time, only yields a binucleate frequency of <10% whilst HepG2 exhibited a binucleate frequency of >30%.^[70,73,83] As a result, DNA damage and genotoxicity assessment are usually performed using alternative methods such as the comet assay or integrated GFP-reporters. However, recently the CBMN assay has been successfully used to detect DNA damage and genotoxicity in 3D HepG2 hanging drop spheroids following acute exposure to aflatoxin B1 and benzopyrene.^[70] This research further highlighted the importance of enhanced metabolic competence in 3D model systems relative to 2D models when assessing toxicological outcomes associated with compounds which require metabolic activation. Even when restricted by the necrotic core, the proliferative capacity of the HepG2 cells on the outer surface of the spheroids is still able to support the CBMN assay.^[70,80] Furthermore, the micronucleus assay was adapted and used to successfully support both acute (1 day) and long-term (5 days) genotoxicity hazard assessment of 10 µg mL⁻¹ of TiO₂ and Ag ENMs.^[80] Careful consideration must be taken when using the “cytokinesis-block” version of this assay for long-term or repeated exposure regimes though, as any DNA damage induced within the first few cell cycles is distributed across the mononucleated cell population, as opposed to being retained and scored within the binucleated cells. This could lead to false negatives, as the DNA damage accumulated over the period of chronic exposure can be masked. As a result, Llewellyn et al. suggested that the mononuclear version of the micronucleus assay may be more suitable for long-term or repeated exposure regimes. The micronucleus assay is a valuable tool when assessing the genotoxic effects associated with both acute and long-term ENM exposure, as to the best of our knowledge, there has been no reported interaction between the assay and ENMs.

The comet assay is commonly used for assessing DNA strand breaks and oxidized or alkylated base lesions following ENM exposure in order to provide an indication of the mutagenic and carcinogenic potential of the ENM under evaluation.^[76] The comet assay can assess a few hundred to several thousand strand breaks per eukaryotic cell; a biologically relevant sensitivity range which can detect DNA damage extending from low, endogenous levels to high, almost lethal levels of damage. Previous work, using PHH models have found that exposure to ZnO, Ag, TiO₂, and multiwalled carbon nanotubes (MWCNT) induced DNA damage at varying exposure concentrations (0.5–8.0 µg mL⁻¹ of ZnO and Ag, and 16–250 µg mL⁻¹ of TiO₂ and MWCNT), with ZnO and Ag exhibiting the greatest DNA damaging potential and subsequent repeated ENM exposure elevating the DNA damage levels significantly.^[93] Similarly, Elje et al. found that ZnO and Ag ENMs, which both display a tendency to dissociate into ions, were found to exhibit a concentration-dependent increase (0–75 µg cm⁻²) in DNA strand breaks following acute, 24 h exposure in both 2D and 3D HepG2 cultures. However, no effect of DNA damage was observed after exposure to TiO₂ ENMs in either 2D or 3D HepG2 cultures.^[76] Whilst these studies highlight that the PHH and HepG2 3D models predict a similar ENM genotoxicity outcome, they also show that the comet assay can be applied with

multiple 3D models contributing to its popularity as a method for assessing ENM associated genotoxicity in vitro. Unlike the CBMN assay mentioned above, the comet assay is not restricted by cells that do not proliferate, in fact, it is a useful tool to circumvent this limitation. The main drawback of this assay is that whilst it highlights the potential of an exogenous agent to cause DNA damage, it does not take into account the ability of the cell to undergo DNA damage repair. Thus, some of the lesions detected by the comet assay may be transient, which may result in misleading positive results. To date, there are no standardized standard operating procedures or regulatory test guidelines for the in vitro comet assay, so a diverse range of methods and cell test systems have been employed leading to variable results for both chemicals and ENMs.^[112] With specific respect to ENM genotoxicity assessment, there are some concerns regarding the interactions between ENMs and the comet assay. Some studies have reported the presence of ENMs in the “comet head” which could give rise to misleading results.^[113] However, comparisons between the in vitro comet and micronucleus assays have shown that out of a total 70 ENMs tested, 48 (69%) were reported as positive for genotoxicity consistently in both assays.^[113] It is important to note, just like the aforementioned genotoxicity assays, that high cytotoxicity is a major contributor to the misleading positive rate.^[112,114,115] Yet, there is no definitive consensus on acceptable cytotoxicity ranges for the in vitro comet assay specifically. The limitations with the in vitro comet assay have been illustrated by Elespuru et al., whereby following an extensive literature review, only 55% of the 22 papers identified that used the in vitro comet assay to evaluate ENM for DNA damage induction, met the acceptability criteria.^[112] With specific respect to more complex 3D and coculture models, it is not always possible to discriminate among multiple cell types using the comet assay, as all cells are lysed prior to analysis. Thus, further development of the in vitro comet approach is required to ensure it is both nano-specific and can be robustly applied to the evaluation of 3D models.

Another novel method to detect genotoxicity or DNA damage induced by ENMs utilizes a BAC–GFP transformed HepG2 cell line, cultured in a 3D format.^[75,90,116,117] Here, key genes in the P53-mediated DNA damage response signaling pathway, such as P53, P21, MDM2, and BTG2, are tagged with GFP using a BAC recombineering technique allowing the detection of the activation of DNA damage signaling upon exposure at single cell level when combined with confocal microscopy.^[117,118] In response to double stranded breaks in the DNA induced by a genotoxic agent (e.g., chemicals and ENMs), the DNA damage response will be activated through the recruitment of ataxia telangiectasia mutated and ataxia telangiectasia, and Rad3-related protein at the DNA damage loci. Activation of checkpoint kinases 1 and 2 (CHK1 and CHK2) ensues and subsequent post-translational modification and activation of transcription factor tumor protein 53 (P53) occurs. This, in turn, leads to activation of its downstream target genes, such as P21, MDM2, and BTG2, aiming for cell cycle arrest, DNA repair, or apoptosis.^[119] Therefore, these reporter genes reflect and highlight the DNA damage response pathway mediated by P53 well at different levels within the signaling cascade. Gene activation/deactivation is time sensitive, in that genes at the beginning of the pathway cascade will be activated and initiated much earlier

than those further downstream. Subsequently, it is important to consider the optimum window of opportunity for gene activity to be assessed, as those genes targeted can often reflect the exposure time required to be undertaken.

When combining these HepG2 DNA damage BAC–GFP reporters with live cell confocal microscopy, the activation dynamics of the critical DNA damage signaling genes can be monitored frequently over extended periods of time at single cell level.^[90] Studies have shown that culturing these HepG2 reporter cells in Matrigel for 21 days resulted in the formation of stable spheroids with an improved hepatic phenotype. This includes increased albumin secretion, cytochrome P450 activity, phase II conjugation enzyme and transporter expression, and activation of hepatic differentiation transcription factors, such as HNF4alpha, C/EBP, and STAT1.^[75,90] Furthermore, these spheroids stop proliferating after 7 to 14 days of culture and remain stable for multiple weeks allowing the testing of long-term repeated exposures.^[75,90] By utilizing these DNA damage HepG2 GFP reporters in both 2D and 3D systems, Hiemstra et al. showed a dose and time-dependent activation of the DNA damage response upon exposure to genotoxic compounds emphasizing its suitability to identify genotoxicants.^[90,120] Furthermore, the 3D HepG2 reporter system showed a high resemblance to chemical-induced stress responses seen in PHH transcriptomics. This DNA damage HepG2 reporter system in 3D can also be applied for ENM-induced genotoxicity over long-term exposure regimes. As demonstrated in **Figure 5**, this system allows for the detection of DNA damage following 3-day exposure to both chemicals and ENMs using 3D spheroid HepG2 BAC–GFP reporters. Here, activation of P21-GFP was seen after exposure to aflatoxin B1,

a known liver carcinogen, as well as after repeated ZnO ENM exposure over 3 days. However, since these spheroids were formed using a scaffold, as previously reported, it is likely the penetration of ENMs into the spheroid, and uptake by the cells may be hindered due to the restricted motility of ENM to translocate through the Matrigel scaffold. To validate this, intracellular measurements of ENM uptake within the spheroids should be undertaken. Alternatively, these HepG2 GFP reporters could be used in a scaffold-free 3D setting to overcome hindrance of ENM-penetration by the ECM to allow for improved uptake of ENMs within the spheroids.

In conclusion, there are number of suitable in vitro genotoxicity assays available, but they do require optimization and further development to facilitate their application to 3D liver models, in order to provide a comprehensive evaluation of the genotoxicity induced post-acute and long-term ENM exposure.

8. Discussion and Future Directions

It is important to consider the suitability of the 3D in vitro hepatic models currently available for genotoxicity evaluation, given that DNA damage is an important key event in hepatocellular carcinoma etiology. Although the four AOPs related to human liver cancer development that have been submitted to the OECD AOP-wiki are still under review, they highlight the following key biochemical endpoints: disruption to the hepatic homeostatic balance in favor of cell growth, reduced apoptotic activity, increased cell proliferation, hyperplasia in several liver cell types, and clonal expansion of preneoplastic foci cells.^[35]

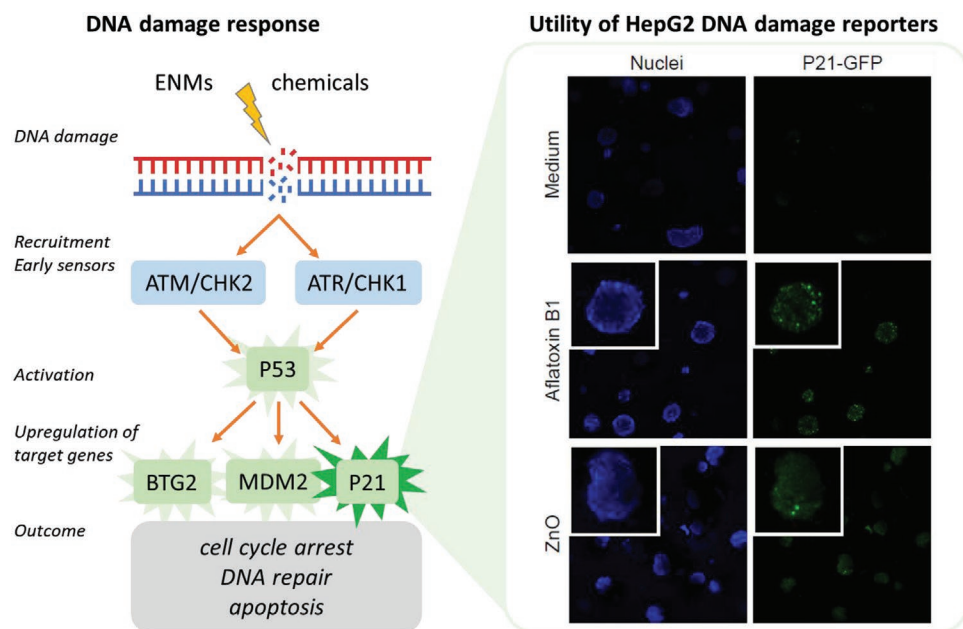


Figure 5. Mapping of the DNA damage response activation by the utility of HepG2 DNA damage reporters P21 induction upon DNA damage signaling in HepG2 cells. In the left panel, a schematic representation of the p53-mediated DNA damage response is shown. Genes in green can be monitored by the usage of specific HepG2 DNA damage reporters (P53, BTG2, MDM2, and P21). In the right panel as an example, the activation of P21-GFP HepG2 reporter upon exposure is shown. HepG2 P21-GFP spheroids grown in Matrigel were repeatedly exposed for 3 days to 5 μM aflatoxin B1 or 100 $\mu\text{g mL}^{-1}$ ZnO and imaged using a confocal microscope with a 20 \times objective. Cells were stained with Hoechst for nuclei visualization and propidium iodide for viability.

These parameters represent important targets that a hepatic 3D model should be able to report upon in order to provide a reliable prediction of carcinogenicity. When selecting key events to target, consideration should be given to the natural timeline of liver adverse outcomes. For example, liver cirrhosis arises as a result of prolonged exposure to hepatotoxicants causing repeated scarring of the hepatic tissue, known as liver fibrosis. Consequently, in order to supersede *in vivo* toxicity testing, 3D *in vitro* liver models must remain viable, while maintaining phenotypic functionality and stable biotransformation competence over an extended period of time. This principle has received a lot of attention in the recent scientific literature, with a number of 3D models adapted to support prolonged culture over 14 days and up to a month in some cases.^[74,83,120] Not only does this development allow for more environmentally relevant long-term, repeated ENM exposures to be assessed, it also provides potential for the evolution of hepatic AOPs to be studied in a more comprehensive manner.

It is necessary to acknowledge that liver cancer progression usually evolves from DNA damage in conjunction with the loss of effective DNA damage repair mechanisms, coupled to induction of oncogenes or loss of tumor suppressor genes, such as P53.^[62] A number of studies using 3D liver models have found that exposure to ENMs can induce genotoxicity in the form of DNA strand breaks and gross chromosomal damage,^[74,80,98] but the majority of these studies do not take into account DNA repair capabilities or the high regeneration capacity of hepatocytes. As a result, regulatory-approved genotoxicity assays, like the CBMN assay or mutation-based assays that accommodate for DNA repair, should be the primary focus when adapting existing 3D liver models to support these endpoints. One major limitation of current 3D models, is the inability to support assays that typically detect point mutations (i.e., the mouse lymphoma assay [OECD 490] and the HPRT assay [OECD 476]). As DNA damage can be induced in multiple forms and no single assay can detect all forms of damage simultaneously, it is important to consider 3D models that are able to support an array of genotoxicity endpoints spanning point mutations, clastogenicity and aneugenicity, or other key events (e.g., cell proliferation, oxidative stress, apoptosis, and inflammation) identified in the AOP frameworks. While several of the key events have been identified to date, the molecular initiating events, particularly associated with ENM exposure, are less understood.^[121] Thus, future studies should aim to identify nano-specific molecular initiating events that should form primary targets for development of novel *in vitro* testing strategies for hepatic disease etiology. In this manner, AOP networks could form part of a decision tree and be utilized as a foundation for establishing the most suitable *in vitro* test systems and biochemical assay endpoints for ENM hazard assessment.^[122]

Another vital aspect of nano(geno)toxicology and the principle mechanism for genotoxicity *in vivo* is secondary genotoxicity, yet it remains largely overlooked within current 3D *in vitro* liver models.^[27–29] To fully emulate the mechanisms underlying ENM associated genotoxicity, further advancement to the current 3D hepatic models needs to incorporate additional immune cell lines (e.g., macrophages and neutrophils). For example, human hepatocyte and Kupffer cell coculture models are well established in a 2D format, but immune cells are not often

incorporated within a 3D approach, especially models with the capability to support genotoxicity assays. Although PHH coculture models are available to provide a more physiologically relevant alternative to *in vivo* toxicology models, consisting not only of human Kupffer cell macrophages but the entire non-parenchymal fraction including LSECs and stellate cells, these models are expensive and exhibit donor–donor variability in comparison to more rudimentary coculture models.^[123] Furthermore, having the addition of multiple cell types means that each cell would have to be individually identified and scored independently for genotoxic events. This process could make an already labor-intensive task even more time-consuming. Based on this, future work should be focused toward developing stable, proliferative 3D coculture liver models. Resident liver macrophages have pre-eminent importance as they play a major role in the mediation of secondary genotoxicity due to their ability to phagocytose ENM and subsequently induce a sustained inflammatory response and oxidative stress.^[27,106] Therefore, models which include multiple cell types, specifically Kupffer cells, in a 3D environment would be beneficial to characterize the hazards and adverse outcomes associated with ENM exposure in a more comprehensive manner.

In conclusion, adverse outcome pathways provide a useful tool for predicting specific mechanisms behind hepatotoxicity and should be taken into consideration throughout the development and refinement of *in vitro* test systems and relevant bioassays. This is necessary to maintain their physiological relevance and support these key events as more data are released. A major challenge has been the development of complex *in vitro* liver models which combine tissue-like functionality, xenobiotic metabolism competency, and retention of hepatic phenotypic characteristics over prolonged culture periods, whilst being compatible with multiparametric hazard endpoint analysis. Consequently, it may be beneficial to coalesce advantageous aspects of the existing 3D *in vitro* model technologies. For example, select the most phenotypically functional hepatic cell line and adapt the current culture system to mimic the setup of another model that has proven to enhance the physiological relevance, longevity, and compatibility for genotoxicity assessment. Conversely, individual models could be developed independently to address particular target endpoints, that is, PHH models for metabolism-based assessments and toxicity screening, whilst HepG2 spheroid models would be utilized for genotoxicity endpoints. Whilst multiple models are likely to be necessary to ensure predictive *in vitro* test systems, it is important to minimize the number of models required to support all relevant hazard characterization endpoints as *in vitro* approaches need to remain cost-effective and easy to implement in an industrial safety assessment setting. Although substantial advancements have been made, a need for high-throughput, robust, and physiologically relevant hepatic models capable of supporting comprehensive genotoxicity assessment following ENM exposure remains to be fully established.

Acknowledgements

The authors would like to acknowledge that this research had received funding from the European Union's Horizon 2020 research and

innovation program for the PATROLS project, under grant agreement No. 760813 as well as from grant agreement No. 681002 (EU-ToxRisk).

Conflict of Interest

The authors declare no conflict of interest.

Keywords

adverse outcome pathways, DNA damage, in vitro liver models, long-term exposure, nano(genotoxicology), nanomaterials

Received: September 28, 2020

Revised: December 10, 2020

Published online:

- [1] X. Yan, A. Sedykh, W. Wang, B. Yan, H. Zhu, *Nat. Commun.* **2020**, *11*, 2519.
- [2] E. Commission, *Definition – Nanomaterials – Environment – European Commission*, **2011**.
- [3] A. Hardy, D. Benford, H. Thorhallur, M. J. Jeger, H. K. Knutsen, S. More, H. Naegeli, H. Noteborn, C. Ockleford, A. Ricci, G. Rychen, J. R. Schlatter, V. Silano, R. Solecki, D. Turck, M. Younes, Q. Chaudhry, F. Cubadda, D. Gott, A. Oomen, S. Weigel, M. Karamitrou, R. Schoonjans, A. Mortensen, *EFSA J.* **2018**, *16*, 5327.
- [4] T. Tervonen, I. Linkov, J. R. Figueira, J. Steevens, M. Chappell, M. Merad, *J. Nanopart. Res.* **2009**, *11*, 757.
- [5] G. Oberdörster, V. Stone, K. Donaldson, *Nanotoxicology* **2007**, *1*, 2.
- [6] V. Stone, M. R. Miller, M. J. D. Clift, A. Elder, N. L. Mills, P. Møller, R. P. F. Schins, U. Vogel, W. G. Kreyling, K. Alstrup Jensen, T. A. J. Kuhlbusch, P. E. Schwarze, P. Hoet, A. Pietroiusti, A. De Vizcaya-Ruiz, A. Baeza-Squiban, J. P. Teixeira, C. L. Tran, F. R. Cassee, *Environ. Health Perspect.* **2017**, *125*, 106002.
- [7] S. Singh, *Toxicol. Mech. Methods* **2019**, *29*, 300.
- [8] M. Shakeel, F. Jabeen, S. Shabbir, M. S. Asghar, M. S. Khan, A. S. Chaudhry, *Biol. Trace Elem. Res.* **2016**, *172*, 1.
- [9] C. H. Li, S. Chuan-Chou, C. Yu-Wen, H. Shih-Hsuan, W. Chung-Che, K. Chen-Chieh, L. Jiunn-Wang, K. Jaw-Jou, *Nanotoxicology* **2012**, *6*, 746.
- [10] L. Geraets, A. G. Oomen, P. Krystek, N. R. Jacobsen, H. Wallin, M. Laurentie, H. W. Verharen, E. F. A. Brandon, W. H. d. Jong, *Part. Fibre Toxicol.* **2014**, *11*, 30.
- [11] C. Lopez-Chaves, J. Soto-Alvaredo, M. Montes-Bayon, J. Bettmer, J. Llopis, C. Sanchez-Gonzalez, *Nanomedicine* **2018**, *14*, 1.
- [12] K. Park, J. Park, H. Lee, J. Choi, W. J. Yu, J. Lee, *Arch. Pharm. Res.* **2018**, *41*, 1108.
- [13] S. K. Balasubramanian, J. Jittiwat, J. Manikandan, C. N. Ong, L. E. Yu, W. Y. Ong, *Biomaterials* **2010**, *31*, 2034.
- [14] B. K. Gaiser, S. Hirn, A. Kermanizadeh, N. Kanase, K. Fytianos, A. Wenk, N. Haberl, A. Brunelli, W. G. Kreyling, V. Stone, *Toxicol. Sci.* **2013**, *131*, 537.
- [15] S. Hirn, M. Semmler-Behnke, C. Schleh, A. Wenk, J. Lipka, M. Schäffler, S. Takenaka, W. Möller, G. Schmid, U. Simon, W. G. Kreyling, *Eur. J. Pharm. Biopharm.* **2011**, *77*, 407.
- [16] A. Kermanizadeh, B. K. Gaiser, H. Johnston, D. M. Brown, V. Stone, *Br. J. Pharmacol.* **2014**, *171*, 3980.
- [17] W.-K. Oh, K. Sojin, M. Choi, C. Kim, Y. S. Jeong, B. Cho, J. Hahn, J. Jang, *ACS Nano* **2010**, *4*, 5301.
- [18] C. Schleh, M. Semmler-Behnke, J. Lipka, A. Wenk, S. Hirn, M. Schäffler, G. Schmid, U. Simon, W. G. Kreyling, *Nanotoxicology* **2012**, *6*, 36.
- [19] V. M. Lauschke, D. F. G. Hendriks, C. C. Bell, T. B. Andersson, M. Ingelman-Sundberg, *Chem. Res. Toxicol.* **2016**, *29*, 1936.
- [20] W. G. Kreyling, U. Holzwarth, N. Haber, J. Kozempel, S. Hirn, A. Wenk, C. Schleh, M. Schäffler, J. Lipka, M. Semmler-Behnke, N. Gibson, *Nanotoxicology* **2017**, *11*, 434.
- [21] A. Buckley, J. Warren, A. Hodgson, T. Marczylo, K. Ignatyev, C. Guo, R. Smith, *Part. Fibre Toxicol.* **2017**, *14*, 5.
- [22] A. Kermanizadeh, D. Balharry, H. Wallin, S. Loft, P. Møller, *Crit. Rev. Toxicol.* **2015**, *45*, 837.
- [23] J. Modrzynska, *Toxicological Effects of Nanoparticle Deposition in the Liver*, Technical University of Denmark, Kongens Lyngby **2018**.
- [24] M. R. Miller, J. B. Raftis, J. P. Langrish, S. G. McLean, P. Samutritai, S. P. Connell, S. Wilson, A. T. Vesey, P. H. B. Fokkens, A. J. F. Boerel, P. Krystek, C. J. Campbell, P. W. F. Hadoke, K. Donaldson, F. R. Cassee, D. E. Newby, R. Duffin, N. L. Mills, *ACS Nano* **2017**, *11*, 4542.
- [25] Regulation (EC) No 1907/2006 – Registration, Evaluation, Authorisation and Restriction of Chemicals (REACH) – Safety and Health at Work, [https://osha.europa.eu/en/legislation/directives/regulation-ec-no-1907-2006-of-the-european-parliament-and-of-the-council#:~:text=2019-,Regulation%20\(CE\)%20No%201907%2F2006%20%2D%20R%20Registration%2C%20Evaluation,and%20Restriction%20of%20Chemicals%20\(REACH\)&text=The%20purpose%20of%20this%20regulation,Community%20workplace%20and%20environmental%20legislation](https://osha.europa.eu/en/legislation/directives/regulation-ec-no-1907-2006-of-the-european-parliament-and-of-the-council#:~:text=2019-,Regulation%20(CE)%20No%201907%2F2006%20%2D%20R%20Registration%2C%20Evaluation,and%20Restriction%20of%20Chemicals%20(REACH)&text=The%20purpose%20of%20this%20regulation,Community%20workplace%20and%20environmental%20legislation) (accessed: August 21, 2020).
- [26] H. Bahadar, F. Maqbool, K. Niaz, M. Abdollahi, *Iran. Biomed. J.* **2016**, *20*, 1.
- [27] H. Barabadi, M. Najafi, H. Samadian, A. Azarnezhad, H. Vahidi, M. A. Mahjoub, M. Koohiyan, A. Ahmadi, *Medicina* **2019**, *55*, 439.
- [28] S. J. Evans, M. J. D. Clift, N. Singh, J. Mallia, M. Burgum, J. W. Wills, T. S. Wilkinson, G. J. S. Jenkins, S. H. Doak, *Mutagenesis* **2017**, *32*, 233.
- [29] V. M. Lauschke, R. Z. Shafagh, D. F. G. Hendriks, M. Ingelman-Sundberg, *Biotechnol. J.* **2019**, *14*, 1800347.
- [30] C. Ding, Y. Li, F. Guo, Y. Jiang, W. Ying, D. Li, D. Yang, X. Xia, W. Liu, Y. Zhao, Y. He, X. Li, W. Sun, Q. Liu, L. Song, B. Zhen, P. Zhang, X. Qian, J. Qin, F. He, *Mol. Cell. Proteomics* **2016**, *15*, 3190.
- [31] E. Trefts, M. Gannon, D. H. Wasserman, *Curr. Biol.* **2017**, *27*, R1147.
- [32] L. A. van Grunsven, *Adv. Drug Delivery Rev.* **2017**, *121*, 133.
- [33] M. Leist, A. Ghallab, R. Graepel, R. Marchan, R. Hassan, S. H. Bennekou, A. Limonciel, M. Vinken, S. Schildknecht, T. Waldmann, E. Danen, B. van Ravenzwaay, H. Kamp, I. Gardner, P. Godoy, F. Y. Bois, A. Braeuning, R. Reif, F. Oesch, D. Drasdo, S. Höhme, M. Schwarz, T. Hartung, T. Braunbeck, J. Beltman, H. Vrieling, F. Sanz, A. Forsby, D. Gadaleta, C. Fisher, J. Kelm, D. Fluri, G. Ecker, B. Zdrzil, A. Terron, P. Jennings, B. van der Burg, S. Dooley, A. H. Meijer, E. Willighagen, C. E. M. Martens, E. Mombelli, O. Taboureau, A. Mantovani, B. Hardy, B. Koch, S. Escher, C. van Thriel, C. Cadenas, D. Kroese, B. van de Water, J. G. Hengstler, *Arch. Toxicol.* **2017**, *91*, 3477.
- [34] G. T. Ankley, S. W. Edwards, *Curr. Opin. Toxicol.* **2018**, *9*, 1.
- [35] E. Gijbels, M. Vinken, *Appl. In Vitro Toxicol.* **2017**, *3*, 283.
- [36] K. Iwaisako, D. A. Brenner, T. Kisseleva, *J. Gastroenterol. Hepatol.* **2012**, *27*, 65.
- [37] M. Brovold, D. Keller, S. Soker, *Biotechnol. Bioeng.* **2020**, *117*, 2516.
- [38] S. Han, L. Han, Y. Yao, H. Sun, X. Zan, Q. Liu, *Oncol. Rep.* **2014**, *31*, 641.
- [39] W.-H. Huang, M.-W. Zhou, Y.-F. Zhu, J.-B. Xiang, Z.-Y. Li, Z.-H. Wang, Y.-M. Zhou, Y. Yang, Z.-Y. Chen, X.-D. Gu, *OncoTargets Ther.* **2019**, *12*, 7573.
- [40] J. M. Crawford, P. Bioulac-Sage, P. Hytioglou, in *MacSween's Pathology of the Liver*, 7th ed. (Eds: A. D. Burt, L. D. Ferrell, S. G. Hübscher), Elsevier, Amsterdam **2018**, pp. 1–87.

- [41] J. Petrasek, T. Csak, G. Szabo, *Adv. Clin. Chem.* **2013**, 59, 155.
- [42] L. J. Dixon, M. Barnes, H. Tang, M. T. Pritchard, L. E. Nagy, in *Comprehensive Physiology*, (Ed: R. Terjung), American Physiological Society, Rockville, MD **2013**, pp. 785–797.
- [43] G. Kolios, V. Valatas, E. Kouroumalis, *World J. Gastroenterol.* **2006**, 12, 7413.
- [44] P. Godoy, N. J. Hewitt, U. Albrecht, M. E. Andersen, N. Ansari, S. Bhattacharya, J. G. Bode, J. Bolleyn, C. Borner, J. Böttger, A. Braeuning, R. A. Budinsky, B. Burkhardt, N. R. Cameron, G. Camussi, C.-S. Cho, Y.-J. Choi, J. C. Rowlands, U. Dahmen, G. Damm, O. Dirsch, M. T. Donato, J. Dong, S. Dooley, D. Drasdo, R. Eakins, K. S. Ferreira, V. Fonsato, J. Fraczek, R. Gebhardt, A. Gibson, M. Glanemann, C. E. P. Goldring, M. J. Gómez-Lechón, G. M. M. Groothuis, L. Gustavsson, C. Guyot, D. Hallifax, S. Hammad, A. Hayward, D. Häussinger, C. Hellerbrand, P. Hewitt, S. Hoehme, H.-G. Holzhütter, J. B. Houston, J. Hrach, K. Ito, H. Jaeschke, V. Keitel, J. M. Kelm, B. K. Park, C. Kordes, G. A. Kullak-Ublick, E. L. LeCluyse, P. Lu, J. Luebke-Wheeler, A. Lutz, D. J. Maltman, M. Matz-Soja, P. McMullen, I. Merfort, S. Messner, C. Meyer, J. Mwinyi, D. J. Naisbitt, A. K. Nussler, P. Olinga, F. Pampaloni, J. Pi, L. Pluta, S. A. Przyborski, A. Ramachandran, V. Rogiers, C. Rowe, C. Schelcher, K. Schmich, M. Schwarz, B. Singh, E. H. K. Stelzer, B. Stieger, R. Stöber, Y. Sugiyama, C. Tetta, W. E. Thasler, T. Vanhaecke, M. Vinken, T. S. Weiss, A. Widera, C. G. Woods, J. J. Xu, K. M. Yarborough, J. G. Hengstler, *Arch. Toxicol.* **2013**, 87, 1315.
- [45] R. A. Roberts, P. E. Ganey, C. Ju, L. M. Kamendulis, I. Rusyn, J. E. Klaunig, *Toxicol. Sci.* **2007**, 96, 2.
- [46] Y. Li, Y. Zhang, C. Zhang, H. Wang, X. Wei, P. Chen, L. Lu, *Proc. Natl. Acad. Sci. USA* **2020**, 117, 1711.
- [47] A. T. Nguyen-Lefebvre, A. Horuzsko, *Enzymol. Metab. J.* **2015**, 1, 101.
- [48] A. Manke, L. Wang, Y. Rojanasakul, *Biomed Res. Int.* **2013**, 2013, 942916.
- [49] P. Khanna, C. Ong, B. Bay, G. Baeg, *Nanomaterials* **2015**, 5, 1163.
- [50] P. Møller, N. R. Jacobsen, J. K. Folkmann, P. H. Danielsen, L. Mikkelsen, J. G. Hemmingsen, L. K. Vesterdal, L. Forchhammer, H. Wallin, S. Loft, *Free Radic. Res.* **2010**, 44, 1.
- [51] C. Buzea, I. I. Pacheco Blandino, K. Robbie, *Biointerphases* **2007**, 2, MR17.
- [52] M. J. D. Clift, B. Rothen-Rutishauser, in *Oxidative Stress and Nanotechnology*, (Eds: D. Armstrong, D. J. Bharali) Humana Press, Totowa, NJ **2013**, pp. 115–133.
- [53] J. W. Han, S. Gurunathan, J.-K. Jeong, Y.-J. Choi, D.-N. Kwon, J.-K. Park, J.-H. Kim, *Nanoscale Res. Lett.* **2014**, 9, 459.
- [54] N. Singh, G. J. S. Jenkins, B. C. Nelson, B. J. Marquis, T. G. G. Maffeis, A. P. Brown, P. M. Williams, C. J. Wright, S. H. Doak, *Biomaterials* **2012**, 33, 163.
- [55] T. V. Nguyen, O. Ukairo, S. R. Khetani, M. McVay, C. Kanchagar, W. Seghezzi, G. Ayanoglu, O. Irrechukwu, R. Evers, *Drug Metab. Dispos.* **2015**, 43, 774.
- [56] R. Kostadinova, F. Boessa, D. Applegate, L. Sutura, T. Weiser, T. Singer, B. Naughton, A. Roth, *Toxicol. Appl. Pharmacol.* **2013**, 268, 1.
- [57] J. M. O'Rourke, V. M. Sagar, T. Shah, S. Shetty, *World J. Gastroenterol.* **2018**, 24, 4436.
- [58] G. Ramakrishna, A. Rastogi, N. Trehanpati, B. Sen, R. Khosla, S. K. Sarin, *Liver Cancer* **2013**, 2, 367.
- [59] P. Rawla, T. Sunkara, P. Muralidharan, J. P. Raj, *Wspolczesna Onkol.* **2018**, 22, 141.
- [60] A. Nakagawara, T. Ozaki, *J. Biomed. Biotechnol.* **2011**, 2011, 603925.
- [61] B. R. Rushing, M. I. Selim, *Food Chem. Toxicol.* **2019**, 124, 81.
- [62] J. C. Nault, J. Zucman-Rossi, *Semin. Liver Dis.* **2011**, 31, 173.
- [63] N. Singh, B. Manshian, G. J. S. Jenkins, S. M. Griffiths, P. M. Williams, T. G. G. Maffeis, C. J. Wright, S. H. Doak, *Biomaterials* **2009**, 30, 3891.
- [64] J. W. Wills, H. D. Summers, N. Hondow, A. Sooresh, K. E. Meissner, P. A. White, P. Rees, A. Brown, S. H. Doak, *ACS Nano* **2017**, 11, 11986.
- [65] L. Guo, S. Dial, L. Shi, W. Branham, J. Liu, J.-L. Fang, B. Green, H. Deng, J. Kaput, B. Ning, *Drug Metab. Dispos.* **2011**, 39, 528.
- [66] S. M. Huang, J. M. Strong, L. Zhang, K. S. Reynolds, S. Nallani, R. Temple, S. Abraham, S. A. Habet, R. K. Baweja, G. J. Burckart, S. Chung, P. Colangelo, D. Frucht, M. D. Green, P. Hepp, E. Karnaukhova, H.-S. Ko, J.-I. Lee, P. J. Marroum, J. M. Norden, W. Qiu, A. Rahman, S. Sobel, T. Stifano, K. Thummel, X.-X. Wei, S. Yasuda, J. H. Zheng, H. Zhao, L. J. Lesko, *J. Clin. Pharmacol.* **2008**, 48, 662.
- [67] C. C. Bell, A. C. A. Dankers, V. M. Lauschke, R. Sison-Young, R. Jenkins, C. Rowe, C. E. Goldring, K. Park, S. L. Regan, T. Walker, C. Schofield, A. Baze, A. J. Foster, D. P. Williams, A. W. M. van de Ven, F. Jacobs, J. van Houdt, T. Lähteenmäki, J. Snoeys, S. Juhila, L. Richert, M. Ingelman-Sundberg, *Toxicol. Sci.* **2018**, 162, 655.
- [68] Y. Higuchi, K. Kawai, T. Kanaki, H. Yamazaki, C. Chesné, C. Guguen-Guillouzo, H. Suemizu, *Hepatol. Res.* **2016**, 46, 1045.
- [69] S. Ramaiahgari, S. Waidyanatha, D. Dixon, M. DeVito, R. Paules, S. Ferguson, *Toxicol. Sci.* **2017**, 160, 189.
- [70] U.-K. Shah, J. de O. Mallia, N. Singh, K. E. Chapman, S. H. Doak, G. J. S. Jenkins, *Mutat. Res., Genet. Toxicol. Environ. Mutagen.* **2018**, 825, 51.
- [71] J. Dumont, R. Jossé, C. Lambert, S. Anthérieu, L. Le Hegarat, C. Aninat, M.-A. Robin, C. Guguen-Guillouzo, A. Guillouzo, *Toxicol. Appl. Pharmacol.* **2010**, 245, 256.
- [72] L. Le Hégarat, A. Mourot, S. Huet, L. Vasseur, S. Camus, C. Chesné, V. Fessard, *Toxicol. Sci.* **2014**, 138, 300.
- [73] M. Mandon, S. Huet, E. Dubreil, V. Fessard, L. Le Hégarat, *Sci. Rep.* **2019**, 9, 10548.
- [74] A. Keramanizadeh, T. Berthing, E. Guzniczak, M. Wheeldon, G. Whyte, U. Vogel, W. Moritz, V. Stone, *Part. Fibre Toxicol.* **2019**, 16, 42.
- [75] S. C. Ramaiahgari, M. W. den Braver, B. Herpers, V. Terpstra, J. N. M. Commandeur, B. van de Water, L. S. Price, *Arch. Toxicol.* **2014**, 88, 1083.
- [76] E. Elje, M. Hesler, E. Rundén-Pran, P. Mann, E. Mariussen, S. Wagner, M. Dusinska, Y. Kohl, *Mutat. Res., Genet. Toxicol. Environ. Mutagen.* **2019**, 845, 403033.
- [77] R. L. Sison-Young, V. M. Lauschke, E. Johann, E. Alexandre, S. Antherieu, H. Aerts, H. H. J. Gerets, G. Labbe, D. Hoët, M. Dorau, C. A. Schofield, C. A. Lovatt, J. C. Holder, S. H. Stahl, L. Richert, N. R. Kitteringham, R. P. Jones, M. Elmasry, R. J. Weaver, P. G. Hewitt, M. Ingelman-Sundberg, C. E. Goldring, B. Kevin Park, *Arch. Toxicol.* **2017**, 91, 1385.
- [78] P. Guinness, D. Mueller, V. Shevchenko, E. Heinzle, M. Ingelman-Sundberg, F. Noor, *Toxicol. Sci.* **2013**, 133, 67.
- [79] S. B. Leite, I. Wilk-Zasadna, J. M. Zaldivar, E. Airola, M. A. Reis-Fernandes, M. Mennecozzi, C. Guguen-Guillouzo, C. Chesne, C. Guillou, P. M. Alves, S. Coecke, *Toxicol. Sci.* **2012**, 130, 106.
- [80] S. V. Llewellyn, G. E. Conway, U.-K. Shah, S. J. Evans, G. J. S. Jenkins, M. J. D. Clift, S. H. Doak, *J. Visualized Exp.* **2020**, 160, e61141.
- [81] K. Zeilinger, N. Freyer, G. Damm, D. Seehofer, F. Knöspel, *Exp. Biol. Med.* **2016**, 241, 1684.
- [82] P. Gripon, S. Rumin, S. Urban, J. Le Seyec, D. Glaise, I. Cannie, C. Guyomard, J. Lucas, C. Trepo, C. Guguen-Guillouzo, *Proc. Natl. Acad. Sci. USA* **2002**, 99, 15655.
- [83] G. E. Conway, U.-K. Shah, S. Llewellyn, T. Cervena, S. J. Evans, A. S. A. Ali, G. J. Jenkins, M. J. D. Clift, S. H. Doak, *Mutagenesis* **2020**, 35, 319.
- [84] OECD, *Test No. 487: In Vitro Mammalian Cell Micronucleus Test*, OECD Publishing, Paris **2016**.

- [85] F. A. Atienzar, E. I. Novik, H. H. Gerets, A. Parekh, C. Delatour, A. Cardenas, J. MacDonald, M. L. Yarmush, S. Dhalluin, *Toxicol. Appl. Pharmacol.* **2014**, 275, 44.
- [86] S. N. Hart, Y. Li, K. Nakamoto, E. A. Subileau, D. Steen, X. B. Zhong, *Drug Metab. Dispos.* **2010**, 38, 988.
- [87] A. Kyffin, P. Sharma, J. Leedale, H. E. Colley, C. Murdoch, P. Mistry, S. D. Webb, *Toxicol. In Vitro* **2018**, 48, 262.
- [88] M. Dubiak-Szepietowska, A. Karczmarczyk, M. Jönsson-Niedziółka, T. Winckler, K. H. Feller, *Toxicol. Appl. Pharmacol.* **2016**, 294, 78.
- [89] A. Higuchi, P. Vadgama, R. Narayan, *Biomaterial Control of Therapeutic Stem Cells by Akon Higuchi*, The Royal Society of Chemistry **2019**, pp. 12–85, Ch. 2, <https://doi.org/10.1039/9781788012690>.
- [90] S. Hiemstra, S. C. Ramaiahgari, S. Wink, G. Callegaro, M. Coonen, J. Meerman, D. Jennen, K. van den Nieuwendijk, A. Dankers, J. Snoeys, H. de Bont, L. Price, B. van de Water, *Arch. Toxicol.* **2019**, 93, 2895.
- [91] J. Theobald, A. Ghanem, P. Wallisch, A. A. Banaeiyan, M. A. Andrade-Navarro, K. Taškova, M. Haltmeier, A. Kurtz, H. Becker, S. Reuter, R. Mrowka, X. Cheng, S. Wölfel, *ACS Biomater. Sci. Eng.* **2018**, 4, 78.
- [92] Y.-S. Weng, S.-F. Chang, M.-C. Shih, S.-H. Tseng, C.-H. Lai, *Adv. Mater.* **2017**, 29, 1701545.
- [93] A. Keramanizadeh, M. Lohr, M. Roursgaard, S. Messner, P. Gunness, J. M. Kelm, P. Möller, V. Stone, S. Loft, *Part. Fibre Toxicol.* **2014**, 11, 56.
- [94] E. Curcio, S. Salerno, G. Barbieri, L. De Bartolo, E. Drioli, A. Bader, *Biomaterials* **2007**, 28, 5487.
- [95] R. Glicklis, J. C. Merchuk, S. Cohen, *Biotechnol. Bioeng.* **2004**, 86, 672.
- [96] J. M. Cohen, G. M. Deloid, P. Demokritou, *Nanomedicine* **2015**, 10, 3015.
- [97] D. G. Thomas, J. N. Smith, B. D. Thrall, D. R. Baer, H. Jolley, P. Munusamy, V. Demokritou, J. Cohen, J. G. Teeguarden, *Part. Fibre Toxicol.* **2018**, 15, 6.
- [98] E. Elje, E. Mariussen, O. H. Moriones, N. G. Bastús, V. Puentes, Y. Kohl, M. Dusinska, E. Rundén-Pran, *Nanomaterials* **2020**, 10, 545.
- [99] R. Agarwal, P. Journey, M. Raythatha, V. Singh, S. V. Sreenivasan, L. Shi, K. Roy, *Adv. Healthcare Mater.* **2015**, 4, 2269.
- [100] J. Fleddermann, J. Susewind, H. Peuschel, M. Koch, I. Tavernaro, A. Kraegeloh, *Int. J. Nanomed.* **2019**, 14, 1411.
- [101] K. Huang, H. Ma, J. Liu, S. Huo, A. Kumar, T. Wei, X. Zhang, S. Jin, Y. Gan, P. C. Wang, S. He, X. Zhang, X.-J. Liang, *ACS Nano* **2012**, 6, 4483.
- [102] J. Zhao, H. Lu, S. Wong, M. Lu, P. Xiao, M. H. Stenzel, *Polym. Chem.* **2017**, 8, 3317.
- [103] D. Allan Drummond, C. O. Wilke, *Nat. Rev. Genet.* **2009**, 10, 715.
- [104] T. Papp, D. Schiffmann, D. Weiss, V. Castranova, V. Vallyathan, Q. Rahman, *Nanotoxicology* **2008**, 2, 9.
- [105] A. Pietroiusti, H. Stockmann-Juvala, F. Lucaroni, K. Savolainen, *Wiley Interdiscip. Rev.: Nanomed. Nanobiotechnol.* **2018**, 10, e1513.
- [106] Z. Magdolenova, A. Collins, A. Kumar, A. Dhawan, V. Stone, M. Dusinska, *Nanotoxicology* **2014**, 8, 233.
- [107] S. H. Doak, B. Manshian, G. J. S. Jenkins, N. Singh, *Mutat. Res., Genet. Toxicol. Environ. Mutagen.* **2012**, 745, 104.
- [108] F. Finot, A. Kaddour, L. Morat, I. Mouche, N. Zaguia, C. Cuceu, D. Souverville, S. Négrault, O. Cariou, A. Essahli, N. Prigent, J. Saul, F. Paillard, L. Heidingsfelder, P. Lafouge, M. Al Jawhari, W. M. Hempel, M. El May, B. Colicchio, A. Dieterlen, E. Jeandidier, L. Sabatier, J. Clements, R. M'Kacher, *J. Appl. Toxicol.* **2017**, 37, 758.
- [109] E. M. Parry, J. M. Parry, C. Corso, A. Doherty, F. Haddad, T. F. Hermine, G. Johnson, M. Kayani, E. Quick, T. Warr, J. Williamson, *Mutagenesis* **2002**, 17, 509.
- [110] M. Fenech, *Mutat. Res., Fundam. Mol. Mech. Mutagen.* **2000**, 455, 81.
- [111] M. Fenech, *Nat. Protoc.* **2007**, 2, 1084.
- [112] R. Elespuru, S. Pfuhrer, M. J. Aardema, T. Chen, S. H. Doak, A. Doherty, C. S. Farabaugh, J. Kenny, M. Manjanatha, B. Mahadevan, M. M. Moore, G. Ouédraogo, L. F. Stankowski Jr., J. Y. Tanir, *Toxicol. Sci.* **2018**, 164, 391.
- [113] H. L. Karlsson, S. Di Bucchianico, A. R. Collins, M. Dusinska, *Environ. Mol. Mutagen.* **2015**, 56, 82.
- [114] S. Costa, J. P. Teixeira, *Encycl. Toxicol.* **2014**, 3, 1020.
- [115] D. Kirkland, *Expert Opin. Drug Metab. Toxicol.* **2011**, 7, 1513.
- [116] S. Wink, S. Hiemstra, B. Herpers, B. van de Water, *Arch. Toxicol.* **2017**, 91, 1367.
- [117] M. Niemeijer, S. Hiemstra, S. Wink, W. den Hollander, B. Braak, B. van de Water, in *Drug-Induced Liver Toxicity*, (Eds: M. Chen, Y. Will), Humana, New York **2018**, pp. 611–625.
- [118] I. Poser, M. Sarov, J. R. A. Hutchins, J.-K. Hériché, Y. Toyoda, A. Pozniakovskiy, D. Weigl, A. Nitzsche, B. Hegemann, A. W. Bird, L. Pelletier, R. Kittler, S. Hua, R. Naumann, M. Augsburg, M. M. Sykora, H. Hofemeister, Y. Zhang, K. Nasmyth, K. P. White, S. Dietzel, K. Mechtler, R. Durbin, A. F. Stewart, J.-M. Peters, F. Buchholz, A. A. Hyman, *Nature Methods* **2008**, 5, 409.
- [119] S. L. Harris, A. J. Levine, *Oncogene* **2005**, 24, 2899.
- [120] S. Hiemstra, M. Niemeijer, E. Koedoot, S. Wink, J. E. Klip, M. Vlasveld, E. de Zeeuw, B. van Os, A. White, B. van de Water, *Chem. Res. Toxicol.* **2017**, 30, 923.
- [121] K. Gerloff, B. Landesmann, A. Worth, S. Munn, T. Palosaari, M. Whelan, *Comput. Toxicol.* **2017**, 1, 3.
- [122] S. Halappanavar, S. van den Brule, P. Nymark, L. Gaté, C. Seidel, S. Valentino, V. Zhernovkov, P. H. Danielsen, A. de Vizcaya, H. Wolff, T. Stöger, A. Boyadziev, S. S. Poulsen, J. B. Sørli, U. Vogel, *Part. Fibre Toxicol.* **2020**, 17, 16.
- [123] A. Keramanizadeh, D. M. Brown, W. Moritz, V. Stone, *Sci. Rep.* **2019**, 9, 7295.



Samantha V. Llewellyn is an early career researcher, whose journey into the world of in vitro toxicology began with a research master's degree at Swansea University, assessing the effects of gold and silver engineered nanomaterial exposure upon human lung epithelial cells and telomere integrity. Currently, Samantha is a research assistant for the In Vitro Toxicology Group at Swansea University working on the Horizon 2020 PATROLS project developing advanced 3D liver models for ENM hazard assessment in vitro and chairs the Early Career Research Network at PATROLS.



Marije Niemeijer works as researcher at the division of Drug Discovery and Safety of Leiden Academic Centre for Drug Research (LACDR) at Leiden University on the development of 3D in vitro liver models for toxicity screening within the Horizon 2020 PATROLS project. Previously, she obtained her Biopharmaceutical Sciences master's degree, after which she studied the regulation of unfolded protein response upon chemical-induced stress in the liver during her Ph.D. at Leiden University within the IMI MIP DILI and Horizon 2020 EU-ToxRisk project.



Shareen H. Doak is professor of Genotoxicology and Cancer in Swansea University Medical School's In Vitro Toxicology Group. Shareen is a UK and EUROTOX registered toxicologist. Her research interests focus on genotoxic profiles of engineered nanomaterials, mechanisms underlying their DNA damaging potential and subsequent human health consequences. Her interests extend to development of advanced 3D culture models and mechanism-based bioassays for safety assessment, to reduce the need for animal testing. Shareen is the Mutagenesis' editor-in-chief.

4.2 Publication II

Advanced 3D Liver Models for In vitro Genotoxicity Testing Following Long-Term Nanomaterial Exposure

Samantha V. Llewellyn¹, Gillian E. Conway¹, Ume-Kulsoom Shah¹, Stephen J. Evans¹, Gareth J.S. Jenkins¹, Martin J.D. Clift¹, Shareen H. Doak¹

¹In Vitro Toxicology Group, Swansea University Medical School

Correspondence to: Shareen H. Doak at s.h.doak@swansea.ac.uk

URL: <https://www.jove.com/video/61141>

DOI: [doi:10.3791/61141](https://doi.org/10.3791/61141)

Keywords: In Vitro Liver Models, Nanomaterials, Hazard Assessment, Long-term Exposure, Nano(genotoxicology), DNA Damage

Date Published: 5/12/2020

Citation: Llewellyn, S.V., Conway, G.E., Shah, U.K., Evans, S.J., Jenkins, G.J., Clift, M.J., Doak, S.H. Advanced 3D Liver Models for In vitro Genotoxicity Testing Following Long-Term Nanomaterial Exposure. *J. Vis. Exp.* (), e61141, doi:10.3791/61141 (2020).

Abstract

Due to the rapid development and implementation of a diverse array of engineered nanomaterials (ENM), exposure to ENM is inevitable and the development of robust, predictive in vitro test systems is essential. Hepatic toxicology is key when considering ENM exposure, as the liver serves a vital role in metabolic homeostasis and detoxification as well as being a major site of ENM accumulation post exposure. Based upon this and the accepted understanding that 2D hepatocyte models do not accurately mimic the complexities of intricate multi-cellular interactions and metabolic activity observed in vivo, there is a greater focus on the development of physiologically relevant 3D liver models tailored for ENM hazard assessment purposes in vitro. In line with the principles of the 3Rs to replace, reduce and refine animal experimentation, a 3D HepG2 cell-line based liver model has been developed, which is a user friendly, cost effective system that can support both extended and repeated ENM exposure regimes (≤ 14 days). These spheroid models ($\geq 500 \mu\text{m}$ in diameter) retain their proliferative capacity (i.e., dividing cell models) allowing them to be coupled with the 'gold standard' micronucleus assay to effectively assess genotoxicity in vitro. Their ability to report on a range of toxicological endpoints (e.g., liver function, (pro-)inflammatory response, cytotoxicity and genotoxicity) has been characterized using several ENMs across both acute (24 h) and long-term (120 h) exposure regimes. This 3D in vitro hepatic model has the capacity to be utilized for evaluating more realistic ENM exposures, thereby providing a future in vitro approach to better support ENM hazard assessment in a routine and easily accessible manner.

Introduction

Due to the rapid development and implementation of a diverse array of engineered nanomaterials (ENM) across a plethora of human-based applications (e.g., food, cosmetics, clothing, sporting equipment, electronics, transport and medicine), it is inevitable that humans will be exposed to ENM on a regular basis. With this, there are heightened concerns that the novel, size specific physio-chemical characteristics that deem these materials advantageous in numerous applications could cause adverse effects upon human health and the environment concomitantly. Currently many international activities are in place to actively reflect more physiologically relevant exposures to these ENM and assess the potential toxicity of these materials over acute, long-term, and repeated low-dose exposure scenarios.

Hepatic toxicology is key when considering ENM exposure, as it is widely known that the liver is a major site of ENM accumulation post exposure^{1,2}. Moreover, the liver is the primary organ system for metabolism and detoxification of substances that enter systemic circulation³. Based upon the accepted understanding that 2D hepatocyte models do not accurately mimic the complexities of intricate multicellular interactions or appropriately represent metabolic activity observed in vivo, a greater focus into developing robust and physiologically relevant in vitro 3D liver models for in vivo substitute technologies has been established^{4,5}. Utilizing advanced 3D culture technologies improves the longevity of in vitro hepatic models allowing for long term, repeated exposure regimes to be investigated. Additionally, this advanced culture format promotes the formation of enhanced physiological, organotypic features such as bile canaliculi, active transporter processes and improved CYP450 drug metabolizing capabilities, thus improving the predictivity of the models⁶. Current 3D in vitro hepatic models consisting of mono-cultures (hepatocytes only) or co-cultures (hepatocytes with nonparenchymal cells) exist in several formats, ranging from microtissues or spheroids in ultralow adhesion plates, hanging drop spheroids, cells embedded in matrices and/or scaffolds and microfluidic cell culture platforms, all of which are deemed effective advanced in vitro models for hepatic toxicity assessment^{6,7}. However, the majority of these model systems are high maintenance, require specialized equipment and are expensive. Furthermore, these models are often static (i.e., nondividing cell models) that prevents their use in the assessment of hazard endpoints, such as genotoxicity testing utilizing methods that quantify fixed DNA damage. Genotoxicity is a core prerequisite in regulatory toxicology, and it is a vital component of the risk assessment of any toxicant⁸.

There is no single assay that can be applied to quantify all forms of DNA damage that may arise following exposure to an exogenous agent. However, a core component of the in vitro genotoxicity testing battery is the micronucleus assay, which is a reliable and multifaceted technique that measures gross chromosomal damage⁹. It is a gold standard technique described by the OECD Test Guideline 487, for assessing in vitro DNA damage and genotoxicity and is part of the test battery requirement for regulatory hazard assessment^{10,11}.

The human hepatocellular carcinoma cell line, HepG2, is used widely for initial hazard assessment screening as the cells are readily available, relatively inexpensive to source, simple to culture and amenable to high throughput screening^{12,13}. When cultured into 3D spherical structures, they have been shown to recapitulate the liver microenvironment well and offer a hepatic model with sufficient proliferative capabilities to support

the micronucleus assay³. Further development of the HepG2 spheroid models was established to improve the longevity and liver-like functionality of the model in order to support genotoxicity hazard assessment over long-term, repeated exposure regimes (≤ 14 days). Thus, in line with the principles of the 3Rs to replace, reduce and refine animal experimentation, the present protocol has been established to provide an advanced 3D in vitro hepatic model capable of reliably evaluating multiple toxicological endpoints (e.g., liver functionality, (pro-)inflammatory markers, cytotoxicity and genotoxicity) following acute, long-term and repeated chemical and ENM exposures in a routine and easily accessible manner.

Here, we present a method to establish a physiologically relevant 3D hepatocyte cell line based in vitro model system for genotoxicity hazard assessment following acute or long-term, repeated ENM exposures. The protocol can be broken down into 6 key stages: culturing cryopreserved HepG2 cells; HepG2 spheroid preparation; HepG2 spheroid transfer from hanging drop to agarose suspension; HepG2 spheroid harvest; micronucleus assay and scoring; and data analysis.

Protocol

1. Culturing cryopreserved HepG2 cells

NOTE: HepG2 cells, obtained from American Type Culture Collection (ATCC) were cultured in 1x Dulbecco's Modified Eagle Medium (DMEM) with 4.5g/L D-glucose and L-glutamine supplemented with 10% foetal bovine serum (FBS) and 1% penicillin/streptomycin antibiotic.

1. Pre-warm DMEM cell culture medium (including the supplements) in a 37 °C water bath for 30 min.
2. Remove one vial of HepG2 cells from liquid nitrogen and thaw in a 37 °C water bath for 2-3 min, whilst gently swirling the vial to allow for uniform thawing of the cell suspension. Take care not to submerge the vial above the O-ring in order to reduce the potential for contamination.
3. Once thawed, remove the vial from the water bath and spray generously with 70% ethanol to decontaminate the outer surface of the vial before placing under a sterile, Class II laminar tissue culture hood.
4. Carefully pipette the contents of the cryovial of HepG2 cells into a centrifuge tube containing 9 mL of pre-warmed DMEM cell culture medium (with supplements).
5. Using a 10 mL strippette, transfer 10 mL of the cell suspension into a 25 cm² disposable cell culture flask and incubate the culture for 3 days (from seeding) at 5% CO₂ and 37 °C until ~80% confluency is reached before undergoing sub-culture into a larger 75 cm² disposable cell culture flask.
6. Once 80% confluency is reached, sub-culture cells under sterile conditions by trypsinization with 0.05% trypsin/EDTA solution pre-warmed in a 37°C water bath for 30 min. At no point should the cells be allowed to dry out.
7. As cells form an adherent monolayer, remove the media by tipping into a disinfectant waste pot. Then immediately wash the monolayer to remove all traces of existing media by rinsing the flask twice with 3 mL of sterile 1x PBS solution kept at room temperature. Also, discard PBS into disinfectant waste pot.
8. Once PBS wash is removed, add 5 mL of pre-warmed 0.05% trypsin-EDTA solution, ensuring to cover the entire surface of the cells and incubate cells for 6-8 min at 37 °C and 5% CO₂.
9. Gently tap the flask to dislodge the cells from the bottom of the flask and then add 5 mL of DMEM cell culture medium (with supplements) to neutralize the trypsin enzyme.
10. Transfer the cell suspension into a 50 mL centrifuge tube and pipette the cell suspension up and down thoroughly to ensure that cells are completely disassociated.
11. Centrifuge the diluted cell suspension at 230 x *g* for 5 min. Discard the supernatant into disinfectant and re-suspend cell pellet in 25mL of DMEM cell culture medium (with supplements).
12. Transfer cell suspension into a 75 cm² disposable cell culture flask and incubate at 37 °C and 5% CO₂ for a further 3 days before undergoing spheroid preparation. Once the HepG2s have had time to acclimatize and once again reach ~80% confluency, determine the cell concentration in preparation for spheroid seeding.

2. HepG2 spheroid preparation

1. Repeat sub-culture steps stated above, except after centrifugation, re-suspend the cell-pellet in 1 mL of DMEM culture medium pre-warmed in a 37 °C water bath. Pipette cell suspension up and down thoroughly.
2. Score cell viability using the Trypan Blue Exclusion Assay (see OSHA SOP 3.21 Reproductive Toxins, Mutagens, Teratogens and Embryotoxins – Procedures for Safe Handling and Storage (2019) for health and safety guidance)¹⁴ with a 1:1 ratio of cell suspension to prefiltered 0.4% Trypan blue solution.
3. Prior to cell counting, take 1 mL of Trypan blue solution using a 1 mL syringe and filter with a 0.45 µm filter unit into a sterile, 1 mL tube.
4. Transfer 10 µL of filtered, Trypan blue solution into a 0.2 mL tube and add 10 µL of cell suspension. Remaining filtered Trypan blue solution can be stored up to 3 months at room temperature for future use.
5. Spray the haemocytometer thoroughly with 70% ethanol and wipe dry with a sterile paper towel before securing the coverslip on top using breath vapor. Sliding the coverslip across the breath moistened surface induces cohesive forces by generating Newton rings.
6. Gently pipette the Trypan blue cell suspension up and down using a 1000 µL pipette (to reduce sheer stress) before adding 10 µL to the haemocytometer. Ensure that the solution is dispersed underneath the cover slip and covers the entire grid without air bubbles.

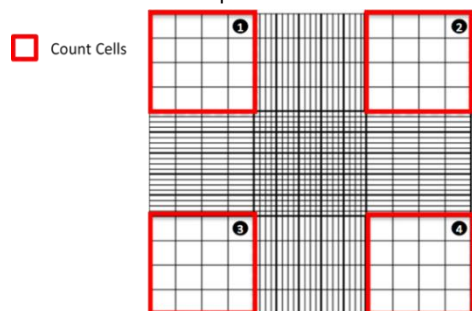


Figure 1: Counting cells using a haemocytometer. Diagrammatic representation of a haemocytometer highlighting which quadrant to count cells from. [Please click here to view a larger version of this figure.](#)

7. Under the microscope, count the live (unstained) and dead (stained blue) cells found in the four large corner squares (**Figure 1**). Exclude any cells found to overlap or sit on the interior two edges of the large corner squares (i.e., on the lines) in the count.
8. Using the following calculation, calculate the average number of live, viable cells (unstained) present in the sample:

$$\text{Total Number of Cells/mL} = \text{Live Cell Count} \times \frac{\text{dilution}}{\text{\# of squares counted}} \times 10,000$$

where dilution refers to how many times the stock solution was diluted in Trypan blue (2x in this case) and # of squares counted refers to the four large corner squares of the haemocytometer counted

9. Based on the viable HepG2 cell count and using the following formula:

$$C_1V_1=C_2V_2$$

where C_1 = the concentration of viable cells currently, V_1

= the volume of cell suspension currently,

C_2 = the concentration of cell suspension wanted,

V_2 = the volume of cell suspension wanted

10. Prepare a 10 mL stock solution of HepG2 cell suspension with DMEM cell culture medium at a concentration of 2.0×10^5 cells/mL in order to achieve 4000 HepG2 cells per 20 μ L hanging drop. Mix the cell suspension thoroughly by gently pipetting up and down using a 1000 μ L pipette to ensure all cells are fully suspended within the media.
11. To the wells of a 96-well cell culture plate, add 100 μ L of sterile, room temperature PBS to prevent the hanging drops from drying out during incubation.
12. Take the lid of a standard flat bottom 96-well cell culture plate, invert it and carefully pipette 20 μ L drops of the cell suspension into the center of each well groove of the lid, as shown in **Figure 2**. Use a multi-channel pipette but add only 2 - 4 drops at once as multiple seeding can affect the accuracy and placement of the drops.
 1. Center the drops within the grooves of the wells laid out on the lid; otherwise they will not hang in the center of the wells when the lid of the plate is turned over and are at risk of falling off into the plate. Gently flip the lid of the 96-well plate, so the drops are now hanging and carefully place on top of the 96-well plate.
13. Place the whole 96 well plate with lid gently into an incubator at 37 °C and 5% CO₂ for 3 days prior to spheroid transfer onto agarose. **NOTE:** Extra care must be taken not only when transporting the plates to/from the incubators, but when opening and closing the incubator in general as excessive movement can cause the plates to shift and the spheroids to either fall or form incorrectly.

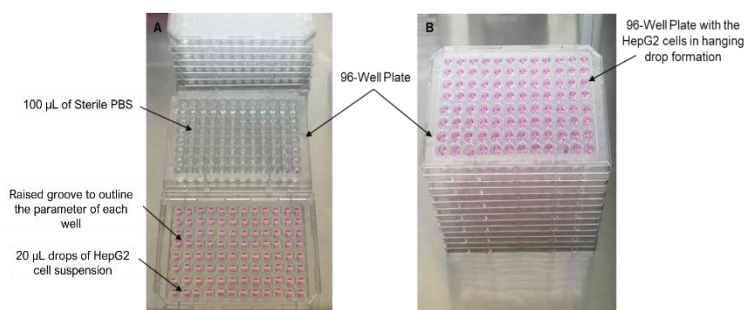


Figure 2: 3D HepG2 in vitro spheroid model preparation. (A) The HepG2 cells seeded in 20 μ L drops onto the lid of a 96-well plate. (B) The HepG2 cells post-seeding in the hanging drop model to allow for spheroid formation. [Please click here to view a larger version of this figure.](#)

3. HepG2 spheroid transfer from hanging drop to agarose suspension

NOTE: On Day 3 post seeding into hanging drops, the spheroids are transferred into the wells of the same 96-well plate all of which have been previously coated with a fine layer of 1.5% agarose gel.

1. Prepare agarose gels and autoclave (i.e., day 2 post seeding) prior to the day of plate coating (i.e., day 3 post seeding).

1. To prepare a 1.5% agarose gel, weigh 0.30 g of agarose into a clean, glass bottle and then add 20 mL of phenol-red free DMEM medium. Autoclave the agarose for 1 h at 230 °C for sterilization. The agarose coating prevents the HepG2 spheroids from adhering to the base of wells and forming a cellular monolayer instead of retaining their 3D spheroid structure.
2. On Day 3 post seeding, remove the 96-well plate containing the HepG2 hanging drop spheroids out of the incubator and carefully flip the lid so the spheroids are no longer hanging.
3. Using a multichannel pipette, remove and discard the 100 μ L of PBS previously added to the base of the 96-well plate. Allow the plates to air dry for 2-3 min whilst heating the agarose in preparation for coating.
CAUTION: This procedure results in very hot, liquid agarose which if spilt onto the skin may burn and cause injury. Furthermore, care must be taken when handling the glass bottle containing the liquid agarose as this too can be very hot.
4. Using the 1.5% agarose gels previously prepared, heat the glass bottle containing the 20 mL agarose gel for 30 s in a microwave at the maximum watt (i.e., 900 W). To coat two 96-well plates, one 20 mL bottle of pre-prepared 1.5% agarose gel should be sufficient.
5. Once melted, gently swirl the agarose by rotating the glass bottle to remove any bubbles and then add 50 μ L of agarose into the base of each well.
NOTE: When adding the agarose, ensure not to angle the plate $>45^\circ$ as the agarose sets quickly and will not form a flat, level layer that can disrupt spheroid growth. It is important to work efficiently at this stage to prevent the agarose from solidifying before the plate is completely coated.
6. Allow the plate to stand for 2 min at room temperature before adding 100 μ L of pre-warmed DMEM cell culture medium (with supplements) on top of the solid agarose layer in each well.
7. Flip the lid of the 96-well plate and place back on top of the 96-well plate so the spheroids are now hanging once again.
8. Centrifuge the plate for 3 min at 200 x g in order to transfer the spheroids from the hanging droplet into the individual wells of the 96-well plate. Following the transfer, the HepG2 spheroids should now be suspended in the cell culture medium. Allow them to settle for 24 h in the incubator at 37 °C and 5% CO₂.
9. Expose HepG2 spheroids of this size to either chemical or ENM treatments on Day 4 post seeding (i.e., 24 h after transfer to agarose coated plates).
10. In order to maintain cell viability over extended culture periods, refresh the cell culture medium every 3 days. To do this, gently aspirate 50 μ L of the cell culture medium from the surface of the well and replace with a fresh 50 μ L of DMEM cell culture medium. Take care not to remove or disturb the spheroid when performing a medium change.

4. Nanomaterial/Chemical exposure

NOTE: The HepG2 liver spheroid model can support both ENM and chemical based exposure regimes, but the primary focus of this protocol is ENM exposures. Prior to exposure, the test ENM must be suitably dispersed; this can be performed as directed by the NanoGenoTox Dispersion Protocol (Grant Agreement No. 20092101, 2018)¹⁵.

1. Following dispersion according to the NanoGenoTox Dispersion Protocol, dilute the ENM suspension from the starting concentration of 2.56 mg/mL to the final desired concentration in pre-warmed DMEM cell culture medium (including the supplements). A total volume of 5 mL is required to dose one 96 well plate.
2. To expose the HepG2 spheroid to either a chemical or ENM, using a 200 μ L pipette, aspirate 50 μ L of cell culture medium from the surface of each well (leaving 50 μ L in the well so as not to disturb the spheroids) and replace with 50 μ L medium containing the test toxicant at the required dose.
3. Once the test material has been applied, incubate the plates for the desired exposure time at 37 °C and 5% CO₂.
4. If a long-term (≥ 24 h) exposure regime is conducted, then immediately after the desired exposure timeframe has elapsed, harvest the spheroids for micronucleus endpoint analysis as described below in steps 6.1 – 6.4.
5. However, with acute exposure regimes (e.g., ≤ 24 h), once the exposure period has ended, harvest, pool, and store 50 μ L of supernatant from each well in the 96 well plate at -80 °C for further biochemical analysis later. Replace the cell culture medium with 50 μ L of fresh medium containing 6 μ g/mL of Cytochalasin B and leave to incubate for 1 – 1.5 cell cycles (i.e., 24 – 26 h for HepG2) in preparation for the cytokinesis block micronucleus assay harvest.

NOTE: For Acute (≤ 24 h) exposure regimes, the cytokinesis block micronucleus assay with Cytochalasin B can be applied but for long-term (≥ 24 h) exposure regimes, the mononuclear version (without Cytochalasin B) of the assay must be utilized as described below in **Figure 4**.

5. HepG2 spheroid harvesting

NOTE: Following either chemical or ENM exposure treatments, both cell culture medium or spheroid tissue can be harvested for multiple endpoint analysis. Depending on the endpoint analysis, spheroids can either be harvested individually (e.g., for image analysis) or pooled together (e.g., for cytokinesis block micronucleus assay).

1. Remove the 96-well plate from the incubator.
2. Using a 200 μ L pipette, aspirate the 100 μ L of cell culture medium including the spheroid tissue from each well and collect in a sterile, 15 mL centrifuge tube. Take care to avoid contact with the agarose.
3. Once collected, centrifuge the spheroid suspension at 230 x g for 5 min. Remove the supernatant and store at -80 °C for further endpoint analysis (e.g., liver function tests) later.
4. Re-suspend the pellet of spheroids in 1 mL of sterile, room temperature PBS (1x).
5. Once washed, centrifuge the spheroid suspension again at 230 x g for 3 min. Discard the supernatant, re-suspend in 500 μ L of 0.05% trypsin-EDTA solution and incubate for 6-8 min at 37 °C and 5% CO₂.

6. Following incubation, gently pipette the trypsinized cells up and down to fully disassociate and re-suspend the HepG2 cells prior to neutralizing with 1 mL of DMEM cell culture medium.
7. Centrifuge the diluted cell suspension at 230 x g for 5 min. Discard the supernatant into disinfectant and re-suspend cell pellet in 2mL of room temperature PBS (1x).
8. Centrifuge the cell suspension at 230 x g for 5 min. Discard the supernatant into disinfectant and then re-suspend the cell pellet once more in 2 mL of cold PBS (1x). Ensure the cells are well dispersed to prevent clumps of cells obscuring the field of view when mounted onto microscope slides.

6. Micronucleus assay and scoring

For the manual method of the micronucleus assay, a cytocentrifuge is required to produce a cytodot (a defined, concentrated region of cells) in the centre of the microscope slide. This process supports more efficient scoring of the slide as it allows the scorer to easily locate the cells of interest, as opposed to evaluating a whole slide where the cells can be widely spread.

1. Dip frosted microscope slides (three per dose) in 70% ethanol followed by ddH₂O and leave to air dry for 5 min.
2. Place prepared microscope slides into cuvette funnel as shown in **Figure 3A**, where the glass slide (iii) is placed in the metal support (iv) with a filter card (ii) and cuvette funnel (i) secured on top.
3. Arrange cuvette funnels in the cytocentrifuge with the funnel facing up, so 100 µL of cell suspension can be directly added into each one.
4. Cytospin for 5 min at 500 x g to ensure cells are evenly distributed onto the surface of the slide.



Figure 3: Cytospin setup to prepare treated cells on microscope slides. (A) Displays the individual components, (i) cuvette funnel, (ii) filter card, (iii) glass microscope slide and (iv) metal support required to cytospin HepG2 cells onto microscope slides. (B) The final cuvette funnel set up. (C) The correct placement of the cuvette funnel within the cytocentrifuge. [Please click here to view a larger version of this figure.](#)

5. Leave slides to air dry before fixation in ice-cold, 90% methanol for 10 min.
6. Once fixed, leave the slides to air dry overnight at room temperature before storing at -20 °C for up to 6 months.
7. When required, remove the pre-prepared microscope slides from -20 °C freezer and allow to warm to room temperature before undertaking Giemsa staining.
CAUTION: According to Regulation (EC) No. 1272/2008 [CLP], Giemsa staining solution is a highly flammable liquid which can be toxic if swallowed and cause damage on contact with the eyes, skin or if inhaled. Refer to the associated SDS sheet for detailed storage, handling and health and safety advice on this chemical prior to use.
8. Whilst the slides are defrosting, prepare a 20% Giemsa staining solution (25 mL required to stain ~30 slides) diluted in phosphatase buffer (pH 6.8). Mix thoroughly by gently swirling the solution before filtering using folded filter paper placed in a funnel.
9. Using a Pasteur pipette, add 3 – 5 drops of filtered Giemsa solution to the cytodot on each slide and leave for 8 – 10 min.
10. Wash slides in two successive phosphatase buffer washes before briefly rinsing under cold water to remove any excess stain leftover. Leave slides to air dry.
11. Once dry, in a fume hood, dip stained slides in xylene for 10 s before adding a drop of mounting medium to the center of the cytodot and a place a glass coverslip on top.
12. Leave microscope slides in the fume hood overnight to dry before manual scoring; they can be stored indefinitely at room temperature.

7. Data analysis

1. As described in the OECD Test Guidelines 487 (2014)¹¹, to assess and quantify DNA damage induced as a result of exposure to an ENM or chemical agent, use a light microscope (100x objective with immersion oil) 2000 mononucleated or 1000 binucleated cells per biological replicate to score for the presence of micronuclei, as shown in **Figure 4**.

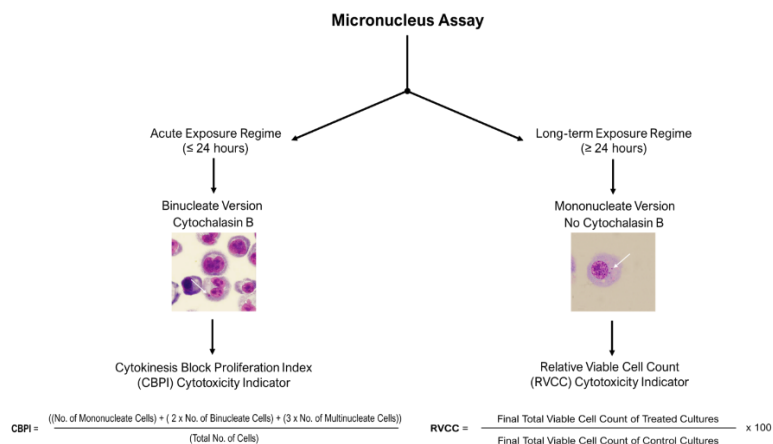


Figure 4: Micronucleus assay scoring decision tree. Schematic decision tree to highlight the necessity for different scoring and cytotoxicity assessment procedures when using the micronucleus assay with 3D models following acute or long-term exposure regimes. Acute (≤24 h) exposures allow use of the cytokinesis blocked micronucleus assay, while long-term (≥24 h) exposures require the mononuclear version of the assay; both of which are described in OECD Test Guideline 487. [Please click here to view a larger version of this figure.](#)

2. Based on the proportion of micronuclei present per number of mononucleated or binucleated cells scored, calculate a percentage of genotoxicity value.
3. In order to assess the DNA damage observed is not as a result of cell debris caused by a high proportion of apoptotic cells, take a measure of cytotoxicity alongside. In this case, depending on the presence of Cytochalasin B, use either CPBI or RVCC calculation (as described in **Figure 4**). Genotoxicity must only be evaluated in samples where cytotoxicity is less than 55% ± 5% as defined in OECD Test Guideline 487¹¹.

Representative Results

Suitability of this cell-line based 3D liver spheroid model for long-term culture and genotoxic hazard assessment was evaluated by conducting baseline characterization to determine the viability and liver-like functionality of the model over the duration of 14 days in culture as well as its applicability for the micronucleus assay.

Baseline Characterization of the 3D HepG2 Liver Spheroid Model

Prior to any in vitro toxicological assessment, it is important to check that the 3D HepG2 spheroids have formed properly before performing the agarose transfer or chemical/ENM treatment. HepG2 spheroids produced using the hanging drop method usually take 2 - 3 days post seeding (4000 cells/spheroid) to form compact, spherical shaped spheroids with an average diameter of 495.52 μm W x 482.69 μm H as shown in **Figure 5A-5C**. HepG2 spheroids that have formed correctly and are acceptable to be used for in vitro toxicological assessment must have a compact, spherical shaped structure with a smooth surface and no visual projections. **Figure 5** provides examples of good quality (**Figure 5D-F**) and a poor quality (**Figure 5G-I**) spheroids. The latter of which should be discarded. Typically, 90-95% of spheroids formed per plate will form correctly and be viable for further experimentation.

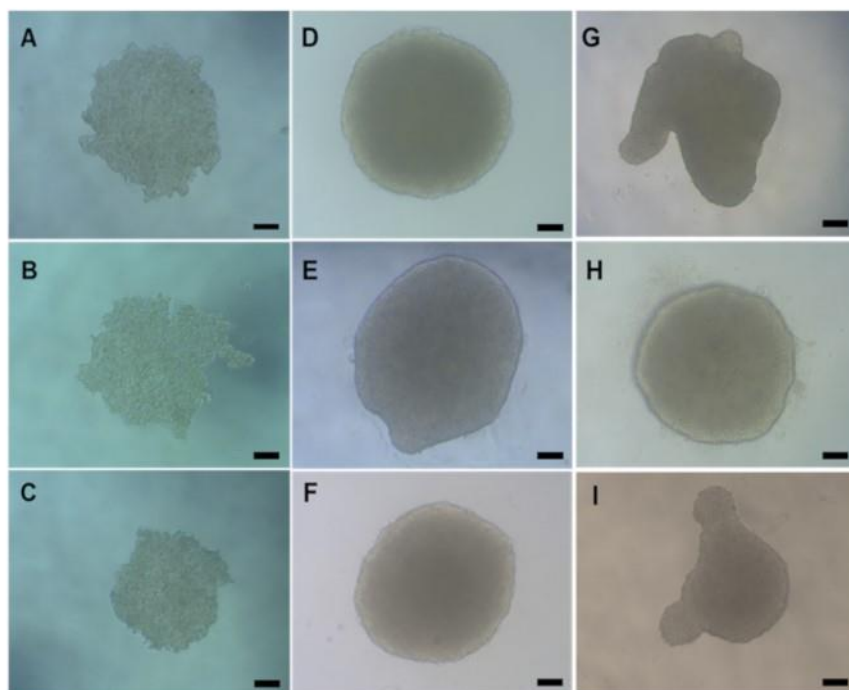


Figure 5: Light microscopy images displaying the natural morphology of the HepG2 spheroids formed via the hanging drop method. (A-C) show Day 2 and (D-I) Day 4 HepG2 liver spheroids post seeding. (D-F) are examples of good quality HepG2 spheroids whilst (G-I) shows poorly formed spheroids. All images were taken on a X20 objective using a microscope. The scale bar represents 20 µm. [Please click here to view a larger version of this figure.](#)

To further confirm HepG2 spheroid viability, a basic colorimetric Bromocresol Green Albumin (BCG) Assay or Urea Assay can be performed to assess their liver-like functionality. Liver-like functionality was assessed in line with viability using the Trypan Blue Exclusion Assay over a 14 day culture period to determine the longevity of the liver spheroid model and establish if it could support long-term or repeated ENM/chemical based hazard assessment (**Figure 6**). Albumin concentration remained consistent over the duration of the culture period. Urea production displays an increase in the concentration of urea produced per spheroid over a week in culture before reaching a plateau by day 7. It is important to note that the levels of albumin and urea produced in the 3D HepG2 spheroids are substantially higher than that observed in the same cell line cultured in a 2D format. Indeed, 2D cultures of HepG2 cells, peak albumin and urea levels were 0.001 mg/mL and 0.010 ng/µL respectively. Furthermore, in previous work published by Shah et al. using an almost identical HepG2 spheroid system, the authors highlight a notable improvement in metabolic activity (CYP1A1 and CYP1A2) in the 3D HepG2 in vitro model systems when compared to the 2D cultured HepG2 cells⁵.

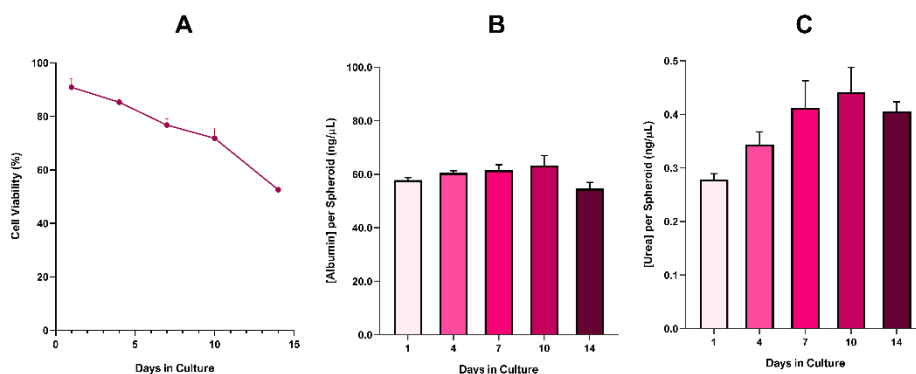


Figure 6: 14-Day baseline characterisation data for HepG2 liver spheroids. Following transfer from hanging drop, (A) highlights the viability of the HepG2 spheroid model over a 14 day period whilst (B) and (C) highlight the liver-like albumin and urea functionality respectively. Mean data ± SEM presented, n = 4. [Please click here to view a larger version of this figure.](#)

With the inevitable development of a necrotic core, a known limitation of 3D liver spheroid cultures, the viability of this HepG2 based model had to be established to demonstrate it was able to sustain long-term (5-10 day) exposure regimes whilst maintaining the proliferative capability required to support the micronucleus assay⁵. Indeed, this 3D liver spheroid model has been shown to retain >70% viability over 10 days in culture. Based on this and in conjunction with the sustained liver-like functionality observed over the ≥14 day culture period, this 3D liver spheroid model can thus support long-term, repeated ENM exposure regimes up to 10 days long (i.e., before viability of the spheroids drop below 70%). For reference, it is

advised that albumin levels for HepG2 spheroids seeded at 4000 cells/spheroid should be ≥ 50.0 ng/ μ L whilst urea production should be ≥ 0.25 ng/ μ L before conducting an in vitro toxicological assessment with this model.

Genotoxicity Assessment of Engineered Nanomaterials

For genotoxicity assessment, the micronucleus assay was used to determine the presence of micronuclei following both acute (24 h) and long-term (120 h) ENM exposures. Aflatoxin B1 is a known liver carcinogen^{16,17} and is a recommended positive control for the micronucleus assay. Optimization experiments have shown that 0.1 μ M of Aflatoxin B1 induces a significant positive (≥ 2.0 fold increase) genotoxic response in 3D HepG2 liver spheroids and thus is used in every micronucleus assay conducted with this model. To ensure the validity of the micronucleus assay results using the HepG2 spheroid model, the background micronucleus frequency for HepG2 cells used in this 3D in vitro model should lie within a range of 0.6% – 1.2%. As a result, Aflatoxin B1 should induce a genotoxic response of at least two-fold higher than that seen with the negative control; thus, 0.1 μ M of Aflatoxin B1 should induce a micronuclei frequency between 1.5% – 3.0%. Using these control parameters, ENM associated genotoxicity in vitro can then be reliably assessed. Based on OECD Test Guideline 487, it is important to note that when testing an ENM or chemical, the concentrations selected should not induce more than 55% \pm 5% cytotoxicity (indicated by a reduction in CPBI or RVCC values in relation to the negative control)¹¹. **Figure 7** illustrates the data generated when Aflatoxin B1 and two ENMs (titanium dioxide (TiO₂) and silver (Ag)) were evaluated following both acute and long-term exposures in the HepG2 spheroids, and subsequent genotoxic potential was analyzed using the micronucleus assay. Both ENMs assessed were tested at a noncytotoxic, low dose of 5.00 μ g/mL over an acute (24 h) exposure and long-term (120 h) exposure regime. A similar trend for genotoxicity across both TiO₂ and Ag ENMs can be observed, whereby the elevated genotoxicity response that resulted following 24 h exposure was not evident after a long-term 5 day exposure. This was despite sustained genotoxicity induced by the Aflatoxin B1 positive control at both time-points.

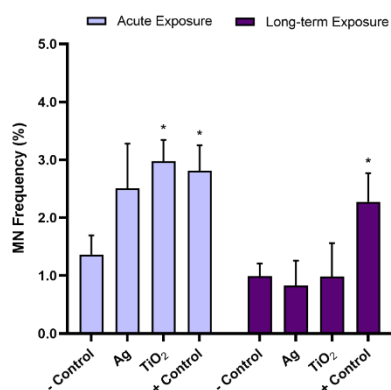


Figure 7: Genotoxicity assessment following TiO₂ and Ag ENM exposure on HepG2 liver spheroids. Genotoxicity (micronucleus frequency) assessment using the micronucleus assay post (A) acute (24 hour) and (B) long-term (120 hour) exposure to 5.00 μ g/mL of TiO₂ and Ag ENM. Negative control is a media only, whilst the positive control is 0.1 μ M of Aflatoxin B1. Mean data (n=2) presented \pm SD. Significance indicated in relation to the negative control: * = $p \leq 0.05$. [Please click here to view a larger version of this figure.](#)

Discussion

Applications for 3D hepatic models vary considerably depending on the particular biochemical endpoint or adverse outcome pathway being targeted. Each model has its benefits and limitations, from interdonor variation in primary human hepatocyte (PHH) models to reduced cytochrome p450 activity in cell-line based models, but all are valuable in their own right^{6,12,18,19}. When assessing genotoxicity there are limitations in the models compatibility with regulatory approved endpoints such as the in vitro micronucleus assay, as active proliferation is required. This is necessary, as genotoxicity assessment requires the quantification of fixed DNA damage to be assessed post cell division when there is opportunity for DNA repair to correct transient lesions. Unfortunately, highly differentiated hepatocyte (i.e., HepaRG) based spheroids or PHH microtissues, which are deemed to exhibit the most physiologically relevant liver-like characteristics form static (non-proliferative) models^{12,19,20}. As a result, the 3D HepG2 spheroid model presented here provides a suitable, alternative model able to support genotoxicity testing. HepG2 cell-line based spheroids have sufficient actively dividing cells on the outer surface of the spheroids whilst maintaining basic liverlike characteristics, such as albumin and urea production and some CYP450 activity^{5,12,19}. Principally this in vitro liver model has been developed to complement the micronucleus assay, as this is one of the two in vitro assays recommended in the battery for genotoxicity testing^{8,10,11,21}. However, the model can be readily applied to DNA sequencing analysis and gene expression (RNA) technologies, while it has the potential to be further adapted and utilized for other DNA damage endpoints, such as the comet assay. Nonetheless, it is important to consider the role that ENM interference plays in some endpoint analyses. For example, flow cytometry-based analyses may not be suitable for ENM genotoxicity assessment specifically due to particle interference²².

One limiting factor of spheroid models that actively undergo cell division is their size. Optimization of seeding density is critical as there needs to be enough cells that allow the model to continue to proliferate; but not too high a cell number, which results in the spheroid becoming overly compact, leading to an increased necrotic core. The cause of this necrosis is believed to be restricted oxygen and nutrient diffusion, as the limit of this diffusion is thought to be approximately 100 – 150 μ m of tissue^{23,24}. However, this does depend of the cell type, cell number, scaffold interactions and culture conditions²⁵. Since, it has been shown that approximately 700 μ m diameter is the limit for avoiding premature onset of necrosis in the center of C3A spheroids, seeding 4000 HepG2 cells per spheroid ensures the diameter of the model at the time of exposure is ≤ 500 μ m²⁶. Furthermore, Shah et al. established that HepG2 cells seeded above 5000 cells per spheroid exhibited a 25% reduction in viability following 7 days in culture, which could pertain to the average diameter of 680 μ m and limited availability of nutrients in a 20 μ L hanging drop⁵. To overcome this, the model devised in the present protocol undergoes a critical step where the hanging drop is transferred to agarose coated wells following initial formation of the spheroid. This ensures a greater volume of culture medium is present to sustain the ever-growing number

of cells within the spheroids. As a result, the HepG2 spheroid model remains over 70% viable following 10 days in culture and can be utilized for long-term hazard assessment in vitro.

Whilst the HepG2 spheroid model can support both acute and long-term exposure regimes, refreshing cell culture medium during extended culture periods is restricted for this model as complete replacement of the medium is not advised due to the potential loss of the spheroids. It is presumed that with ENM exposures, the tendency for homogenous ENM dispersions to agglomerate and sediment is high. However, it is notable that the rate at which an ENM sediments can vary depending on the particle parameters (e.g., size, shape and density) and can be determined theoretically using the in vitro sedimentation, diffusion and dosimetry (ISDD) model, or its recent derivatives, often referred to when regarding ENM (suspension) exposure approaches^{27,28}. With this in mind, it is assumed that if only 50% of the cell culture medium is carefully removed from the surface of the cell culture, the disruption and subsequent removal of the ENM dose should be minimal. However, with Brownian motion at play, this may not strictly be the case and further work into the deposition and sedimentation of each particular ENM to be tested should be undertaken to ensure the correct dosimetry is retained throughout the long-term exposure regimes²⁷. Principally this is a potential limitation to consider when performing repeated dosing regimes as this could be critical to the final, accumulated concentration. Chemical based exposures on the other hand, whilst not without their own limitations to consider, offer a more simplistic approach in that chemical substances tend to remain in solution and thus a direct replacement of the original chemical concentration in addition to the newly added concentration ensures that any chemical lost during media refreshment is replaced accordingly²⁹. Future applications would include evaluating the suitability of the model for repeated exposure regimes over long-term culture periods as repeated dosing strategies are crucially important for assessing the ability of a particular organ system to ameliorate or overcome the adverse effects, if any, induced by bioaccumulation of a xenobiotic substance.

In conclusion, this 3D in vitro hepatic model has the capacity to be utilized for evaluating a range of realistic exposure scenarios, thereby providing a future in vitro approach to better support both ENM and chemical hazard assessment in a routine and easily accessible manner.

Disclosures

The authors have nothing to disclose.

Acknowledgments

The authors would like to acknowledge that this research has received funding from the European Union's Horizon 2020 research and innovation programme for the PATROLS project, under grant agreement No.760813

References

1. Geiser, M., Kreyling, W. G. Deposition and biokinetics of inhaled nanoparticles. *Particle and Fibre Toxicology*. **7**, 2 (2010).
2. Modrzynska, J. Toxicological effects of nanoparticle deposition in the liver. *Kgs. Lyngby, Denmark: Technical University of Denmark*. (2018).
3. Elje, E. et al. The comet assay applied to HepG2 liver spheroids. *Mutation Research/Genetic Toxicology and Environmental Mutagenesis*. **845**, p403033 (2019).
4. Breslin, S., O'Driscoll, L. Three-dimensional cell culture: the missing link in drug discovery. *Drug Discovery Today*. **18**, p240-249 (2013).
5. Shah, U.-K. et al. A three-dimensional in vitro HepG2 cells liver spheroid model for genotoxicity studies. *Mutation Research/Genetic Toxicology and Environmental Mutagenesis*. **825**, p51-58 (2018).
6. Lauschke, V. M., Hendriks, D. F. G., Bell, C. C., Andersson, T. B., Ingelman-Sundberg, M. Novel 3D Culture Systems for Studies of Human Liver Function and Assessments of the Hepatotoxicity of Drugs and Drug Candidates. *Chemical Research in Toxicology*. **29**, 1936-1955 (2016).
7. van Grunsven, L. A. 3D in vitro models of liver fibrosis. *Advanced Drug Delivery Reviews*. **121**, 133-146 (2017).
8. Corvi, R., Madia, F. In vitro genotoxicity testing – can the performance be enhanced? *Food and Chemical Toxicology*. **106**, p600-608 (2017).
9. Doak, S. H., Manshian, B., Jenkins, G. J. S., Singh, N. In vitro genotoxicity testing strategy for nanomaterials and the adaptation of current OECD guidelines. *Mutation Research/Genetic Toxicology and Environmental Mutagenesis*. **745**, 104-111 (2012).
10. Fenech, M. Cytokinesis-block micronucleus cytome assay. *Nature Protocols*. **2**, 1084-1104 (2007).
11. OECD Guidelines. *Test No. 489: In vivo Mammalian Alkaline Comet Assay*. (2016).
12. Gerets, H. H. J. et al. Characterization of primary human hepatocytes, HepG2 cells, and HepaRG cells at the mRNA level and CYP activity in response to inducers and their predictivity for the detection of human hepatotoxins. *Cell Biology and Toxicology*. **28**, 69-87 (2012).
13. Sison-Young, R. L. et al. A multicenter assessment of single-cell models aligned to standard measures of cell health for prediction of acute hepatotoxicity. *Archives of Toxicology*. **91**, 1385-1400 (2017).
14. European Agency for Safety and Health at Work. *European Guidelines 2019*. <https://osha.europa.eu/en/safety-and-health-legislation/european-guidelines> (2019).
15. Jensen, K.A. The NANOGENTOX Dispersion Protocol for NANoREG. *European Union Grant Agreement n° 2009 21 01*. (2014).
16. Marchese, S. et al. Aflatoxin B1 and M1: Biological Properties and Their Involvement in Cancer Development. *Toxins*. **10**, 214 (2018).
17. Rushing, B. R., Selim, M. I. Aflatoxin B1: A review on metabolism, toxicity, occurrence in food, occupational exposure, and detoxification methods. *Food and Chemical Toxicology*. **124**, 81-100 (2019).
18. Keramanizadeh, A., Brown, D. M., Moritz, W., Stone, V. The importance of inter-individual Kupffer cell variability in the governance of hepatic toxicity in a 3D primary human liver microtissue model. *Scientific Reports*. **9**, 7295 (2019).
19. Berger, B. et al. Comparison of Liver Cell Models Using the Basel Phenotyping Cocktail. *Frontiers in Pharmacology*. **7**, 443 (2016).
20. Ramaiahgari, S. C. et al. A 3D in vitro model of differentiated HepG2 cell spheroids with improved liver-like properties for repeated dose highthroughput toxicity studies. *Archives of Toxicology*. (2014).
21. Li, Y. et al. Factors affecting the in vitro micronucleus assay for evaluation of nanomaterials. *Mutagenesis*. **32** (1), 151-159 (2016).

22. Kirkland, D., Reeve, L., Gatehouse, D. and Vanparys, P. A core in vitro genotoxicity battery comprising the Ames test plus the in vitro micronucleus test is sufficient to detect rodent carcinogens and in vivo genotoxins. *Mutation Research/Genetic Toxicology and Environmental Mutagenesis*. **721** (1), 27-73 (2011).
23. Curcio, E. et al. Mass transfer and metabolic reactions in hepatocyte spheroids cultured in rotating wall gas-permeable membrane system. *Biomaterials*. **28**, 5487-5497 (2007).
24. Glicklis, R., Merchuk, J. C., Cohen, S. Modeling mass transfer in hepatocyte spheroids via cell viability, spheroid size, and hepatocellular functions. *Biotechnology and Bioengineering*. **86**, 672-680 (2004).
25. Asthana, A., Kisaalita, W. S. Microtissue size and hypoxia in HTS with 3D cultures. *Drug Discovery Today*. **17**, 810-817 (2012).
26. Gaskell, H. et al. Characterization of a functional C3A liver spheroid model. *Toxicology Research*. **5**, 1053-1065 (2016).
27. Cho, E. C., Zhang, Q., Xia, Y. The effect of sedimentation and diffusion on cellular uptake of gold nanoparticles. *Nature Nanotechnology*. **6**, 385-91 (2011).
28. Hinderliter, P. M. et al. ISDD: A computational model of particle sedimentation, diffusion and target cell dosimetry for in vitro toxicity studies. *Particle and Fiber Toxicology*. **7**, 36 (2010).
29. Kramer, N. I., di Consiglio, E., Blaauboer, B. J., Testai, E. Biokinetics in repeated-dosing in vitro drug toxicity studies. *Toxicology in vitro*. **30**, 217-224 (2015).

4.3 Publication III

Original Manuscript

Adaptation of the *in vitro* micronucleus assay for genotoxicity testing using 3D liver models supporting longer-term exposure durations

Gillian E. Conway^{1,✉}, Ume-Kulsoom Shah¹, Samantha Llewellyn¹, Tereza Cervena^{1,2}, Stephen J. Evans¹, Abdullah S. Al Ali¹, Gareth J. Jenkins¹, Martin J. D. Clift¹ and Shareen H. Doak^{1,*}

¹In Vitro Toxicology Group, Institute of Life Science, Swansea University Medical School, Singleton Park Campus, Swansea, Wales SA2 8PP, UK and ²Department of Nanotoxicology and Molecular Epidemiology, Institute of Experimental Medicine of the CAS, Vídeňská 1083 142 20 Prague 4, Czech Republic

*To whom correspondence should be addressed. Tel: 0044 (0)1792 295388; Email: s.h.doak@swansea.ac.uk

Received 15 May 2020; Editorial decision 22 June 2020; Accepted 23 June 2020.

Abstract

Following advancements in the field of genotoxicology, it has become widely accepted that 3D models are not only more physiologically relevant but also have the capacity to elucidate more complex biological processes that standard 2D monocultures are unable to. Whilst 3D liver models have been developed to evaluate the short-term genotoxicity of chemicals, the aim of this study was to develop a 3D model that could be used with the regulatory accepted *in vitro* micronucleus (MN) following low-dose, longer-term (5 days) exposure to engineered nanomaterials (ENMs). A comparison study was carried out between advanced models generated from two commonly used liver cell lines, namely HepaRG and HepG2, in spheroid format. While both spheroid systems displayed good liver functionality and viability over 14 days, the HepaRG spheroids lacked the capacity to actively proliferate and, therefore, were considered unsuitable for use with the MN assay. This study further demonstrated the efficacy of the *in vitro* 3D HepG2 model to be used for short-term (24 h) exposures to genotoxic chemicals, aflatoxin B1 (AFB1) and methylmethanesulfonate (MMS). The 3D HepG2 liver spheroids were shown to be more sensitive to DNA damage induced by AFB1 and MMS when compared to the HepG2 2D monoculture. This 3D model was further developed to allow for longer-term (5 day) ENM exposure. Four days after seeding, HepG2 spheroids were exposed to Zinc Oxide ENM (0–2 µg/ml) for 5 days and assessed using both the cytokinesis-block MN (CBMN) version of the MN assay and the mononuclear MN assay. Following a 5-day exposure, differences in MN frequency were observed between the CBMN and mononuclear MN assay, demonstrating that DNA damage induced within the first few cell cycles is distributed across the mononucleated cell population. Together, this study demonstrates the necessity to adapt the MN assay accordingly, to allow for the accurate assessment of genotoxicity following longer-term, low-dose ENM exposure.

Introduction

In recent years, 3D *in vitro* liver models have become increasingly useful tools for the genotoxic assessment of hazardous materials as they more accurately represent the physiological environment of

the liver (1–5). It is widely accepted that the traditional *in vitro* 2D monocultures poorly represent the intricacies of the liver cells metabolic activity *in vivo* and, therefore, are limited in their ability to elucidate complex biological processes (5–7). It has been shown that

the expression of liver-specific enzymes and drug metabolism in primary human hepatocytes (albumin and cytochrome P450) were at much lower levels in 2D culture (8,9). Recent advances in tissue engineering allow researchers to better simulate the liver environment using 3D cultures, providing a valuable tool for advancing the study of hepatotoxicity. At the International Workshop on Genotoxicity Testing (IWGT) it was recognised that 3D models, including those representing the liver, were deemed more physiologically relevant than the standard 2D monocultures (1).

Primary 2D human hepatocytes have been widely used in hepatotoxicity; however, they are not without limitations; for example, phenotypic variation between donors, rapid dedifferentiation and common loss of liver functionality (as indicated by reduced albumin and urea production) (7,10). The more physiologically relevant primary hepatocyte 3D liver model outperforms the standard 2D *in vitro* system, demonstrating long-term stability and the ability to maintain similar *in vivo* liver functionality (10). Primary hepatocyte 3D models have been reported to be efficacious in assessing longer-term toxicity using a variety of endpoints, such as cytotoxicity, cytokine production and DNA damage induction, following repeated exposure to engineered nanomaterials (ENMs) (11). Whilst 3D primary hepatocytes are relevant for longer-term toxicity testing, they are not suitable for use with the regulatory accepted micronucleus (MN) assay. The success of this assay relies on cellular proliferation; however, many primary or differentiated 3D hepatic models are static (12).

Genotoxicity assessment involves the need for a battery of tests that are capable of quantifying the induction of point mutation, structural chromosomal damage and numerical changes in chromosome number. The key *in vitro* assays utilised to evaluate these endpoints include the bacterial reverse mutation test, the MN assay and mammalian cell gene mutation tests (e.g. using the *HPRT* and *xprt* genes). Other DNA damage reporter assays that are used for screening purposes include the comet assay, gamma-H2AX staining and, in more recent years, the use of ‘-omics’ technologies, that is, transcriptomics have been applied to screen for modifications and alternations in gene expression profiles following DNA damage induction. The MN assay is a reliable technique that measures fixed chromosomal damage demonstrated by the frequency of MN in cells that have undergone cell division, which results from aneuploidic or clastogenic damage (13) and is, therefore, recommended as the ‘benchmark’ technique for assessing DNA damage and genotoxicity *in vitro* (14,15). The MN assay has previously been adapted to accommodate advanced 3D tissue culture models for the assessment of hazardous materials. For example, Curren *et al.* successfully modified the traditional MN assay for use with 3D EpiDerm Skin model, measuring genotoxicity using the reconstructed skin MN (RSMN) assay following chemical exposures for up to 72 h (16). Similarly, Wills *et al.* have also adapted the *in vitro* MN assay for genotoxic assessment of the EpiDerm Skin model and TK6 cells following 24 h nanoparticle exposure (17). Shah *et al.* have recently developed a cost-effective, low-maintenance 3D HepG2 liver model that has been shown to maintain liver functionality and can be used for genotoxicity assessment using the cytokinesis-block MN assay (CBMN). The use and applicability of this 3D liver genotoxicity approach has been demonstrated with the chemicals benzo[a]pyrene (BaP) and 2-amino-1-methyl-6-phenylimidazo[4,5-b]pyridine (PhIP), where interestingly, the 3D liver spheroid system was more sensitive to the induction of damage induced by these pro-genotoxins than the comparative 2D HepG2 monocultures (3). The reason for this difference was the substantially higher expression levels of metabolic enzymes in the 3D liver spheroid models

than in the 2D HepG2 cultured cells. Thus, the capability of the 3D models to more efficiently metabolise the BaP and PhIP exposures into their genotoxic metabolites resulted in greater genotoxicity being reported in the more complex culture system than when the standard CBMN assay was applied in 2D cell cultures.

The efficacy of the MN assay in 3D culture systems following exposure to ENMs must, however, also be considered, as it has long been recognised that the Organisation for Economic Co-operation and Development (OECD) test guidelines, which were primarily developed for chemicals, are not wholly appropriate for ENMs (13). For example, the CBMN assay requires the addition of cytochalasin B (Cyto B), a cytostatic agent that will halt cell division after one cell cycle and block cytokinesis, therefore resulting in the formation of clearly identifiable bi-nucleated cells (15). When exposing cells to chemicals, Cyto B can be added during or after the addition of the chemical. However, for ENM exposures, co-treatment of Cyto B with ENM has been shown to prevent cellular uptake of ENM; therefore, it is critical that Cyto B is added post-ENM exposure (13,18). More recently, a review of published data resulted in a series of recommendations on the genotoxic assessment of ENM (19). When evaluating the MN assay, of the 36 studies that satisfied the inclusion criteria, the conclusion was that there was a large degree of variation amongst assay approach and that standardisation of the MN assay to evaluate ENM is required (19). The MN assay is routinely used to evaluate genotoxicity associated with chemical compounds. However, unlike chemical compounds which often can have short half-lives, many ENMs are biopersistent. They, therefore, do not always readily breakdown in biological systems and can result in a gradual intracellular accumulation with prolonged and/or repeated exposures (18). To further develop our understanding and accurately assess the impact of more realistic longer-term, low-dose ENM exposure using the MN assay, it is necessary to have biological test systems and assays that facilitate this. The aim of this study, therefore, was to develop an advanced 3D liver spheroid model that could be used with the MN assay for genotoxicity assessment following longer-term exposure to test agents at low doses that are more representative to an *in vivo* exposure system. This will be achieved *via* the modification of the protocol previously described in Shah *et al.* (3) to sustain extended culture periods of HepG2 and HepaRG liver spheroids *in vitro* while maintaining liver functionality and also adapt the approach to support the analysis of fixed DNA damage using the MN assay following longer-term ENM exposures.

Materials and Methods

Chemicals

Aflatoxin B1 (AFB1; Sigma Aldrich, UK), Cyto B and methylmethanesulfonate (MMS; Sigma Aldrich, UK) were prepared according to manufacturer’s instructions. Stock solutions of AFB1 (3 mM), MMS (1 mM) and Cyto B (1.5 mg/ml) were prepared in DMSO and stored at -20°C . ZnO ENM (JRC Nanomaterials Repository, Belgium) stock solutions (2.56 mg/ml) were prepared and dispersed as per the NanoGenoTox Dispersion Protocol (grant agreement no. 20092101, 2018) (20). Working stocks of both chemicals and ENMs were subsequently made fresh for each experiment.

Cell culture and maintenance

The human Caucasian hepatocellular carcinoma-derived epithelial cell line HepG2 (ECACC 85011430) was cultured in Dulbecco’s Modified Eagle Medium (DMEM) with 4.5 g/l D-glucose and L-glutamine (GIBCO, Paisley, UK) supplemented with 10% foetal

bovine serum and 1% penicillin/streptomycin (GIBCO, Paisley, UK). HepG2 cells were sub-cultured with trypsin/EDTA (0.05%) solution (GIBCO, Paisley, UK). HepG2 cells were sub-cultured every 3–5 days when 80% confluency was reached.

HepaRG cells (Biopredic International, HPR116) were thawed in HepaRG™ Thawing/Plating/General Purpose medium (Biopredic International, MIL600C with ADD670C), counted and seeded immediately into spheroids using HepaRG™ Maintenance/Metabolism medium (Biopredic International, MIL600C with ADD620C). Both cell types were examined for morphology using a Zeiss Axiovert 25 light microscope at ×40 objective.

3D spheroid liver models for acute exposures

HepG2 monolayers were used to form spheroids using the previously described hanging drop method (3). In short, HepG2 cells were trypsinised and a cell stock (2.0×10^5 cells/ml) was prepared. HepaRG cells were thawed straight from liquid nitrogen and viability assessed using the trypan blue cell exclusion (TB) assay prior to preparing a cell stock of 2.0×10^5 cells/ml. A total of cell suspension (~4000 cells per 20 µl drop) was pipetted onto an inverted 9.4-cm square petri dish lid (Greiner Bio-One, UK). Approximately 100 drops were placed on each inverted petri dish lid. Subsequently, 20 ml of phosphate buffered saline (PBS) was added to the base petri dish to prevent the drops from drying out during the culture period. The petri dish was placed into the incubator at 37°C and 5% CO₂ atmosphere. To maintain cell viability in the hanging drop, 6 µl of media was added to each drop on Day 3. Assessment of the spheroid morphology was examined using a Zeiss Axiovert 25 light microscope at ×40 objective.

3D spheroid liver models for longer-term exposures

To support the growth of 3D spheroids over longer time periods, we have adapted the protocol previously described by Shah *et al.* (3). Following trypsinisation of 2D HepG2 cells, a stock solution of cells was prepared. Next, 20 µl of the cell suspension (4000 HepG2 cells per 20 µl hanging drop) was pipetted onto the inverted side of a 96-well tissue culture plate. To prevent the hanging drops from drying out, 100 µl PBS was transferred into the wells of the 96-well plates. The lid of the 96-well plate was gently inverted and placed onto the 96-well plate. The plate was then placed in the incubator at 37°C with 5% CO₂. Three days after seeding (into hanging drops), the PBS was removed from each of the wells. The base of each well was coated with 50 µl of 1.5% agarose gel (Figure 1). Once dried, 100 µl fresh media was added to the wells. The spheroids were then transferred into the wells by centrifugation at 200g for 3 min. The HepG2 spheroids, suspended in the cell culture medium, were left to settle for 24 h, after which, they were ready to be exposed. To maintain cell viability over extended culture periods, the cell culture medium was refreshed every 3 days, whereby 50 µl of media was aspirated and replaced with a fresh 50 µl of DMEM. Assessment of the spheroid morphology was examined using a Zeiss Axiovert 25 light microscope at ×40 objective.

Exposures

Short term

The spheroids were left in the hanging drop positions for 3 days (Figure 1). On Day 4, the hanging drops were treated with either AFB1 or MMS for 24 h, after which, Cyto B [6 µg/ml (Merck)] was added for an additional 24 h. The spheroids were harvested and

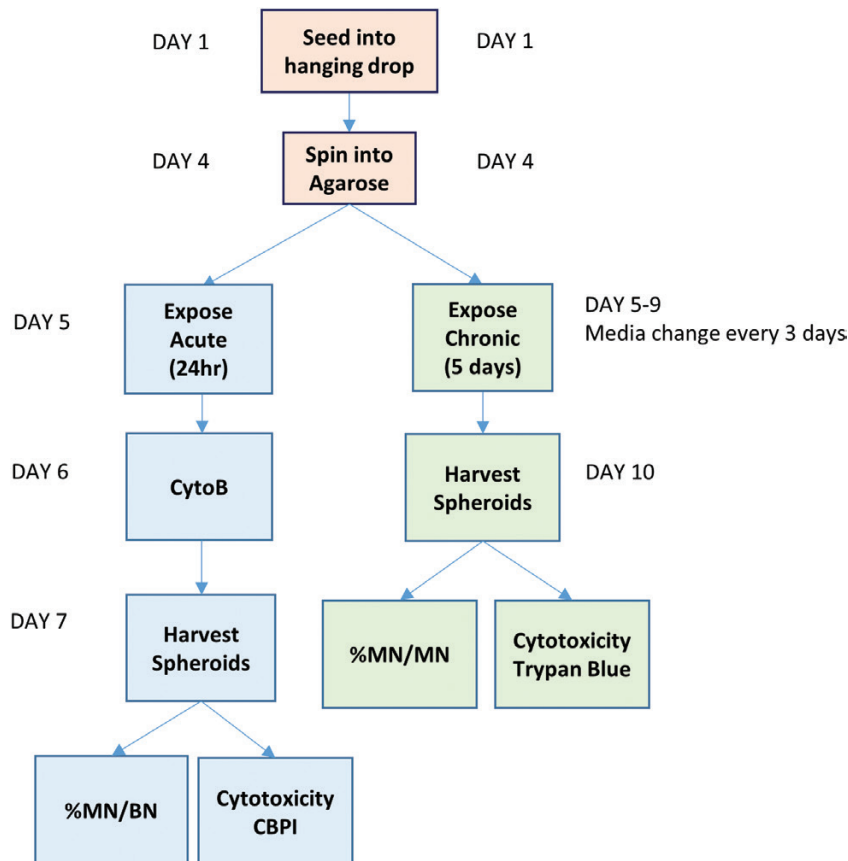


Fig. 1. A schematic of the spheroid-ENM exposure timeline and MN assay specific adaptations.

trypsinised as described below for the TB cytotoxicity assay. After the final centrifugation step, the pellet was re-suspended in 400 μ l PBS. Slides were prepared for both cytokinesis-block proliferation index (CBPI) and semi-automated MN scoring as previously described by Shah *et al.* and Chapman *et al.* (3,21).

Longer term

As detailed in the NanoGenoTox Dispersion Protocol (grant agreement no. 20092101, 2018) (20), ZnO ENM was dispersed by sonication (Branson Sonifier 250, \emptyset 13 mm, 400 W output power, 20 kHz) in 0.05% bovine serum albumin. Stock solution of ZnO was prepared at a concentration of 2.56 mg/ml, which was diluted in cell culture media to the required concentration (0.2–2 μ g/ml). The protocol for exposing 3D liver spheroids to ENM was recently published by Llewellyn *et al.* (5). In brief, on Day 5, 50 μ l of media was removed from the 96-well plate, taking caution not to disturb the spheroids, and replaced with 50 μ l of ZnO ENM or AFB1. The plates were then incubated at 37°C for 5 days (Figure 1). AFB1 (0.1 μ M) was used as a positive chemical control. Three days following exposure, the media was replenished. Being careful not to disrupt the settled ENM and spheroids, 50 μ l of media was aspirated from each well and replaced with 50 μ l of fresh media. On Day 10, 5 days post-ENM exposure, the spheroids were pooled and analysed for relative viable cell count (RVCC) using the TB assay and for genotoxicity using the mononuclear MN assay (as described below).

Cytotoxicity

Cell viability of the spheroids was assessed using the TB assay (GIBCO, Paisley, UK). Pooled spheroids were centrifuged at 230g for 5 min. To remove any residual media, the cell pellet was re-suspended in 1 ml PBS (GIBCO, Paisley, UK) and centrifuged at 230g for 5 min. To dissociate the spheroids, the cell pellet was re-suspended in trypsin/EDTA for 8–10 min. Fresh media was added in equal volumes to neutralise the trypsin. The cells were centrifuged at 230g for 5 min and re-suspended in fresh media. Cell viability was then analysed using the standard TB assay (22). RVCC was calculated in accordance with the OECD guidelines and that previously described by (5,15).

Liver functionality assays

Spheroid albumin and urea levels were examined to assess HepG2 and HepaRG spheroid liver-like functionality (BCG Albumin Assay Kit, MAK124 and Urea Assay Kit, MAK006, Sigma Aldrich, UK). All assays were performed as per manufacturer's instructions. However, to ensure that samples fell within the standard curve, for the urea assay, the supernatants were diluted 1:10 with urea assay. On the day of harvest, spheroids were pooled and centrifuged at 230g for 5 min. Cell culture supernatant was collected (1.5 ml) for use with the albumin and urea secretion assays. Samples were stored at -80°C until the assays were performed.

MN assay

Manual slide preparation for CBPI

Manual slides were prepared to calculate the CBPI. Glass slides were cleaned with 70% ethanol and left to air dry. Slides were prepared using the previously described cytospin method (23). In short, 100 μ l of cell suspension in PBS was added to the cytospin cassette. The cassettes were centrifuged at 500g for 5 min. Once dried, the slides were fixed with cold 90% methanol for 10 min. The slides were then left to dry overnight at room temperature and stained using 20% Giemsa stain diluted in phosphate buffer (pH 6.8). The CBPI was calculated using the Olympus BH2 microscope at $\times 100$ objective on the first 500 cells according to the OECD guidelines (15).

Preparation of slides for scoring MN frequency using the automated Metafer System

The remaining cells in PBS are then fixed and placed on slides as previously described (23). The cell density on the slide was examined accordingly using the Olympus BH2 microscope at $\times 100$ objective. Once the slides were dry, they were stored at -20°C until scoring. Prior to automated scoring using the Metafer system, 30 μ l of Vectashield Mounting Medium with 4',6-diamidino-2-phenylindole (DAPI) (Vector Laboratories, Peterborough, UK) was added in the dark and a coverslip applied. When scoring, detection of MN in binucleated (BN) or mononucleated cells were performed as previously described by Chapman *et al.* and Manshian *et al.* (21,23). A minimum of 1000 BN cells or 2000 mononucleated cells were counted per exposure dose per replicate using the principles previously established by Fenech *et al.* (24) and in accordance with the OECD guidelines (15).

Statistical analysis

All experiments were performed three times independently ($n = 3$) with data presented as mean \pm standard deviation (SD), unless stated otherwise. Statistical analysis was performed using Prism 8, GraphPad Software, Inc. Shapiro–Wilk test was used to calculate normality for each data set. For normally distributed data, either a one-way analysis of variance (ANOVA; HepG2 and HepaRG cell viability, HepG2 Cyto B; 2D and 3D HepG2 AFB1, MMS) or two-way ANOVA (HepG2 vs. HepaRG; cell viability, albumin, urea; 2D vs. 3D HepG2 AFB1, MMS) with Bonferroni *post hoc* were used. Fisher's Exact test was used to determine statistical significance of MN/BN% and MN/MN% when compared to the untreated control ($P < 0.05$). For non-parametric data, a Kruskal–Wallis test was used to calculate significance when there were more than two variables (MN/MN% vs. MN/BN%, RVCC vs. CBPI, ZnO ENM) or to compare to the untreated control (RVCC and CBPI; $P < 0.05$).

Results

Characterisation of HepG2 and HepaRG 3D models for genotoxic assessment using the MN assay

HepG2 and HepaRG cells are commonly used in liver toxicology studies due to their capacity to retain many of the metabolic functions of human liver cells. Urea and albumin production were assessed using the supernatant from both models on Days 4, 7, 10 and 14. As demonstrated in Figure 2A, there was a significant difference between the HepaRG and HepG2 cells ($P < 0.001$). Bonferroni's *post hoc* test further revealed significant differences in the level of urea on Days 1 and 7 between the two cell types ($P < 0.033$). HepG2 spheroids demonstrated an overall reduced capacity to produce urea compared to HepaRG; however, this difference was less notable after 10 days of culture. Additionally, no significant difference in albumin production was observed between the two cell types over the 14-day period (Figure 2B). Within the HepaRG model, a significant reduction in cell viability was observed on Days 10 and 14 when compared to Day 1 ($P < 0.05$); no significant differences were observed for HepG2 spheroids over the 14 days when compared to Day 1 (Figure 2C). When then two models were compared, there was a main effect for time ($P < 0.001$); however, over that time period, *post hoc* analysis demonstrated no significant difference in viability between the two models (Figure 2C).

As currently described by the OECD test guideline 487 for the 'in vitro mammalian cell micronucleus assay', it is necessary to ensure that, after cells have been exposed to a chemical, they must

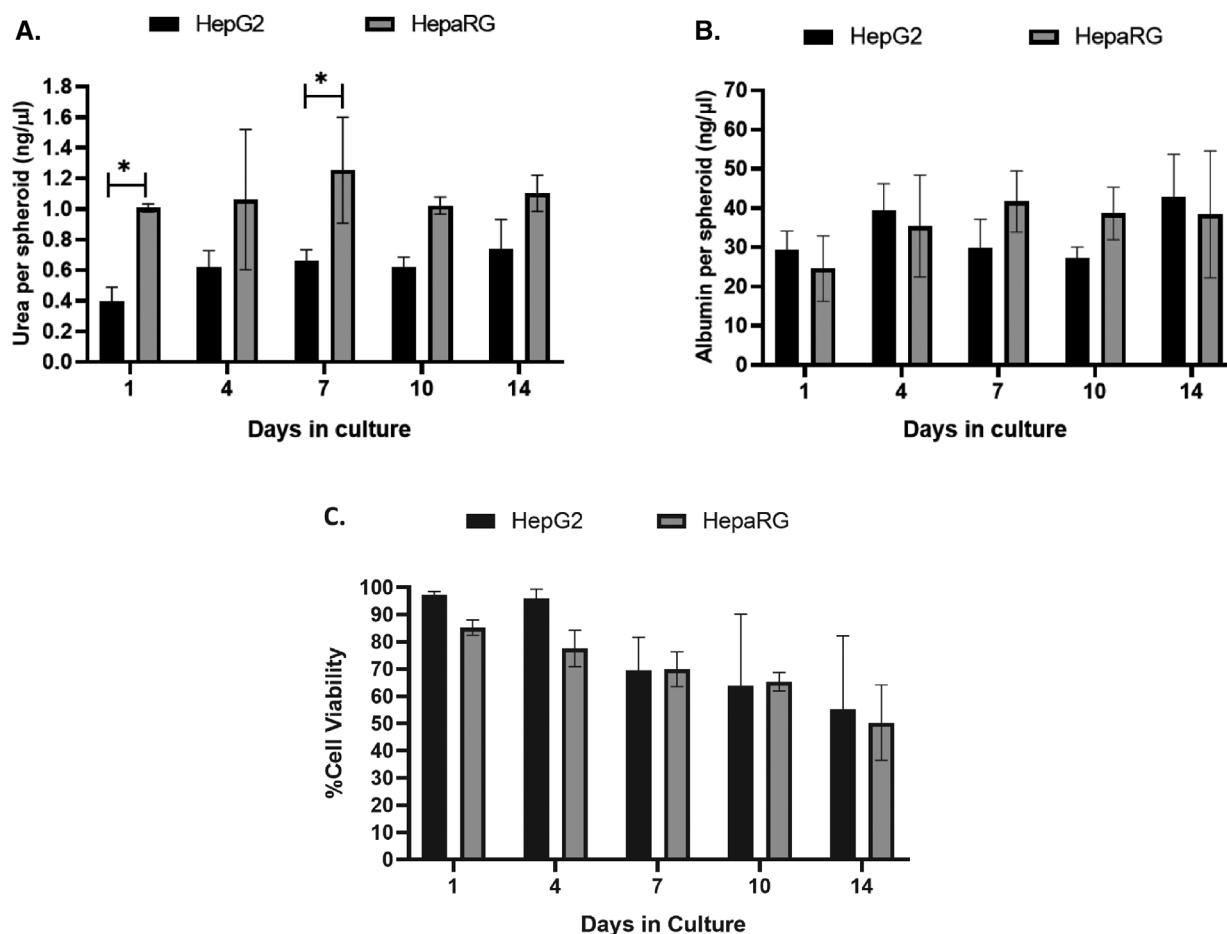


Fig. 2. Characterisation of HepG2 and HepaRG liver cells over 14 days in culture. (A) Urea and (B) albumin production and (C) viability of 3D HepG2 and HepaRG spheroids were evaluated over 14 days. Statistical differences between HepG2 and HepaRG spheroids were analysed using two-way ANOVA with Bonferroni *post hoc* (* $P < 0.05$). Data shown are expressed as mean \pm SD, $n = 3$.

undergo mitosis prior to being scored. The addition of Cyto B prior to nuclear division blocks the actin ring filaments, preventing the complete formation of two new daughter cells, resulting in the formation of a BN cell. Figure 3A and B demonstrates the optimisation of the incorporation of Cyto B into the CBMN assay in HepG2 3D spheroids. When evaluating the most appropriate Cyto B concentration to use, a small (1.997%) yet statistically significant increase in the frequency of BN cells was recorded when exposed to 9 $\mu\text{g}/\text{ml}$ ($P = 0.021$) when compared to 6 $\mu\text{g}/\text{ml}$ of Cyto B (Figure 3A). However, upon visual assessment following exposure to 9 $\mu\text{g}/\text{ml}$, the spheroids displayed irregular morphology demonstrating loss of integrity of the outer layers and evidence of membrane blebbing that was not observed in cells treated with 6 $\mu\text{g}/\text{ml}$ (data not shown). Therefore, 6 $\mu\text{g}/\text{ml}$ was selected for experiments going forward. In addition to concentration, it is also important to consider the time of Cyto B application. As illustrated in Figure 3B, whilst no significant cytotoxicity was observed at any time point, a significantly higher BN cell frequency was apparent at 24 h post-treatment than that compared with any other time point ($P < 0.01$).

To determine the proliferative capacity of HepaRG spheroids, cells were exposed to increasing concentrations of Cyto B for 24 and 30 h to capture a full cell cycle. No statistically significant differences were observed between the two time points or at any concentration

of Cyto B for either genotoxicity or cytotoxicity (Figure 3C). However, what was apparent was the very low proliferative capacity of differentiated HepaRG 3D spheroids, which regardless of Cyto B concentration or exposure time, generated no more than a 9% BN cell frequency compared to 31% observed in HepG2 spheroids. This low induction of BN cells deems the HepaRG spheroid model unsuitable for genotoxicity assessment using the MN assay. Therefore, HepG2 cell spheroids were selected for further development as a model for longer-term ENM exposures.

HepG2 3D liver model demonstrates increased sensitivity to pro-carcinogens compared to HepG2 monolayers following acute exposures.

To investigate the sensitivity of 3D spheroids to a known genotoxic insult, both 2D and 3D HepG2 models were exposed to increasing concentrations of the well-known liver carcinogen AFB1 for 24 h and analysed using the CBMN assay. Figure 4A demonstrates a significant dose-dependent increase in MN frequency following exposure to AFB1 for both 2D ($P < 0.001$; 0.05–0.2 μM) and 3D ($P < 0.05$; 0.025–0.2 μM) HepG2 models when compared to the untreated control. When both 2D and 3D models were compared, the 3D model demonstrates a greater genotoxic effect. Bonferroni *post hoc* revealed a significant difference in MN frequency

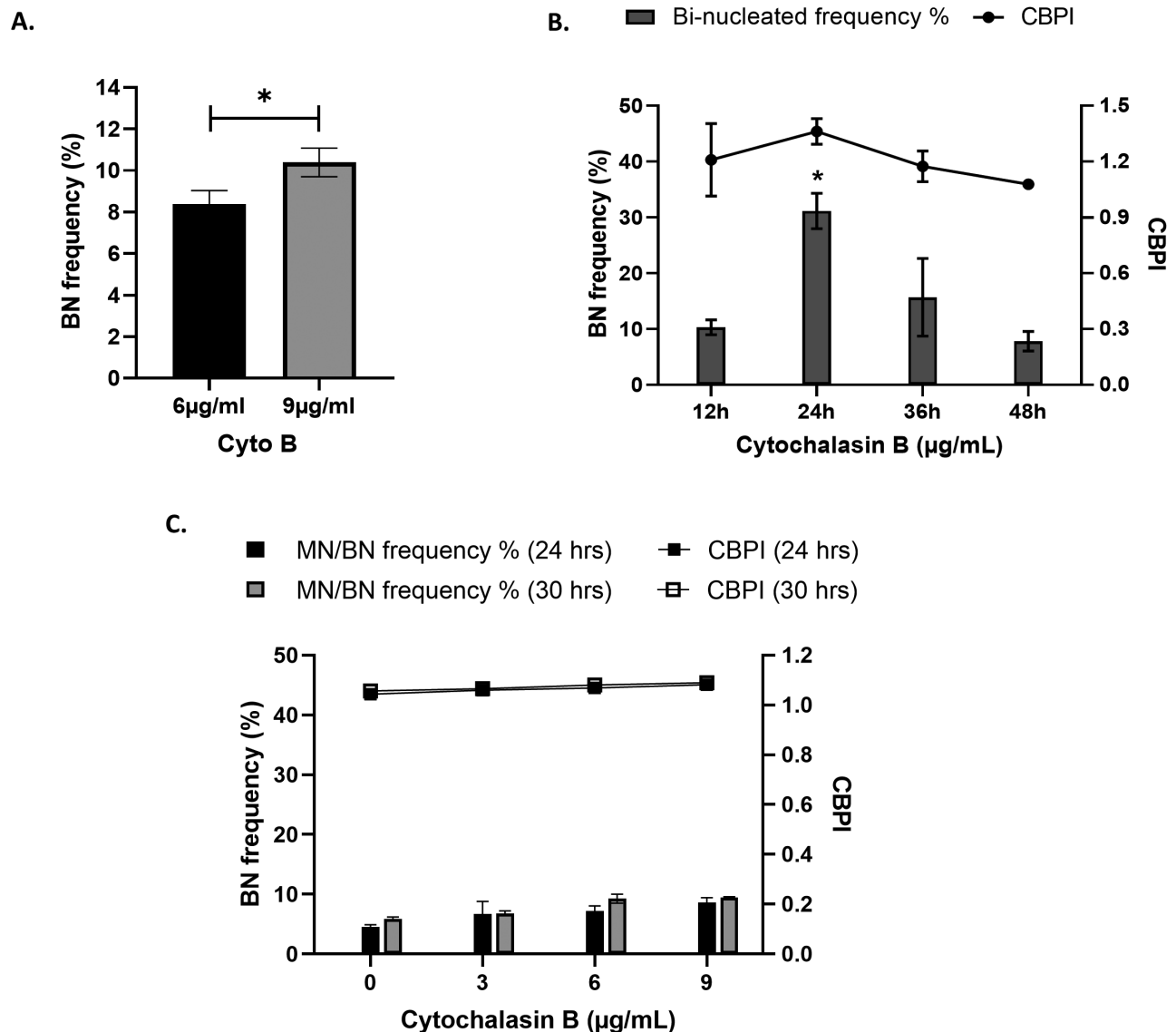


Fig. 3. Optimisation of Cyto B application for use with the CBMN assay. HepG2 3D liver spheroids were exposed to (A) 6 and 9 µg/ml Cyto B for 24 h and (B) 6 µg/ml Cyto B for 12, 24, 36 and 48 h and analysed for percentage BN cell frequency. Statistical differences were analysed using (A) unpaired *t*-test ($*P = 0.021$) and (B) one-way ANOVA with Bonferroni *post hoc* ($*P < 0.01$). (C) HepaRG spheroids were exposed to increasing concentrations of Cyto B (3, 6 and 9 µg/ml) for 24 and 30 h and analysed for percentage BN cell frequency and CBPI. Data shown are expressed as mean \pm SD, $n = 2$.

detected between both 2D and 3D HepG2 cells at 0.025–0.2 µM ($P < 0.001$). At top dose (0.2 µM) in the 2D model, there is 3-fold (3.1) difference in MN when compared to the untreated control; on the other hand, in the 3D model, the MN frequency is nearly 4-fold (3.7) higher than the untreated control. The CBPI demonstrates no cytotoxicity as a result of AFB1 over the concentration range applied. This data demonstrates that 3D HepG2 spheroids are more sensitive to the DNA damage induced by AFB1 than the 2D monoculture. It is suggested that this may be due to the increased metabolic activity of 3D HepG2 models previously demonstrated by Shah *et al.* (3) and, therefore, they are more efficient at converting AFB1 to the genotoxic metabolite than the same cells grown as 2D monocultures.

To investigate whether 3D HepG2 spheroids also demonstrated increased sensitivity to DNA damage induced by direct-acting genotoxins, both cell culture formats were exposed to increasing concentrations of the alkylating agent and direct-acting genotoxin MMS for 24 h (Figure 4B). Similarly, as demonstrated with AFB1,

Figure 4B demonstrates a significant dose-dependent increase in MN frequency for both 2D ($P < 0.05$; 20–30 µM) and 3D ($P < 0.001$; 10–30 µM) HepG2 models when compared to the untreated control. No cytotoxicity was observed following MMS treatment. In contrast, Bonferroni *post hoc* testing revealed a significant difference in MN frequency when comparing the induction of DNA damage between the 2D and 3D model formats at 10 and 15 µM ($P < 0.05$). Generally, however, there was little difference between the fold difference in the induction of genotoxicity over the control when comparing the 2D and 3D model formats, thus indicating that they had a very similar sensitivity to the induction of DNA damage by the direct-acting genotoxin MMS.

Modified hanging drop approach supports longer-term viability of HepG2 spheroids

To maintain cell viability in the hanging drop during short-term exposures, 6 µl of media was added to each 20 µl drop on Day 3;

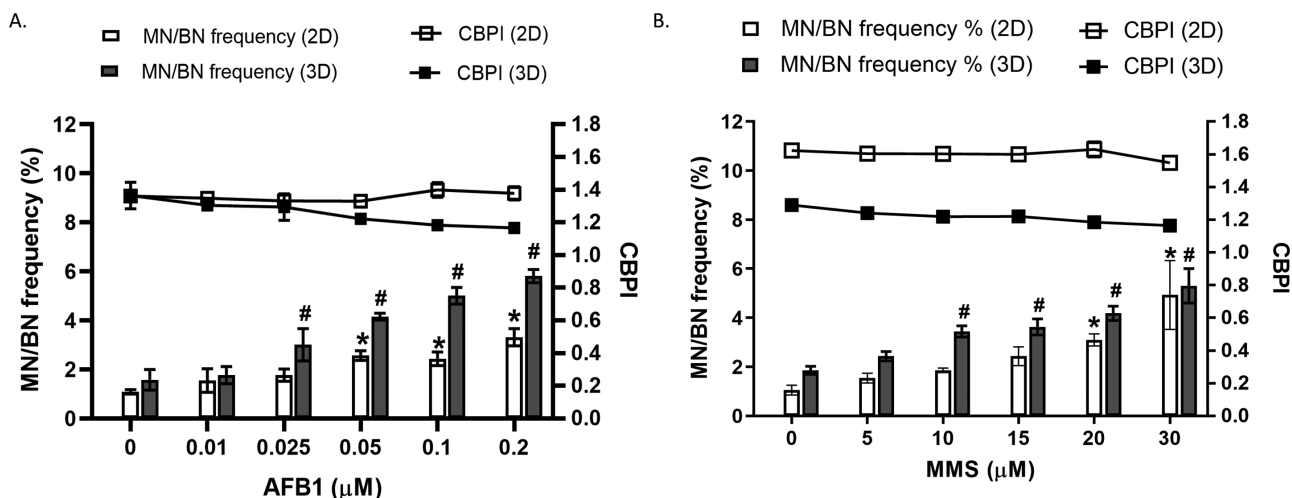


Fig. 4. Assessment of micronuclei frequency in 2D monocultures and 3D HepG2 spheroids following a genotoxic insult. 2D HepG2 monocultures and 3D spheroids were exposed to increasing concentrations of (A) Aflatoxin B1 (0–0.2 μM) and (B) MMS (0–30 μM) for 24 h and analysed for MN in BN cells (MN/BN%) and CBPI. Statistical significance was compared to the untreated control and was analysed by one-way ANOVA with Bonferroni *post hoc* (* $P < 0.007$). Data shown are expressed as mean \pm SD, $n = 3$.

however, for longer-term exposures, continued addition of media to the droplet would result in the droplet becoming too large and, thus, would fall from the lid of the petri dish. In an effort to overcome this, spheroids were seeded onto the lid of a 96-well plate. After 3 days, 100 μl of fresh media was added to the base of each well of the plate. The spheroids were then transferred into each of the wells containing fresh media by centrifugation. As seen in Figure 5A, after 72 h, the HepG2 cells within the spheroid begin to elongate and form protrusions in an effort to reform a monolayer on the base of the 96-well plate. To combat this issue and extend the longevity of the spheroid model, a layer of agarose (1.5% agarose in DMEM without phenol red) was added to the base of the 96-well plate (Figure 5C). Following the addition of the agarose layer, the spheroid forms a defined round spheroid, with no protrusions (Figure 5B).

Table 1 below demonstrates the results of a comparison study of spheroid viability and urea and albumin production in both the presence and absence of an agarose layer added to the base of the 96-well plate. A significant increase in urea production was observed on day 10 in the presence of agarose ($P = 0.014$). No difference was observed between the two methods for albumin. Similarly, when comparing the viability at each time point, no significance was observed; however, a significant difference is demonstrated in the total mean difference with cell viability in the presence and absence of agarose ($P = 0.013$; Figure 5D). To maintain the structural integrity of the spheroids and prolong viability of the culture over 10 days, it was concluded that the addition of a 1.5% agarose layer to the base of the 96-well plates prior to the addition of media was necessary to support longer-term exposures. This approach was implemented for the remainder of this study.

***In vitro* MN assay for longer-term ENM genotoxicity assessment**

As demonstrated previously, the CBMN version of the MN assay with CBPI was performed, where, after a 24-h exposure, Cyto B was added for an additional 24 h, which results in the formation of BN cells. However, it was postulated that the damage encountered following longer-term exposure may occur at an earlier stage; therefore, the addition of Cyto B and counting MN in BN cells after a 5-day exposure could fail to accurately capture the true genotoxic insult.

To investigate this, firstly using the CBMN approach, all MN in BN cells (MN/BN%) were scored with CBPI calculated as a measure of cytotoxicity (Figure 6A). A non-dose-dependent induction of genotoxicity was observed, with the only significant difference noted between the untreated control and the lowest concentration 0.2 μg/ml of ZnO ($P = 0.037$) and, as expected, with the positive control (0.1 μM AFB1, $P < 0.001$). Second, in the absence of Cyto B, cells were scored for MN in mononucleated cells (MN/MN %) and RVCC calculated as the measure of cytotoxicity (Figure 6B). A significant increase in MN frequency was observed in all concentrations of ZnO ENM compared to the untreated control ($P < 0.007$, 0.025–30 μg/ml). Additionally, when compared, a significant difference ($P = 0.021$) was observed between the two methods for assessing MN frequency (MN/BN% and MN/MN%). No significant difference was observed between the two methods for cytotoxicity (CBPI and RVCC).

Discussion

The purpose of this study was to develop a 3D liver spheroid model that would support ENM genotoxicity assessment following exposure over a prolonged period (i.e. up to 5 days). Over the last decade, there have been a number of protocols published demonstrating the development of 3D liver models. However, a model that supports DNA damage testing using the MN assay following longer-term ENM exposure and associated genotoxic assessment using the MN assay is yet to be established. Herein describes a method that supports the growth and maintenance of 3D liver spheroids over a total of 10, allowing for an extended exposure period of 5 days.

In an effort to replace, reduce and refine the reliance on animal experimentation, substantial efforts have been placed on developing 3D *in vitro* model systems that demonstrate greater physiological relevance and that mimic the liver-like functionality and metabolism seen *in vivo*. It is thought that the enhanced features of 3D models are due to the compact density of the spheroid, complex cell to cell interactions and signalling, making them an ideal candidate to improve the state-of-the-art for genotoxicological testing (25). Using

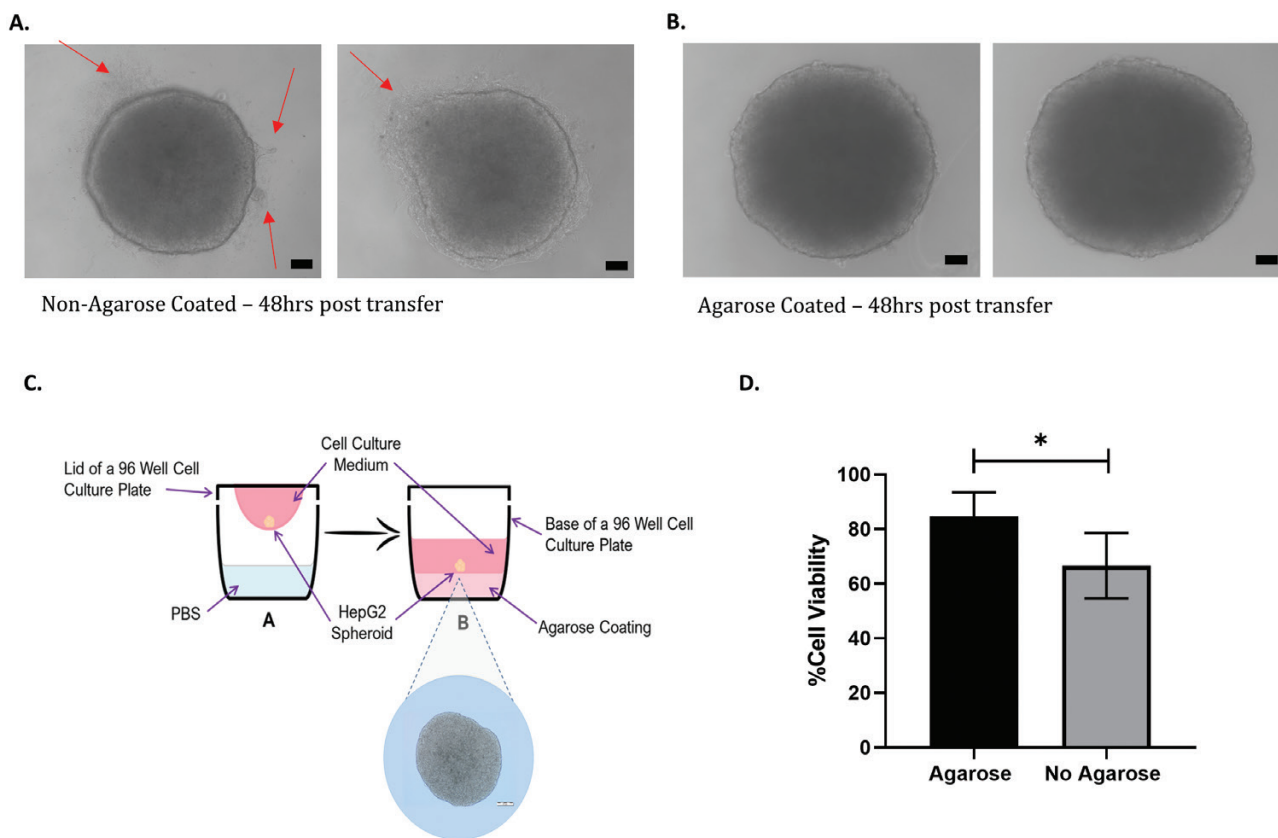


Fig. 5. Modification of the hanging drop method to support longer-term ENM exposures. Spheroids were grown on the lid of a 96-well plate for 3 days; on Day 4, they were transferred by centrifugation into the base of the plate containing media that was either (A) not coated in agarose or (B) coated in agarose. Images of the spheroids were obtained using light microscopy ($\times 40$ objective) after 72 h. Changes to spheroid structure are denoted by red arrows. Scale bar 20 μm . (C) Schematic of the modified hanging drop method with the addition of a 1.5% agarose layer that is used for the remainder of the study. (D) Viability of HepG2 spheroids was calculated using the Trypan Blue assay in the presence and absence of agarose. Statistical significance was determined using an unpaired *t*-test ($*P < 0.01$). Data shown are expressed as mean \pm SD, $n = 3$.

Table 1. Characterisation of 3D liver spheroids in the presence and absence of agarose.

HepG2 cells	No Agarose		Agarose	
	Day 7	Day 10	Day 7	Day 10
% Viability (95% CI)	73.5% (90.07–56.03)	60.09% (93.99–26.20)	89.98% (102.03–77.95)	79.6% (102.42–56.82)
Albumin per spheroid (ng/ μl) (95% CI)	32.56 (39.17–25.94)	29.83 (33.50–26.15)	34.23 (63.99–4.46)	48.51 (94.82–2.19)
Urea per spheroid (ng/ μl) (95% CI)	0.64 (0.70–0.58)	0.63 (0.68–0.58)	0.66 (0.79–0.52)	0.82* (1.09–0.54)

*Significant at $P < 0.014$. CI, confidence interval.

liver-specific functionality assays, our data demonstrates that 3D HepG2 spheroids maintain functionality for up to 14 days in culture as fully formed spheroids. HepaRG liver cells are widely used in drug development and toxicology, as they retain liver-like functionality. Using the same protocol, we generated a differentiated HepaRG 3D model and the two models showed comparable liver-like functionality. However, there was some variance between the two models in urea production, with the HepaRG model demonstrating the ability to maintain consistently high levels of urea over the 14 days, albeit only significant at Days 1 and 7. There was no significant difference in albumin levels over the 14 days between the two models;

however, HepG2 levels appear to be lower. No differences in cell viability were observed over the 14 days. Based on this metabolic data, it would appear that the HepaRG model exhibits a slight advantage over HepG2, which agrees with observations by others, although they are largely comparable (12).

An important feature of the MN assay is the requirement for cells to demonstrate a high proliferative capacity. This study demonstrates a basal-level BN cell frequency following treatment with 6 $\mu\text{g}/\text{ml}$ Cyto B in 3D HepG2 cells, indicating that the cells within the spheroid (particularly at the periphery) are actively proliferating. Whilst this is lower than typically observed in 2D culture,

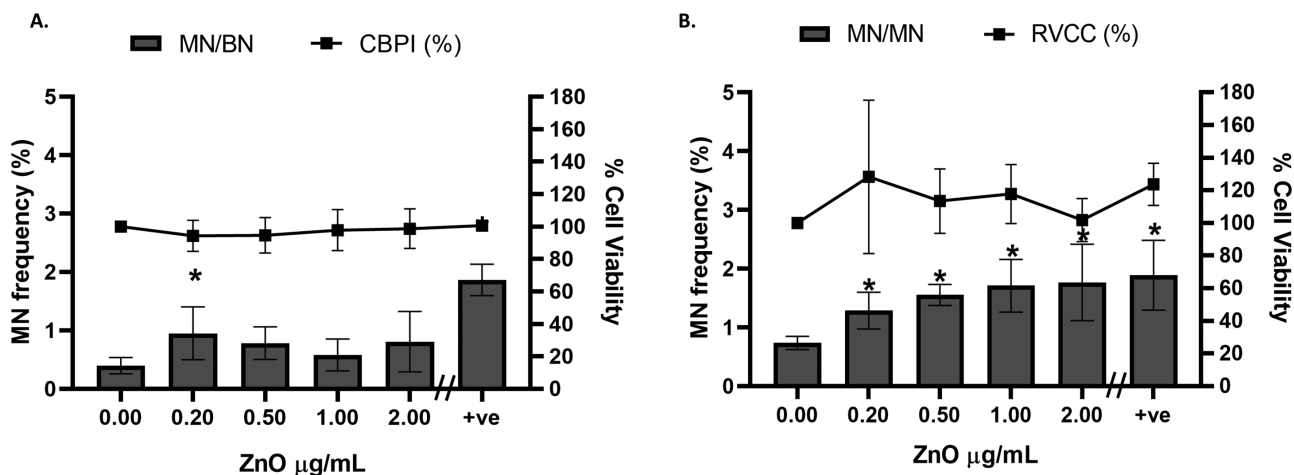


Fig. 6. Optimisation of the *in vitro* micronucleus assay for longer-term ENM genotoxicity assessment. 3D HepG2 spheroids were exposed to increasing concentrations of ZnO ENM (0–2.0 $\mu\text{g/ml}$) and 0.1 μM AFB1 (positive control, +ve) for 5 days and analysed for MN in (A) BN cells (MN/BN %, $n = 2$) with CBPI ($n = 2$) and (B) mononucleated cells (MN/MN %, $n = 3$) with RVCC. Statistical significance compared to the untreated control was analysed by Fisher's exact ($*P < 0.05$). Data shown are expressed as mean \pm SD.

this level of proliferation is sufficient to support the MN assay. We found that 24 h was the optimal time point to capture cells that have been arrested after one cell cycle and presented as BN cells. In contrast to this, our data showed that HepaRG cells exhibit a very low proliferation rate. Despite adjusting the Cyto B concentration and exposure duration, the BN frequency for 24 h was 7.2%, whilst, for HepG2 spheroids, it reached 31.13%. The very low proliferative capacity of differentiated HepaRG 3D spheroids deems them unsuitable for genotoxicity assessment using the MN assay. Interestingly, as demonstrated by others, this does not seem to be the case when HepaRG cells are cultured in 2D (26,27). However, for 3D spheroids, this data agrees with Mandon *et al.*, who demonstrated that HepaRG 3D spheroids had low levels of DNA topoisomerase II, a specific marker for cell division (2), confirming the quiescent nature of differentiated HepaRG spheroids. Therefore, if the endpoint for analysis is the MN assay, HepaRG in 3D spheroid format are not a practical cell model to be used. Jossé *et al.* previously described the adaptation of the HepaRG cell line to the MN assay for genotoxicity testing, which was facilitated by treating the HepaRG cells in 2D with epidermal growth factor to stimulate cell proliferation (27). To the best of our knowledge, this has not been explored in 3D HepaRG models but offers a potential strategy to overcome the quiescent nature of 3D HepaRG spheroids.

Shah *et al.* have previously determined that HepG2 spheroids demonstrate increased efficacy over the standard 2D monoculture and can readily metabolise the pro-carcinogens B[a]-P and PhIP into their genotoxic metabolites, thus initiating an enhanced genotoxic response compared to 2D cultures (3). Similarly, our data confirms that 3D HepG2 spheroids detect greater levels of genotoxicity at low concentrations of the liver pro-carcinogen AFB1 compared to 2D monocultures. This may be due to the increase in metabolic function observed in 3D models (3,28,29). We also establish that the direct-acting genotoxin, MMS, induced similar levels of genotoxicity in both 2D and 3D models. The data demonstrates that the elevated number of MN observed in the 3D models with pro-carcinogens is not an artefact of the 3D system (e.g. DNA damage induced through enhanced metabolism). Although no significant cytotoxicity was observed between the two models, the CBPI was lower in the 3D spheroid model than the 2D monoculture following both AFB1 and

MMS exposure. This coincides with that observed by Shah *et al.* who suggested that, due to the compact nature of the spheroid, it is primarily the outer layer of cells that are rapidly dividing, whereas the cells within the spheroid core have a lower proliferation index (3).

In an effort to increase the longevity of the 3D culture, spheroids were seeded onto the lid of a 96-well plate as opposed to the lid of a square petri dish as previously described by Shah *et al.* (3). Following a 3-day incubation period to allow for spheroid formation, the spheroids were dropped by centrifugation into each well of the 96-well plate, which contained 100 μl media. However, during visual examination of the HepG2 spheroids, it was apparent that the naturally adherent nature of the HepG2 cells began affecting the structural integrity of the spheroid. The spheroids began to form protrusions in an effort to reform a monolayer on the base of each well. HepG2 cells are, by nature, an adherent cell line and, when given the opportunity to attach to a surface, they will try to form a monolayer as demonstrated in the present study. To overcome this obstacle, 1.5% agarose was added to the base of each well prior to the addition of media. A small change was demonstrated in urea production on day 10 that was in favour of the presence of agarose. This agrees with numerous studies that demonstrate the use of agarose in 3D spheroid formation (30–32). Interestingly, our data also showed an increase in cell viability when agarose was added, similarly to that observed by Friedrich *et al.* who noted that spheroid formation and growth were superior when wells were coated in agarose (31). It was also clear that the integrity and structure of the spheroids were not compromised. Therefore, it was determined for this reason that we would use the modified hanging drop setup going forward. Agarose not only inhibits cell adhesion and is non-toxic but also offers a cost-effective alternative to ultra-low adhesion plates.

It is evident from our data that using the CBMN form of the MN assay to measure genotoxicity following longer-term exposures (over 24 h) underestimates the true level of genotoxicity. A significant difference between the two methods was observed and there is a clear trend of a higher MN frequency in mononucleated cells. When compared to the untreated control, there was a significant increase in MN frequency in mononucleated cells at all ZnO ENM concentrations. In contrast, a significant increase in MN frequency in BN cells was only observed at the lower concentration

(0.2 µg/ml). It was hypothesised that the damage encountered is occurring early on and, therefore, the addition of Cyto B and counting of MN in BN cells on the final day is missing the initial genotoxic insult. Following longer-term exposures, cells will have undergone numerous cell divisions and, thus, the addition of Cyto B will only capture the cells that have divided in the last cell cycle. According to the OECD test guideline 487, measuring cytotoxicity by CBPI should only be used following the addition of Cyto B (15). Therefore, we suggest that, as an alternative, when performing longer-term exposures, cytotoxicity is measured using an alternative method, such as RVCC using the TB assay instead. It is noted that the OECD test guideline 487 suggests relative population doubling (RPD) or relative increase in cell count (RICC) as alternative methods when Cyto B is not used to ensure that the cells have undergone cell division after extended treatment periods. However, based on the nature of the experimental setup of this 3D spheroid assay, it would be impractical and costly to set up a satellite plate of spheroids for every concentration to perform the RPD. The RICC was also considered, however, as the cells are replicating and dividing in the hanging drop during the spheroid formation phase, that is, the first 4 days post-seeding and prior to exposure, this would also underestimate cytotoxicity. Consequently, due to the complex structure of the 3D liver models, the RVCC was calculated using the TB assay. This method was previously described by Roy *et al.* as a measure of cytotoxicity in the 3D RSMN assay (33). The authors measure cytotoxicity using both the CBPI and RVCC, identifying that the RVCC was the more sensitive measure of cell viability for treatment with *N*-ethyl-*N*-nitrosourea and 2-ethyl-1,3-hexanediol in their 3D skin model. Our data demonstrates no significant difference between the RVCC and CBPI and, therefore, is put forward as a feasible method for measuring cytotoxicity when assessing longer-term genotoxicity using the MN assay in 3D liver spheroid models.

In recent decades, there has been a rapid development and implementation of a variety of ENMs used in fields such as food and agricultural industry, medical devices and drug delivery. The investigation of the potential genotoxicity of these materials over acute and longer-term exposure scenarios is a vital component of their safety assessment. The *in vitro* MN assay is deemed the gold standard when assessing chromosomal damage induction (specifically clastogenicity and/or aneugenicity); however, this method was originally established for use with chemicals and 2D culture systems. There are many limitations of 2D systems for genotoxicity assessment, which have previously been extensively reviewed (34). In addition, the regulated genotoxicity *in vitro* testing methods (i.e. for pharmaceuticals) demonstrate ‘low specificity’ and ‘misleading false positives’ which, at present, results in the requirement for additional animal tests (1,35). It is vital that there is continued development of novel advanced *in vitro* test systems and robust protocols, such as 3D *in vitro* models, that can be used as reliable alternatives to animal testing. More importantly, the European directive (Directive 2010/63/EU) driving the ‘3Rs’ to reduce, replace and refine *in vivo* animal-based experiments aims to advance *in vitro*-based systems as alternative methods to provide predictive and reliable results for hazard assessment (36). With advancements in 3D *in vitro* systems and continuous development of novel ENMs, it is essential that we also adapt our current methodologies to evolve with the field. Investigative studies into the use of the MN assay for short-term ENM exposures using the CBMN assay have identified that Cyto B can halt cellular uptake of the novel materials (13,18). Therefore, it was established that

Cyto B should only be added to the cells post-ENM exposure and not as a co-exposure with the ENM, a method that is commonly performed with chemical compounds. Recently, Wills *et al.* have successfully adapted the RSMN version of the MN assay for the genotoxic assessment of silica nanoparticles in both 2D and 3D *in vitro* models following 24-h exposures (17). Having modified the 3D liver spheroid system and accompanying MN assay to support a longer-term ENM exposure regime, this study demonstrates a dose-dependent increase in the frequency of MN following 5 days of exposure to ZnO ENM. This would not have been observed had methodology alterations not been made. Careful consideration must be taken when using the ‘cytokinesis-block’ version of this assay for longer-term exposure regimes, as any DNA damage induced within the first few cell cycles is distributed across the mononucleated cell population as opposed to being retained and scored within the BN cells. This study demonstrates the potential to score false negatives, as the DNA damage accumulated over the period of chronic exposure can be masked when using the CBMN version of the MN assay.

In conclusion, this study has developed a physiologically relevant, advanced 3D HepG2 hepatocyte model that demonstrates increased efficacy for genotoxicity over 2D monoculture. It also maintains stability and liver functionality over extended culture periods. Herein, the present study has demonstrated the suitability of this model for assessing genotoxicity of direct and indirect acting mutagens using the regulatory approved *in vitro* MN assay. Additionally, taking into consideration the necessary adaptations, our study demonstrates that this model can also be used for the genotoxic assessment of ENMs using the MN assay.

Acknowledgements

The authors would like to acknowledge that this research has received funding from the Horizon 2020 Research and Innovation Programme for the PATROLS project, under grant agreement no. 760813.

Conflict of interest statement: The authors declare no competing interests.

Availability of data and material

The authors will freely release all data underlying the published paper upon direct request to the corresponding author.

Author contributions

S.H.D and G.J. J conceived the project and designed the experiments. U.K.S, S.L., T.C., S.J.E., A.S.A.A. and G.E.C. performed the experiments and collected and analysed the data. G.E.C., U.K.S., S.L., S.H.D and M.J.D.C co-wrote the paper. All authors discussed the results and reviewed the manuscript.

References

1. Pfulher, S., van Benthem, J., Curren, R., *et al.* (2020) Use of *in vitro* 3D tissue models in genotoxicity testing: strategic fit, validation status and way forward. Report of the working group from the 7th International Workshop on Genotoxicity Testing (IWGT). *Mutat. Res.*, 850–851, 503135.
2. Mandon, M., Huet, S., Dubreil, E., Fessard, V. and Le Hégarat, L. (2019) Three-dimensional HepaRG spheroids as a liver model to study human genotoxicity *in vitro* with the single cell gel electrophoresis assay. *Sci. Rep.*, 9, 10548.
3. Shah, U.K., Mallia, J. de O., Singh, N., Chapman, K.E., Doak, S.H. and Jenkins, G.J.S. (2018) A three-dimensional *in vitro* HepG2 cells liver spheroid model for genotoxicity studies. *Mutat. Res. Genet. Toxicol. Environ. Mutagen.*, 834, 35–41. doi:10.1016/j.mrgentox.2018.06.020.

4. Štampar, M., Tomc, J., Filipič, M. and Žegura, B. (2019) Development of in vitro 3D cell model from hepatocellular carcinoma (HepG2) cell line and its application for genotoxicity testing. *Arch. Toxicol.*, 93, 3321–3333.
5. Llewellyn, S. V., Conway, G.E., Shah, U.K., Evans, S.J., Jenkins, G.J.S., Clift, M.J.D. and Doak, S.H. (2020) Advanced 3D liver models for in vitro genotoxicity testing following long-term nanomaterial exposure. *J. Vis. Exp.* 2020, 1–10.
6. Yamada, K. M. and Cukierman, E. (2007) Modeling tissue morphogenesis and cancer in 3D. *Cell*, 130, 601–610.
7. Lauschke, V.M., Hendriks, D.F.G., Bell, C.C., Andersson, T.B. and Ingelman-Sundberg, M. (2016) Novel 3D culture systems for studies of human liver function and assessments of the hepatotoxicity of drugs and drug candidates. *Chem. Res. Toxicol.*, 29, 1936–1955.
8. Schwartz, R. E., Fleming, H. E., Khetani, S. R. and Bhatia, S. N. (2014) Pluripotent stem cell-derived hepatocyte-like cells. *Biotechnol. Adv.*, 32, 504–513.
9. Kondo, Y., Iwao, T., Nakamura, K., et al. (2014) An efficient method for differentiation of human induced pluripotent stem cells into hepatocyte-like cells retaining drug metabolizing activity. *Drug Metab. Pharmacokin.*, 29, 237–243.
10. Bell, C. C., Hendriks, D. F., Moro, S. M., et al. (2016) Characterization of primary human hepatocyte spheroids as a model system for drug-induced liver injury, liver function and disease. *Sci. Rep.*, 6, 25187.
11. Keramanzadeh, A., Løhr, M., Roursgaard, M., Messner, S., Gunness, P., Kelm, J. M., Møller, P., Stone, V. and Loft, S. (2014) Hepatic toxicology following single and multiple exposure of engineered nanomaterials utilising a novel primary human 3D liver microtissue model. *Part. Fibre Toxicol.*, 11, 56.
12. Kammerer, S. and Küpper, J.-H. (2018) Human hepatocyte systems for in vitro toxicology analysis. *J. Cell. Biotechnol.*, 3, 85–93. doi:10.3233/jcb-179012.
13. Doak, S.H., Manshian, B., Jenkins, G.J.S. and Singh, N. (2012) In vitro genotoxicity testing strategy for nanomaterials and the adaptation of current OECD guidelines. *Mutat. Res. Genet. Toxicol. Environ. Mutagen.*, 745, 104–111.
14. Doherty, A., Bryce, S.M. and Bemis, J.C. (2016) *The In Vitro Micronucleus Assay*. Elsevier Inc., Amsterdam, pp. 161–205.
15. OECD (2016) *Test No. 487: In Vitro Mammalian Cell Micronucleus Test*. OECD Publishing, Paris, p. 29.
16. Curren, R. D., Mun, G. C., Gibson, D. P. and Aardema, M. J. (2006) Development of a method for assessing micronucleus induction in a 3D human skin model (EpiDerm™). *Mutat. Res.*, 607, 192–204.
17. Wills, J.W., Hondow, N., Thomas, A.D., et al. (2016) Genetic toxicity assessment of engineered nanoparticles using a 3D in vitro skin model (EpiDerm™). *Part. Fibre Toxicol.*, 13, 50.
18. Doak, S. H., Griffiths, S. M., Manshian, B., Singh, N., Williams, P. M., Brown, A. P. and Jenkins, G. J. (2009) Confounding experimental considerations in nanogenotoxicology. *Mutagenesis*, 24, 285–293.
19. Elespuru, R., Pfuhler, S., Aardema, M. J., et al. (2018) Genotoxicity assessment of nanomaterials: recommendations on best practices, assays, and methods. *Toxicol. Sci.*, 164, 391–416.
20. Jensen, K.A. and Thieret, N. (2014) *The NANOGENOTOX Dispersion Protocol for NANoREG*, 13. <http://safenano.re.kr/download.do?SEQ=175> (accessed April 15, 2020).
21. Chapman, K. E., Thomas, A. D., Wills, J. W., Pfuhler, S., Doak, S. H. and Jenkins, G. J. (2014) Automation and validation of micronucleus detection in the 3D EpiDerm™ human reconstructed skin assay and correlation with 2D dose responses. *Mutagenesis*, 29, 165–175.
22. Louis, K. S. and Siegel, A. C. (2011) Cell viability analysis using trypan blue: manual and automated methods. *Methods Mol. Biol.*, 740, 7–12.
23. Manshian, B. B., Singh, N. and Doak, S. H. (2013) The in vitro micronucleus assay and kinetochore staining: methodology and criteria for the accurate assessment of genotoxicity and cytotoxicity. *Methods Mol. Biol.*, 1044, 269–289.
24. Fenech, M., Chang, W. P., Kirsch-Volders, M., Holland, N., Bonassi, S. and Zeiger, E.; HUMAN MICRONUCLEUS PROJECT. (2003) HUMN project: detailed description of the scoring criteria for the cytokinesis-block micronucleus assay using isolated human lymphocyte cultures. *Mutat. Res.*, 534, 65–75.
25. Otieno, M.A., Gan, J. and Proctor, W. (2018) Status and future of 3D cell culture in toxicity testing. In Chen M., Will Y. (eds.), *Drug-Induced Liver Toxicity. Methods in Pharmacology and Toxicology*. Humana Press Inc., New York, pp. 249–261. Accessed 29 February 2020.
26. Le Hégarat, L., Mourot, A., Huet, S., Vasseur, L., Camus, S., Chesné, C. and Fessard, V. (2014) Performance of comet and micronucleus assays in metabolic competent HepaRG cells to predict in vivo genotoxicity. *Toxicol. Sci.*, 138, 300–309.
27. Jossé, R., Rogue, A., Lorge, E. and Guillouzo, A. (2012) An adaptation of the human HepaRG cells to the in vitro micronucleus assay. *Mutagenesis*, 27, 295–304.
28. Foster, A. J., Chouhan, B., Regan, S. L., et al. (2019) Integrated in vitro models for hepatic safety and metabolism: evaluation of a human Liver-Chip and liver spheroid. *Arch. Toxicol.*, 93, 1021–1037.
29. Bell, C. C., Dankers, A. C. A., Lauschke, V. M., et al. (2018) Comparison of hepatic 2D sandwich cultures and 3D spheroids for long-term toxicity applications: a multicenter study. *Toxicol. Sci.*, 162, 655–666.
30. Mirab, F., Kang, Y. J. and Majd, S. (2019) Preparation and characterization of size-controlled glioma spheroids using agarose hydrogel microwells. *PLoS One*, 14, e0211078.
31. Friedrich, J., Seidel, C., Ebner, R. and Kunz-Schughart, L. A. (2009) Spheroid-based drug screen: considerations and practical approach. *Nat. Protoc.*, 4, 309–324.
32. Wenzel, C., Otto, S., Prechtel, S., Parczyk, K. and Steigemann, P. (2015) A novel 3D high-content assay identifies compounds that prevent fibroblast invasion into tissue surrogates. *Exp. Cell Res.*, 339, 35–43.
33. Roy, S., Kulkarni, R., Hewitt, N.J. and Aardema, M.J. (2016) The EpiDerm™ 3D human reconstructed skin micronucleus (RSMN) assay: historical control data and proof of principle studies for mechanistic assay adaptations. *Mutat. Res. Genet. Toxicol. Environ. Mutagen.*, 805, 25–37. doi:10.1016/j.mrgentox.2016.05.010.
34. Evans, S. J., Clift, M. J., Singh, N., de Oliveira Mallia, J., Burgum, M., Wills, J. W., Wilkinson, T. S., Jenkins, G. J. and Doak, S. H. (2017) Critical review of the current and future challenges associated with advanced in vitro systems towards the study of nanoparticle (secondary) genotoxicity. *Mutagenesis*, 32, 233–241.
35. Corvi, R. and Madia, F. (2017) In vitro genotoxicity testing—can the performance be enhanced? *Food Chem. Toxicol.*, 106, 600–608.
36. Council Directive 2010/63/EU (2010) Council Directive 2010/63/EU on the protection of animals used for scientific purposes. *Off. J. Eur. Union*, 53, 84. doi:10.3000/17252555.L_2010.276.eng.

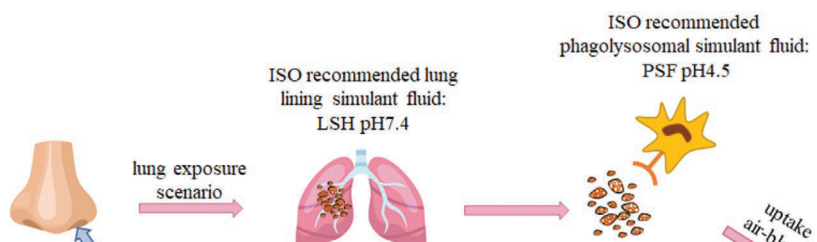
4.4 Publication IV

Simulating Nanomaterial Transformation in Cascaded Biological Compartments to Enhance the Physiological Relevance of In Vitro Dosing Regimes: Optional or Required?

Samantha V. Llewellyn, Angela Kämpfer, Johannes G. Keller, Klaus Vilsmeier, Veronika Büttner, Didem Ag Selesi, Roel P. F. Schins, Shareen H. Doak, and Wendel Wohlleben**

Would an engineered nanomaterial (ENM) still have the same identity once it reaches a secondary target tissue after a journey through several physiolog-

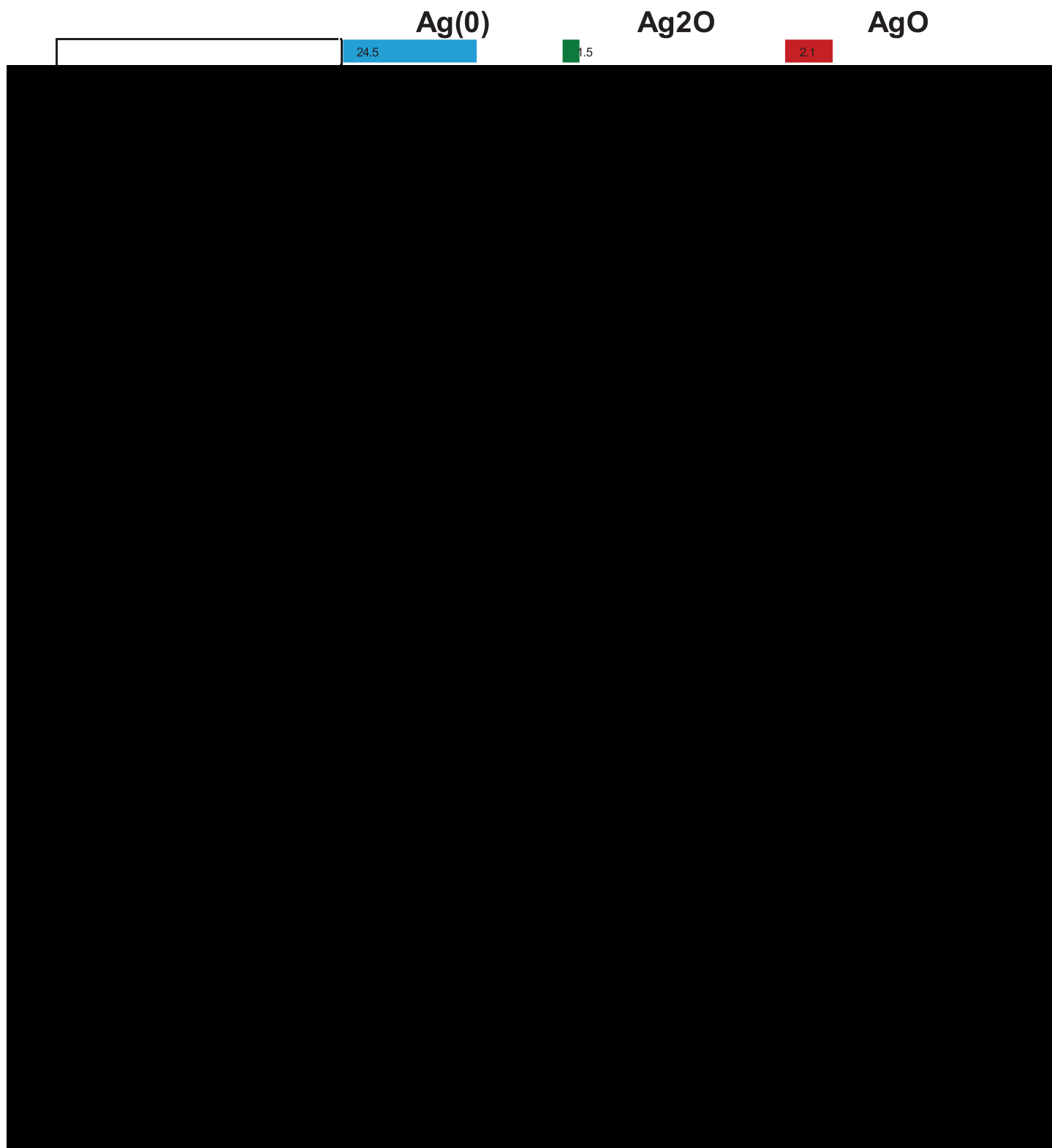
human blood plasma, and may not change much with prolonged incubation.^[4] It has been demonstrated that some fraction



cade of ENM transformation from site of exposure through to secondary organ systems and the direct toxicological impact of such material modifications is yet to be fully evaluated.

To address this, the approach employed in the present study was to firstly expand the pre-treatment concept that mimics

inflammatory response, and genotoxicity) can be assessed following exposure to pristine and PT ENMs to determine if ENM GIT exposure pre-treatments are a necessary step to improve the predictive capabilities of in vitro test systems for ENM hazard assessment.



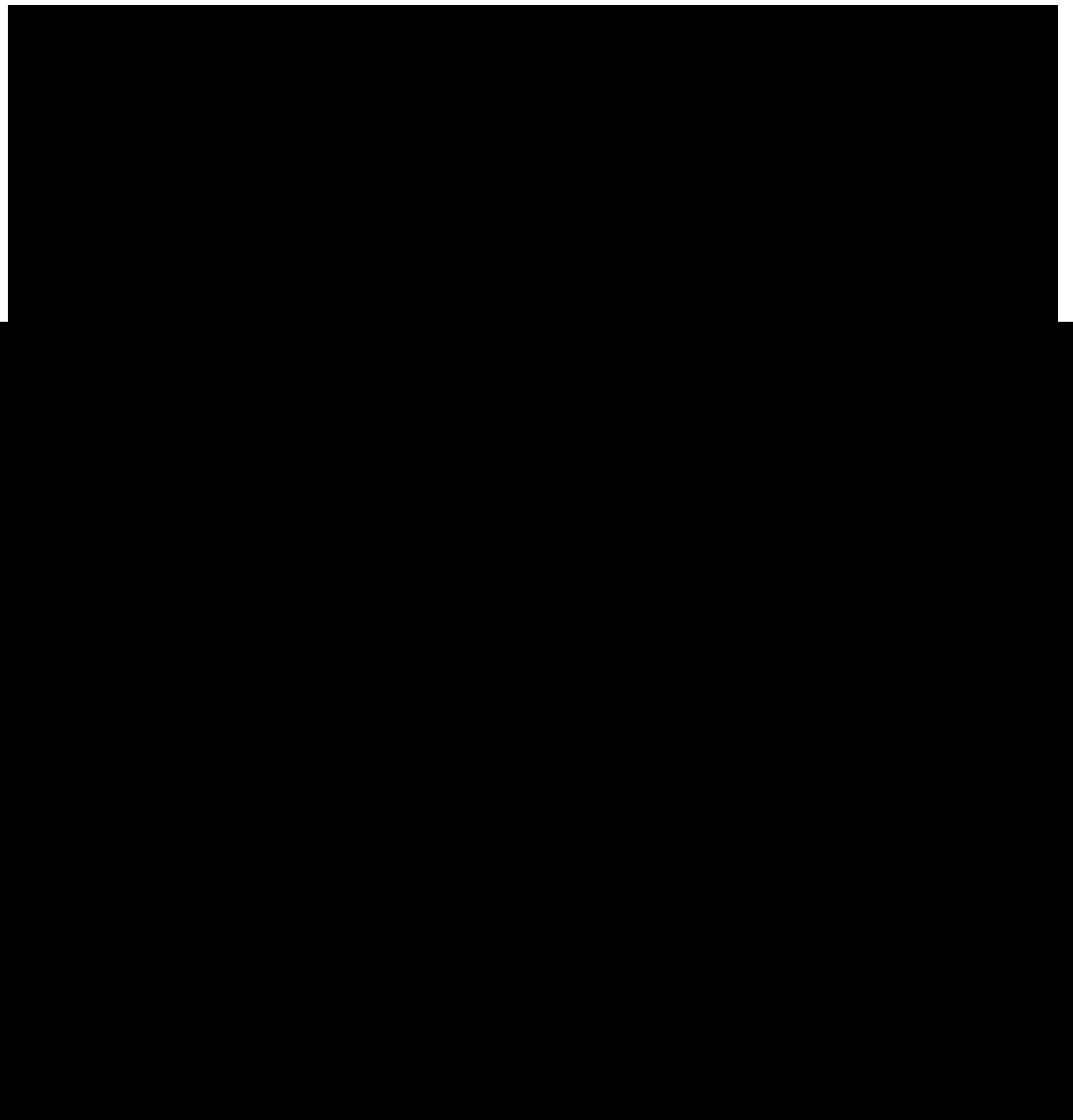
any specific media except lung simulant fluid (LSF).

We then proceeded to simulate pathways through several biological compartments. Ag Sigma generated significantly more ions in the combination of LSF—foetal bovine serum (FBS) and IUF—phagolysosomal simulant fluid (PSF), but not

We then again proceeded to simulate pathways through several biological compartments. After sequential incubations, we applied the same size distribution analysis, as described in Table 1. The detailed results for two Ag and two SiO₂ materials are given in Table S5, Supporting Information, with one

A

Table 1. In vivo journey emulated by sequential incubation in physiologi-



trifugation (AUC) technique.^[33,34] Only the dispersion directly in LSF induced minor agglomeration (see Figure 3A, black dash-dotted line), but none of the sequential incubations modulated the D50 (Table S5, Supporting Information). This was also

imen, which represents an approach to design “what ENM” is exposed to the cells. However, even for Ag this cannot be generalized: the counter example is Ag NM300, which is chemically oxidized already and colloidally stabilized by polymers

Table 2. Particle size median (D50) after normalization to the median size distribution when dispersed directly into the second medium. The color code is normalized on the entire data set to highlight cases where the sequential incubation leads to results that have very similar (white), lower (blue), or higher (red) levels of agglomeration as compared to single incubation in either the first or the second medium of the sequence.

	Relative to 1st medium	Relative to 2nd medium	Relative to 1st medium	Relative to 2nd medium
--	---------------------------	---------------------------	---------------------------	---------------------------

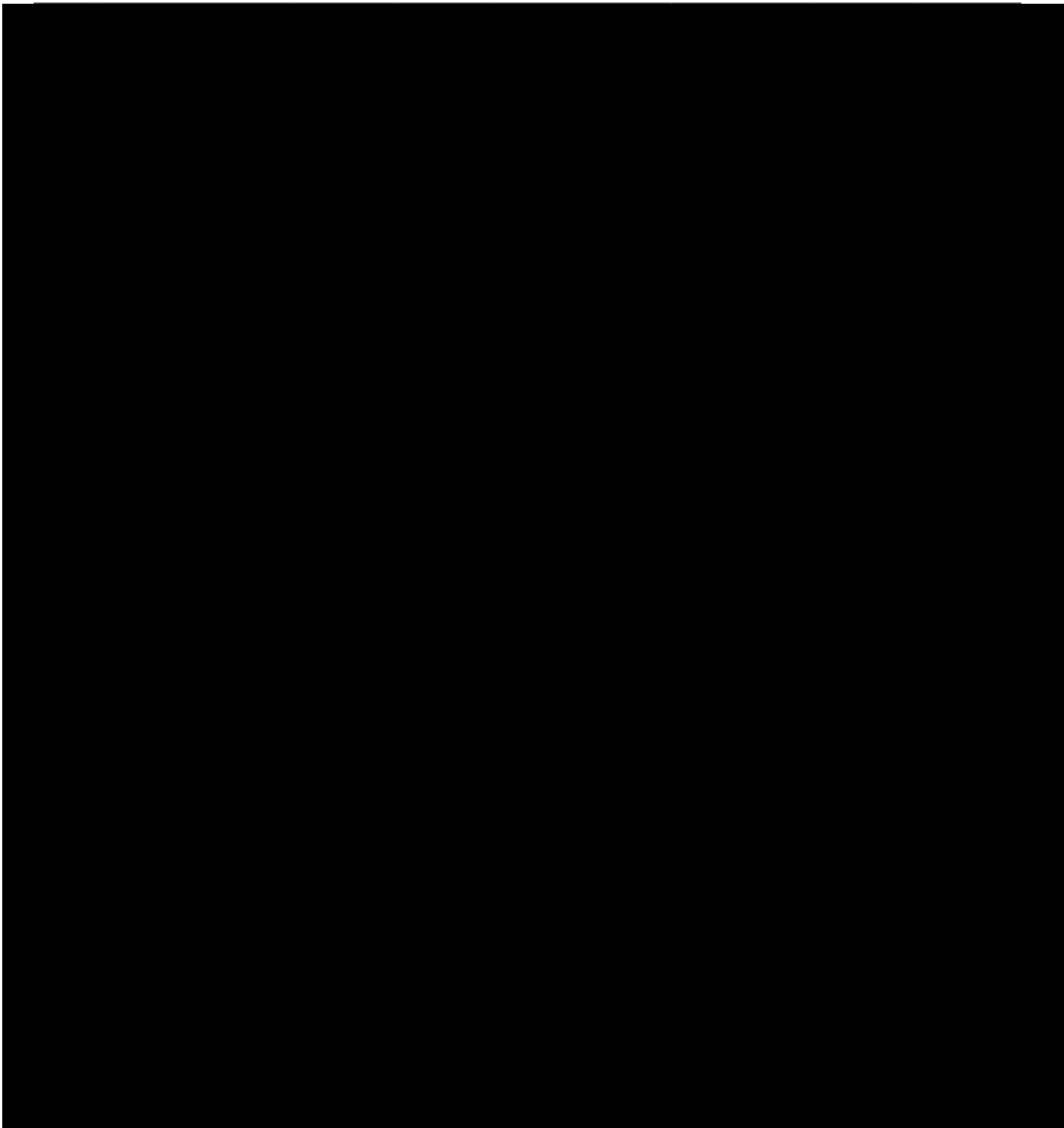


Figure 4. FRAS results on amorphous SiO₂ and Ag Sigma without (orgi) and with the IUF GIT pre-treatment. shown to induce an higher concentration of IL-8 release relative to the pristine particles, (Figure 7A). This suggested that ENM



F
*
T

tr

a
h
a
p
a
G
p
t
r
f
s

P
P
a
f

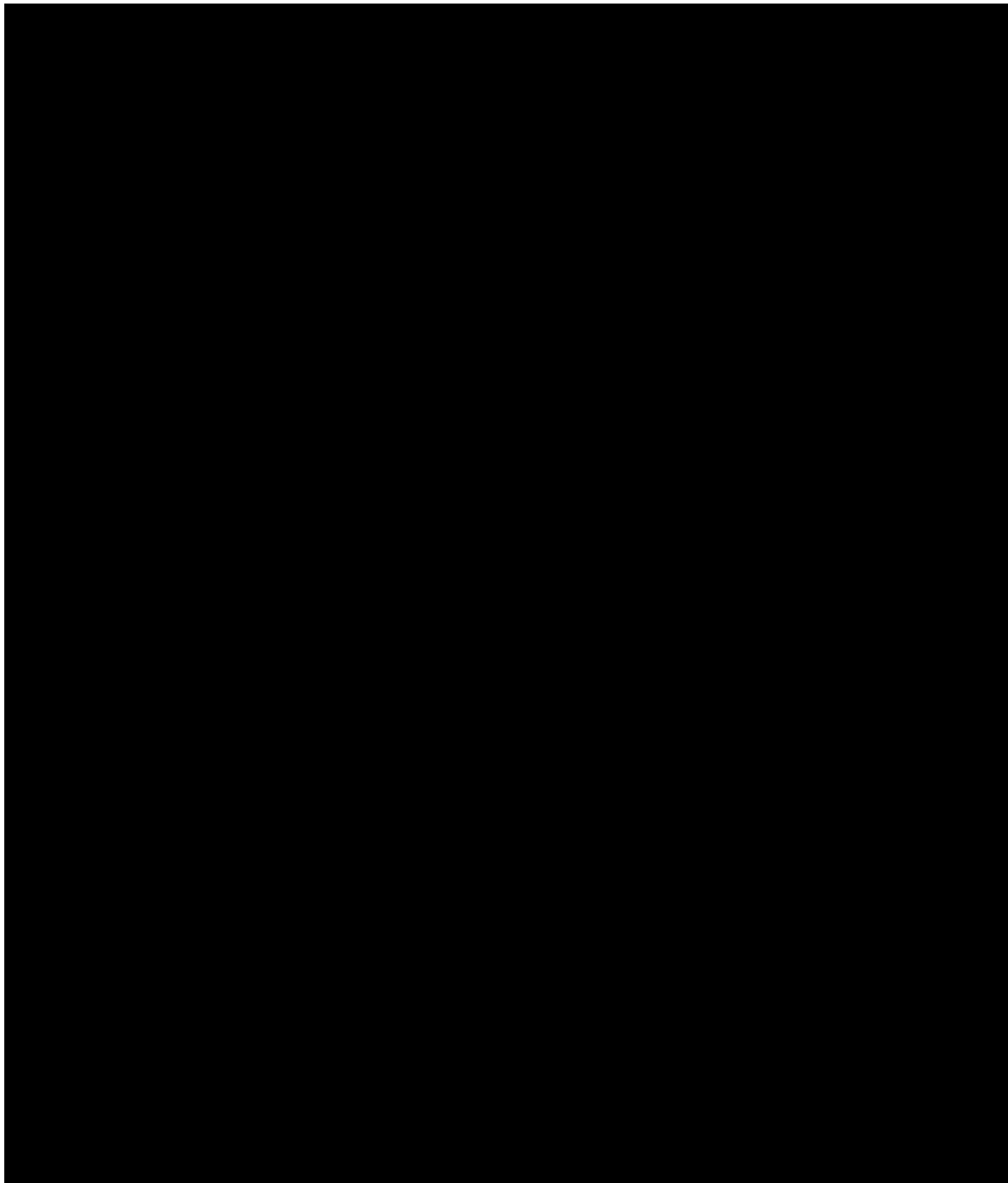
w
o
t
r
c
a
(
f
A
s

i
D
E
P

2
I

We expanded and critically assessed a concept to increase the realism of in vitro testing, by undertaking ENM pre-treatment

transformation of the particles. When proposing complex pre-treatment in tests of particle-induced effects,^[40] future work



have been successfully implemented in three independent labs and can serve as standard protocols. Furthermore, the impact

the physico-chemical transformation and reactivity would be assessed post pre-treatment in human cell-based systems, only

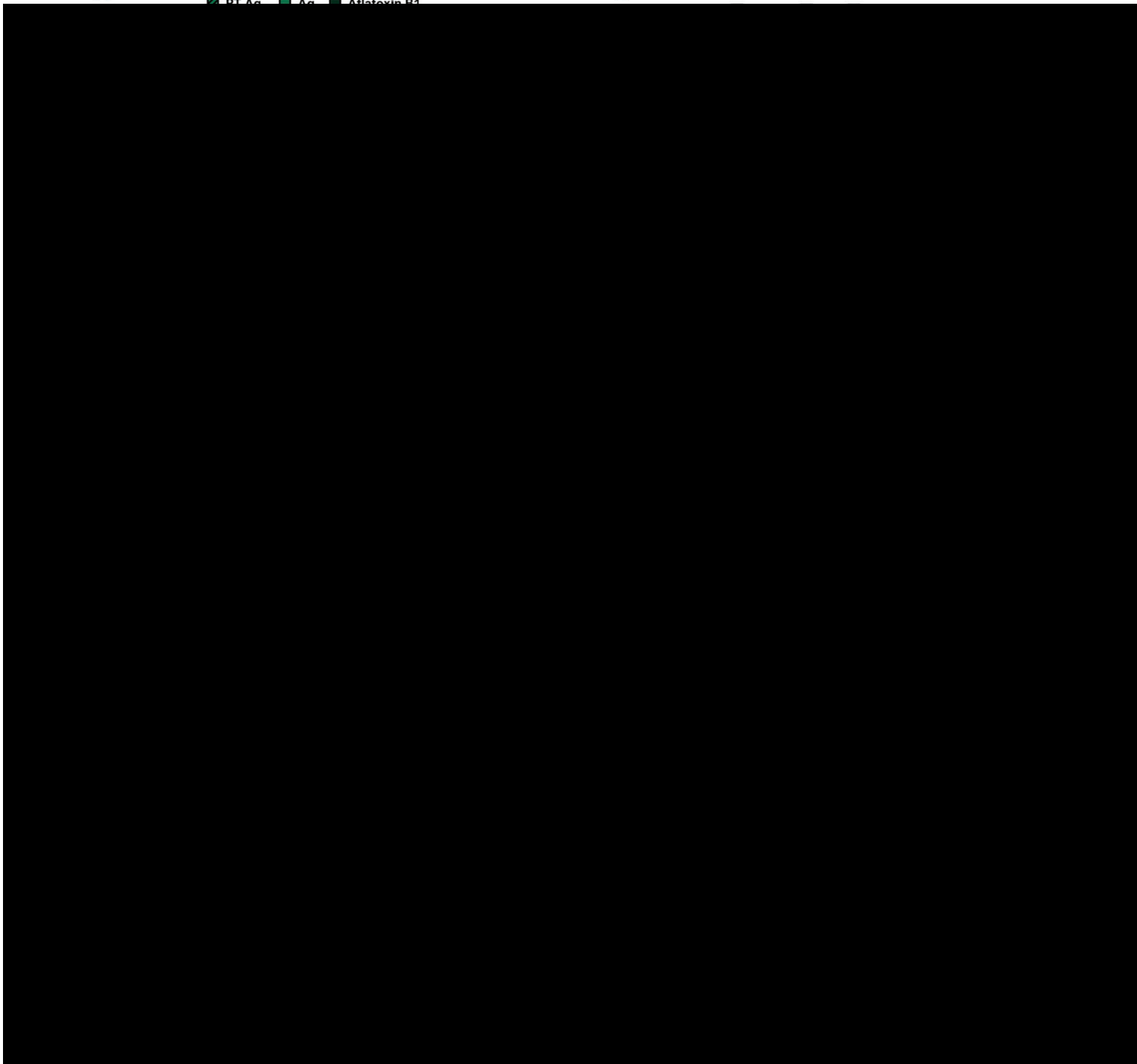
A

Negative All Simulants

PT Ag Ag Aflatoxin B1

B

Negative All Simulants



Sequential Incubation Standard Protocol: To simulate oral ENM exposure in vivo, 4.0 mg mL⁻¹ of ENMs were incubated in IUF_G gastric simulant fluid (pH 2.7) for 30 min at 37 °C/5% CO₂, followed by a 30 min incubation in IUF_I intestinal simulant fluid (pH 9.5). For exposure scenarios (Table 1) that required an additional simulant fluid, the ENM were added to the first medium to obtain 4.0 mg mL⁻¹ and stirred for 1 h at 350 rpm, 37 °C. The second medium (third medium, for the IUF_G and IUF_I sequence) was added in excess at a ratio of 10:1 to minimize influences (e.g., pH) of the previous medium.^[32] The sample was then dispersed through ultrasonic power at an amplitude of

The authors acknowledge the funding received from the European Union's Horizon 2020 research and innovation program for the PATROLS project, under grant agreement No. 760813.

Conflict of Interest

The authors declare no conflict of interest.

Keywords

engineered nanomaterial pre-treatment, gastro-intestinal digestion, in vitro hazard assessment, nanomaterials, physico-chemical characterisation

- [20] A. P. Walczak, R. Fokkink, R. Peters, P. Tromp, Z. E. H. Rivera, I. M. C. M. Rietjens, P. J. M. Hendriksen, H. Bouwmeester, *Nanotoxicology* **2012**, *7*, 1198.
- [21] K. Gerloff, D. I. A. Pereira, N. Faria, A. W. Boots, J. Kolling, I. Förster, C. Albrecht, J. J. Powell, R. P. F. Schins, *Nanotoxicology* **2013**, *7*, 353.
- [22] X. Cai, X. Liu, J. Jiang, M. Gao, W. Wang, H. Zheng, S. Xu, R. Li,

- Environ. Health Perspect.* **1994**, *102*, 103.
- [18] B. J. Phillips, E. Kranz, P. S. Elias, R. Münzner, *Food Cosmet. Toxicol.* **1980**, *18*, 371.
- [19] A. G. Oomen, A. Hack, M. Minekus, E. Zeijdner, C. Cornelis, G. Schoeters, W. Verstraete, T. V. de Wiele, J. Wragg, C. J. M. Rempelberg, A. J. A. M. Sips, J. H. V. Wijnen, *Environ. Sci. Technol.* **2002**, *36*, 3326.
- P. Schuck, W. Wohlleben, *NanoImpact* **2018**, *10*, 87.
- [42] A. Gandon, K. Werle, N. Neubauer, W. Wohlleben, *J. Phys.: Conf. Ser.* **2017**, *838*, 012033.
- [43] W. Thongkam, K. Gerloff, D. van Berlo, C. Albrecht, R. Schins, *Mutagenesis* **2016**, *32*, 105.
- [44] A. Kinsner, M. Boveri, L. Hareng, G. C. Brown, S. Coecke, T. Hartung, A. Bal-Price, *J. Neurochem.* **2006**, *99*, 596.



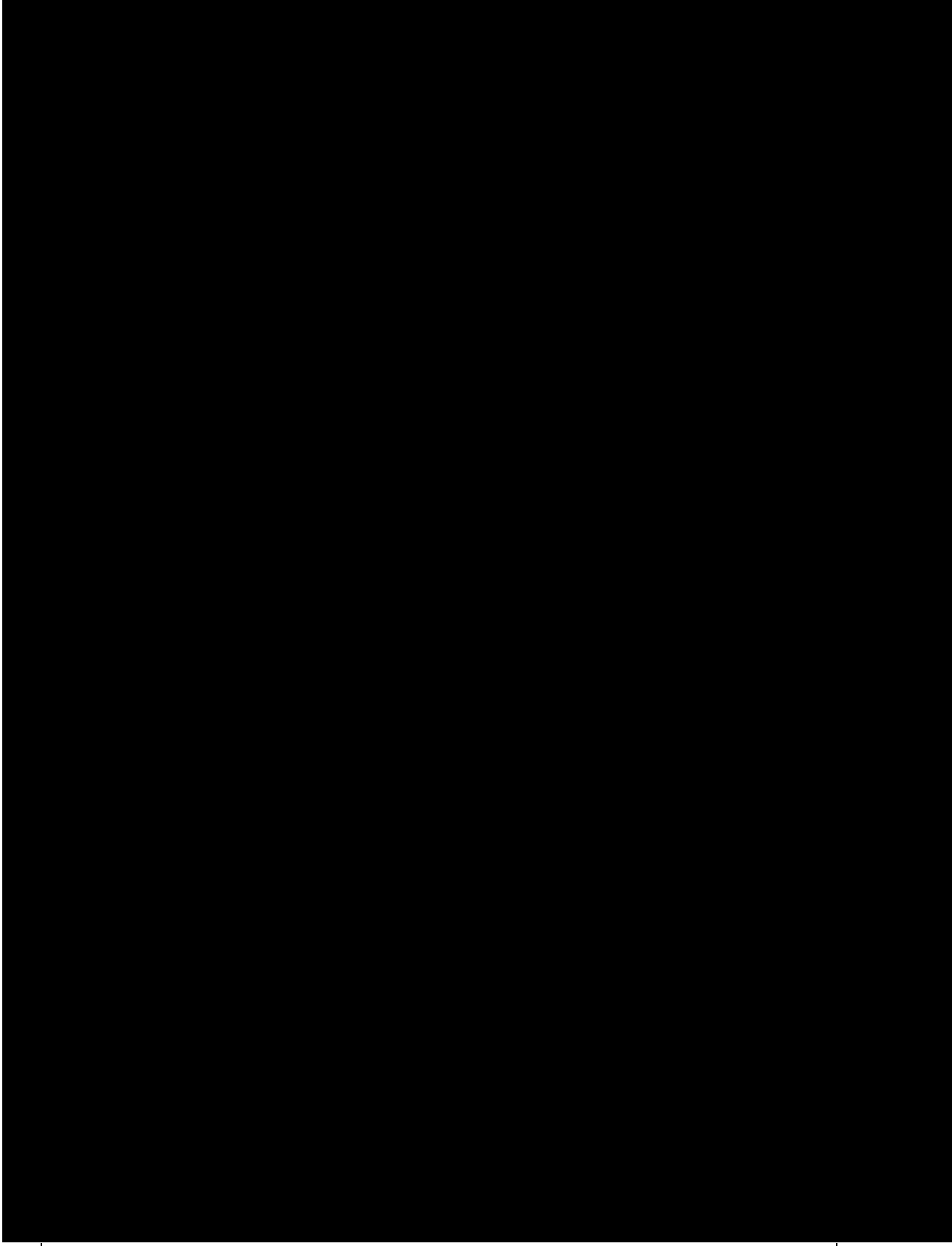
Supporting Information

for *Small*, DOI: 10.1002/smll.202004630

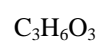
Simulating Nanomaterial Transformation in Cascaded Biological Compartments to Enhance the Physiological Relevance of In Vitro Dosing Regimes: Optional or Required?

Samantha V. Llewellyn, Angela Kämpfer, Johannes G. Keller, Klaus Vilsmeier, Veronika Büttner, Didem Ag Seleci, Roel P. F. Schins, Shareen H. Doak, and Wendel Wohlleben**

icibly



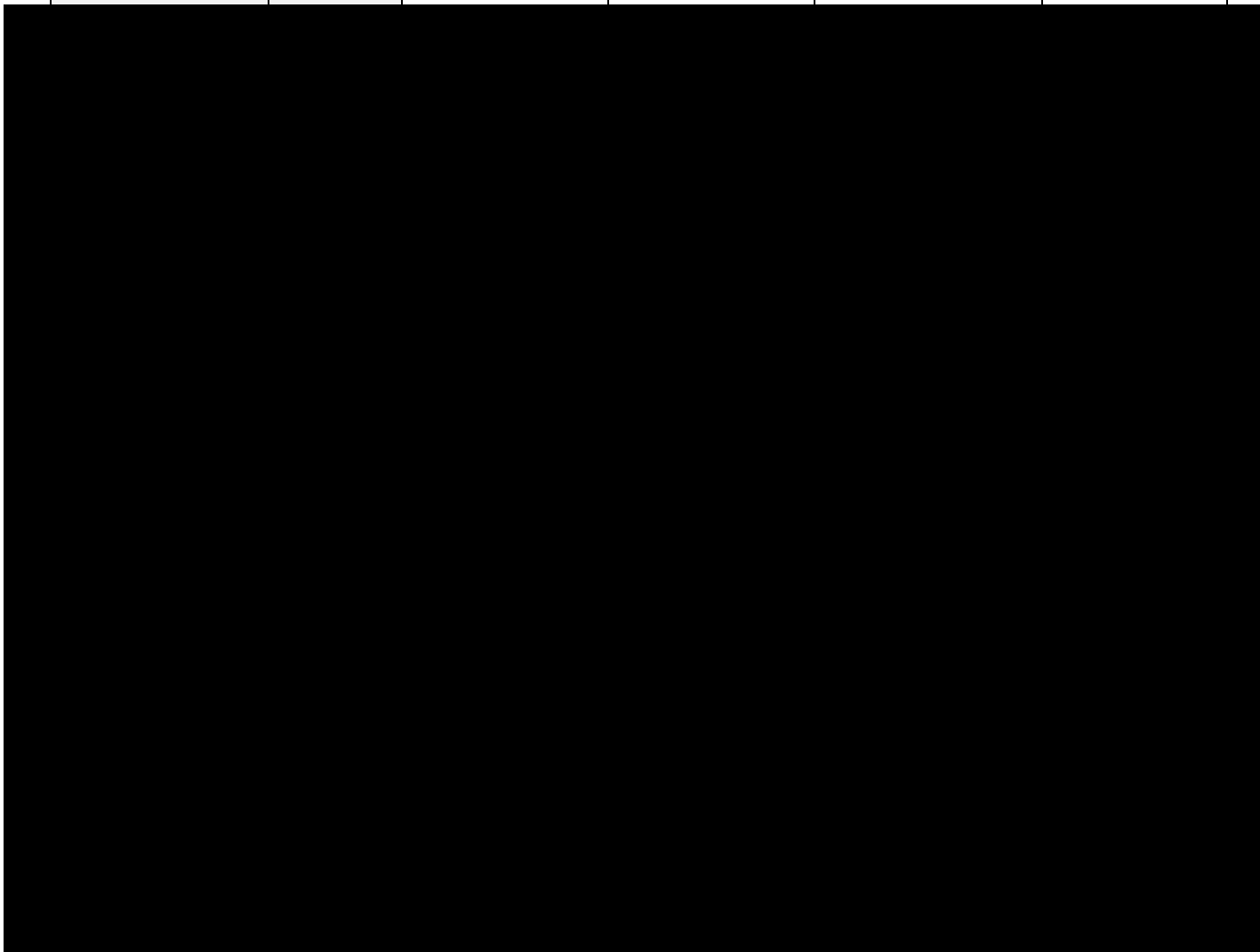
90% lactic acid



79

Table S2: Physical-chemical properties of the ENMs evaluated.

Property & Method of Analysis	Unit	Amorphous SiO ₂	SiO ₂ NM200	Ag Sigma (Cat#: 576832, PVP)	Ag NM300
Composition: CAS	n/a	7631-86-9		7440-22-4	
XRD: composition,					Ag ₂ O + Ag (93%



Surface charge	mV	-35	-22	-30	-22
Water contact angle: surface hydrophobicity	°	77.1 ± 1.4°	<10°	140.8 ± 1°	not measurable (suspension)

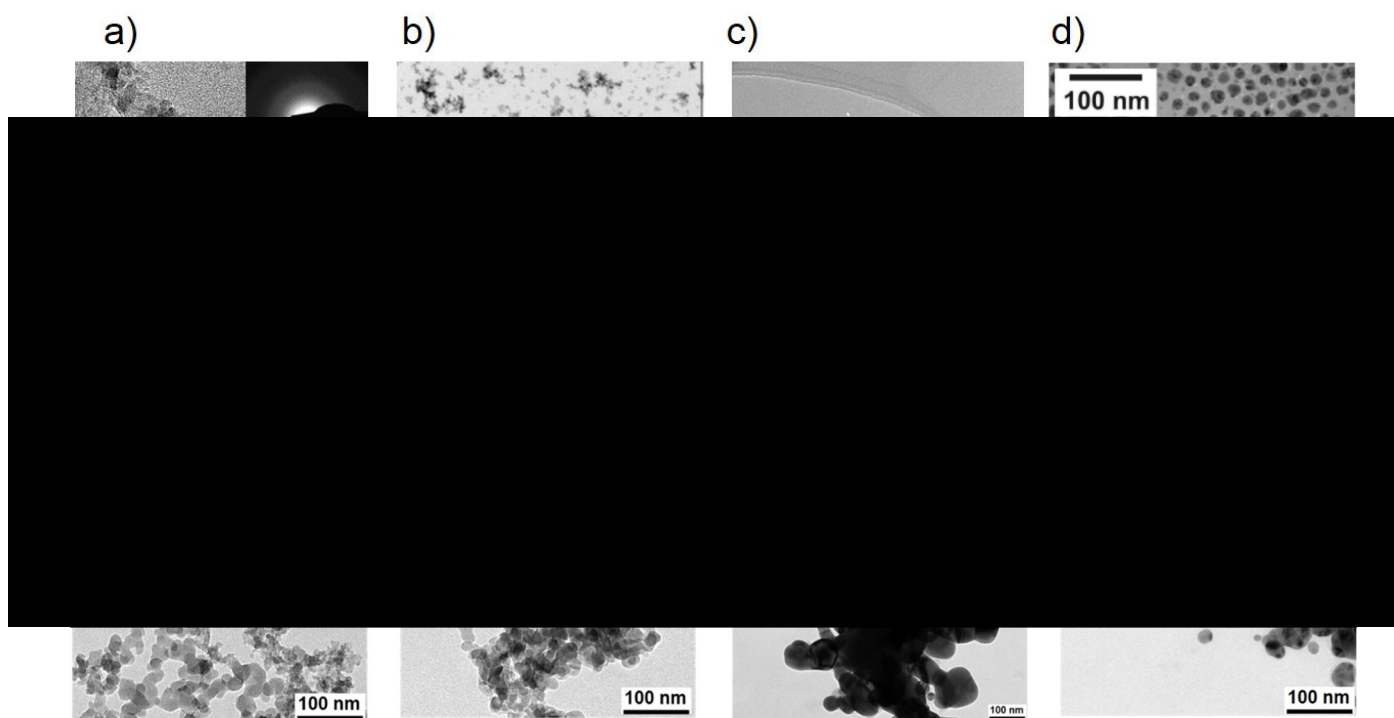


Figure S1: TEM micrographs of the ENM: a)-d) show the pristine ENM, and e)-h) show the aged ENM after sequential IUF_S and IUF_I treatment. a,e) Amorphous SiO₂; b,f) SiO₂ NM200; c,g) Ag Sigma; d,h) Ag NM300. Figure d) reproduced from Klein et al. (2011) JRC report 60709 (DOI 10.2788/23079).

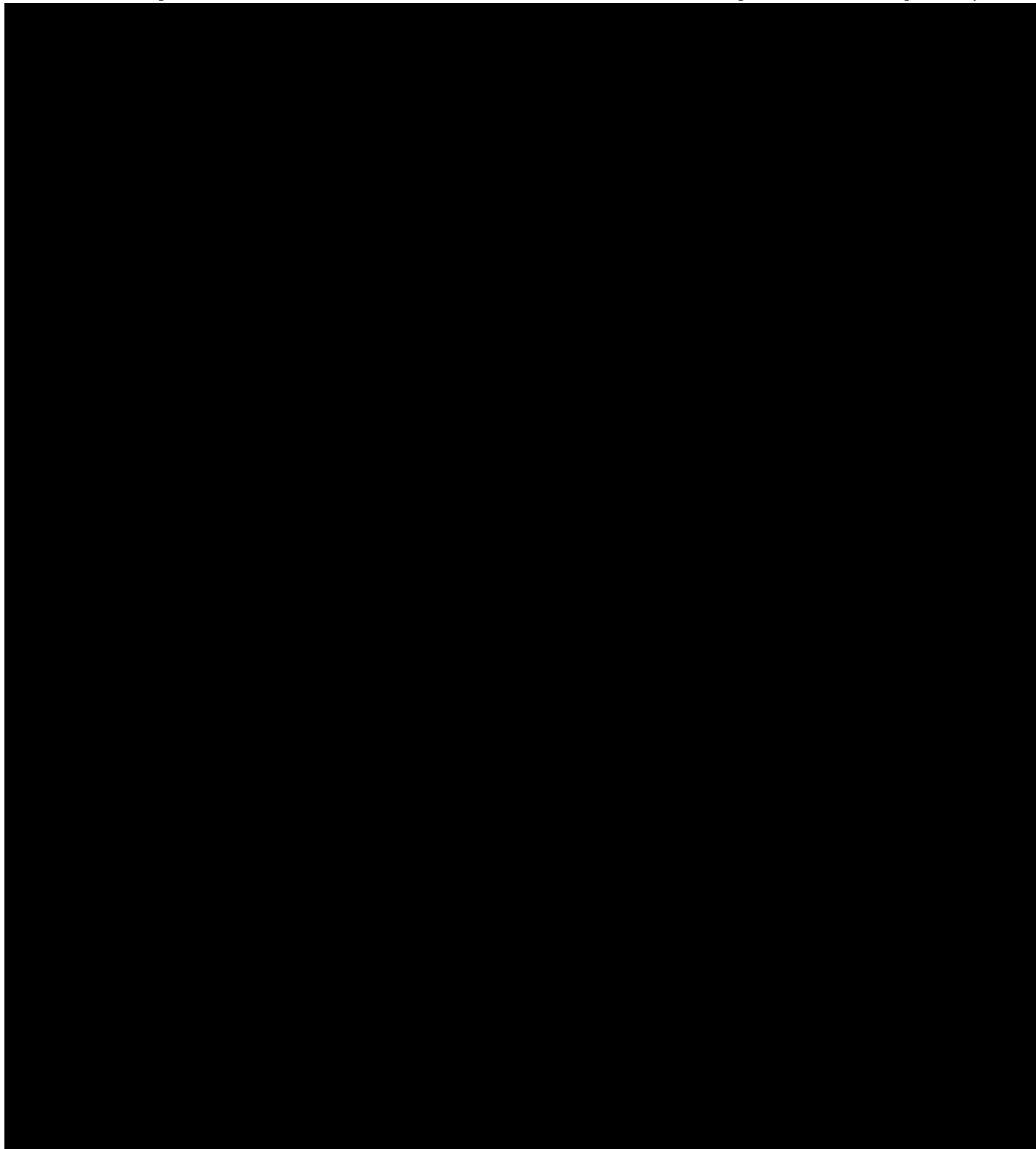
	C 1s	O 1s	Ag 3d	Cl 2p	Na 1s
Ag_Sigma_org1	50.6	19.1	28.2	2.4	
	51.0	15.6	29.6	3.8	
	50.8	16.2	31.2	1.8	
	47.5	14.4	34.4	3.8	

and 23% O from the polymer functionalization. With the additional remains from the GIT pre-treatment (observed as Na in both cases), the total Ag content on the surface remained below the detection limit of 0.5%, such that no oxidation state could be determined for Ag NM300 after GIT pre-treatment.

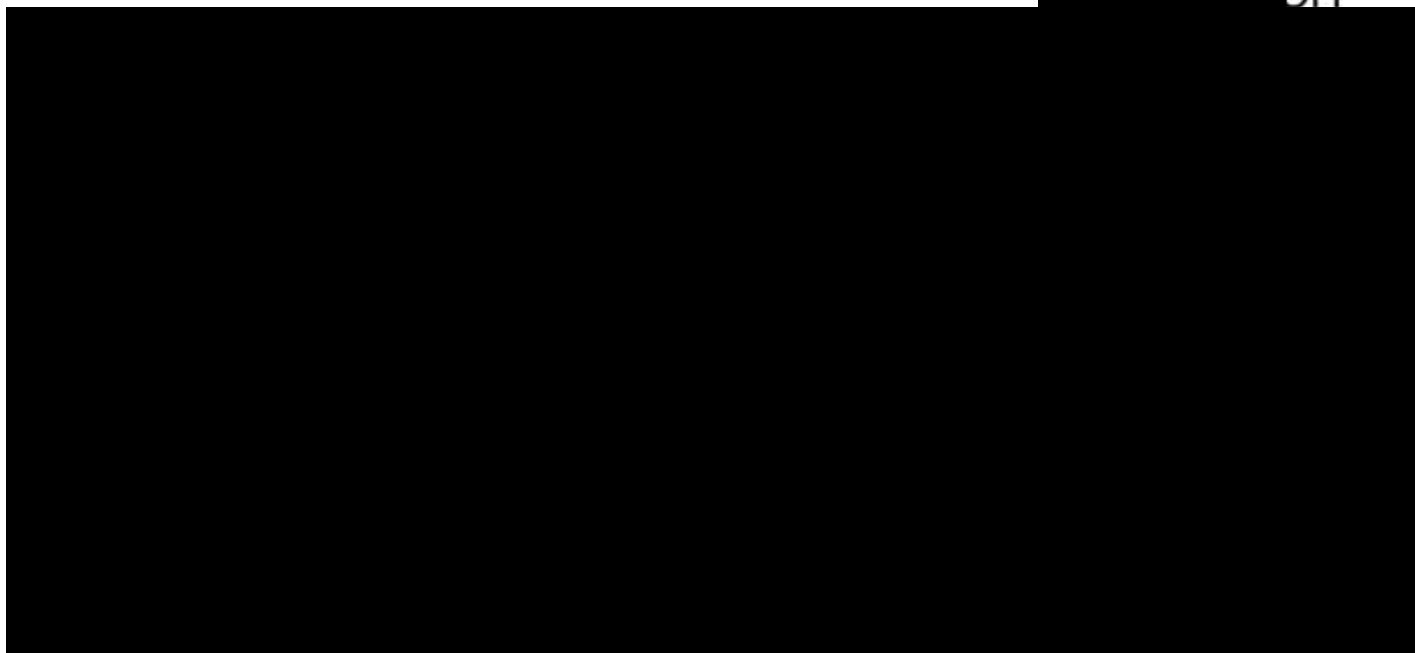
Table S3: Ion concentrations in mg/L of a total solid content of 4000 mg/L of Ag Sigma and amorphous SiO₂ after filtration through a 5kDa membrane in different media. Concentrations measured through ICP-MS.

		Ag	SiO ₂		
Ag Sig	IUF_1	26	88	289	
SiO ₂ am	IUF_1	117	263	598	

Table S5: Particle size distribution descriptors D10, D50 and D90 after sequential incubation for Ag Sigma, Ag NM300, amorphous SiO₂ and SiO₂ NM200. The code “FBS to PSF” means that the particles are first dispersed by



shows that it is not the length of incubation, and not a single medium, but indeed the sequence that is decisive for the final size of Ag Sigma:



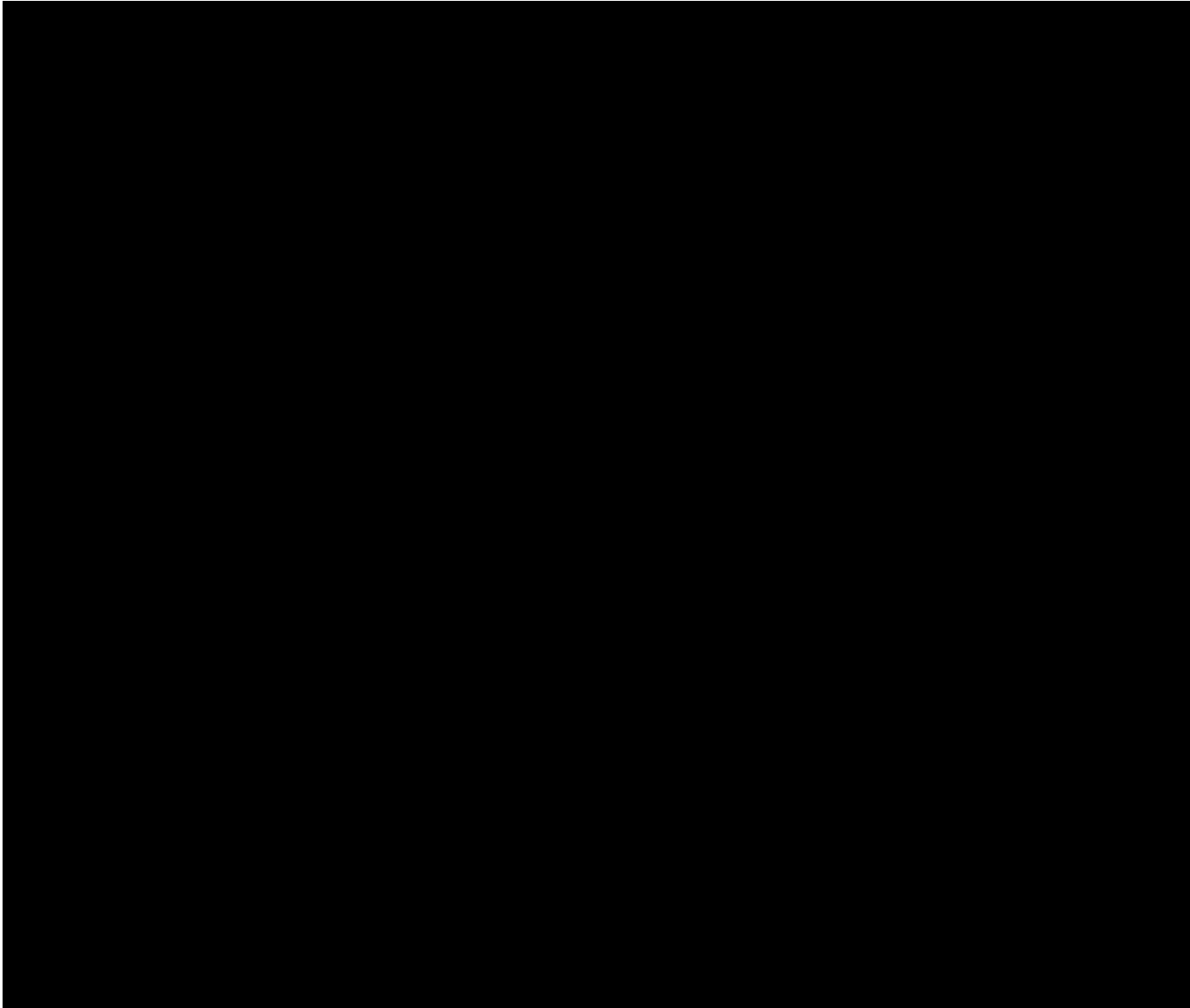
leads to results very similar (white) or lower (blue) or higher (red)

LSF to LSF		100%
PSF to PSF		128%

agglomeration as compared to single incubation in either the first or the second medium of the sequence.

3. Additional Results on Genotoxicity

The pre-treatment of Ag Sigma ENM with artificial GIT digestive fluids significantly reduced the



pristine or P1 Ag Sigma ENM (Average \pm SD, N=3; * $p \leq 0.05$ compared to respective control, # $p \leq 0.05$ compared to corresponding pristine Ag Sigma concentration by One-way ANOVA and Tukey's *post hoc* test)

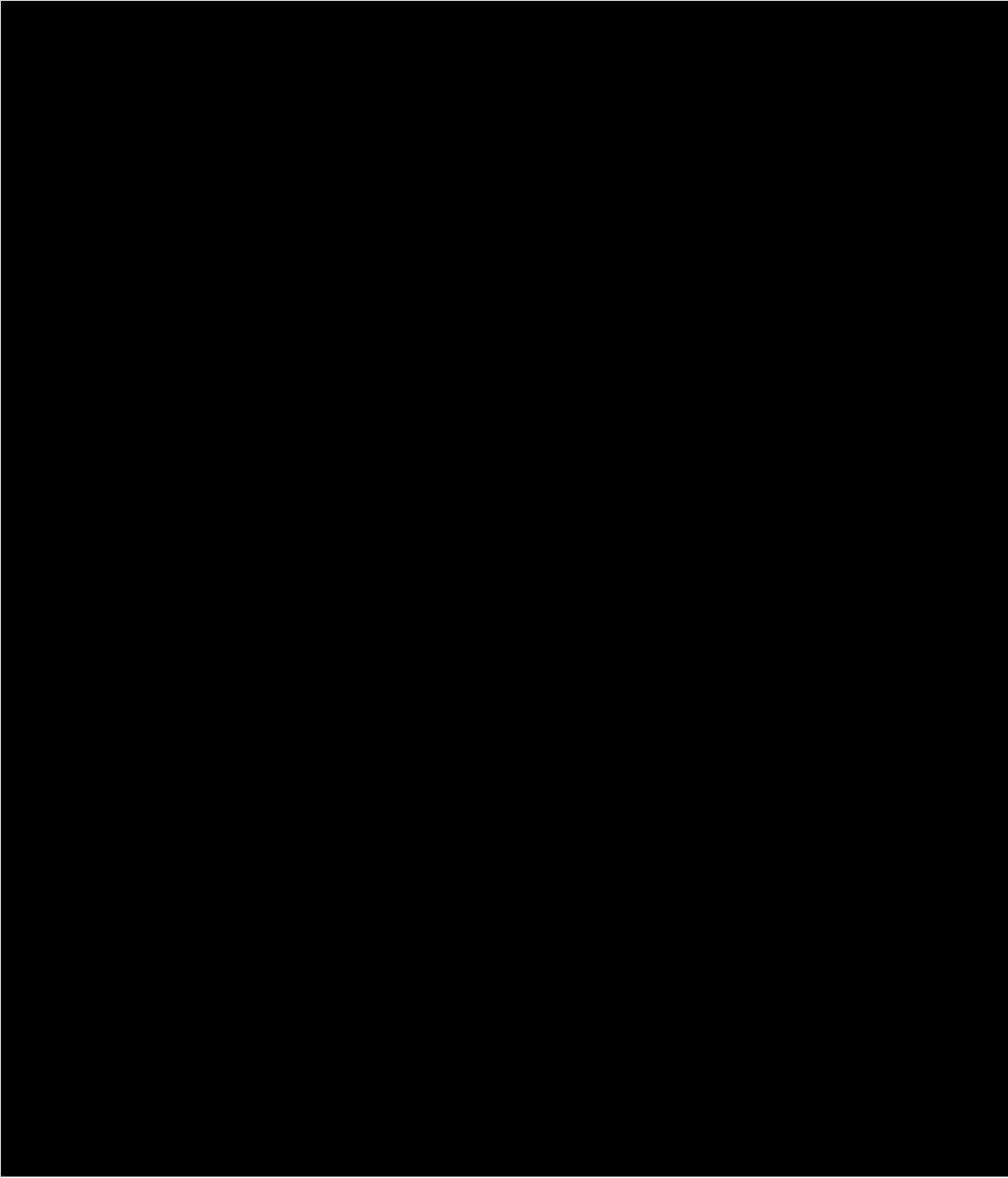
Cytokinesis-block Micronucleus (CBMN) Assay for Genotoxicity

Aflatoxin B1, a known liver carcinogen, was used as a positive control for genotoxicity. For acute exposures, 1000 binucleated cells were scored per dose per replicate using the cytokinesis-block version of the MN assay (3000 binucleate cells scored in total). Mean data of three biological replicates (n=3) is presented \pm SD.

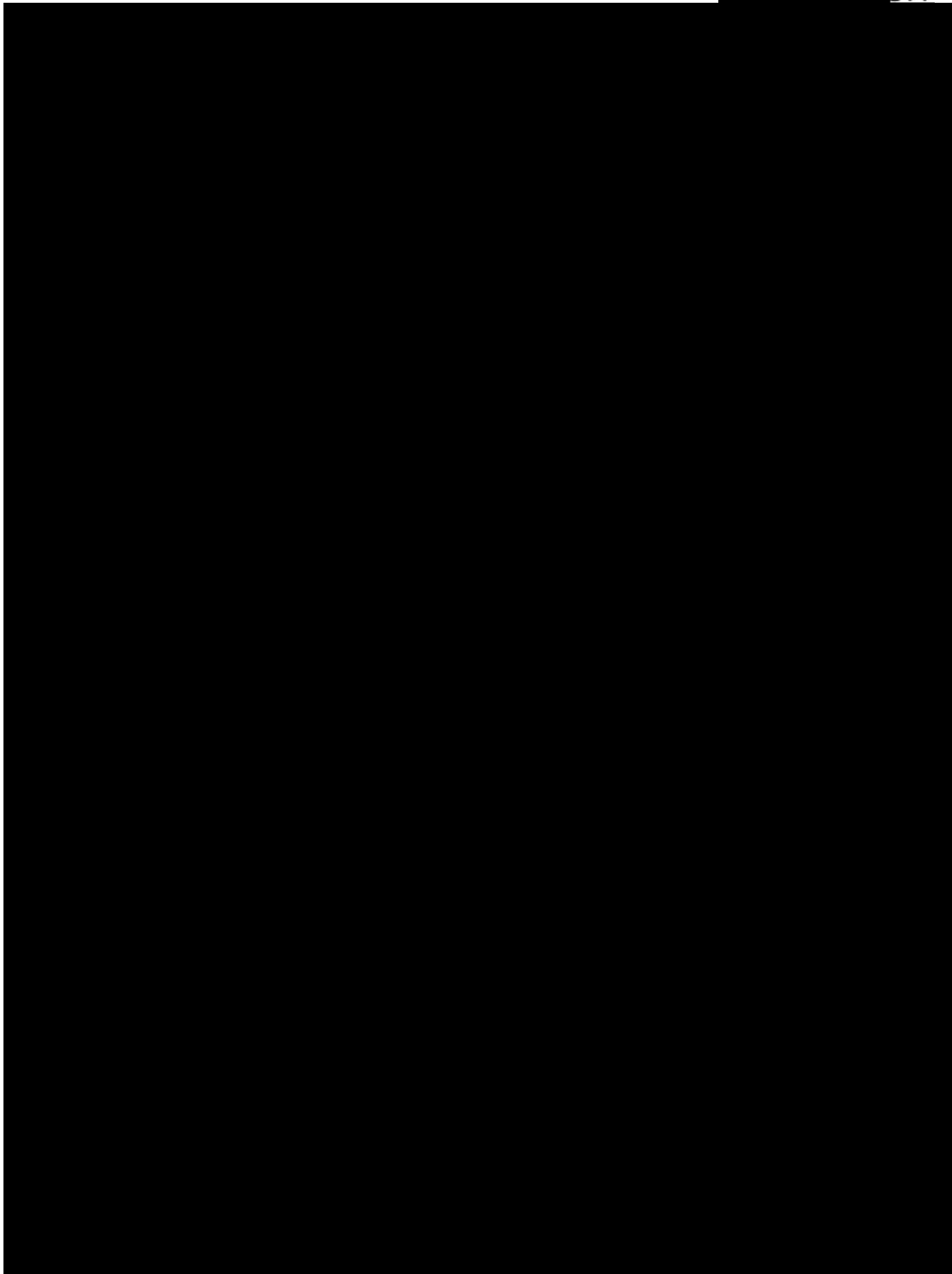
2. Experimental Section

2.1 Gastrointestinal (GIT) Model

Experiments were performed using monocultures of Caco-2 (DSMZ), HT29-MTX-E12 (previously

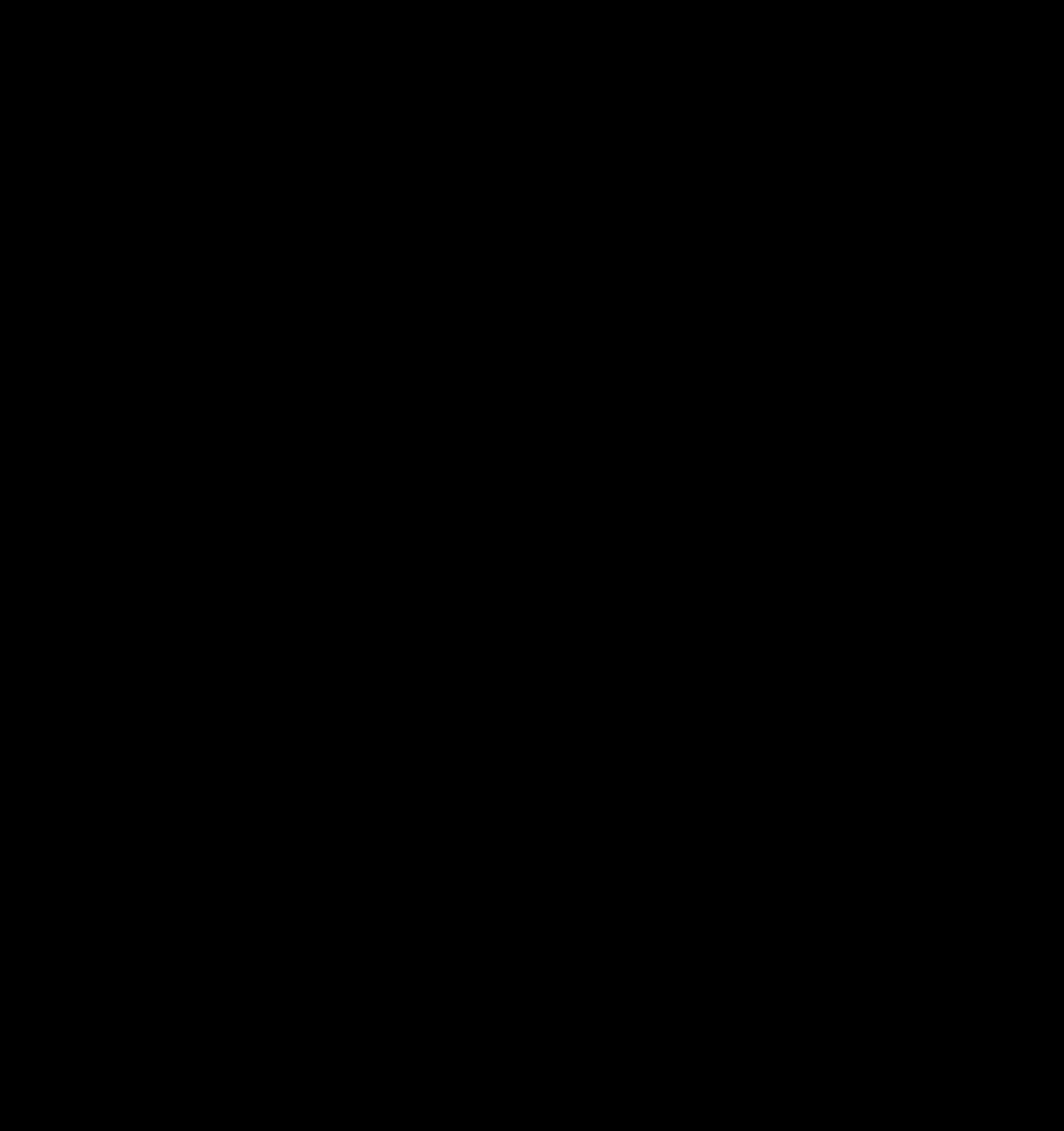


spectrophotometrically (Thermo Scientific, Multiskan Go) at 450 and 630 nm.



third pre-treatment fluid for 1hr to simulate their translocation into the circulatory system prior to reaching the liver.

In parallel, 2.56mg/mL of pristine Ag Sigma were dispersed for 16 mins in 0.05% Bovine



ANOVA with Sidak's post hoc were used. For non-parametric data, Kruskal-Wallis test was used to calculate significance when there were more than two variables, with Dunn's multiple comparisons test.


4.5 Publication V

RESEARCH

Open Access



Understanding the impact of more realistic low-dose, prolonged engineered nanomaterial exposure on genotoxicity using 3D models of the human liver

Samantha V. Llewellyn¹ , Gillian E. Conway¹, Ilaria Zanoni⁴, Amalie Kofoed Jørgensen⁵, Ume-Kulsoom Shah¹, Didem Ag Seleci^{2,3}, Johannes G. Keller^{2,3}, Jeong Won Kim⁶, Wendel Wohlleben^{2,3}, Keld Alstrup Jensen⁵, Anna Costa⁴, Gareth J. S. Jenkins¹, Martin J. D. Clift¹ and Shareen H. Doak^{1*}

Abstract

Background: With the continued integration of engineered nanomaterials (ENMs) into everyday applications, it is important to understand their potential for inducing adverse human health effects. However, standard in vitro hazard characterisation approaches suffer limitations for evaluating ENM and so it is imperative to determine these potential hazards under more physiologically relevant and realistic exposure scenarios in target organ systems, to minimise the necessity for in vivo testing. The aim of this study was to determine if acute (24 h) and prolonged (120 h) exposures to five ENMs (TiO₂, ZnO, Ag, BaSO₄ and CeO₂) would have a significantly different toxicological outcome (cytotoxicity, (pro-)inflammatory and genotoxic response) upon 3D human HepG2 liver spheroids. In addition, this study evaluated whether a more realistic, prolonged fractionated and repeated ENM dosing regime induces a significantly different toxicity outcome in liver spheroids as compared to a single, bolus prolonged exposure.

Results: Whilst it was found that the five ENMs did not impede liver functionality (e.g. albumin and urea production), induce cytotoxicity or an IL-8 (pro-)inflammatory response, all were found to cause significant genotoxicity following acute exposure. Most statistically significant genotoxic responses were not dose-dependent, with the exception of TiO₂. Interestingly, the DNA damage effects observed following acute exposures, were not mirrored in the prolonged exposures, where only 0.2–5.0 µg/mL of ZnO ENMs were found to elicit significant ($p \leq 0.05$) genotoxicity. When fractionated, repeated exposure regimes were performed with the test ENMs, no significant ($p \geq 0.05$) difference was observed when compared to the single, bolus exposure regime. There was < 5.0% cytotoxicity observed across all exposures, and the mean difference in IL-8 cytokine release and genotoxicity between exposure regimes was 3.425 pg/mL and 0.181%, respectively.

Conclusion: In conclusion, whilst there was no difference between a single, bolus or fractionated, repeated ENM prolonged exposure regimes upon the toxicological output of 3D HepG2 liver spheroids, there was a difference between acute and prolonged exposures. This study highlights the importance of evaluating more realistic ENM exposures, thereby providing a future in vitro approach to better support ENM hazard assessment in a routine and easily accessible manner.

Keywords: In vitro liver models, Engineered nanomaterials, Physiologically relevant exposure, Nanotoxicology, Genotoxicity

*Correspondence: S.H.Doak@swansea.ac.uk

¹ In Vitro Toxicology Group, Institute of Life Science, Swansea University Medical School, Swansea University, Singleton Park, Swansea SA2 8PP, UK
Full list of author information is available at the end of the article



© The Author(s) 2021. This article is licensed under a Creative Commons Attribution 4.0 International License, which permits use, sharing, adaptation, distribution and reproduction in any medium or format, as long as you give appropriate credit to the original author(s) and the source, provide a link to the Creative Commons licence, and indicate if changes were made. The images or other third party material in this article are included in the article's Creative Commons licence, unless indicated otherwise in a credit line to the material. If material is not included in the article's Creative Commons licence and your intended use is not permitted by statutory regulation or exceeds the permitted use, you will need to obtain permission directly from the copyright holder. To view a copy of this licence, visit <http://creativecommons.org/licenses/by/4.0/>. The Creative Commons Public Domain Dedication waiver (<http://creativecommons.org/publicdomain/zero/1.0/>) applies to the data made available in this article, unless otherwise stated in a credit line to the data.

Background

Nanotechnology is considered an important Key Enabling Technology (KET), underpinning a variety of novel applications across wide ranging sectors. As a global market, nanotechnology reached \$75.8 billion in 2020 and is predicted to exceed \$125 billion in the next three years, with engineered nanomaterials (ENMs) defined as having the greatest share of the global nanotechnology market [1]. ENMs are manufactured materials with advanced size specific physico-chemical properties derived from an unbound, monodispersed state, or as an aggregate/agglomerate where 50% or more of the particles possess one or more external dimensions in the size range 1–100 nm [2]. This greater surface area to volume ratio enables ENMs to harbour advantageous properties that improve the functionality of a plethora of applications (e.g. cosmetics, medicine, electronics, construction and energy industries) providing great opportunities for economic growth and life improving technologies. Consequently, with increasing human and environmental exposure comes the need to understand any potential associated safety risks.

Human ENM exposure occurs via four primary routes; inhalation, ingestion, injection and dermal penetration. With the exception of certain medical treatments, the prospect of injecting ENMs into the body is relatively low for the majority of individuals. While for most ENM, the likelihood of occupational inhalation exposure is predominant, such as the use of barium sulfate (BaSO_4) and cerium dioxide (CeO_2) in the automotive industry; other routes of potential relevant exposure could arise from the use of consumer products, with some examples being the ingestion of food grade titanium dioxide (TiO_2) or dermal penetration of sunscreen enhancing zinc oxide (ZnO) [3–6]. Silver (Ag) ENMs, with its popular anti-microbial properties, are deemed the most readily applied ENM in consumer products included in the top three applications found in medicine, textiles and cosmetic products [7–9]. Consequently, understanding the impact of repeated ENM exposure to human health over prolonged periods of time is imperative.

Once ENMs have entered the body, if they have the ability to traverse biological barriers and enter circulation, the materials can translocate to secondary sites of deposition, including the spleen, liver and kidneys [10, 11]. Of these sites, the liver is of particular toxicological importance due to its high susceptibility to ENM deposition and accumulation, as well as its role in maintaining metabolic homeostasis and the detoxification of both endogenous and exogenous substances [12, 13]. Secondary ENM deposition in the liver is commonly reported, but it is becoming more evident that translocation following inhalation or ingestion in particular, is

low with < 1.0% of the insoluble ENM exposure concentration reaching the secondary organs [14]. A previous *in vivo* study undertaken to assess the effects of an occupational 14-day pulmonary exposure, found that only 1.24% and 2.87% of the original intratracheal instilled dose of 162 μg of TiO_2 and CeO_2 ENMs per mouse reached the liver [15]. This corresponds to a translocated dose of 1 $\mu\text{g}/\text{g}$ *in vivo* or 1 $\mu\text{g}/\text{mL}$ *in vitro* [15], illustrating the necessity for low-dose exposures when evaluating the effect of ENM exposure upon secondary sites of exposure, such as the liver. Even at low-doses, ENMs have been found to induce hepatic dysfunction and severe organ damage *in vivo*. Liver damage caused by the long-term (90 days), daily intragastric exposure of 2.5–10 $\mu\text{g}/\text{g}$ of TiO_2 resulted in bioaccumulation and aggregation in the liver over time, significant changes in tissue morphology and the expression of genes involved in immune and inflammatory responses (e.g. CXCII over-expression), apoptosis, oxidative stress and metabolic process [16]. Similarly, low dose (< 10.0 $\mu\text{g}/\text{mL}$) *in vitro* ENM exposures of Ag and ZnO were sufficient to induce biological effects, including DNA damage and elevated levels of reactive oxygen species (ROS). Yet, many *in vitro* studies have previously focused on the acute effects of high ENM concentrations, which is beneficial for establishing potential toxicity and hazard, but does not allow for evaluation of the chronic effects that may be associated with the more realistic long-term human exposure scenarios [14, 17]. Prolonged exposure to ENMs may induce repetitive injury leading to chronic liver disease, whereby the regenerative capabilities are impaired, and the hepatocytes begin to undergo cell death as a result of inflammation [12, 18]. Therefore, continued ENM exposure raises concerns regarding the gradual accumulation and chronic health effects that may be induced.

With the vast range of ENMs available on the market, each with its own unique specification, it is untenable to rely on *in vivo* based methods to fully elucidate the immediate and lasting effects of ENM exposure upon the human body [19]. In recent years, international bodies such as the Organisation for Economic Cooperation and Development (OECD) Working Party on Manufactured Nanomaterials, the International Organization for Standardization (ISO) and the European Committee for Standardization (CEN) have published a series of test guidelines, guidance documents and regulatory standards to help drive the development of physiologically relevant, high-throughput *in vitro* test systems and regulated protocols for ENM hazard assessment [20]. To align with these new test guidelines and the 3Rs directive to replace, reduce and refine the use of *in vivo* based testing systems, researchers have

been developing advanced in vitro models to emulate human organ systems and sustain long-term culture, to provide viable alternatives to in vivo test systems and to propel in vitro ENM hazard assessment screening forward.

The development of 3D liver models has been an important advancement as they have been shown to better encapsulate organ morphology and intricate multicellular interactions, while demonstrating improved hepatic function, metabolic activity, and extended culture longevity [12, 21–24]. To date, the longest viable hepatic model in vitro is described to be functional for up to 5 months with the use of an inverted colloidal crystal extracellular matrix (ECM) to aid the formation of hepatic hexagonal architecture with primary human foetal hepatocytes [25]. Though this model has the capability to parallel in vivo based long-term exposure studies, the use of an ECM scaffold, however, poses different challenges for ENM hazard assessment [26, 27]. Some 3D hepatic in vitro models based on primary human hepatocytes (PHH) can remain viable for up to 21 days in culture; whilst they can be utilised for the evaluation of e.g. viability, hepatic functionality, metabolic activity and pro-inflammatory response, they do not actively proliferate and so cannot be used for genotoxicity testing which often requires proliferating cells [14]. To overcome this, a proliferating cell-line based 3D in vitro HepG2 spheroid model has been developed, which can be utilised to evaluate multiple toxicological endpoints including genotoxicity [28, 29]. HepG2 cells have shown phenotypic secretion of hepatic plasma proteins (e.g. albumin, fibrinogen and transferrin), phase II gene expression and the capability to positively identify pro-carcinogens and six out of nine drug-induced liver injury (DILI) compounds [24, 30, 31].

Given the limitations associated with standard in vitro hazard testing approaches, this study aimed to determine if more realistic prolonged and repeated ENM exposure regimes exhibited different (geno)toxicological outcomes as compared to standard acute exposures when utilising 3D liver spheroids. Five ENMs were selected based on the ECETOC DF4nanoGrouping decision-making framework for the grouping and testing of ENM, to provide a range of materials that possess different physico-chemical characteristics and exhibit varying dissolution and transformation capacities in a biological environment; TiO₂ and CeO₂ defined as active, insoluble materials, ZnO and Ag defined as soluble, ionic materials and BaSO₄ defined as a passive, non-reactive material [32, 33]. Furthermore, this study sought to determine the genotoxic potency of these materials, at physiologically relevant, low exposure concentrations of 0.2–10.0 µg/mL, upon the 3D in vitro liver models.

Results

ENM intrinsic and extrinsic physico-chemical characterisation

Deemed as the defining features responsible for the beneficial integration of ENMs into various applications and the drivers of ENM toxicity, the characterisation of individual ENM physico-chemical properties is crucial in understanding the interaction, uptake, translocation and potential adverse effects of these materials within biological systems. Five different metallic ENMs were evaluated using physico-chemical characterisation techniques to assess ENM composition, crystallinity, size, surface area, surface properties (e.g. coating, charge, reactivity), solubility, dissolution and bio-persistence.

A summary of all the intrinsic and extrinsic physico-chemical characteristics of the test ENMs are provided in Table 1. The five materials, whilst composed of varying metals, share a similar size and density of 10–50 nm in diameter and 3.5–8.5 g/cm³, respectively. All the ENMs exhibit a similar primary particle size, but they have different specific surface areas (as measured by BET) with Ag possessing the lowest specific surface area of 6.4 m²/g and TiO₂ possessing the highest specific surface area of 51.0 m²/g. All the ENMs have a negative surface charge at pH 7 in 10 mM of KCl water solution, with the exception of CeO₂ with a positive surface charge of +35.2 mV. Only two ENMs, Ag and ZnO, both of which are commonly found to dissociate into ions, have a surface coating; functionalized PVP and UV activated silicon, respectively. Further to this, according to the definitions set out by Arts et al., they are the only two ENMs tested in this study that are hydrophobic, with a water contact angle >90°. Yet, they were both originally categorized as 'soluble, non-persistent ENMs' by the ECETOC DF4nanoGrouping decision-making framework, pertaining to the high rates of dissolution observed [32, 33].

The colloidal behaviour of the five ENMs in the test medium (DMEM) over a period of 24 and 120 h was determined using dynamic light scattering (DLS), as shown in Table 2. In conjunction, the polydispersity index (PDI; measure of ENM sample heterogeneity based on size), and zeta potential (ZP; surface charge), of the materials was measured. For TiO₂, we observed a concentration dependent increase in size distribution, from ~20 nm (0.2 µg/mL) to 300 nm (10 µg/mL). We found comparable results in the size distribution after 24 and 120 h exposure that confirms the ability of complete DMEM medium to preserve colloidal stability of TiO₂ ENMs, even after prolonged exposure. However, all the samples showed high PDI values, presenting polydispersion in the size distribution (3 main populations were detected at all concentrations). The ZP data was set around –10 mV which aligns with ZP value

of complete DMEM and confirms the presence of a uniform protein corona surrounding the ENMs at all exposure concentrations and time points. The only difference detected with ZnO ENMs in complete DMEM, in comparison with TiO₂, is that the size remained below 50 nm for all the samples tested and thus do not exhibit a tendency to actively agglomerate. As for TiO₂, the ZnO ZP values do not significantly change as a function of time and exposure concentration, remaining within 0 to -10 mV, illustrating little surface charge to encourage agglomeration. In Ag samples, after 24 h, the samples showed a broad distribution, with an abrupt increase in diameter for more concentrated samples (2.0–10.0 µg/mL). However, after 120 h, the particle size distribution was narrower and the mean size values are reduced (1.0–10.0 µg/mL samples). Also, in this case, the most reliable hypothesis is that the larger diameter particles sedimented and the complete DMEM stabilized the nano-fraction left in suspension. BaSO₄ ENMs appear very small and exhibit a narrow size distribution for all the samples, resulting in a standard deviation around a few nanometers. The ENM agglomerate size almost doubles from 0.2 to 10.0 µg/mL at both time points, but this material demonstrated the greatest stability and dispersion. In a similarly manner to TiO₂, CeO₂ ENMs displayed an increase in size distribution correlated with an increase in the exposure concentration. However, following 120 h exposure, the difference in size data between the lower and higher concentrations were very low. In fact, even if there is a 2-fold increase in CeO₂ concentration, the mean diameter only slightly increases in size and retains a narrow distribution. Whilst this behaviour is indicative of an increase in colloidal stability versus time, it is more likely due to a partial sedimentation of larger particles that reduce particle size distribution over time.

Dissolution studies in the cell incubation media showed similar trends as the biological clearance data summarized by Arts et al., but there are apparent disagreements with the REACH grouping categories [32]. ZnO showed high 24 h solubility (~10.0 µg/mL) followed by BaSO₄ (2.4 µg/mL) and Ag (0.01 µg/mL), while dissolution of TiO₂ and CeO₂ was not observed (Table 1) [32]. This information suggests that the applied realistic doses for ZnO are borderline to the 24 h solubility level in the test media. As a result, the associated detrimental effects to the HepG2 cells in the experiments with ZnO may, to a great extent, be induced by the dissolved Zn²⁺ ions and not the ENM. With regards to CeO₂, it was observed that 2.4 µg/mL was dissolved after 24 h. Consequently, particle-induced effects were not expected until the second-highest dose applied in this study, unless the effects are very acute.

Analysis of the particle pH and oxygen (O₂) reactivities (Fig. 1) in the test medium showed minor effect with an increase in pH (~0.2–0.3 pH units) for ZnO. This is a lower pH effect than reported in Da Silva et al., where pH increased to above pH 9 in Hams F12 + 10% FBS + 1% Pen/Strep [36, 37]. Changes in the pH of the test medium are driven by the dissolution of the ENMs into different ions. For example, the observed pH increase for ZnO, which mainly occurred within the first 15 mins of the test, is explained by the dissolution of ZnO into Zn²⁺ ions and two hydroxide ions. Similar fast kinetics was observed by the pH increase in this study too. In contrast to ZnO, all the other 4 materials resulted in a pH decrease. For BaSO₄, the decrease was minor, while it was pronounced and persistent for Ag (~ -0.2 pH units).

The temporal oxidative (dO₂) reactivity is understood directly as the extent by which the test material, as a result of redox reactivities and potential dissolution, causes changes in the O₂ concentration dissolved in the test medium with and without the presence of the ENM. With regards to the oxidative behaviour (Fig. 1B), BaSO₄, Ag, and TiO₂ showed a moderate increase in O₂ within the first 500–700 mins after which the oxidative reaction is neutralised. On a relative scale between the 5 test materials, TiO₂ followed by BaSO₄ appear to be the materials with the highest initial dO₂ reactivity. The relatively short duration of the observed reactivity suggests that the potential biological effect of material-induced changes in dO₂ will be due to reactions within the first 200–600 mins after exposure is initiated.

Single bolus, acute and prolonged ENM exposures

Acute, single bolus ENM exposures are commonly used for in vitro ENM hazard assessment and were undertaken to establish a foundation for which to compare prolonged and repeated ENM exposure regimes against.

Liver functionality: albumin and urea

To establish that no significant loss to liver functionality in the 3D HepG2 models occurred and that their fidelity was maintained following either acute (24 h) or prolonged (120 h) ENM exposures, the levels of both albumin and urea were assessed.

Albumin levels were found to remain relatively stable across the dose-range for each test ENM evaluated (Table 3). The concentration of albumin was generally greater following longer-term culture than acute exposure periods, which is to be expected as albumin accumulates with increasing culture time of the 3D spheroids [29]. There was no significant change in albumin levels following longer-term exposure to any of the ENMs tested, nor with acute exposure to TiO₂, ZnO or CeO₂. However, a significant ($p \leq 0.05$) reduction in albumin

Table 1 Physico-chemical characteristics of TiO₂, ZnO, Ag, BaSO₄ and CeO₂ ENMs

ENM physico-chemical characterisation	TiO ₂ NM-105	ZnO NM-111	Ag Sigma 576832	BaSO ₄ NM-220	CeO ₂ NM-212
Core composition and CAS	Titanium Dioxide CAS: 1317-80-2	Zinc Oxide CAS: 1314-13-2	Silver CAS: 7440-22-4	Barium Sulfate CAS: 7727-43-7	Cerium Dioxide CAS: 1306-38-3
Crystalline phases (XRD) ^a	86.9% Anatase + 13.1% Rutile	Zincite	Metallic	Barite	Cerianite
Surface coating	N/A	UV active silicon coating—tri-ethoxycapylsilane	PVP (polyvinylpyrrolidone) functionalized polymer	N/A	N/A
Impurities (XRF)	None (purity > 99%)	P ₂ O ₅ , SiO ₂ , CaO, CuO, Fe ₂ O ₃ , NiO (All < 1.0%)	Pd, Cl (< 1.0%) Rh, Fe, Cu, Ni (< 0.1%) (purity > 99.5%)	Na, Ca, Sr, F, Cl, organic contaminations (purity > 93.8%)	P ₂ O ₅ , CaO, Cl (< 1.0%) V ₂ O ₅ , SO ₃ , CoO, MgO, SiO ₂ , CuO, Fe ₂ O ₃ , ZnO (< 0.1%)
Size (MinFerret; TEM) ^b	25 nm	40.6 nm	30.0 nm	31.5 nm	13.7 nm
3D aspect ratio and circulatory (TEM) ^b	N/A	A.R: 1.88 ± 0.78 C: 0.80 ± 0.12	A.R: 1.36 ± 0.30 C: 0.88 ± 0.09	A.R: 1.22 ± 0.19 C: 0.98 ± 0.04	A.R: 1.21 ± 0.25 C: 0.97 ± 0.06
Surface area (BET)	51.0 m ² /g	12.0 m ² /g	6.4 m ² /g	33.0 m ² /g	27.0 m ² /g
Relative density (He pycnometer)	3.95 g/cm ³	4.99 g/cm ³	8.36 g/cm ³	4.13 g/cm ³	7.2 g/cm ³
Chemical nature of the surface (XPS) ^c	Ti: 24.5% O: 65.0% C: 10.5%	Zn: 34.6% C: 22.2% O: 43.1%	Ag: 38.9% C: 47.6% O: 13.5%	Ba: 21.5% S: 12.5% O: 65.8%	Ce: 25.6% O: 74.4%
Surface charge (zeta potential at pH 7 in 10 mM KCl water solution)	− 17.0 mv	N/A	− 30.0 mV	− 30.2 mV	+ 35.2 mV
Surface reactivity (FRAS)	18.6 (nmol TEU/m ² ENM)	20.3 (nmol TEU/m ² ENM)	2240.0 (nmol TEU/m ² ENM)	13.9 (nmol TEU/m ² ENM)	16.7 (nmol TEU/m ² ENM)
Surface reactivity (EPR DMPO and CPH spin count)	DMPO: 3.01e ⁺¹² CPH: 8.29e ⁺¹²	DMPO: 1.21e ⁺¹³ CPH: 1.28e ⁺¹³	DMPO: 8.00e ⁺¹¹ CPH: 5.58e ⁺¹³	DMPO: 4.92e ⁺¹² CPH: 8.89e ⁺¹²	DMPO: 5.86e ⁺¹² CPH: 1.22e ⁺¹⁴
Hydrophobicity (water contact angle)	Hydrophilic (60°)	Hydrophobic (152°)	Hydrophobic (141°)	Hydrophilic (< 10°)	Hydrophilic (60°)
Dissolution ^d	Low dissolution (in PBS)	High dissolution (in biological media DMEM + FCS)	Unknown	Low dissolution (in PBS)	Low dissolution (in biological media DMEM + FCS)
Dissolution (24 h) in DMEM + 10% FBS + 1% Pen/Strep	Not detectable	10.11 ± 0.31 µg/mL	0.01 ± 0.01 µg/mL	2.40 ± 0.01 µg/mL	Not detectable
Biological clearance in vivo (t50) ^d	Physiological clearance (> 40 days)	Rapid clearance	Unknown	Accelerated clearance (< 40 days)	Decelerated clearance (> 40 days)
Previous REACH grouping category ^d	4—active, biopersistent, non-fibrous ENMs	1—soluble, non-persistent ENMs	1—soluble, non-persistent ENMs	3—passive, biopersistent, non-fibrous ENM	4—active, biopersistent, non-fibrous ENMs

Characterisation techniques are abbreviated, in order of appearance, as follows: CAS chemical abstracts service, XRD X-ray diffraction, XRF X-ray fluorescence, TEM transmission electron microscopy, BET Brunauer–Emmett–Teller, XPS X-ray photoelectron spectroscopy, FRAS ferric reduction ability of serum, EPR electron paramagnetic resonance spectroscopy, DMPO 5,5-dimethyl-1-pyrroline-N-oxide, CPH 1-hydroxy-3-carboxy-pyrrolidine, REACH registration, evaluation, authorisation and restriction of chemicals

All data indicated with a ^a is complemented by TEM images, sourced from Keller et al. and Yin et al. ^b is complemented by XRD graphs is complemented by XPS graphs located in the Additional file 1: Figure S1, S2 and S3, respectively. All data with a ^d was sourced from Arts et al. 2016 [32, 34, 35]

Table 2 The colloidal behaviour of TiO₂, ZnO, Ag, BaSO₄ and CeO₂ ENMs once exposed to DMEM complete media for 24 and 120 h.

ENM sample	ENM concentration (µg/mL)	Exposure time (h)	pH	Size DLS (nm)		PDI	Zeta Pot. (mV)	
				Mean	Stdev		Mean	Stdev
TiO ₂ NM 105	0.2	24	7.6	23	1	0.6	- 8.8	0.6
	0.5	24	7.7	108	64	0.3	- 10.2	0.6
	1	24	7.6	112	49	0.4	- 9.9	0.4
	2	24	7.7	226	46	0.3	- 8.0	0.4
	5	24	7.7	216	24	0.7	- 10.3	0.8
	10	24	7.6	282	22	0.6	- 9.8	0.6
	0.2	120	7.8	37	2	0.6	- 5.9	0.5
	0.5	120	7.8	97	21	0.3	- 10.0	0.8
	1	120	7.9	71	2	1.0	- 10.2	0.3
	2	120	7.9	232	24	0.5	- 13.1	0.9
ZnO NM 111	0.2	24	7.6	21	3	0.4	- 7.8	0.9
	0.5	24	7.7	25	3	0.6	- 6.7	1.6
	1	24	7.7	22	4	0.4	- 4.3	0.8
	2	24	7.7	20	1	0.4	- 7.7	0.5
	5	24	7.7	50	12	0.4	- 4.4	0.9
	10	24	7.7	74	43	0.2	- 8.3	0.8
	0.2	120	7.8	30	1	0.5	- 7.5	0.8
	0.5	120	7.8	28	1	0.8	- 5.8	1.2
	1	120	7.8	28	4	0.6	- 6.9	0.6
	2	120	7.8	40	3	0.6	- 6.8	1.8
Ag Sigma 576832	0.2	24	7.8	26	1	0.7	- 7.9	1.3
	0.5	24	7.8	43	13	0.4	- 9.5	0.7
	1	24	7.8	138	11	0.2	- 10.9	1.6
	2	24	7.8	244	166	0.3	- 10.0	0.8
	5	24	7.8	273	186	0.4	- 10.4	1.3
	10	24	7.8	308	36	0.3	- 11.3	0.8
	0.2	120	8.1	79	2	0.4	- 11.1	1.6
	0.5	120	8.0	73	2	0.4	- 11.2	0.3
	1	120	7.9	117	3	0.6	- 7.7	0.8
	2	120	8.1	89	3	0.4	- 10.8	0.9
BaSO ₄ NM 220	0.2	24	7.6	20	1	0.4	- 8.6	0.5
	0.5	24	7.6	27	2	0.7	- 9.5	0.8
	1	24	7.6	21	1	0.5	- 8.1	0.9
	2	24	7.6	21	1	0.6	- 9.6	0.9
	5	24	7.7	32	1	0.8	- 9.6	0.2
	10	24	7.7	41	3	1.0	- 11.6	0.8
	0.2	120	7.8	51	1	0.6	- 4.1	0.9
	0.5	120	7.8	54	2	0.6	- 7.7	0.4
	1	120	7.8	59	1	0.6	- 8.1	0.7
	2	120	7.8	66	2	0.6	- 4.6	1.3
5	120	7.8	80	1	0.6	- 8.3	1.0	
10	120	7.8	95	1	0.6	- 10.0	0.8	

Table 2 (continued)

ENM sample	ENM concentration (µg/mL)	Exposure time (h)	pH	Size DLS (nm)		PDI	Zeta Pot. (mV)	
				Mean	Stdev		Mean	Stdev
CeO ₂ NM 212	0.2	24	7.6	21	2	0.5	-6.5	0.4
	0.5	24	7.6	24	1	0.7	-7.4	0.8
	1	24	7.7	109	53	0.4	-6.6	0.2
	2	24	7.7	351	218	0.4	-10.2	0.6
	5	24	7.7	598	446	0.8	-8.1	0.9
	10	24	7.7	392	116	0.5	-10.7	1.0
	0.2	120	8.2	76	1	0.4	-7.0	1.3
	0.5	120	7.9	56	3	0.6	-7.3	0.4
	1	120	7.8	98	4	0.8	-4.5	0.5
	2	120	7.8	90	42	0.7	-6.7	0.3
	5	120	7.9	114	1	0.6	-9.4	0.7
	10	120	7.9	194	29	0.4	-9.1	0.6

was observed following 24 h exposure to the higher doses (5.0 µg/mL and 10.0 µg/mL) of Ag and BaSO₄ ENMs.

In a similar manner to albumin, the concentration of urea produced by the HepG2 spheroids also remained consistent across all ENM exposures (Table 4). A significant reduction ($p = 0.0061$) in urea was only observed following acute exposure to 10.0 µg/mL of ZnO and longer-term exposure to 5.0 µg/mL of TiO₂.

(Pro)-inflammatory response: IL-8, IL-6 and TNF-α cytokine release

Following ENM exposure, IL-6, IL-8 and TNF-α cytokine levels were assessed to investigate the induction of any potential (pro-)inflammatory response. Attributable to the 3D liver spheroid model being a monoculture of HepG2 epithelial-like cells, all IL-6 and TNF-α results were found to be below detectable limits regardless of ENM tested or exposure-regime applied and so these cytokines were not considered further (data not shown). In contrast, IL-8, an acute phase chemokine released by hepatic epithelial cells, was modified in response to the ENM exposures as illustrated in Fig. 2. When comparing the IL-8 response between acute and prolonged exposure regimes for TiO₂, ZnO, BaSO₄ and CeO₂, there was an increase in the concentration of IL-8 present across the dose range. Exposure to 0.5 µg/mL of TiO₂ induced the only significant ($p = 0.0042$) increase in IL-8 following acute exposure, which was no longer observed after 120 h (Fig. 1A). Instead, as the concentration of TiO₂ increased in the longer-term exposure, the concentration of IL-8 present decreased with 5.0 µg/mL and 10.0 µg/mL

TiO₂ inducing a significant ($p \leq 0.01$) reduction in IL-8. Neither ZnO (Fig. 2B), or Ag (Fig. 2C) induced any significant changes in IL-8 production following either acute or prolonged low-dose ENM exposure with both showing a similar trend to the control across the dose range. Fig. 2D demonstrates that BaSO₄ was the only material to induce an increase in IL-8 across the 2.0–10.0 µg/mL dose range. However, significance ($p = 0.0261$) was only achieved at the single dose of 0.2 µg/mL BaSO₄. Exposure to CeO₂, Fig. 2E, resulted in IL-8 induction at 0.2 µg/mL and 0.5 µg/mL following acute exposures and across the prolonged exposure dose range (0.2 and 2.0 µg/mL). However, none of these IL-8 peaks were found to be significant despite being up to 3-fold higher than the negative control.

Cytotoxicity and genotoxicity

To determine if the test materials induced fixed DNA damage following both acute and prolonged exposure, the micronucleus (MN) assay was employed in conjunction with an appropriate cytotoxicity assay.

As shown in Fig. 3, cytotoxicity was not induced following either acute or prolonged exposure to any of the test ENM up to a top dose of 10.0 µg/mL of material. In contrast, a significant dose-dependent increase in genotoxicity was observed with all test ENMs following acute exposure. With TiO₂, the lowest observed adverse effect level (LOAEL) was 2.0 µg/mL ($p = 0.0052$); the frequency of MN induction increased further at 5.0 µg/mL ($p < 0.0001$), where the MN frequency was 2.4-fold higher than the negative control. Similar to TiO₂,

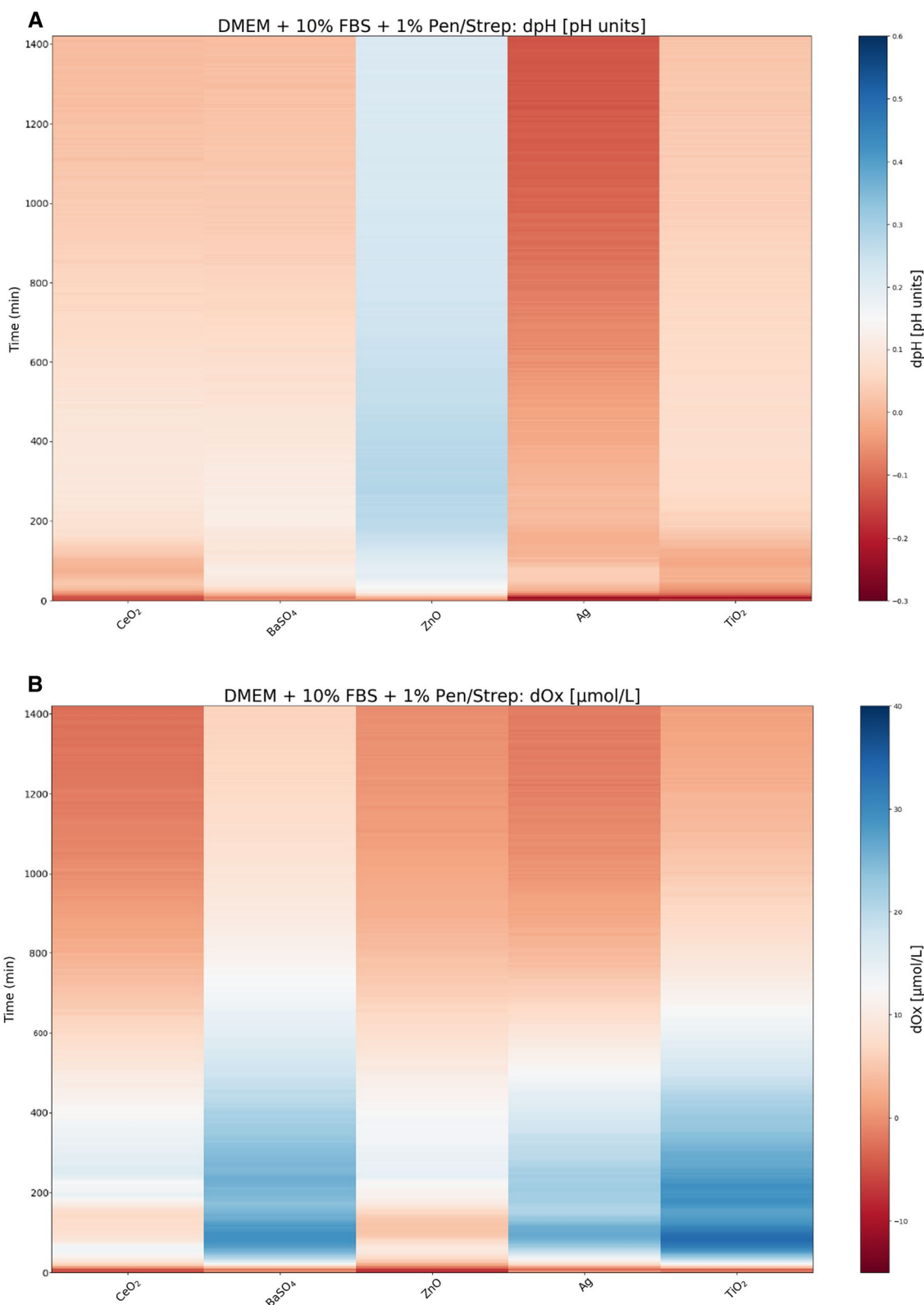


Fig. 1 Surface plot shows the 24 h (1400 min) temporal pH reactivity (dpH) **(A)** and temporal oxidative reactivity (dOx) **(B)** for CeO₂ (NM-212), BaSO₄ (NM-220), ZnO (NM-111), Ag (Sigma 576832) and TiO₂ (NM-105) in DMEM + 10% FBS + 1% Pen/Strep cell culture medium, during in vitro test conditions using the SDR method

whilst Ag, BaSO₄ and CeO₂ did not induce a significant increase in genotoxicity following prolonged exposures, each material was shown to induce a significant acute genotoxic response. Ag (Fig. 3C) displayed a significant increase in genotoxicity following 24 h exposure to 0.5 µg/mL ($p = 0.0033$), 1.0 µg/mL ($p = 0.0004$) and 5.0 µg/mL ($p = 0.0032$); although the observed effect was a plateau with all doses exhibiting an MN frequency 2.05–2.51%. BaSO₄ induced a significant genotoxic response with all but one concentration, 1.0 µg/mL, following acute exposure as illustrated in Fig. 3D. Similarly to Ag, acute exposure to CeO₂ (Fig. 3E) induced a significant genotoxicity response at 3 concentrations: 0.5 µg/mL ($p = 0.0185$), 5.0 µg/mL ($p = 0.0191$) and 10.0 µg/mL ($p = 0.0209$). ZnO (Fig. 3B) was the only material to exhibit both an acute and prolonged effect upon genotoxicity in 3D HepG2 liver spheroids. ZnO appears to induce different patterns of genotoxicity between the acute and prolonged exposure regimes. The acute genotoxic response appears to peak and trough, whereby ZnO induces a significant increase in genotoxicity at 0.5 µg/mL ($p < 0.0001$), 1.0 µg/mL ($p = 0.0083$), 5.0 µg/mL ($p < 0.0001$) and 10.0 µg/mL ($p = 0.0001$). In contrast, following the prolonged exposure, genotoxicity increased in a dose dependent manner up to 1.0 µg/mL and then plateaued, with the top dose reducing back to control levels. As shown by Fig. 3, none of the other test materials induced a significant positive induction of genotoxicity following prolonged exposure. Considering the acute (24 h) data, the genotoxicity potency ranking based on the dose response relationship and the greatest fold-change in MN induction is: ZnO > TiO₂ > BaSO₄ = CeO₂ > Ag.

Fractionated repeated, prolonged ENM exposures

Fractionated, repeated prolonged ENM exposures were also investigated to more accurately simulate human ENM exposure and to determine if the added complexity of the exposure regime would significantly affect the toxicological outcome in 3D HepG2 liver spheroids. Whilst both exposure regimes resulted in the same final exposure concentration, the manner in which the ENMs were exposed to the spheroids differed between a single, bolus dose on day one and a repeated, fractionated dose given every day for the entire five day exposure, as illustrated in Fig. 4.

Liver functionality: albumin and urea

To ensure the HepG2 spheroids maintained their phenotypic functionality following both ENM prolonged exposure regimes, the levels of both albumin and urea

were measured post exposure. For both albumin and urea concentrations, there was no significant difference between prolonged single, bolus, and repeated, fractionated exposure regimes irrespective of the test ENM applied or the dose. Based on the values in Table 5, the average range between the mean albumin and urea values for each exposure regime was 3.84 ng/µL of albumin and 0.06 ng/µL of urea. Thus, the manner in which the 3D HepG2 liver spheroids are exposed to ENM over prolonged exposure regimes was not observed to significantly impede liver functionality.

(Pro)-inflammatory response: IL-8, IL-6 and TNF- α cytokine release

With the complex interplay of inflammatory mediators, feedback loops and pathway cascades, timing is crucial with inducing a (pro-)inflammatory response. Therefore, it was important to establish if modifying the prolonged exposure regime to a repeated, fractionated exposure method as opposed to a single, bolus exposure on day one, would affect the (pro-)inflammatory response in HepG2 spheroids. In a similar manner to the acute and prolonged exposure studies described earlier, IL-6, IL-8 and TNF- α cytokine release was assessed for both the prolonged single, bolus and the repeated, fractionated ENM exposure regimes, but only an IL-8 (pro-)inflammatory release was detectable (Fig. 5). Prolonged exposure to both 0.5 µg/mL and 5.0 µg/mL of TiO₂ and ZnO ENMs dosed via the two different methods, showed no significant difference in the IL-8 (pro-)inflammatory response in the HepG2 liver spheroids. For the individual test ENMs, there appears to be little to no difference at all in the concentration of IL-8 released following exposure to either material.

Cytotoxicity and genotoxicity

To mimic a gradual accumulation of ENMs and determine the effect this may have on DNA damage and cytotoxicity in HepG2 liver spheroids, spheroids were dosed with TiO₂ and ZnO ENMs via two techniques; a single, bolus dose or a repeated, fractionated dose. Exposing 3D HepG2 liver spheroids to either TiO₂ or ZnO, irrespective of dose, did not induce a significant increase in cell death or MN frequency as compared to the untreated control (Fig. 6). Furthermore, there was no significant difference in the cytotoxicity or genotoxicity observed when comparing the single, bolus dose on day one versus the repeated, fractionated dose every day in 3D HepG2 liver spheroids.

Table 3 Albumin concentration per HepG2 spheroid following both acute (24 h) and prolonged (120 h) ENM exposure to increasing concentrations (0.2–10.0 µg/mL) of ENMs

ENM concentration (µg/mL)	Albumin per spheroid (ng/µL) following Acute (24 h) exposure (95% CI)					Albumin per spheroid (ng/µL) following Prolonged (120 h) exposure (95% CI)				
	TiO ₂	ZnO	Ag	BaSO ₄	CeO ₂	TiO ₂	ZnO	Ag	BaSO ₄	CeO ₂
Untreated negative control	29.660 (4.85–24.47)	23.171 (15.14–30.20)	27.785 (10.61–44.96)	30.703 (15.06–46.35)	52.878 (42.54–63.22)	35.783 (31.02–40.54)	27.510 (21.82–33.20)	36.944 (25.88–38.01)	32.550 (16.19–48.91)	49.851 (41.15–58.56)
0.2	28.235 (23.88–32.59)	24.715 (19.06–30.37)	24.903 (19.12–30.69)	27.002 (21.50–32.51)	52.235 (45.47–59.00)	35.245 (26.64–43.85)	28.506 (21.66–35.35)	33.821 (23.58–44.06)	31.043 (25.36–36.72)	50.506 (45.50–55.52)
0.5	28.622 (22.52–34.72)	24.232 (17.51–30.95)	33.376 (5.90–60.86)	26.915 (20.44–33.39)	55.154 (47.86–62.45)	37.734 (34.45–41.02)	26.990 (21.17–32.81)	45.420 (37.39–53.45)	32.922 (29.74–36.11)	49.160 (35.30–63.02)
1.0	29.108 (26.00–32.22)	23.943 (16.90–30.99)	24.207 (16.36–32.06)	25.417 (16.71–34.12)	56.472 (41.31–71.63)	34.880 (24.30–45.46)	27.748 (21.07–34.42)	30.996 (25.10–36.90)	35.691 (31.84–39.54)	52.407 (51.08–53.74)
2.0	32.104 (24.97–39.24)	24.343 (14.05–34.64)	33.428 (19.10–47.76)	29.790 (17.75–41.83)	52.620 (47.75–57.49)	33.071 (26.30–39.85)	27.132 (23.13–31.13)	40.737 (35.84–45.63)	38.078 (22.41–53.57)	50.857 (43.77–57.94)
5.0	30.114 (16.48–43.75)	24.611 (21.88–27.34)	9.520* (–7.69 to 26.74)	18.216* (6.51–29.92)	55.937 (42.99–68.88)	33.236 (28.45–38.02)	28.740 (23.08–34.40)	35.984 (25.21–46.76)	30.937 (29.41–32.46)	56.619 (45.51–67.73)
10.0	28.137 (21.96–34.32)	22.989 (14.95–31.03)	12.666* (–5.14 to 30.47)	14.032* (4.27–23.79)	51.445 (43.73–59.16)	30.494 (24.01–36.97)	31.111 (15.22–47.01)	35.342 (32.29–38.39)	33.686 (30.99–36.39)	50.287 (46.88–53.70)
Aflatoxin B1 positive control	24.488 (4.24–44.74)	22.925 (20.29–25.56)	32.943 (5.80–60.08)	35.329 (10.87–59.79)	52.907 (47.02–58.80)	36.650 (31.60–41.70)	30.789 (13.38–49.20)	38.405 (33.32–43.49)	31.139 (30.14–32.14)	48.498 (44.01–52.99)

Mean data of three biological replicates, analysed in triplicate (n = 9) are presented with 95% confidence intervals. Significance is indicated in relation to the negative control, where * = p ≤ 0.05

Table 4 Urea concentration per HepG2 spheroid following both acute (24 h) and prolonged (120 h) exposure to increasing concentrations (0.2–10.0 µg/mL) of ENMs

ENM concentration (µg/mL)	Urea per spheroid (ng/µL) following Acute (24 h) exposure (95% CI)					Urea per spheroid (ng/µL) following Prolonged (120 h) exposure (95% CI)				
	TiO ₂	ZnO	Ag	BaSO ₄	CeO ₂	TiO ₂	ZnO	Ag	BaSO ₄	CeO ₂
Untreated negative control	0.690 (0.625–0.754)	0.937 (0.786–1.088)	0.455 (0.217–0.693)	0.394 (0.235–0.553)	0.675 (0.564–0.785)	1.021 (0.981–1.061)	0.744 (0.365–1.123)	0.389 (0.188–0.589)	0.292 (0.126–0.459)	0.927 (0.746–1.107)
0.2	0.813 (0.676–0.950)	1.245 (1.097–1.393)	0.520 (0.337–0.703)	0.498 (0.379–0.618)	0.724 (0.697–0.752)	1.108 (0.902–1.314)	0.832 (0.565–1.098)	0.523 (0.431–0.615)	0.402 (0.276–0.527)	0.968 (0.812–1.124)
0.5	0.889 (0.809–0.970)	1.036 (0.969–1.103)	0.550 (0.307–0.793)	0.505 (0.312–0.698)	0.762 (0.649–0.874)	1.273 (0.811–1.725)	0.769 (0.563–0.974)	0.563 (0.440–0.686)	0.409 (0.207–0.611)	0.920 (0.761–1.078)
1.0	0.859 (0.693–1.025)	1.145 (1.056–1.234)	0.539 (0.414–0.664)	0.638 (0.571–0.706)	0.775 (0.735–0.816)	1.213 (1.092–1.334)	0.794 (0.675–0.914)	0.490 (0.264–0.716)	0.549 (0.478–0.621)	0.940 (0.710–1.170)
2.0	0.930 (0.783–1.076)	1.120 (0.873–1.366)	0.567 (0.423–0.771)	0.573 (0.376–0.771)	0.717 (0.549–0.885)	1.197 (0.902–1.492)	0.795 (0.502–1.089)	0.521 (0.428–0.688)	0.481 (0.274–0.688)	0.971 (0.706–1.236)
5.0	0.699 (0.565–0.834)	0.793 (0.668–0.919)	0.596 (0.324–0.869)	0.643 (0.487–0.799)	0.782 (0.645–0.919)	0.805* (0.636–0.974)	0.832 (0.729–0.935)	0.703 (0.595–0.811)	0.781 (0.515–1.047)	0.955 (0.672–1.238)
10.0	0.628 (0.371–0.885)	0.728* (0.635–0.821)	0.571 (0.518–0.624)	0.618 (0.214–1.021)	0.792 (0.617–0.967)	0.846 (0.771–0.921)	0.737 (0.532–0.942)	0.726 (0.367–1.085)	0.899 (0.735–1.063)	0.909 (0.755–1.064)
Aflatoxin B1 Positive Control	0.773 (0.718–0.828)	0.881 (0.729–1.033)	0.515 (0.332–0.698)	0.423 (0.330–0.517)	0.755 (0.500–1.010)	0.846 (0.771–0.921)	0.488* (0.212–0.763)	0.516 (0.432–0.600)	0.323 (0.224–0.422)	0.953 (0.878–1.029)

Mean data of three biological replicates, analysed in triplicate (n = 9) are presented with 95% confidence intervals. Significance is indicated in relation to the negative control, where * = p ≤ 0.05

Discussion

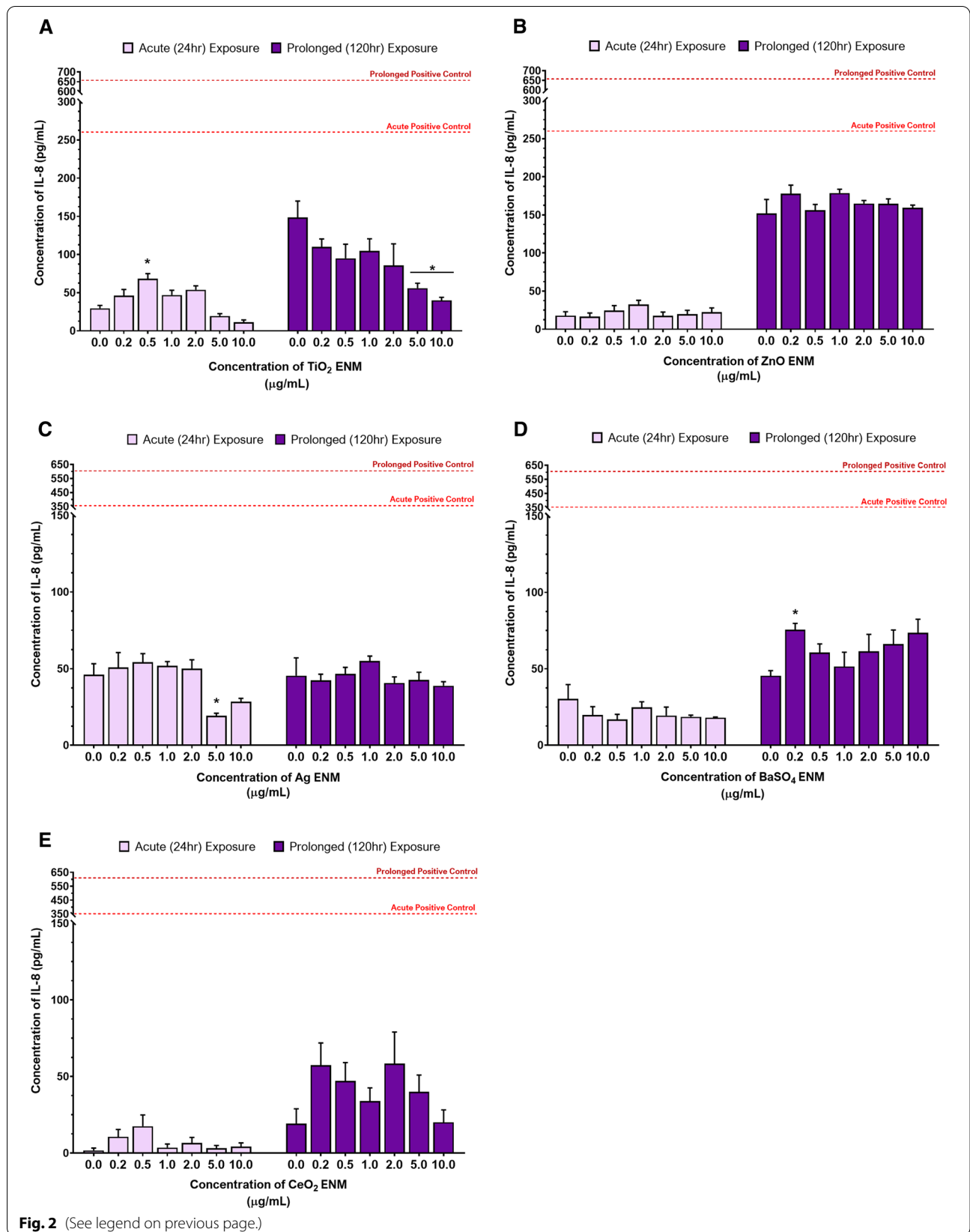
It is widely acknowledged that it is unsustainable and ethically divisive to rely primarily on in vivo based test systems for comprehensive ENM hazard assessment, as such, research into suitable, physiologically relevant in vitro alternatives has been at the forefront of nanotoxicology in recent years. Not only have scientists strived to alleviate the limitations of current in vitro models to enhance the longevity and predictivity of the models, but, as in the present study, there have been recent efforts to start addressing the manner in which humans are exposed to ENMs in natural life [38, 39]. This study aimed to determine, firstly, if a more realistic, low-dose prolonged ENM exposure would provoke a significantly different (geno)toxicological effect compared to an acute exposure in 3D HepG2 spheroids. Secondly, this study aimed to determine if a daily repeated, fractionated ENM exposure regime would significantly alter the toxicological outcome in 3D HepG2 spheroids compared to a single, bolus prolonged exposure. To assess this, a cell-line based 3D in vitro HepG2 spheroid model able to evaluate cytotoxicity, (pro-)inflammatory response and genotoxicity associated with both acute and longer-term (≤ 10 days) ENM exposure upon the liver was utilised. In this system, hepatocyte spheroids recapitulated basic in vivo hepatic functions and structure, whilst maintaining specific parameters required for multiple biochemical endpoint testing [28, 29]. Applying this liver model, a range of five different ENMs were evaluated, across a low concentration range of 0.2–10.0 $\mu\text{g}/\text{mL}$, to determine whether the individual physico-chemical characteristics would elicit a different biological response following either an acute (24 h) or longer-term (120 h) exposure scenario in vitro. A low-dose concentration range was selected to not only simulate physiological relevant concentrations of translated ENMs in the liver, but to ensure that the in vitro test system is not over saturated by the sheer volume of material, which increases the risk of a misleading positive toxicity result [14, 15].

Previously, many in vitro studies have focused on the acute effects of high concentrations of ENMs [17, 40]. Acute exposure regimes are a less laborious and generally a more efficient way to quickly determine whether a substance has the potential to illicit an adverse reaction or be hazardous. However, it does not provide an accurate

representation of the prolonged effects this acute exposure may have nor does it provide any indication of the accumulated effects were this exposure to be a recurring event. In order to address this, a longer-term exposure regime of five days (120 h; bolus and repeated) was established to provide a more realistic dosing scenario, as most individuals are likely to be exposed to multiple, low doses of ENMs over time [17, 41]. Alongside the evaluation of key toxicological endpoints, such as cytotoxicity, (pro-)inflammatory response and genotoxicity, the viability and fidelity of the liver model had to be assessed throughout the duration of this study. As biomarkers of hepatic metabolism and functionality, albumin and urea production were measured. Albumin is a stable, 66.5 kDa plasma protein primarily synthesised in the liver and is principally responsible for maintaining oncotic pressure within in the blood, in order to prevent excess volumes of water being leaked into the surrounding tissues [42]. In addition to this, albumin has been found to play a role in immunomodulation, antioxidant effects and binding to multiple drugs, toxins, and other molecules, including ENMs. Albumin is one of the most abundant proteins frequently found in the protein corona of ENMs [43, 44]. Urea is an organic, 60 Da, metabolic end product of protein catabolism; a process which happens within the liver as it is the sole organ that has enzymes for urea synthesis [45]. Urea synthesis is crucial in the breakdown and excretion of nitrogen waste products, such as ammonia, which are toxic to the mammalian body if not metabolised to urea and excreted as urine [46]. Across all acute ENM exposures, the viability and liver functionality was not significantly reduced, with the exception of exposure to the top concentrations (5.0 $\mu\text{g}/\text{mL}$ and 10.0 $\mu\text{g}/\text{mL}$) of Ag and BaSO₄ which did significantly reduce albumin production. As this reduction was not mirrored in the production of urea, one suggestion for this decrease could be the tendency of ENMs to actively adsorb proteins, like albumin, to their surface as part of the protein corona; the reduction may therefore be an artifact [47, 48]. Over the duration of the prolonged exposures, as expected, the albumin levels increased as a result of the actively proliferating cells on the outer layers of the spheroid. Subsequently, the higher prevalence of albumin could saturate the ENM corona and so the previously observed decrease in albumin may have been compensated for. Overall, neither acute nor prolonged exposure to these test ENMs significantly reduced the fidelity of

(See figure on next page.)

Fig. 2 Release of IL-8 (pro-)inflammatory cytokines in 3D HepG2 liver spheroids following both acute (24 h) and longer-term (120 h) exposure to 0.2–10.0 $\mu\text{g}/\text{mL}$ of (A) TiO₂, (B) ZnO, (C) Ag, (D) BaSO₄ and (E) CeO₂ ENMs. An untreated, media only sample was used as the negative control. The positive assay control was 0.25 $\mu\text{g}/\text{mL}$ of TNF- α protein (NBP2-35076-50 μg , Biotechnie, UK), as indicated by the dotted line, which represents the mean positive control response for both acute (light red line) and prolonged (dark red line) exposures. Mean data of three biological replicates, analysed in triplicate (n = 9) are presented \pm SEM. Significance is indicated in relation to the negative control, where * = $p \leq 0.05$



these HepG2 spheroids, which also correlates with the limited cytotoxicity observed over the concentration-ranges and exposure regimes applied.

Each ENM has a unique set of physico-chemical characteristics (e.g. size, shape, composition, surface charge, coating, crystallinity and solubility) which determine how these materials interact with biological systems; influencing cellular uptake, bio-durability, translocation and deposition around the body [49]. Not only is it important to fully characterize an ENM prior to exposure, it is equally as important to characterize these materials under biological exposure conditions as these materials may undergo transformation (e.g. dissolution, aggregation and reprecipitation) when they come into contact with different biological fluids [39]. As a result, these novel size-specific characteristics often heavily influence the toxicological potential for such materials. Therefore, it is particularly important to consider the physico-chemical characteristics and biotransformation potential of these materials when evaluating the toxicity outcomes observed.

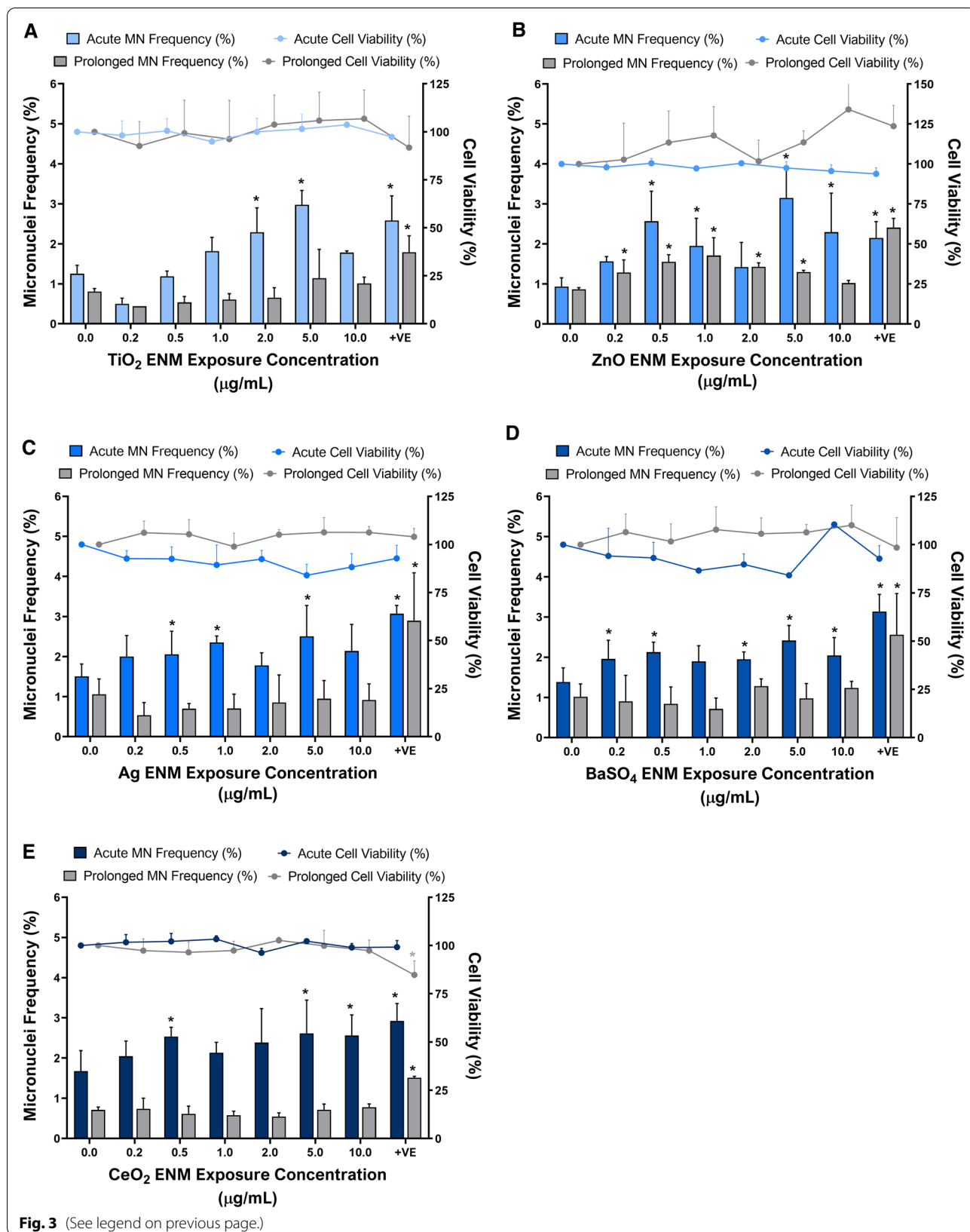
Many ENMs are known reactive oxygen species (ROS)/reactive nitrogen species (RNS) inducers, and directly or indirectly cause an imbalance in the redox homeostasis of the cell [50–52]. Most metal based ENMs, particularly transition metals, elicit ROS and free radical mediated toxicity via Fenton-type reactions. As a result, their ability to influence intracellular calcium concentrations, activate (pro-)inflammatory transcription factors (e.g., nuclear factor kappa B [NF- κ B]) and modulate cytokine release via the production of free radicals, is believed to be linked to the greater surface area, therefore increased surface reactivity, as well as the addition of pro-oxidant thiol groups on the surface of the materials [50–52]. Interestingly, the ENM with greatest surface area (TiO₂) did exhibit the greatest O₂ reactivity and induced the greatest IL-8 response over any other material, with a significant increase in IL-8 release observed following acute exposure to 0.50 μ g/mL. This was no longer the case following prolonged exposures. Instead, as the concentration of TiO₂ increased in the prolonged exposure studies, the concentration of IL-8 decreased. This may be attributable to the increased agglomeration observed, restricting cellular uptake and reducing the surface area

available for oxidative reactions to occur. In addition, the likelihood is that any REDOX or Fenton-type reactions will have occurred within the first 24 h of the exposure. As a result, the production of free radicals that trigger the release of (pro-)inflammatory cytokines, like IL-8 via the activation of REDOX sensitive Nf- κ β or MAPK signalling pathways, may no longer be as actively expressed 120 h later. The differences in ENM associated IL-8 release between acute and prolonged exposures could suggest that other factors (e.g. dissolution, agglomeration, rate of cellular uptake) may be more influential in orchestrating the (pro-)inflammatory response during this time. It appears the two materials (Ag and ZnO) with the greatest solubility and lowest surface area, exhibit minimal dose-dependent effects in IL-8 release, with a consistent IL-8 response observed across almost all doses following either an acute or prolonged exposure. In contrast, ENMs with a more bio-persistent nature, which take longer to breakdown and clear, could cause a greater and more variable inflammatory response in the prolonged exposure. For example, BaSO₄ induced the only significant increase in IL-8 release following prolonged exposure. The overall increase in IL-8 release observed between the acute and prolonged ENM exposures is likely caused by the reduced oxygen diffusion towards the centre of the spheroid over time. This will result in increased hypoxic conditions within the spheroid core, which is associated with increased IL-8 production [29, 53–55].

Genotoxicity of the five test ENMs was assessed using the 'gold standard' in vitro MN assay, which is the recommended test for evaluating fixed gross chromosomal damage for regulatory purposes. Whilst there is an OECD Test Guideline (TG487) for this assay, it has long been recognised that nano-specific adaptations to the method are required, which were included in the approach taken within this study [56, 57]. No significant cytotoxicity was detected following either acute or prolonged exposure to any of the ENMs tested, regardless of the concentration or dosing regimen employed. However, all five ENMs tested positive for genotoxicity following acute exposure, albeit not in a dose-dependent manner, due to variation in agglomeration across dose ranges. A genotoxicity potency ranking was established based on the dose response and the greatest fold-change in MN

(See figure on next page.)

Fig. 3 Cytotoxicity and genotoxicity responses in HepG2 spheroids following both acute (24 h) and prolonged (120 h) exposure to 0.2–10.0 μ g/mL of (A) TiO₂, (B) ZnO, (C) Ag, (D) BaSO₄ and (E) CeO₂ ENMs. Cytotoxicity was assessed using the cytokinesis-block proliferation index (CBPI) for acute exposures, whilst trypan blue was assessed for the prolonged exposures, both of which are presented relative to the negative, untreated control. A known liver carcinogen, aflatoxin B1 (0.1 μ M) was used as a positive control for genotoxicity. For acute exposures, 1000 binucleated cells were scored per replicate for each dose point using the cytokinesis-block version of the MN assay (2000 binucleate cells scored in total per dose). For prolonged exposures, 2000 mononucleated cells were scored per replicate for each dose point using the mononuclear MN assay (4000 mononucleate cells scored in total per dose). Mean data of two and three biological replicates (n = 2, n = 3) for genotoxicity and cytotoxicity respectively is presented \pm SD. Significance indicated in relation to the negative control: * = $p \leq 0.05$



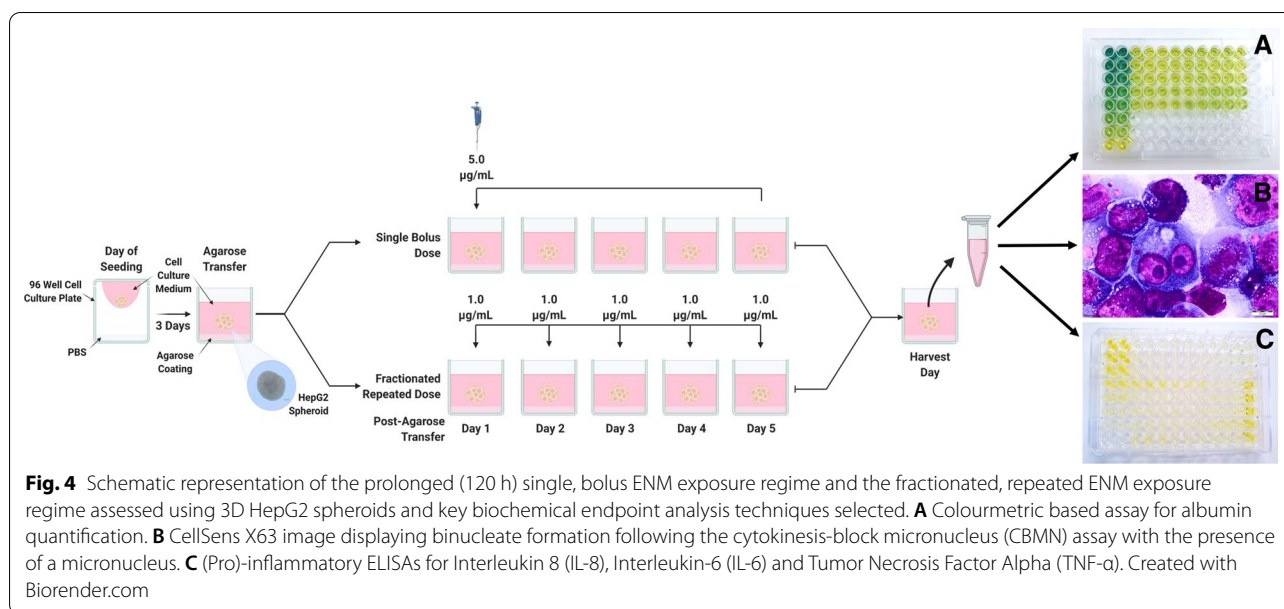


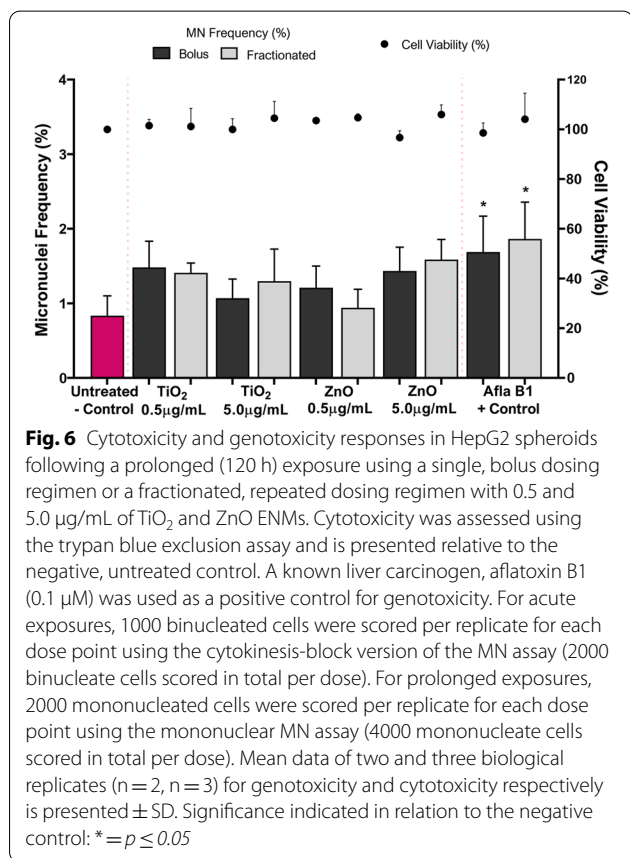
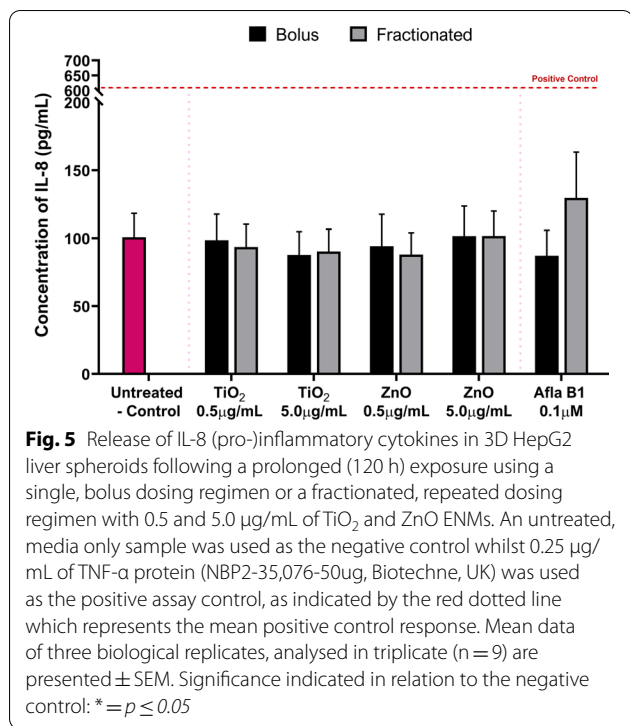
Table 5 Concentration of albumin and urea produced per HepG2 spheroid following a prolonged (120 h) exposure using a single, bolus dosing regime or a fractionated, repeated dosing regime with 0.5 and 5.0 $\mu\text{g/mL}$ of TiO_2 and ZnO ENMs

3D HepG2 liver spheroid liver functionality	Albumin per spheroid (ng/ μL) (95% CI)		Urea per spheroid (ng/ μL) (95% CI)	
	Bolus	Fractionated	Bolus	Fractionated
Untreated negative control	32.807 (29.323–36.291)		0.805 (0.729–0.880)	
TiO_2 0.5 $\mu\text{g/mL}$	37.736 (29.973–45.499)	33.716 (30.426–37.007)	0.885 (0.722–1.048)	0.806 (0.616–0.995)
TiO_2 5.0 $\mu\text{g/mL}$	32.740 (29.457–36.022)	31.289 (25.383–37.195)	0.818 (0.757–0.878)	0.815 (0.772–0.858)
ZnO 0.5 $\mu\text{g/mL}$	42.960 (30.320–55.601)	32.948 (28.644–37.252)	0.790 (0.585–0.996)	0.819 (0.781–0.858)
ZnO 5.0 $\mu\text{g/mL}$	33.971 (31.280–36.662)	36.665 (33.365–39.965)	0.854 (0.775–0.932)	0.666 (0.492–0.840)
Aflatoxin B1 positive control	35.969 (25.594–46.344)	36.978 (30.590–43.366)	0.769 (0.707–0.885)	0.792 (0.758–0.826)

Mean data of three biological replicates, analysed in triplicate ($n=9$) are presented with 95% confidence intervals. Significance is indicated in relation to the negative control, where $*=p \leq 0.05$

induction, as follows: $\text{ZnO} > \text{TiO}_2 > \text{BaSO}_4 = \text{CeO}_2 > \text{Ag}$. This genotoxicity potency ranking could help provide an insight into the DNA damaging potential of these ENMs if exposed to the human liver. However, it is also important to note that whilst for each material there is evidence of genotoxicity, there is also evidence of dose ranges where DNA damage does not occur and so there may be opportunity for safe exposure limits to be established. The average LOAEL post-acute exposure was induced by an ENM concentration of 0.5 $\mu\text{g/mL}$, with ZnO, BaSO_4 , CeO_2 and Ag eliciting a 2.75-, 1.54-, 1.51- and 1.37-fold change in MN induction, respectively. For, TiO_2 , whilst the LOAEL was reached at 2.0 $\mu\text{g/mL}$

with 1.83-fold increase in MN frequency over control, this material induced the second greatest increase in MN induction behind ZnO, with a 2.4-fold increase in MN fold following acute exposure to 5.0 $\mu\text{g/mL}$. The significant increase in MN induction following acute 24 h exposure to higher concentrations of TiO_2 , could be attributed to the high oxidative potential TiO_2 exhibits within the first 24 h of exposure, Fig. 1B. This potent O_2 reactivity suggests that the elevated DNA damage observed could be a result of ROS and oxidative stress. DNA is one of the major targets for oxidative stress induced damage (e.g. DNA–protein crosslinks, alkali-labile sites, DNA adducts, mutations), with OH^\bullet , a highly



potent free radical, known to react with all components of DNA and causing strand breaks via the formation of 8-OHdG DNA adducts [58, 59]. Whilst TiO₂ ENM O₂ reactivity is very active during the first few hours of the exposure, this oxidative potential appears to decrease as exposure duration increases and so may no longer be as prominent following prolonged exposure, resulting in the lower MN frequency at 120 h. In all cases, the top dose of 10.0 µg/mL resulted in a lower MN frequency following acute exposure than that of the former dose of 5.0 µg/mL. This is most likely due to greater material agglomeration at the top dose, restricting ENM translocation through the compact spheroid structure, thus reducing cellular uptake and biological interaction. It is well known that at higher ENM concentrations, the degree of agglomeration tends to be greater than that at the lower concentrations of ENMs, as the high number of particles within a given space increases the chance of particle–particle interaction and subsequent agglomeration [60]. This was further illustrated in this study by the time- and dose-dependent increase in agglomeration, with the average agglomerate size increasing from 23 nm at 0.2 µg/mL to 282 nm at 10.0 µg/mL, and 37 nm at 0.2 µg/mL to 275 nm at 10.0 µg/mL, respectively (Table 2). Whilst, at the lowest concentration of 0.2 µg/mL, all five ENMs remain monodispersed following acute exposure and only small agglomerates (< 80 nm) had formed over the duration of the 120 h exposure. At lower doses, darkfield imaging of PHH microtissues following exposure to 1.25 µg/mL and 5.0 µg/mL of TiO₂ (NM-105) and CeO₂ (NM-212), illustrated that the ENMs could penetrate deep into the core, with a large proportion of the hepatocytes encountering the ENM [14]. This is further supported with evidence that the microtissues were shown to rotate within the wells, and thus ENM exposure is likely to be even across the surface of the spheroids [14]. Similarly, with the addition of an agarose coating at the base of the spheroids, the HepG2 spheroids are also free to move and rotate within the well enabling the ENMs to access the entire surface layer of actively proliferating HepG2 cells [28].

There was a significant difference in the genotoxicity observed between acute and prolonged ENM exposure, whereby the notable ENM-associated genotoxic effects observed in the first 24 h are not apparent over the prolonged exposure. This could be due to repair mechanisms that, may be efficient at removing DNA damage and / or damaged cells over time, which is not evident in an acute exposure experiment. Additionally, cells developing MN within the first 24 h of exposure can undergo cell death over the remaining duration of the prolonged experiment. It is also important to consider that following the prolonged exposure periods, although more individual

cells were scored in the analysis, there is a greater chance of the DNA damage observed in the first 24 h to have been “diluted” in the ever-growing population. As a result, the probability of scoring a cell with a MN decreases over time. However, these time-dependent differences in genotoxicity could also be as result of extrinsic ENM physico-chemical properties (e.g. surface reactivity, agglomeration and dissolution). For example, ZnO was the only ENM to exhibit genotoxic effects following both acute and prolonged ENM exposure, with a significant response induced at 0.5–10.0 $\mu\text{g}/\text{mL}$ in the acute exposures and 0.2–5.0 $\mu\text{g}/\text{mL}$ in the prolonged exposures. ZnO nanoparticles are known to be highly soluble and readily release ions [61]. Aligned with existing literature, the ZnO ENMs in this study were found to rapidly dissolve into Zn^{2+} ions and two hydroxide ions, the latter causing an increase in pH in the culture medium within 15 min of exposure [37]. For soluble metal ENMs, there is always a question as to whether the toxicity observed is caused directly by the ENMs themselves or from the dissolved ions. ZnO ENMs can dissolve into Zn^{2+} ions, which can trigger signaling cascades leading to an enhanced influx of calcium, the release of (pro-)inflammatory mediators and ROS generation [40]. Interestingly, the greater induction of genotoxicity was observed following 24 h exposure to ZnO ENMs as opposed to 120 h. This is hypothesized to be induced by the rapid dissolution of Zn^{2+} ions within the first 24 h, inducing acute adverse effects similar to those described above, leading to an elevated genotoxic effect which was no longer as prominent following 120 h exposure, as a result of the reduced number of ions released over the 120 h exposure period. This correlates with reports in the literature whereby, an acute 24 h ZnO (NM-111) exposure caused a loss in the glutathione levels and an increase in the levels of ROS in the human hepatoblastoma C3A cell line [62]. Further to this, by employing the anti-oxidant Trolox, a reduction in IL-8 response and a suppression in the toxicity potential of the ZnO ENMs was observed, thus highlighting the important link of ZnO mediated oxidative stress. This elevated ZnO induced oxidative stress and ROS, has been shown to cause oxidative DNA damage, including DNA strand breaks and formamidopyrimidine DNA glycosylase (fpg)-specific DNA lesions in the liver [63, 64]. In addition, there are concerns that even if ZnO ENMs were not able to enter the nucleus, the Zn^{2+} ions could interact and affect DNA integrity, making successful DNA repair even more challenging [40]. These reports in the scientific literature indicate that persistent release and accumulation of ions over time could further induce ongoing oxidative stress and ROS induced DNA damage, as well as impeding DNA repair mechanisms,

resulting in a prolonged genotoxic effect, similar to that found in this study.

Although Ag ENMs release Ag^+ ions in a similar manner to ZnO, the Ag were found to be the least genotoxic out of the five materials tested. It is possible these Ag^+ ions may also induce DNA damage, but they are released much more slowly than the Zn^{2+} ions; thus, it is hypothesized that the gradual dissolution of Ag ENMs over the 24 h period could allow time for the repair of any low level damage induced. Additionally, the Ag ENMs were found to exhibit substantial dose-dependent agglomeration, with almost a 12-fold increase in the average particle diameter between the lowest and the highest concentrations, which could restrict the number of Ag particles internalized by the hepatocytes. Any Ag ENMs not internalized by the cells would remain within the culture medium and subsequently dissolve into Ag ions in situ, where the ions would likely be sequestered by the excess serum proteins in the medium. Consequently, the extrinsic physico-chemical variances between ZnO and Ag ENM are likely to account for the differences in their ability to induce genotoxicity.

Due to the more prominent genotoxic nature of ZnO and TiO_2 , these two materials were taken forward for further assessment into the effects different prolonged exposure regimes may have upon the genotoxic potential of ENMs. It was important to test both materials, as ZnO was known to give a positive genotoxic response following both acute and prolonged exposures, whilst TiO_2 only induced genotoxicity after an acute exposure. Interestingly, the enhanced complexity of the repeated exposure regime, developed to better mimic the natural human exposure scenario, made no difference on the toxicological response (cytotoxicity, (pro-)inflammatory response nor genotoxicity) in the HepG2 liver spheroids. A previous study, using the same materials, ZnO (JRC NM-111) and TiO_2 (JRC NM-105), showed that a repeated exposure of 0.62–10.0 $\mu\text{g}/\text{mL}$ dosed every other day for up to 21 days induced limited cytotoxicity, but a time dependent increase in cytokine levels in PHH microtissues [14]. Kermanizadeh et al., however, did not fractionate the doses over this time period and also included a 24 h recovery period between doses and an extended recovery (≥ 7 days) at the end of the exposure duration, which was shown to help alleviate the (pro-)inflammatory response. In that study, whilst an almost complete refresh of the culture medium was undertaken between repeated exposures, as the doses were not fractionated the final concentration of the ENM exposures will have been greater than those used in the present study as a result of residual material. Consequently, even with a repeated ENM exposure regime that is four-fold longer than the

one described in the present study, neither TiO₂ or ZnO induced any adverse effects in either hepatic model. This could be explained through the liver's unique ability to regenerate itself following acute toxicological insult, and with the low doses used for the repeated exposure in this study, toxicity may have been within limits that did not overwhelm the hepatocytes nor induce adverse outcomes. Another aspect to consider is whether the added complexity of a prolonged, repeated exposure outweighs the benefits of a more simplistic dosing approach. In the present study, the added complexity of repeated, fractionated exposures did not improve the predictive capabilities of the in vitro 3D liver model when evaluating ZnO and TiO₂. Thus, while prolonged repeated ENM exposures performed with in vivo relevant concentrations are more physiologically relevant and provide a better insight into the long-term effects of ENM exposure upon the liver, fractionated, repeated dosing regimens may not provide additional benefit for assessing the toxicological response in hepatocytes over single, bolus dosing regimens.

Conclusion

In conclusion, both acute and prolonged ENM exposures were assessed and were shown to result in different toxicological responses. This highlights the importance of evaluating prolonged ENM exposures to fully understand the longer-term and accumulated effects of ENMs following acute insult. For ZnO and TiO₂, there was no significant difference between prolonged single, bolus or repeated, fractionated exposure regimens. Thus, the added complexity of fractionated dosing did not influence the study outcome. Even given the low doses of ENM applied in this study, all five of the materials tested were shown to induce fixed DNA damage in 3D HepG2 spheroids following acute exposure, leading to the following genotoxicity potency ranking: ZnO > TiO₂ > BaSO₄ = CeO₂ > Ag. This study therefore demonstrates that 3D in vitro hepatic spheroid models have the capacity to be utilised for evaluating more realistic ENM exposures, thereby providing a future in vitro approach to better support ENM hazard assessment in a routine and easily accessible manner.

Materials and methods

In vitro 3D liver model

The Human Caucasian Hepatocellular Carcinoma derived epithelial cell line, HepG2 (ECACC 85011430 and ATCC HB-8065) monolayers were cultured in Dubecco's Modified Eagle Medium (DMEM) with 4.5g/L D-Glucose and L-Glutamine (GIBCO, Paisley, UK) supplemented with 10% Foetal Bovine Serum

(FBS) and 1% Penicillin/Streptomycin antibiotic (GIBCO, Paisley, UK). HepG2 cells were sub-cultured every 3–5 days, once 80% confluency was reached, they were trypsinised (0.05% trypsin/EDTA solution; GIBCO, Paisley, UK) and a cell stock of 2.0×10^5 cells/mL was prepared. To form the 3D spheroid structure, HepG2 cells were cultured in 96-well plates using the hanging drop method developed by Llewellyn et al. and described by Conway et al. [28, 29]. Extensive information regarding the establishment, culture, characterisation, exposure protocol, harvest and application of the 3D HepG2 spheroid model can be found in the published protocol by Llewellyn et al., 2020. In short, 20 μ L of the cell suspension (4000 HepG2 cells per 20 μ L hanging drop) was pipetted onto the inverted side of a 96-well tissue culture plate, before gently inverting the lid and placing back onto the 96-well plate filled with 100 μ L of PBS [28]. The plate was then placed in the incubator at 37 °C with 5% CO₂ for 3 days before agarose transfer.

ENM characterisation

Crystalline phases (XRD)

Powder samples were loaded onto a 20 × 20 mm glass sample holder, and the incident X-rays aligned to enter the centre of the sample. The X-ray is generated by a rotating anode X-ray generator of Copper (Cu). We executed a 2 θ – θ coupled scan from 10 °C to 100 °C with a step width of 0.02 °C and a second duration time per step. Measured data is refined by Rietveld analysis using PDXL from Rigaku SmartLab. XRD analysis were performed in line with ISO 17025 and, technically to, JIS K 0131 and BS EN 13925-4 [65–67].

Impurities (XRF)

Semi-quantitative elemental analysis was conducted on powder samples of the ENMs using a Bruker S8 Tiger wave length dispersive X-ray fluorescence (WDXRF) spectrometer using Rh X-ray source operated at 60 kV. Powdered samples of 2.0–5.0 mg were placed on a XRF thin film (mylar sheet with a thickness of 6.0 μ m), which was fixed in a 40 mm diameter sample cup (Fluxana, Kleve, Germany). The measurement time was 17 min. Results were manually post-processed for each element individually, to account for low concentrations and peak overlaps.

TEM (size, 3D aspect ratio and circulatory)

TEM was carried out for ENMs on an EM208, operating at 200 kV (Philips, Eindhoven, The Netherlands), with a high definition acquisition system based on a

side-mounted TEM camera OSIS Morada and an iTEM soft-ware platform (Olympus Soft Imaging Solutions GmbH, Münster, Germany). ENMs, dispersed in MilliQ water, were placed onto a carbon-coated grid and dried at room temperature under vacuum.

Surface area (BET)

Specific surface area was determined with the BET method using a Micromeritics Gemini V. Samples were degassed at 100 °C under vacuum for 30 mins. Nitrogen adsorption isotherms at 77 K were recorded at five pressures between 0.05 and 0.30 P/P₀. Measurements were performed adhering to the standard DIN ISO 9277-2014-01 [68].

Density (He pycnometer)

Skeletal density of all ENMs was determined using a He pycnometer (Micromeritics AccuPyc II 1340). Samples were measured at 20 °C, applying ten He purging cycles of the chamber before the measurement and analyzed according to DIN EN ISO 1183-3 [69].

XPS

XPS measurements were performed with a VersaProbe II Spectrometer (Ulvac-Phi, Japan) to obtain the chemical composition. The instrument was calibrated with clean Gold (Au) and Cu foils, of which electron binding energies were Au 4f=83.96 ± 0.02 eV and Cu 2p_{3/2}= 932.62 ± 0.05 eV, respectively [70]. The samples were irradiated with monochromatic Al K α X-ray ($h\nu=1486.6$ eV, 25 W) using an X-ray spot size of 100 × 100 μm^2 and a take-off angle of 45 ° with respect to the sample surface. The base pressure of the instrument was better than 1.0 × 10⁻⁹ Torr and the operating pressure better than 3.0 × 10⁻⁹ Torr. The surface chemical compositions (as %) were determined by relative atomic sensitivity factors. The samples were not etched or pre-treated prior to each measurement.

Surface charge

The zeta potential (ZP) was measured at room temperature (25 °C) as a function of pH using a ZP analyzer (Malvern Zetasizer Nano ZS). Each ZP value was calculated in an average of 22–30 runs at pH 7 in 10 mM potassium chloride (KCl) water solution.

FRAS

For ENM reactivity testing under physiological conditions, the FRAS assay multi-dose protocol was undertaken as described by Gandon et al. [71].

EPR spin trap DMPO and CPH

Two standardized EPR methods have been established to assess the surface-induced reactivity of ENMs: method I utilizes the nitron spin trap DMPO, one of the most established spin traps for nanosafety purposes, whilst method II employs the cyclic hydroxylamine spin probe CPH which interacts directly with short-lived ROS (e.g. superoxide radical) on the material surface [72, 73].

Hydrophobicity

The material hydrophilicity was evaluated by a water contact angle measurement using Drop Shape Analyzer - DSA100. Sample powder (~ 0.5 g) was spread as a thin layer on the surface of the sticky sample holder (3M Color Laser Transparency Film plate covered with a homogenous adhesive layer (0.25 mm) of Acronal[®] V 215) by pressing the surface with a spatula. A nitrogen gun is used to gently blow the powder residuals not attached to the sample holder's surface. Finally, contact angle measurement was performed at 23 °C by measuring the diameter of the spherical crown of 2 μL water dropped on the surface of sample layer.

Dynamic light scattering (DLS)/electrophoretic light scattering (ELS) measurements

The colloidal characterization of TiO₂, ZnO, Ag, BaSO₄ and CeO₂ ENMs was determined using a Zetasizer nano ZSP (model ZEN5600, Malvern Instruments, UK), measuring the DLS (ØDLS) and ZP of nanosol. ZP measurements were performed by ELS and the Smoluchowski equation was applied to convert the electrophoretic mobility to ZP. ENMs were diluted at 0.2, 0.5, 1.0, 2.0, 5.0 and 10.0 $\mu\text{g}/\text{mL}$ in DMEM complete for DLS and ZP analysis and measured after 24 and 120 h of exposure at 37 °C in static condition. Samples were measured three times and the mean ØDLS and ZP data presented.

Sensor dish reader reactivity and Dissolution testing

Real-time temporal pH and O₂ reactivity and 24 h end-point dissolution testing was performed using the Sensor Dish[®] reader (SDR) method (PreSens Precision Sensing GmbH, Regensburg, Germany). The test is based on the use of fluorescent pH (HydroDish[™]; range: pH 6–8.5, resolution 0.05 pH units) and O₂ (OxoDish[™]; range: 0–50% dissolved O₂; measured in mmol/L) sensors mounted at the bottom of each well in 24-well multi-dish cell incubation plates. The tests were conducted in DMEM + 10% FBS + 1% Pen/Strep, similar to the medium used in the in vitro assays. A standard material concentration of 320 $\mu\text{g}/\text{mL}$ was used to obtain sufficiently robust reactivity signal from the test materials as compared with the reactivity signal from the pure medium.

Batch-dispersions of 2.56 mg/mL were made in 0.05% BSA-water by 16 min, 13 mm probe-sonication, amplitude 10% (Branson Sonifier S-450D, Branson Ultrasonics Corp., Danbury, CT, USA) after pre-wetting the test materials with ethanol following the NANOGENOTOX dispersion protocol [74] and added by pipette to the test media immediately after dispersion was completed.

For each test, SensorDish® plates with 1.750 mL test medium added to each well were placed on the plate readers in a cell incubation chamber (37 °C; 5% CO₂ atmosphere; 95% Relative humidity; CelCulture® CO₂ Incubator, ESCO Medical, Egaa, Denmark). After thermal equilibration to 37 °C, a batch dispersion was prepared for the test material in question. 250 µL batch dispersion or control dispersion medium were each added to half of the wells, respectively and online measurement of the pH and O₂ concentrations was started immediately. After 24 h the measurements were stopped and medium samples were collected and added to 3 kDa centrifugal filter tubes by pipette and centrifuged at 4000 × RCF for 30 min. The 3 kDa filtered medium were sampled and added 500 µL 2% ultrapure HNO₃. The amount of liquids were weighed for subsequent quantification. Liquid samples were stored in darkness until shipment for inductively coupled plasma mass spectrometry (ICP-MS) analysis. The temporal reactivities (dpH and dO₂) were calculated as the difference between the mean values in wells with a test material minus the mean values in wells without a test material and then plotted as function of time. The SDR-test is explained in detail in Jørgensen et al. (in prep.)

ENM exposures

Five ENMs (TiO₂ NM-105, ZnO NM-111, JRC Nanomaterials Repository, Belgium; BaSO₄ NM-220, CeO₂ NM-212, Fraunhofer IME, Germany; and Ag 576832, Sigma Aldrich, UK) were stored as dry powders at room temperature until the day of exposure. ENM stock solutions were prepared (2.56 mg/mL) and dispersed for 16 mins in 0.05% Bovine Serum Albumin (BSA) using the probe sonication (Branson Sonifier 250, Ø 13 mm, 400 W output power, 20 kHz) method described by Jensen et al. [74]. Working stocks of ENMs were made fresh for each experiment. Following dispersion, ENMs were diluted in cell culture media to the required concentrations with all five ENMs assessed over both an acute 24 h and prolonged 120 h exposure scheme. For prolonged ENM exposures, a partial media change was undertaken after 72 h, whereby the top 50% of the culture medium within the wells was removed and replaced with fresh ENM-free culture medium of the exact same volume. Exposure procedures are described in detail, with a peer-reviewed SOP available, in Llewellyn et al. [29]. TiO₂ and ZnO at two

selected doses of 0.5 and 5.0 µg/mL, were further evaluated following a longer-term (120 h), repeated dosing scheme whereby the original bolus dose was fractionated into five, equal parts of 0.1 and 1.0 µg/mL, respectively to be dosed daily onto the 3D liver spheroids, Fig. 4. The plates were then incubated at 37 °C/5% CO₂ for the desired exposure period. For prolonged exposures, a culture medium replacement was undertaken once, on Day 3 of the exposure, by removing 50 µL of media from the well and replacing with a fresh 50 µL of DMEM. For the repeated ENM exposures however, this was not necessary, as 50% of the culture medium was being refreshed daily with the new dose of ENMs. All experiments were performed with three biological replicates with mean data ± SD presented, unless stated otherwise.

Liver functionality: albumin and urea assays

Following both acute and prolonged ENM exposure, liver-like functionality was evaluated using the BCG Albumin Assay Kit (MAK124, Sigma, UK) and Urea Assay Kit (MAK006, Sigma-Aldrich, UK). A negative, untreated media control was used alongside a chemical positive control; 0.1 µM of a known liver carcinogen, Aflatoxin B1 (Afla B1; Cat# No: A6636, Sigma Aldrich, UK). At the end of the exposure period all supernatants were harvested by pooling 50 µL of media from each well. To sediment any excess ENM from the supernatant, the samples were centrifuged at 230g for 2 mins and the resulting supernatant collected. All assays were performed as per manufacturer's instructions, with three biological replicates assessed in triplicate. For the urea assay, supernatants were diluted 1:10 with urea assay buffer.

(Pro)-inflammatory response: interleukin-6 (IL-6), interleukin 8 (IL-8) and tumour necrosis factor alpha (TNF-α)

Cytokine release was quantified by ELISA, using the cell supernatants described above. DuoSet human antibody kits for IL-8, IL-6, and TNF-α (DY208, DY206 and DY210 DuoSet ELISA, R&D Systems) were used according to the manufacturer's instructions. An ELISA assay positive control, Tumor Necrosis Factor Alpha Protein (TNF-α protein; Cat# No: 2-35076, BioTechne, UK) was re-suspended in ddH₂O according to manufacturer's instructions and diluted to a final working concentration of 0.25µg/mL of TNF-α protein. The detection antibodies were diluted as follows: IL-8: 0.1% BSA, 0.05% Tween 20 in Tris-buffered Saline (TBS) and IL-6/TNF-α: 1% BSA in PBS, and incubated with samples for 2 h at RT. The signal was developed using streptavidin horseradish-peroxidase and TMB Substrate Reagent A and B (Cat# No. DY999,

R&D Systems, UK). Absorbance was measured at 450 nm (PolarStar Omega Plate Reader) and the standard curve was plotted as 4-parameter logistic fit using the MyAssays.com software. Three biological replicates were assessed in triplicate.

Cytotoxicity and genotoxicity: trypan blue exclusion assay, cytokinesis proliferation index and in vitro micronucleus assay

The MN assay was undertaken in conjunction with the cytokinesis-block proliferation index (CPBI) and trypan blue exclusion assay for determining cytotoxicity post-acute and longer-term ENM exposures, respectively. A negative, untreated media control was used alongside 0.1 μM of a known liver carcinogen, Afla B1 as a positive control for genotoxicity. The MN assay was conducted as described by Conway et al. [28]. In short, after both acute and prolonged exposures, the cell culture supernatant was harvested and stored at $-80\text{ }^{\circ}\text{C}$ for future biochemical endpoint analysis. The remaining liver spheroids were then pooled, trypsinised and prepared for cytotoxicity assessment and semi-automated MN scoring as previously described by Llewellyn et al. and Conway et al. [28, 29]. When scoring, detection of micronuclei in bi-nucleated or mono-nucleated cells were performed as previously described by Llewellyn et al. [29]. A minimum of 1000 bi-nucleated cells or 2000 mono-nucleated cells were counted per exposure dose per biological replicate ($n \geq 2$), using the principles established by Fenech et al. and in accordance with the OECD Test No. 487: In Vitro Mammalian Cell Micronucleus Test guidelines [75, 76]. All controls for the MN assay were within the acceptance criteria based on historical ranges, with the average MN frequency for the positive control (Aflatoxin B1) lying between 2.2 and 2.8% and the negative, untreated control data between 0.8 and 1.4%. In all tests, the positive control had to be a minimum of two-fold greater than that of the untreated, negative control.

Data analysis and statistics

Statistical analysis was performed using Prism 8, GraphPad Software, Inc. (USA). Shapiro-Wilk test was used to calculate normality for each data set. For normally distributed data, One-way ANOVA with Sidak's post hoc were used. For non-parametric data, Kruskal-Wallis test was used to calculate significance when there were more than two variables, with Dunn's multiple comparisons test. For genotoxicity data sets, with ≥ 2 biological replicates, a two-tailed Fischer's Exact test was conducted.

Supplementary Information

The online version contains supplementary material available at <https://doi.org/10.1186/s12951-021-00938-w>.

Additional file 1: Figure S1: TEM micrographs of the ENM listed in Table 1: (A) TiO_2 NM-105 (B) Ag Sigma (C) BaSO_4 NM-220 (D) CeO_2 NM-212 and (E) ZnO NM-111. Image (A), (B), (C) and (D) reproduced from Keller et al. (2020) (<https://doi.org/10.1080/17435390.2020.1836281>) and image (E) reproduced from Yin et al. (2015) (<https://doi.org/10.1007/s11051-014-2851-y>). **Figure S2:** A series of XRD patterns for the five ENMs listed in Table 1, (A) TiO_2 (NM-105), (B) Ag (Sigma 576832), (C) ZnO (NM-111), (D) BaSO_4 (NM-220) and (E) CeO_2 (NM-212). These graphs illustrate the crystalline phases for each material as summarised in Table 1. **Figure S3:** A series of XPS core level curves for the five ENMs included in this study and summarized in Table 1: TiO_2 (NM-105), ZnO (NM-111), Ag (Sigma 576832), BaSO_4 (NM-220) and CeO_2 (NM-212). Each curve is fitted by Lorentzian-Gaussian convoluted functions to determine the chemical composition. **Figure S4:** Representative images of micronuclei generated by automated scoring of HepG2 cells using a Metafer MetaSystem 3.9.8. (A) illustrates an enlarged image of a micronucleus shown in the scoring gallery pictured in (D), and highlighted with an orange outline. Representative images of micronuclei found within the HepG2 mononucleate (B, C) and binucleate (E-G) cell populations following prolonged and acute ENM exposures respectively.

Acknowledgements

The authors would like to acknowledge and thank the members of Work Packages 1 and 4, and the PATROLS steering board for their valuable review and feedback of the manuscript prior to submission.

Authors' contributions

SVL produced and analysed the data for all ENM exposures on the 3D liver models, as well as generating the figures for all data and wrote the manuscript itself. GC generated the data for the two different dosing regime experiments. IZ and AC were responsible for the DLS data generated in Table 2, whilst AKJ and KAJ generated the oxygen reactivity and dissolution data in Fig. 1. DAS, JGK and WW produced most of the data in Table 1, with some contributions from IZ, AC, AKJ, KAJ and JWK. SHD provided the study design and supervision on the written manuscript. All authors read and approved the final manuscript.

Funding

The authors would like to acknowledge that this research has received funding from the European Union's Horizon 2020 research and innovation program for the PATROLS project, under Grant Agreement No. 760813.

Availability of data and materials

The datasets generated and analysed during the current study are uploaded to eNanoMapper database repository [<https://search.data.enanomapper.net/projects/patrols>].

Declarations

Ethical approval and consent to participate

Not applicable.

Consent for publication

Not applicable.

Competing interests

The authors declare no competing interests and confirm the funders had no role in the design of the study; in the collection, analyses, or interpretation of data; in the writing of the manuscript, or in the decision to publish the results.

Author details

¹In Vitro Toxicology Group, Institute of Life Science, Swansea University Medical School, Swansea University, Singleton Park, Swansea SA2 8PP, UK.

²Advanced Materials Research, Department of Material Physics and Analytics, BASF SE, 67056 Ludwigshafen, Germany. ³Advanced Materials Research, Department of Experimental Toxicology and Ecology, BASF SE, 67056 Ludwigshafen, Germany. ⁴Institute of Science and Technology for Ceramics, CNR-ISTEC-National Research Council of Italy, Faenza, Italy. ⁵National Research Centre for the Working Environment (NRCWE), Lersø Parkallé 105, 2100 Copenhagen, Denmark. ⁶Korea Research Institute of Standards and Science (KRISS), 267 Gajeong-ro, Daejeon 34113, Korea.

Received: 23 March 2021 Accepted: 13 June 2021

Published online: 28 June 2021

References

- Research and Markets 2018. Global Nanotechnology Market (by Component and Applications), Funding & Investment, Patent Analysis and 27 Companies Profile & Recent Developments-Forecast to 2024 [Internet]. [cited 2021 Feb 28]. Available from: <https://www.researchandmarkets.com/research/zc7qgf/global?w=5>.
- Commission E. Definition—Nanomaterials—Environment—European Commission [Internet]. 2011 [cited 2020 Aug 21]. Available from: https://ec.europa.eu/environment/chemicals/nanotech/faq/definition_en.htm?fbclid=IwAR2eQnhTXXwZb5U1VHmEIQIP1cS0sAJYNTsGMCI9mLbaqLAKUxDkRIsiYWw.
- Molina RM, Konduru Nv, Queiroz PM, Figueroa B, Fu D, Ma-Hock L, et al. Fate of barium sulfate nanoparticles deposited in the lungs of rats. *Sci Rep*. 2019;9(1):1–13. <https://doi.org/10.1038/s41598-019-44551-2>.
- Reed K, Cormack A, Kulkarni A, Mayton M, Sayle D, Klaessig F, et al. Exploring the properties and applications of nanocerium: is there still plenty of room at the bottom? *Environ Sci Nano R Soc Chem*. 2014;1:390–405.
- Koivisto AJ, Kling KI, Fonseca AS, Bluhme AB, Moreman M, Yu M, et al. Dip coating of air purifier ceramic honeycombs with photocatalytic TiO₂ nanoparticles: a case study for occupational exposure. *Sci Total Environ*. 2018;15(630):1283–91.
- Fonseca AS, Viitanen A-K, Kanerva T, Säämänen A, Aguerre-Chariol O, Fable S, et al. Occupational exposure and environmental release: the case study of pouring TiO₂ and filler materials for paint production. *Int J Environ Res Public Health*. 2021;18(2):418.
- Haider A, Kang IK. Preparation of silver nanoparticles and their industrial and biomedical applications: a comprehensive review. *Adv Mater Sci Eng*. 2015;2015:1–16.
- Burduşel AC, Gherasim O, Grumezescu AM, Mogoantă L, Ficaï A, Andronescu E. Biomedical applications of silver nanoparticles: an up-to-date overview. *Nanomaterials*. 2018;8:681.
- StatNano. Home | Nanotechnology Products Database (NPD) [Internet]. 2018 [cited 2018 Sep 9]. Available from: <http://product.statnano.com/>.
- Kreyling WG, Semmler-Behnke M, Takenaka S, Möller W. Differences in the biokinetics of inhaled nano-versus micrometer-sized particles. *Acc Chem Res*. 2013;46(3):714–22. <https://doi.org/10.1021/ar300043r>.
- Geiser M, Kreyling WG. Deposition and biokinetics of inhaled nanoparticles. *Particle Fibre Toxicol BioMed Central*. 2010;7:1–17.
- Lauschke VM, Hendriks DFG, Bell CC, Andersson TB, Ingelman-Sundberg M. Novel 3D culture systems for studies of human liver function and assessments of the hepatotoxicity of drugs and drug candidates. *Chem Res Toxicol*. 2016;29(12):1936–55.
- Sadauskas E, Wallin H, Stoltenberg M, Vogel U, Doering P, Larsen A, et al. Kupffer cells are central in the removal of nanoparticles from the organism. *Particle Fibre Toxicol*. 2007;4:1–10.
- Kermanizadeh A, Berthing T, Guzniczak E, Wheeldon M, Whyte G, Vogel U, et al. Assessment of nanomaterial-induced hepatotoxicity using a 3D human primary multi-cellular microtissue exposed repeatedly over 21 days—the suitability of the in vitro system as an in vivo surrogate. *Particle Fibre Toxicol*. 2019;16(1):42. <https://doi.org/10.1186/s12989-019-0326-0>.
- Modrzynska J, Berthing T, Ravn-Haren G, Kling K, Mortensen A, Rasmussen RR, et al. In vivo-induced size transformation of cerium oxide nanoparticles in both lung and liver does not affect long-term hepatic accumulation following pulmonary exposure. *PLoS ONE*. 2018;13(8):e0202477.
- Cui Y, Liu H, Ze Y, Zengli Z, Hu Y, Cheng Z, et al. Gene expression in liver injury caused by long-term exposure to titanium dioxide nanoparticles in mice. *Toxicol Sci*. 2012;128(1):171–85.
- Kawata K, Osawa M, Okabe S. In vitro toxicity of silver nanoparticles at noncytotoxic doses to HepG2 human hepatoma cells. *Environ Sci Technol*. 2009;43(15):6046–51. <https://doi.org/10.1021/es900754q>.
- van Grunsven LA. 3D in vitro models of liver fibrosis. *Adv Drug Deliv Rev*. 2017;121:133–46.
- Clift MJD, Jenkins GJS, Doak SH. An alternative perspective towards reducing the risk of engineered nanomaterials to human health. *Small*. 2020;16(36):2002002. <https://doi.org/10.1002/sml.202002002>.
- Comandella D, Gottardo S, Rio-Echevarria IM, Rauscher H. Quality of physicochemical data on nanomaterials: an assessment of data completeness and variability. *Nanoscale*. 2020;12(7):4695–708.
- Bell CC, Dankers ACA, Lauschke VM, Sison-Young R, Jenkins R, Rowe C, et al. Comparison of hepatic 2D sandwich cultures and 3D spheroids for long-term toxicity applications: a multicenter study. *Toxicol Sci Off J Soc Toxicol*. 2018;162(2):655–66.
- Ramaiahgari SC, Den Braver MW, Herpers B, Terpstra V, Commandeur JNM, van de Water B, et al. A 3D in vitro model of differentiated HepG2 cell spheroids with improved liver-like properties for repeated dose high-throughput toxicity studies. *Arch Toxicol*. 2014; <https://doi.org/10.1007/s00204-014-1215-9>
- Kermanizadeh A, hr Miller L, Roursgaard M, Messner S, Gunness P, Kelm JM, et al. Hepatic toxicology following single and multiple exposure of engineered nanomaterials utilising a novel primary human 3D liver microtissue model. *Particle Fibre Toxicol*. 2014;11(1):56. <https://doi.org/10.1186/s12989-014-0056-2>.
- Shah U-K, de Mallia JO, Singh N, Chapman KE, Doak SH, Jenkins GJS. A three-dimensional in vitro HepG2 cells liver spheroid model for genotoxicity studies. *Mutat Res/Genetic Toxicol Environ Mutagen*. 2018;825:51–8.
- Ng SS, Xiong A, Nguyen K, Masek M, No DY, Elazar M, et al. Long-term culture of human liver tissue with advanced hepatic functions. *JCI Insight*. 2017;2(11). <https://doi.org/10.1172/jci.insight.90853>.
- Engin AB, Nikitovic D, Neagu M, Henrich-Noack P, Docea AO, Shtilman MI, et al. Mechanistic understanding of nanoparticles' interactions with extracellular matrix: The cell and immune system. *Particle Fibre Toxicol BioMed Central Ltd*. 2017;14:1–16. <https://doi.org/10.1186/s12989-017-0199-z>.
- Llewellyn SV, Niemeijer M, Nymark P, Moné MJ, Water B, Conway GE, et al. In vitro three-dimensional liver models for nanomaterial DNA damage assessment. *Small*. 2021;17:2006055. <https://doi.org/10.1002/sml.202006055>
- Conway GE, Shah U-K, Llewellyn SV, Cervena T, Evans SJ, Al Ali A, et al. Adaptation of the in vitro micronucleus assay for genotoxicity testing using 3D liver models supporting longer-term exposure durations. *Mutagenesis*. 2020;35:319–30.
- Llewellyn S v., Conway GE, Shah U-K, Evans SJ, Jenkins GJS, Clift MJD, et al. Advanced 3D liver models for in vitro genotoxicity testing following long-term nanomaterial exposure. *J Visual Exp*. 2020;(160):e61141. Available from: <https://www.jove.com/video/61141/advanced-3d-liver-models-for-vitro-genotoxicity-testing-following>.
- Wilkening S, Stahl F, Bader A. Comparison of primary human hepatocytes and hepatoma cell line HepG2 with regard to their biotransformation properties. *Drug Metab Disposition*. 2003;31(8):1035–42.
- Sison-Young RL, Lauschke VM, Johann E, Alexandre E, Antherieu S, Aerts H, et al. A multicenter assessment of single-cell models aligned to standard measures of cell health for prediction of acute hepatotoxicity. *Arch Toxicol*. 2017;91(3):1385–400.
- Arts JHE, Irfan MA, Keene AM, Kreiling R, Lyon D, Maier M, et al. Case studies putting the decision-making framework for the grouping and testing of nanomaterials (DF4nanoGrouping) into practice. *Regul Toxicol Pharmacol*. 2016;1(76):234–61.
- Arts JHE, Hadi M, Irfan MA, Keene AM, Kreiling R, Lyon D, et al. A decision-making framework for the grouping and testing of nanomaterials (DF4nanoGrouping). *Regul Toxicol Pharmacol*. 2015;71(2):S1–27.
- Yin H, Coleman VA, Casey PS, Angel B, Catchpoole HJ, Waddington L, et al. A comparative study of the physical and chemical properties of nano-sized ZnO particles from multiple batches of three commercial products. *J Nanopart Res* 2015;17(2).
- Keller JG, Quevedo DF, Faccani L, Costa AL, Landsiedel R, Werle K, et al. Dosimetry in vitro—exploring the sensitivity of deposited dose predictions vs. affinity, polydispersity, freeze-thawing, and analytical methods. *Nanotoxicology*. 2021;15(1):21–34.

36. da Silva E, Kembouche Y, Tegner U, Baun A, Jensen KA. Interaction of biologically relevant proteins with ZnO nanomaterials: a confounding factor for in vitro toxicity endpoints. *Toxicol In Vitro*. 2019;1(56):41–51.
37. da Silva E, Kembouche Y, Tegner U, Baun A, Jensen KA. Data supporting the investigation of interaction of biologically relevant proteins with ZnO nanomaterials: a confounding factor for in vitro toxicity endpoints. *Data Brief*. 2019;23:103795.
38. Kämpfer AAM, Busch M, Schins RPF. Advanced in vitro testing strategies and models of the intestine for nanosafety research. *Chem Res Toxicol Am Chem Soc*. 2020;33:1163–78. <https://doi.org/10.1021/acs.chemrestox.0c00079>.
39. Llewellyn Sv, Kämpfer A, Keller JG, Vilsmeier K, Büttner V, AgSeleci D, et al. Simulating nanomaterial transformation in cascaded biological compartments to enhance the physiological relevance of in vitro dosing regimes: optional or required? *Small*. 2021;17:2004630. <https://doi.org/10.1002/smll.202004630>.
40. Scherzad A, Meyer T, Kleinsasser N, Hackenberg S. Molecular mechanisms of zinc oxide nanoparticle-induced genotoxicity short running title: genotoxicity of ZnO NPs. *Materials*. 2017;10:1427.
41. Yetisgin AA, Cetinel S, Zuvun M, Kosar A, Kutlu O. Therapeutic nanoparticles and their targeted delivery applications. *Molecules*. 2020;25(9):2193.
42. Spinella R, Sawhney R, Jalan R. Albumin in chronic liver disease: structure, functions and therapeutic implications. *Hepato Int*. 2016;10:124–32.
43. Nierenberg D, Khaled AR, Flores O. Formation of a protein corona influences the biological identity of nanomaterials. *Rep Pract Oncol Radiother*. 2018;23(4):300–8.
44. Tenzer S, Docter D, Kuharev J, Musyanovych A, Fetz V, Hecht R, et al. Rapid formation of plasma protein corona critically affects nanoparticle pathophysiology. *Nat Nanotechnol*. 2013;8(10):772–81. <https://doi.org/10.1038/nano.2013.181>.
45. Bikbov B, Perico N, Abbate M, Remuzzi G. The glomerulus: mechanisms and patterns of injury. In: *Comprehensive toxicology*. 3rd Edn. Elsevier Inc., Amsterdam; 2018. pp. 189–206.
46. Barmore W, Stone WL. Physiology, urea cycle [Internet]. *StatPearls*. StatPearls Publishing; 2018 [cited 2021 Feb 28]. Available from: <http://www.ncbi.nlm.nih.gov/pubmed/30020695>.
47. Monopoli MP, Walczyk D, Campbell A, Elia G, Lynch I, Baldelli Bombelli F, et al. Physical–chemical aspects of protein corona: relevance to in vitro and in vivo biological impacts of nanoparticles. *J Am Chem Soc*. 2011;133(8):2525–34. <https://doi.org/10.1021/ja107583h>.
48. Park SJ. Protein–nanoparticle interaction: corona formation and conformational changes in proteins on nanoparticles. *Int J Nanomed*. 2020;15:5783–802.
49. Drasler B, Sayre P, Steinhäuser KG, Petri-Fink A, Rothen-Rutishauser B. In vitro approaches to assess the hazard of nanomaterials. *NanoImpact*. 2017;8:99–116.
50. Møller P, Jacobsen NR, Folkmann JK, Danielsen PH, Mikkelsen L, Hemmingsen JG, et al. Role of oxidative damage in toxicity of particulates. *Free Radical Res*. 2010;44(1):1–46. <https://doi.org/10.3109/10715760903300691>.
51. Khanna P, Ong C, Bay B, Baeg G. Nanotoxicity: an interplay of oxidative stress, inflammation and cell death. *Nanomaterials*. 2015;5(3):1163–80.
52. Manke A, Wang L, Rojanasakul Y, Manke A, Wang L, Rojanasakul Y. Mechanisms of nanoparticle-induced oxidative stress and toxicity. *BioMed Res Int*. 2013;2013:942916.
53. Desbaillets I, Diserens AC, de Tribolet N, Hamou MF, van Meir EG. Upregulation of interleukin 8 by oxygen-deprived cells in glioblastoma suggests a role in leukocyte activation, chemotaxis, and angiogenesis. *J Exp Med*. 1997;186(8):1201–12.
54. Sonna LA, Cullivan ML, Sheldon HK, Pratt RE, Lilly CM. Effect of hypoxia on gene expression by human hepatocytes (HepG2). *Physiol Genomics*. 2003;12(3):195–207. <https://doi.org/10.1152/physiolgenomics.00104.2002>.
55. Li XP, Yang XY, Biskup E, Zhou J, Li HL, Wu YF, et al. Co-expression of CXCL8 and HIF-1 α is associated with metastasis and poor prognosis in hepatocellular carcinoma. *Oncotarget*. 2015;6(26):22880–9.
56. Elespuru R, Pfuhrer S, Aardema MJ, Chen T, Doak SH, Doherty A, et al. Genotoxicity assessment of nanomaterials: recommendations on best practices, assays, and methods. *Toxicol Sci*. 2018;164(2):391–416.
57. Doak SH, Manshian B, Jenkins GJS, Singh N. In vitro genotoxicity testing strategy for nanomaterials and the adaptation of current OECD guidelines. *Mutat Res Genet Toxicol Environ Mutagenesis*. 2012;745(1–2):104–11.
58. Manke A, Wang L, Rojanasakul Y. Mechanisms of nanoparticle-induced oxidative stress and toxicity. *BioMed Res Int*. 2013;2013:1–15.
59. Fu PP, Xia Q, Hwang HM, Ray PC, Yu H. Mechanisms of nanotoxicity: generation of reactive oxygen species. *J Food Drug Anal*. 2014;22:64–75.
60. Bruinink A, Wang J, Wick P. Effect of particle agglomeration in nanotoxicology. *Arch Toxicol*. 2015;89:659–75.
61. Behra R, Sigg L, Clift MJD, Herzog F, Minghetti M, Johnston B, et al. Bioavailability of silver nanoparticles and ions: from a chemical and biochemical perspective. *J R Soc Interface R Soc*. 2013;10:20130396. <https://doi.org/10.1098/rsif.2013.0396>.
62. Keramanizadeh A, Gaiser BK, Hutchison GR, Stone V. An in vitro liver model—assessing oxidative stress and genotoxicity following exposure of hepatocytes to a panel of engineered nanomaterials. *Particle Fibre Toxicol*. 2012;9(1):28. <https://doi.org/10.1186/1743-8977-9-28>.
63. Elje E, Mariussen E, Moriones OH, Bastús NG, Puentes V, Kohl Y, et al. Hepato(Geno)toxicity assessment of nanoparticles in a hepG2 liver spheroid model. *Nanomaterials*. 2020;10(3):545. Available from: [/pmc/articles/PMC7153628/?report=abstract](https://pmc/articles/PMC7153628/?report=abstract).
64. Sharma V, Singh P, Pandey AK, Dhawan A. Induction of oxidative stress, DNA damage and apoptosis in mouse liver after sub-acute oral exposure to zinc oxide nanoparticles. *Mutat Res Genetic Toxicol Environ Mutagenesis*. 2012;745(1–2):84–91.
65. ISO-ISO/IEC 17025-General requirements for the competence of testing and calibration laboratories [Internet]. [cited 2021 Mar 11]. Available from: <https://www.iso.org/publication/PUB100424.html>.
66. JIS K0131 : General Rules for X-Ray Diffractometric Analysis [Internet]. [cited 2021 Mar 11]. Available from: https://global.ihs.com/doc_detail.cfm?document_name=JIS%20K%2020131&item_s_key=00254019#abstract-section.
67. BS EN 13925-2 : Non-destructive testing. X-ray diffraction from polycrystalline and amorphous materials—procedures [Internet]. [cited 2021 Mar 11]. Available from: <https://www.bsibedge.com/productdetails/BSI/BSI30028455/BSEN13925-2>.
68. ISO-ISO 9277:2010-Determination of the specific surface area of solids by gas adsorption—BET method [Internet]. [cited 2021 Mar 11]. Available from: <https://www.iso.org/standard/44941.html>.
69. ISO 1183-1:2019(en), Plastics—methods for determining the density of non-cellular plastics. Part 1: Immersion method, liquid pycnometer method and titration method [Internet]. [cited 2021 Mar 11]. Available from: <https://www.iso.org/obp/ui/#iso:std:iso:1183-1:ed-3:v2:en>.
70. ISO-ISO 15472:2010-Surface chemical analysis—X-ray photoelectron spectrometers—calibration of energy scales [Internet]. [cited 2021 Mar 5]. Available from: <https://www.iso.org/standard/55796.html>.
71. Gandon A, Werle K, Neubauer N, Wohlleben W. Surface reactivity measurements as required for grouping and read-across: an advanced FRAS protocol. *J Phys Conf Ser (Institute of Physics Publishing)*. 2017;838:012033. <https://doi.org/10.1088/1742-6596/838/1/012033>.
72. ISO-ISO/TS 18827:2017-Nanotechnologies—electron spin resonance (ESR) as a method for measuring reactive oxygen species (ROS) generated by metal oxide nanomaterials [Internet]. [cited 2021 Feb 28]. Available from: <https://www.iso.org/standard/63502.html>.
73. Wohlleben W, Driessen MD, Raesch S, Schaefer UF, Schulze C, von Vacano B, et al. Influence of agglomeration and specific lung lining lipid/protein interaction on short-term inhalation toxicity. *Nanotoxicology*. 2016;10(7):970–80. <https://doi.org/10.3109/17435390.2016.1155671>.
74. Alstrup Jensen K. The NANOGENTOX Dispersion Protocol for NANoREG. Grant Agreement n° 2009 21 01 [Internet]. 2014 [cited 2019 Dec 15]; Available from: <file:///C:/Users/Owner/Downloads/20140711+NANoREG+The+NANOGENTOX+dispersion+protocol+for+NANoREG+V1+0.pdf>
75. Fenech M. The in vitro micronucleus technique. *Mutat Res*. 2000;455(1–2):81–95.
76. OECD. Test No. 487: In Vitro Mammalian Cell Micronucleus Test [Internet]. OECD; 2016 [cited 2020 Aug 21]. (OECD Guidelines for the Testing of Chemicals, Section 4). Available from: https://www.oecd-ilibrary.org/environment/test-no-487-in-vitro-mammalian-cell-micronucleus-test_9789264264861-en.

Publisher's Note

Springer Nature remains neutral with regard to jurisdictional claims in published maps and institutional affiliations.

Additional File 1

1. ENM Characterisation

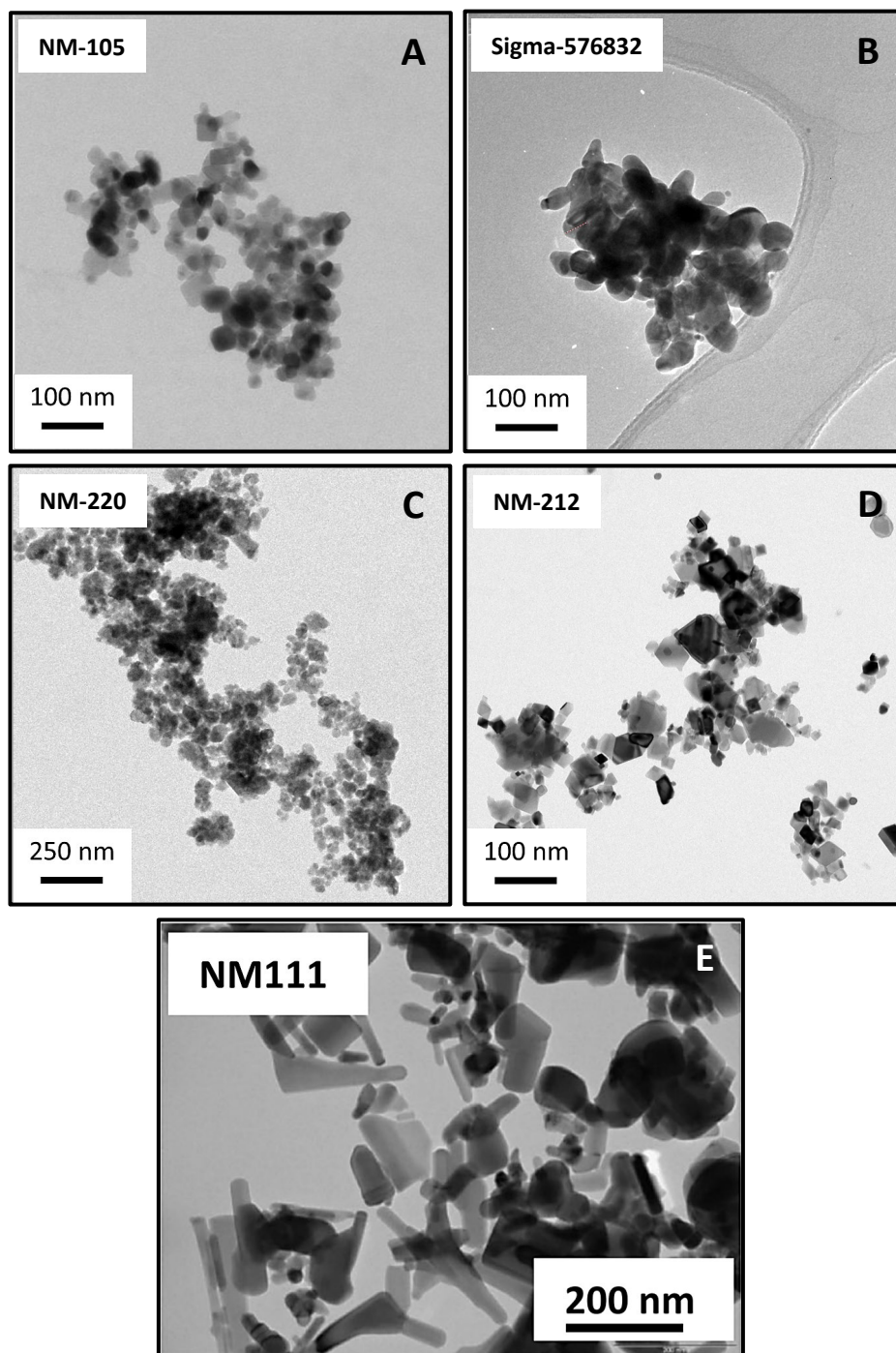
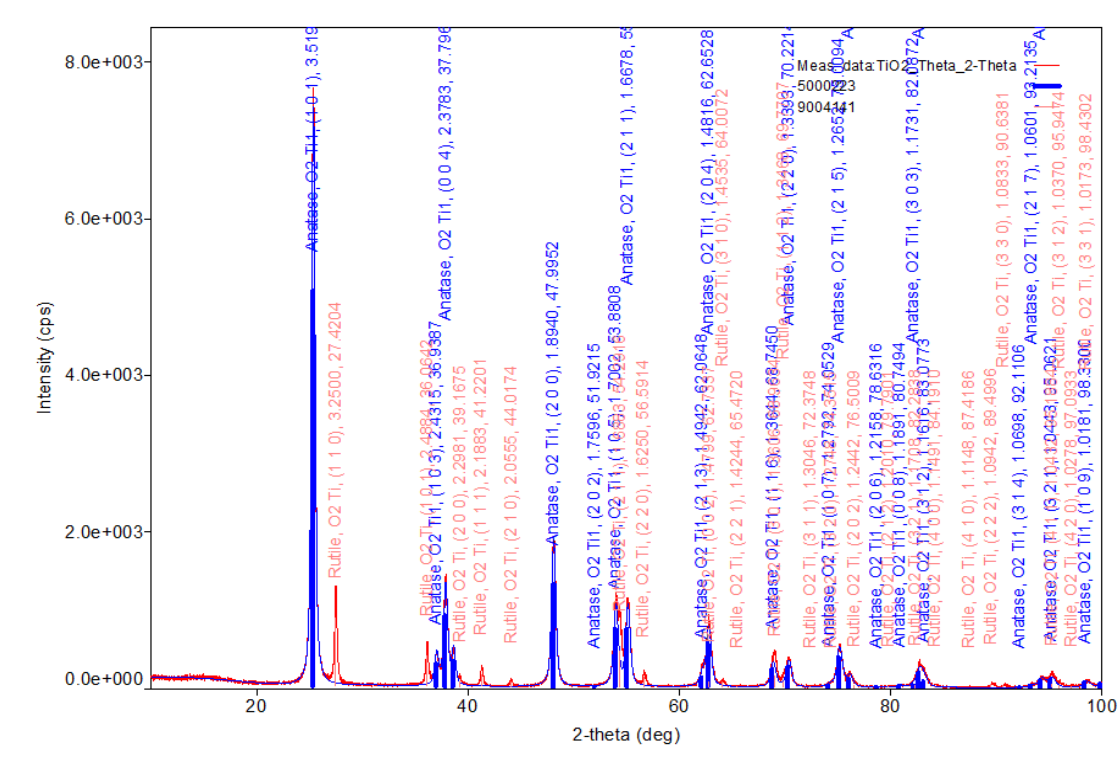
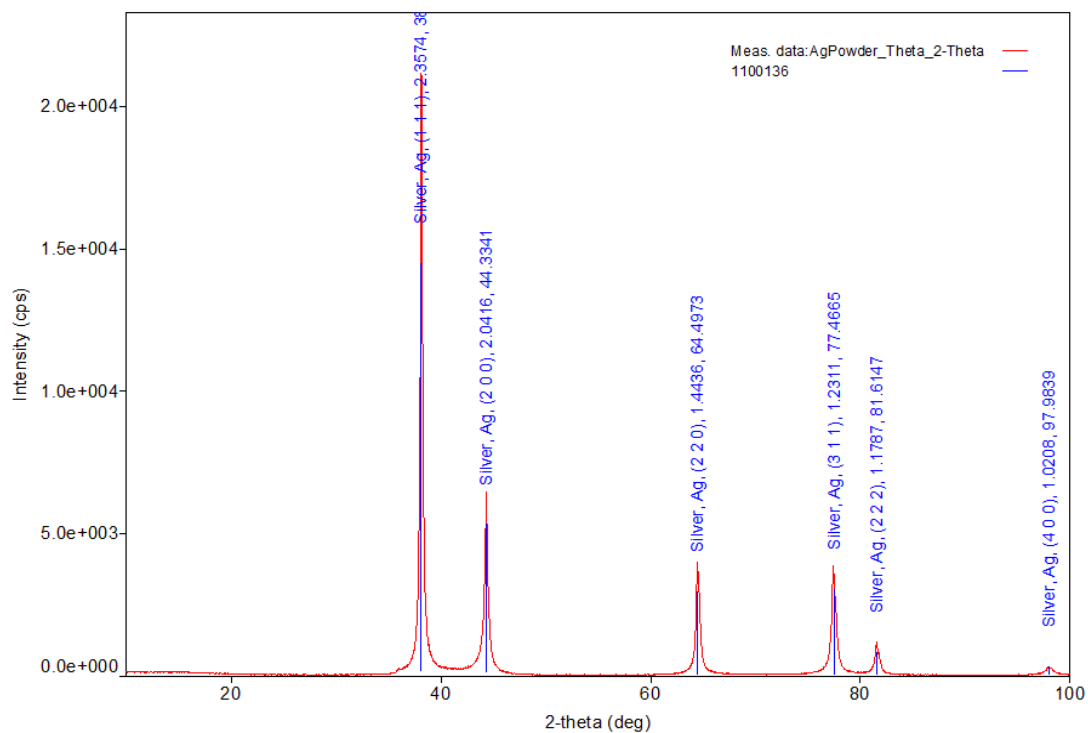


Figure S1: TEM micrographs of the ENM listed in Table 1: (A) TiO₂ NM-105 (B) Ag Sigma (C) BaSO₄ NM-220 (D) CeO₂ NM-212 and (E) ZnO NM-111. Image (A), (B), (C) and (D) reproduced from Keller et al. (2020) (DOI: 10.1080/17435390.2020.1836281) and image (E) reproduced from Yin et al. (2015) (DOI 10.1007/s11051-014-2851-y).

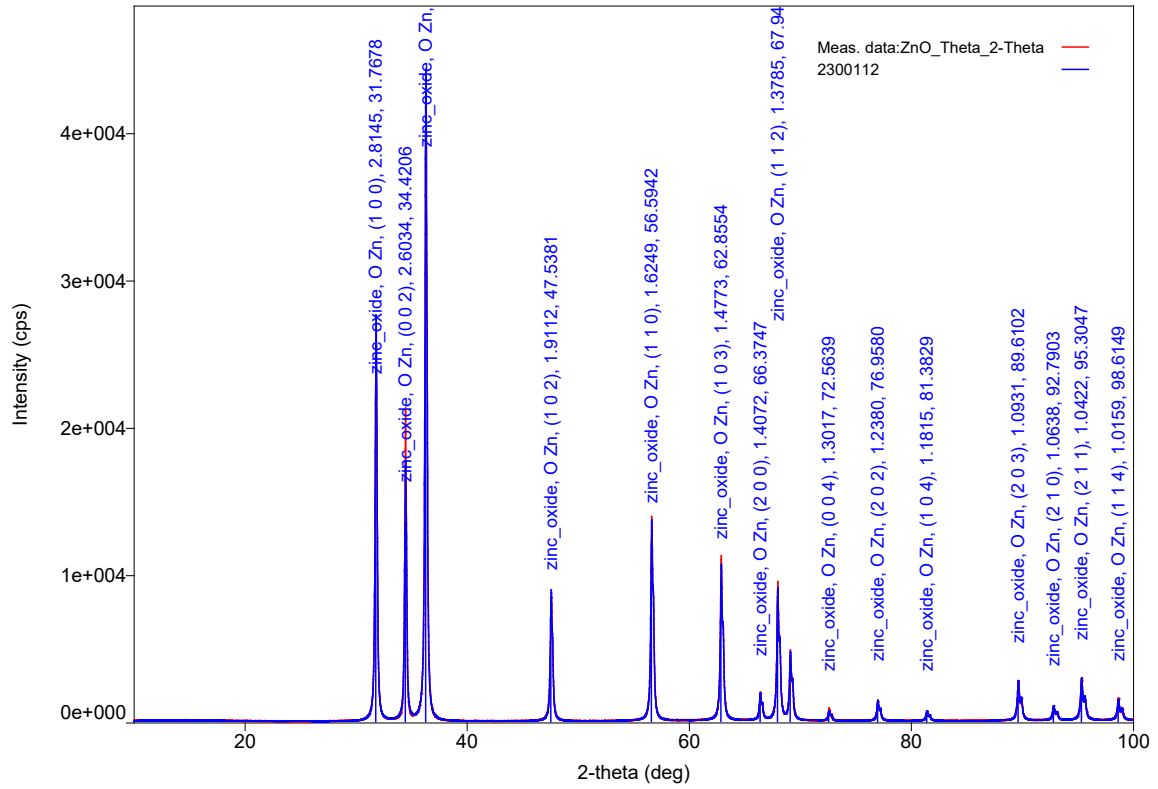
A. TiO₂ NM-105



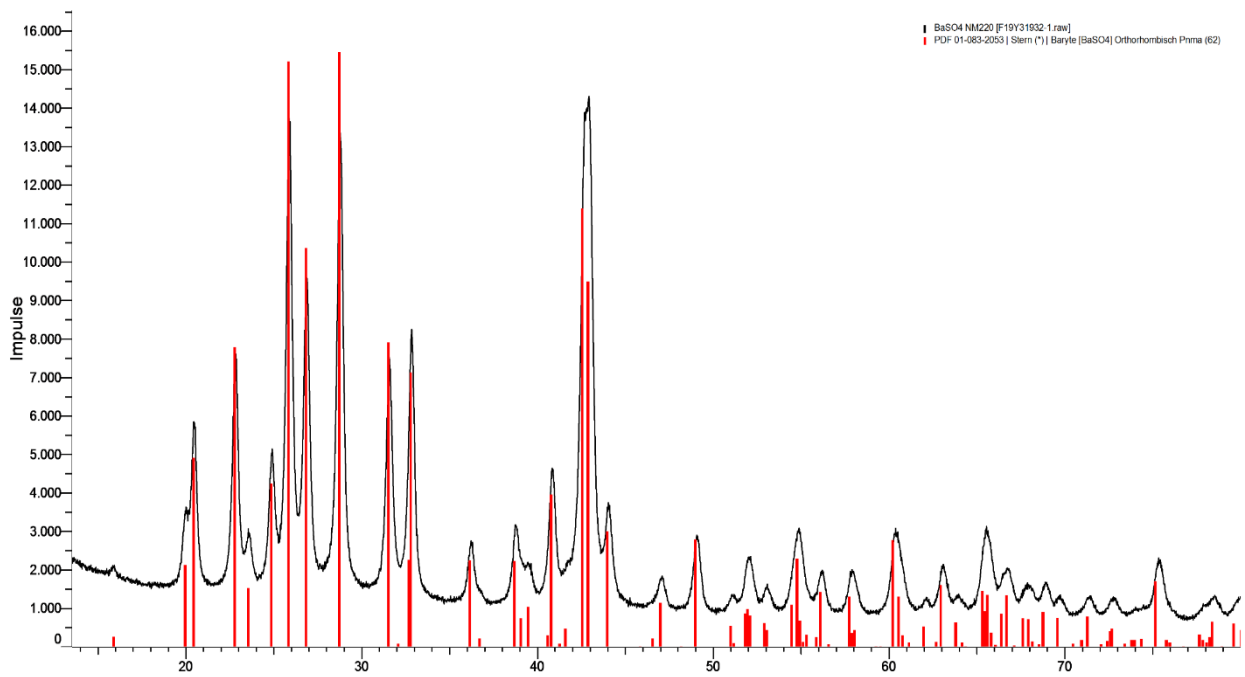
B. Ag Sigma-576832



C. ZnO NM-111



D. BaSO4 NM220



E. CeO₂ NM212

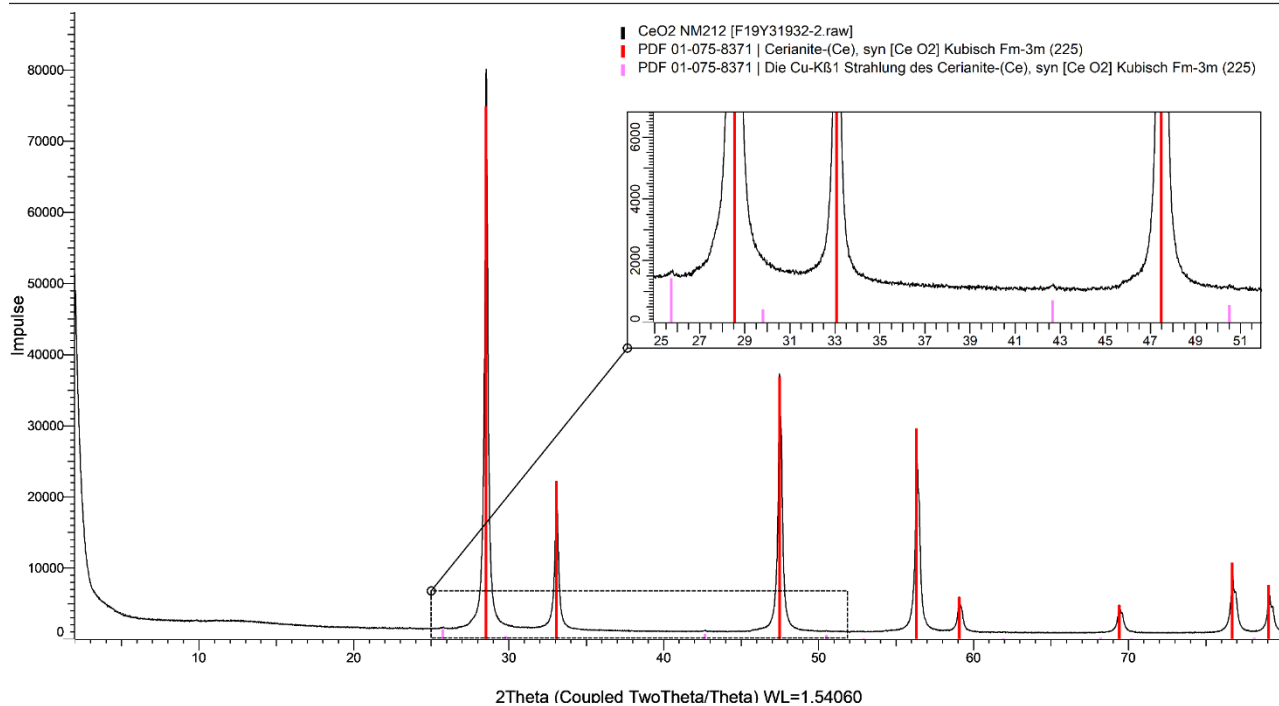


Figure S2: A series of XRD patterns for the five ENMs listed in Table 1, (A) TiO₂ (NM-105), (B) Ag (Sigma 576832), (C) ZnO (NM-111), (D) BaSO₄ (NM-220) and (E) CeO₂ (NM-212). These graphs illustrate the crystalline phases for each material as summarised in Table 1.

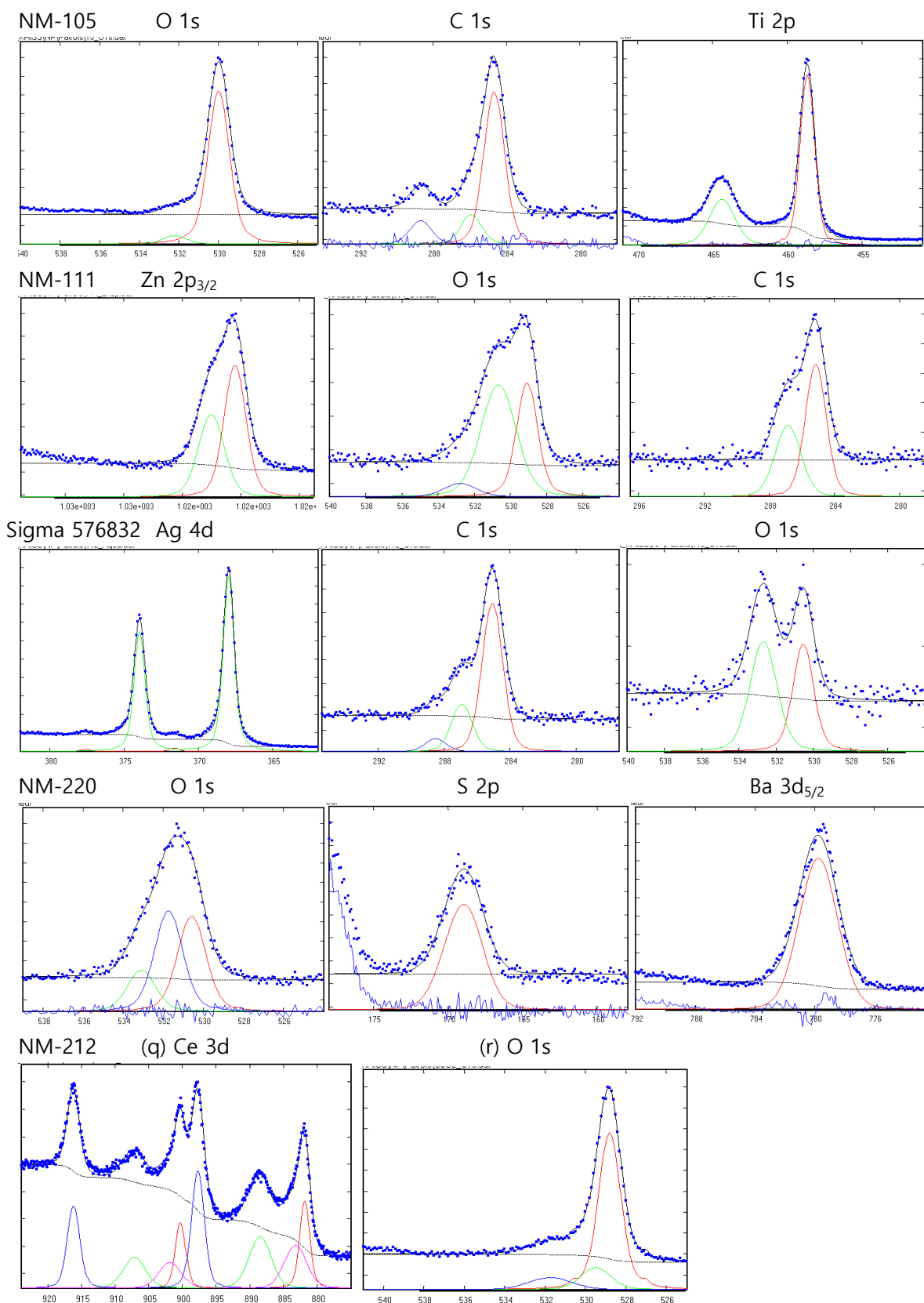


Figure S3: A series of XPS core level curves for the five ENMs included in this study and summarized in Table 1: TiO₂ (NM-105), ZnO (NM-111), Ag (Sigma 576832), BaSO₄ (NM-220) and CeO₂ (NM-212). Each curve is fitted by Lorentzian-Gaussian convoluted functions to determine the chemical composition.

2. Micronucleus Assay

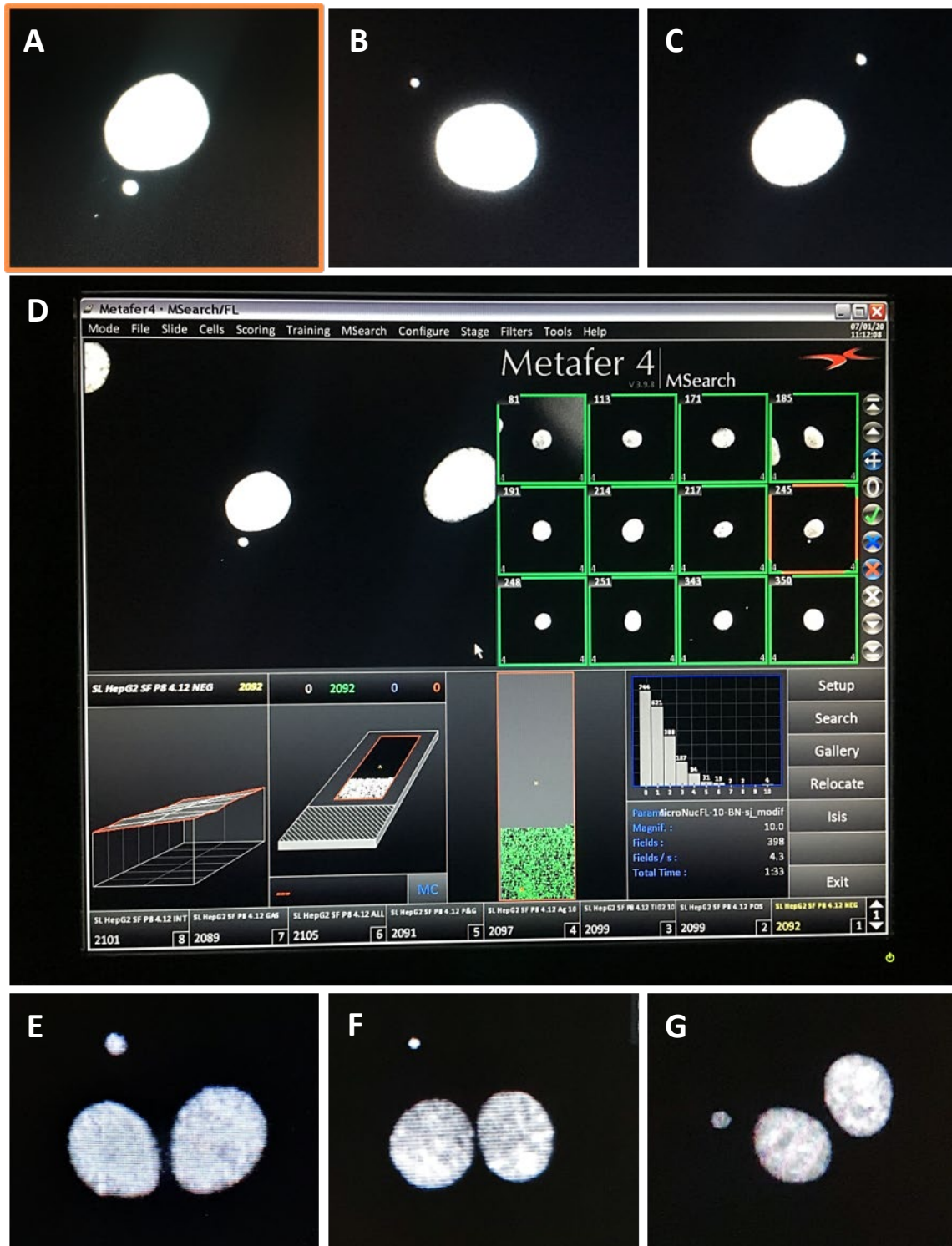


Figure S4: Representative images of micronuclei generated by automated scoring of HepG2 cells using a Metafer MetaSystem 3.9.8. (A) illustrates an enlarged image of a micronucleus shown in the scoring gallery pictured in (D), and highlighted with an orange outline. Representative images of micronuclei found within the HepG2 mononucleate (B, C) and binucleate (E – G) cell populations following prolonged and acute ENM exposures respectively.

5.0 Critical Review

Nanotechnology is an important Key Enabling Technology (KET) that leads the drive for innovative products to alleviate the increasing demand for smaller, lighter, faster, more adaptable and durable technologies. Nanotechnology is the manipulation and production of materials with enhanced unique physico-chemical properties created by manufacturing these materials into particles of 1 – 100 nm in size, increasing the surface area to volume ratio (1,2). As a global market, nanotechnology reached \$75.8 billion in 2020, with engineered nanomaterials (ENMs) defined as having the greatest share of the global nanotechnology market (3). There has been widespread adoption of ENMs in a variety of industries such as food, textiles, cosmetics, medicine, electronics, manufacturing, construction and energy industries. With the continued manufacturing, integration and extensive application of ENMs, there are heightened concerns regarding increased human and environmental exposure, and the potential risk these materials with novel, physico-chemical characteristics may pose to human health and the environment. Due to the diversity in design of these ENMs, it is untenable to rely solely on *in vivo* based test systems to evaluate any potential risks that routine exposure to these materials may pose to human health. With this in mind and in line with the 3R's directive to reduce, replace and refine the use of animal-based testing methods (4), there has been a keen research focus into the development and advancement of robust, physiologically relevant *in vitro* test systems. There are a range of test systems available, each with the own benefits and limitations which often define their compatibility with a specific hazard endpoint. A number of 2D models were initially developed, including the use of organotypic cultures (*e.g.* lung or liver slices), human primary cell types or multiple cell-lines to build both co-cultures and triple-cocultures, which more closely mimic the human cell population. In most cases, the next logical step involved the progression from 2D into 3D *in vitro* test systems, like spheroids, organoids and microtissues. This often results in a better representation of the complex architecture of the intra-cellular network, as well as improved organotypic features (*e.g.* metabolic activity), which enhance the capacity of these models to act as *in vivo* substitute test systems for ENM hazard assessment.

Hepatic toxicology is a fundamental aspect of ENM associated toxicity assessment, as the liver is the main site of secondary ENM deposition and accumulation, as well as the main detoxification centre of the human body. As a secondary site of ENM

exposure, the ENMs have to translocate from the primary site of exposure, following either ingestion, inhalation, injection or dermal penetration and cross a cascade of biological compartments. This results in direct interaction with a variety of biological membranes and fluids, which can result in a transformation of the physico-chemical characteristics of the materials, impacting, for example, ENM surface chemistry, protein corona, morphology, agglomeration and dissolution. Thus, it is highly likely that the ENMs, which reach the liver, are no longer the 'pristine' materials from the original exposure (5). With high ENM surface energy, once in contact with biological fluids, proteins and other biomolecules, bind rapidly to the surface of the particle forming a dynamic surface coating, known as the protein corona. The assembly of this protein corona bestows the ENMs with a new biological identity, which determines colloidal stability, biodistribution, cellular interaction, uptake, clearance and toxicity (5–7). Therefore, it is essential to understand the range of transformation that ENM may undergo within a physiologically relevant environment.

Whilst the translocation of ENMs to the liver is low, with only 1.0% of the original inhaled or ingested dose reportedly found to translocate to the liver, there are more concerns regarding the gradual accumulation of the materials in the liver over time. A previous *in vivo* study undertaken to assess the effects of an occupational 14-day pulmonary exposure, found that only 1.24% and 2.87% of the original intratracheal instilled dose of 162 µg of TiO₂ and CeO₂ ENMs per mouse reached the liver (8). This corresponds to a translocated dose of 1 µg/g *in vivo* or 1 µg/mL *in vitro* (8), illustrating the concentration of material reaching the liver is relatively low and that low-dose exposures should be employed when evaluating the effect of ENM exposure upon secondary sites of exposure. Within this thesis, in addition to enhancing the physiological relevance of the ENM exposures, low-dose ENM exposures have also been performed, with concentrations ranging from 0.20 µg/mL to 10.0 µg/mL.

Furthermore, the duration and manner of ENM exposure is pertinent to identifying their full toxicological potential. Whilst the majority of *in vitro* ENM hazard assessment has been performed under acute exposure, which provide an insight into the potential toxicity of these materials, these exposure regimes do not simulate human exposure. Humans are more likely to be exposed to low concentrations of ENMs repeatedly over a longer duration of time, and so it is important to emulate this within an *in vitro* setting, as studies have already shown ENMs are able to accumulate in the liver and can cause hepatotoxicity upon prolonged, repeated exposure (9–11). One

major limitation behind the paucity of long-term *in vitro* based ENM hazard assessment is the longevity of current hepatic models. In brief, the existing literature highlights a vast range of different 3D liver models from primary human hepatocyte (PHH) microtissues, organoids and cell-line based spheroid models to organ-on-a-chip devices, bioreactor chambers, tissue engineering and 3D printing (12–14). These models all have their own benefits and limitations. Whilst some exhibit the greatest physiological relevance, liver-like functionality and metabolic activity (*e.g.* PHH models), others are more accessible, easily reproducible and adaptable to measure multiple toxicity endpoints (*e.g.* spheroids). Some hepatic models are able to remain viable for longer culture periods than others, but often these models are fully differentiated, non-proliferating models and / or they require additional structural support through scaffolds or matrices, which can make them incompatible with some toxicity assays or hinder ENM cellular exposures (15). For example, PHH models, deemed the ‘gold standard’ for *in vitro* hepatic toxicology, are static, non-dividing models deeming them incompatible with assays that evaluate fixed DNA damage, such as the micronucleus (MN) assay, as fixed DNA damage is only measurable after the cells to have undergone at least one cell cycle. There is no single assay that detects all forms of DNA damage; however the MN assay is the regulatory ‘gold’ standard for assessing chromosomal damage *in vitro*, and thus is considered a robust assay for measuring genotoxicity. Genotoxicity arises as a result of DNA damage, and can disrupt normal development, cause malignancies and other pathogenic events. Multiple *in vivo* and *in vitro* studies have reported that some ENMs exhibit clear cytotoxic, (pro-)inflammatory, and sometimes genotoxic effects, thus raising concerns as to the long-term repercussions on human health (16,17). As a result, a distinct technological gap was identified and a need for a proliferating 3D liver model with the ability to support ENM exposures and facilitate the measurement of fixed DNA damage over both acute and prolonged exposure periods was recognized (15). Whilst there is an Organisation of European Cooperation and Development (OECD) Test Guideline (TG487) for the MN assay, it has long been recognised that nano-specific adaptations to the method are required, which were included in the approach taken within this study (18,19). Therefore, the aim of this thesis was to develop a robust, more physiologically relevant *in vitro* 3D liver model able to support fixed DNA damage assessment and provide a potential *in vivo* alternative test system for ENM hazard screening following more realistic prolonged and repeated ENM exposures.

5.1 *In Vitro* 3D HepG2 Liver Model Development

Publication I involves an extensive literature search with the aim to provide some background into the current research and development status of 3D *in vitro* liver models able to support ENM associated hazard assessment, specifically focusing on genotoxicity. This review considered the benefits, limitations and nano-specific adaptations of *in vitro* approaches to assess hepatic DNA damage following ENM exposure. Alongside this, the review identified adverse outcome pathways (AOPs) as a useful tool for predicting specific mechanisms behind hepatotoxicity, with key events which should be taken into consideration throughout the development and refinement of *in vitro* test systems and relevant bioassays. Following this review, it was evident that there was a distinct paucity of *in vitro* 3D models able to support both prolonged ENM exposure and fixed DNA damage assessment. This outcome led to the focus for publication's II and III on the development and optimisation of a predictive and more physiologically relevant 3D *in vitro* liver model. As detailed in publication II, when designing and developing this model based on the original short-term exposure system described in Shah *et al.*, 2018, there were three main aims:

1. To improve the physiological relevance and longevity of the model
2. To build a model able to actively proliferate to support fixed DNA damage assessment *via* the micronucleus assay.
3. To achieve A and B, without using materials or processes that would be susceptible to ENM interference or hinder cellular uptake (*i.e.* scaffolds and matrigels) (20).

Initial work began with an investigation into enhancing the physiological relevance of the liver model. To do this, a comparison between the easily accessible, cost effective HepG2 cell line versus the more metabolically active, liver-like HepaRG cell line was conducted. HepaRG cells have been shown to express the main xenobiotic-metabolizing enzymes, such as phase I CYP450s (*e.g.* CYP1A2, 2B6, 2C9, 2D6 and 3A4), phase II glucuronosyltransferase, N-acetyltransferase and sulfotransferase enzymes, nuclear receptors (*e.g.* PXR, PPAR α) and transporters (*e.g.* MRP2 and MDR1), deeming them highly suitable cell line for assessing drug hepatotoxicity (21,22). The expression level of these enzymes has additionally been shown to resemble that of the primary human hepatocytes (PHH), giving a closer translation between *in vitro* to *in vivo* results, with no inter-donor variation experienced with the

PHH models (23). Consequently, it was thought that the HepaRG cells may be the most suitable cells to develop a 3D liver model that supported both long term ENM exposure and genotoxicity testing. However, as the HepaRG cells are already differentiated, they do not actively proliferate and even with the optimization of MN test conditions (*i.e.* cytochalasin B concentrations of 3 – 9 $\mu\text{g}/\text{mL}$, and exposure durations of 24 – 30 h) as shown in publication III, Fig. 3C, the binucleate frequency remained below 10%. A low binucleate frequency deems them unsuitable for fixed DNA damage assessment as the cells cannot divide sufficiently to support the detection of micronuclei during cytokinesis. With this, and in conjunction with the fact the HepaRG cells did not significantly outperform the HepG2 cells in liver-like functionality, illustrated in publication III, the HepaRG cell line was no longer considered in the future development of the model.

Once the preferred cell line had been established, the next stage of development was to improve the longevity of the HepG2 spheroid model by enhancing its viability over extended culture durations to support prolonged and repeated ENM exposures. The hanging drop method was selected, as it is a simple, scaffold-free system, that enables spheroid formation without the need for additional synthetic materials or force besides gravity. The original HepG2 spheroid model described by Shah *et al.*, retained the spheroids in 25 μL hanging drops through-out the duration of the culture, including exposure. This restricted availability of fresh culture medium throughout the duration of the experiment, limiting the viability of the model to < 7 days. To overcome this limitation, the hanging drops were grown on 96-well plates, as opposed to square petri dishes, to allow for the spheroids to be transferred to the wells of the culture plate containing fresh culture medium. This enabled a plentiful supply of cell culture medium, with the essential nutrients to aid cell growth and dilute any waste products, to improve the viability of the cells over a longer duration of time. The simplest, most effective way to transfer the hanging drops into a 96-well plate, was to seed them directly onto the lid of the plate then centrifuge them into the bottom of the well as shown in Fig. 1.

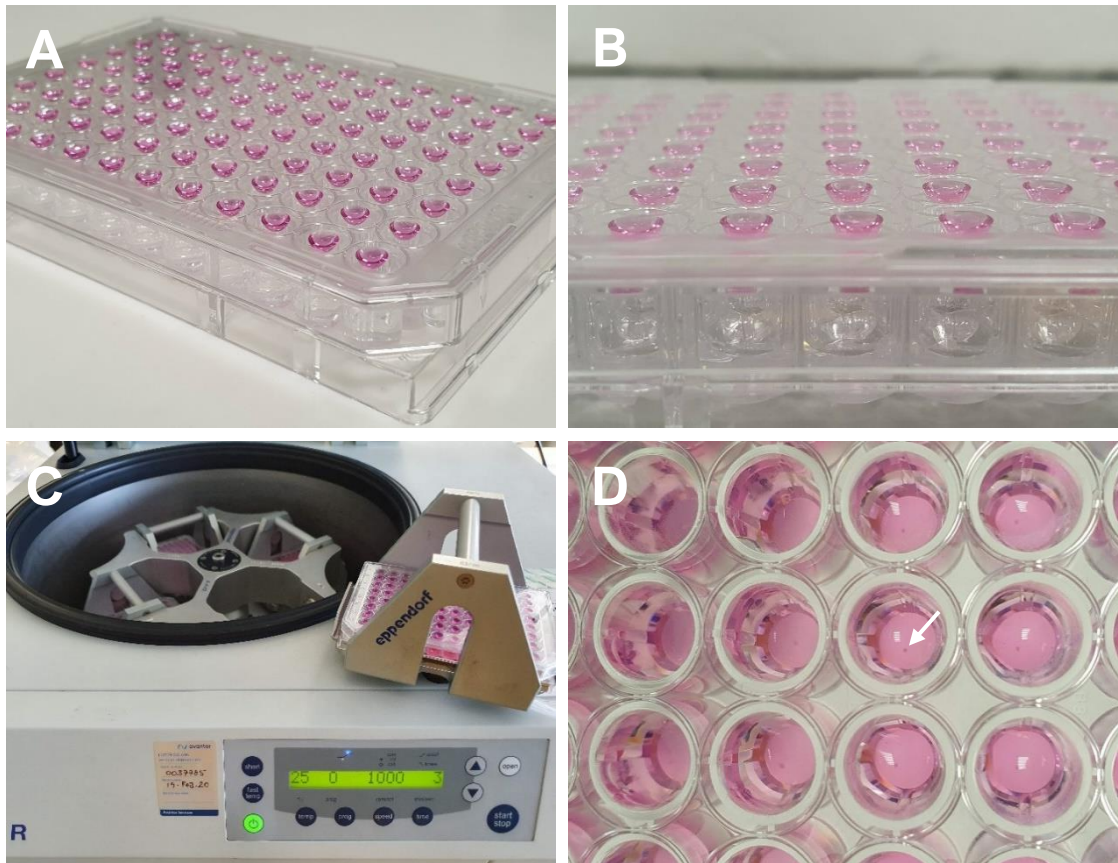


Figure 1: Representative images of (A) the 96-well plate after seeding the HepG2 droplets onto the surface of the lid with (B) PBS added to the wells of the plate to prevent the droplets drying out before the (C) transfer to agarose coated wells three days later *via* centrifugation. Following centrifugation, (D) the HepG2 spheroids, indicated by the white arrow, are now in the base of the wells surrounded by fresh culture medium.

After a few trials with different centrifuge settings, capture medium volumes and cell seeding densities, the most effective method was to seed the cells at 4000 cells per spheroid in a 20 μ L drop, perform a quick short spin with 100 μ L of medium in the base of the wells to catch the spheroids as they fall. One minor issue faced with the new 96-well plate set up was preventing the HepG2 spheroids from settling at the bottom of the well, attaching to the plastic and beginning to grow out into a monolayer once again. This issue was easily resolved by coating the plastic at the base of the well with a fine layer of 1.5% agarose gel. As a result, the 3D HepG2 spheroid model was now over 70% viable for 14 days in culture; an extra 7 days longer than viability of the previous model.

With respect to publications II and III, the majority of relevant data generated as part of the development and characterization of the 3D HepG2 spheroid model was included in these papers. The main outcome of this section of the research was the development of the *in vitro* 3D HepG2 spheroid model, described in publication II, which was shown to retain proliferative capabilities and remain viable for a longer period in culture, deeming it a useful tool for ENM associated DNA damage assessment. Publication III, identified that when employing the 3D HepG2 model for prolonged ENM hazard assessment, the mononuclear version of the MN assay should be used as opposed to the binuclear version, as an entire population of cells with DNA damage can be overlooked leading to a mis-representation of results. The main impact of these two publications was a Standard Operating Procedure (SOP) describing how to set-up and apply the 3D HepG2 liver model for both acute and prolonged ENM genotoxicity assessment using the OECD approved, *in vitro* micronucleus assay.

5.2 ENM Exposure Scheme Design

Whilst the development and optimisation of a more physiologically relevant liver model was the key priority, this was not the only aspect of hepatic ENM hazard assessment that could be advanced further. The manner in which we perform the ENM exposure itself could be improved to better emulate the “true” ENM exposure experienced by the liver. For example, with inhalation and ingestion being the two most common routes of ENM exposure, techniques to mimic these routes of exposure, with a specific focus on the interaction of the materials with particular biological fluids as they translocate through the human body, were investigated. During translocation through the body, ENMs are likely to come into contact with a wide range of different biomolecules, changeable pH environments and microbes; all of which can transform the original ‘pristine’ ENMs in a manner that may change how these materials interact with biological systems, influencing cellular uptake, bio-durability and toxicity. Therefore, not only is it important to fully characterize an ENM prior to exposure, it is equally as important to characterize these materials under biological exposure conditions as they may undergo transformation (*e.g.* dissolution, aggregation and reprecipitation) when they come into contact with different biological fluids (24). As a result, simulating this *in vivo* journey and the key interactions with biological fluids is critical in fully understanding and predicting the potential toxicological effects

ENMs could have upon the liver. Both inhalation and ingestion exposure routes were addressed with a range of potential simulant fluids devised for lung lining fluid (*i.e.* pulmonary surfactant), gastric and intestinal fluid as well as human blood. These simulant fluids were designed to simulate the *in vivo* journey from (A) the lung, across the air-blood barrier and into the blood stream or (B) oral ingestion leading to translocation from the stomach, intestines and then into the blood stream before reaching the liver, as illustrated in Fig. 2. The simulant fluid protocols were developed with the aim to be as physiologically representative as possible, but equally were not to be too complex so that the protocol could be easily reproduced and potential variation minimised. It is important to note that a fraction of the inhaled ENMs could reach the GIT too *via* the hosts primary defence mechanism against inhaled toxicants, known as mucociliary clearance. Mucociliary clearance involves the secretion of mucus, by the goblet cells, onto the surface of the airway epithelium. Inhaled particles, ENMs, allergens or pathogens deposited on the ciliated airways can be trapped in the mucus and cleared up the trachea by the mucociliary escalator before being swallowed and digested *via* the GIT (25). This particular exposure pathway was not simulated in this instance, as we were focusing on the primary routes of exposure, but this pathway could be considered as a valuable addition to the pre-treatment scheme for future investigations.

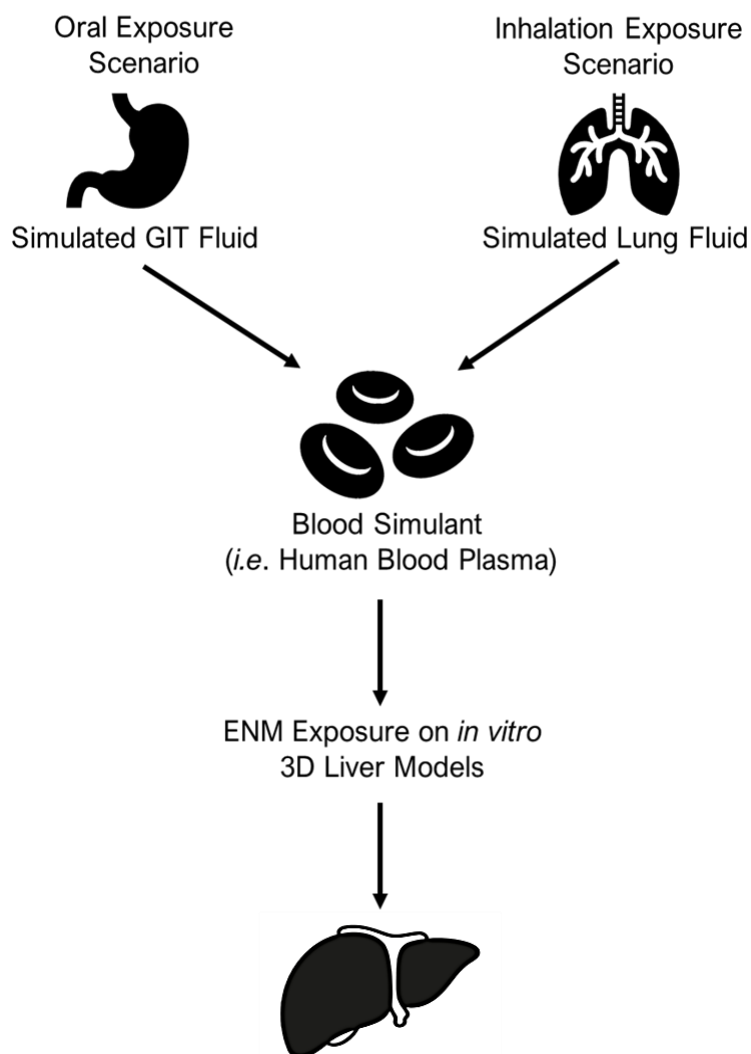


Figure 2: Schematic representation to illustrate the sequential incubations required for simulating the translocation of ENMs to the liver, following both oral and inhalation exposure routes. GIT: Gastrointestinal Tract.

5.2.1 Inhalation Simulant Fluids

After an extensive literature search, a number of lung simulant fluids were shortlisted including Simulated Lung Fluid (SLF), Epithelial Lining Fluid (ELF) and Gamble's solution; but the SLF was selected as the most physiologically representative simulant fluid (Table 1). All of the simulants assessed share a pH of 7.4, and some similar chemical components, particularly when comparing SLF and ELF. Whilst Gamble's solution has been adapted and used frequently in the past, this simulant fluid was first devised in 1979 and omits a number of key proteins, like albumin (26). With ELF

being difficult to source in the UK, the most suitable option to take forward was the SLF, supplied by Professor Ben Forbes and his research group in Kings College London, as described in Hassoun *et al.*, (2018) (27).

Table 1: Compositional breakdown of potential simulant fluids devised as a more physiologically representative alternative to human lung surfactant. Chemical abbreviations, in order of appearance, are as follows: DPPC: dipalmitoylphosphatidylcholine, and DPPG: dipalmitoylphosphatidylglycerol.

Lung Simulant Fluids					
Simulated Lung Fluid (SLF)		Epithelial Lining Fluid (ELF)		Gamble's Solution	
pH 7.4		pH 7.4		pH 7.4	
DPPC	4.8 mg/mL	Serum Albumin	7.4 mg/mL	Magnesium Chloride	0.095 mg/mL
DPPG	0.5 mg/mL	Phosphatidylcholine	10.0 mg/mL	Sodium Chloride	6.019 mg/mL
Cholesterol	0.1 mg/mL	Lysozyme	2.5 mg/mL	Potassium Chloride	0.298 mg/mL
Albumin	8.8 mg/mL	Apotransferrin	0.2 mg/mL	Disodium hydrogen phosphate	0.126 mg/mL
Immunoglobulin G	2.6 mg/mL	Ascorbic Acid	50 µg/mL (280µM)	Sodium sulfate	0.063 mg/mL
Transferrin	1.5 mg/mL	Uric Acid	1 µg/mL (2µM)	Calcium chloride dehydrate	0.368 mg/mL
Ascorbate	140 µM	α-tocopherol	25 µg/mL (150µM)	Sodium acetate	0.574 mg/mL
Urate	95 µM	Glutathione	50 µg/mL (160µM)	Sodium hydrogen carbonate	2.604 mg/mL
Glutathione	170 µM	Hanks Balanced Salt Solution		Sodium citrate dihydrate	0.097 mg/mL

The SLF selected (Table 2) consists of key components found in healthy human respiratory tract lining fluid, including major soluble proteins (Albumin, IgG and Transferrin), abundant lipids (DPPG, DPPC and Cholesterol) and antioxidants (Ascorbate, Glutathione and Urate). Aliquots of stabilized, freeze-dry SLF can be distributed, stored at room temperature for up to three months and then reconstituted in 10mL of de-ionised water on day of ENM exposure. This highlights that SLF is stable, easily accessible and with a long shelf life can support longer-term ENM studies readily.

Table 2: Description of the composition (A) and physicochemical properties (B) of the selected simulant lung fluid proposed for ENM pre-treatment schemes. Chemical abbreviations, in order of appearance, are as follows: DPPC: dipalmitoylphosphatidylcholine, DPPG: dipalmitoylphosphatidylglycerol and HBSS: Hanks' Balanced Salt Solution.

A Simulated Lung Fluid (SLF)		B Simulated Lung Fluid (SLF)	
Ingredient	Concentration in 10mL SLF Aliquots	Physicochemical Property	Reconstituted freeze-dry SLF
DPPC	4.8 mg/mL	pH	7.7 ± 0.1
DPPG	0.5 mg/mL	Conductivity [mS / m]	14.6 ± 0.2
Cholesterol	0.1 mg/mL	Viscosity [Pa.s x 10 ⁻³]	1.111 ± 0.015
Albumin	8.8 mg/mL	Surface Tension [mN / m]	55.6 ± 0.7
IgG	2.6 mg/mL		
Transferrin	1.5 mg/mL		
Ascorbate	122.14 µM		
Urate	95.47 µM		
Glutathione	161.61 µM		
Gentamicin	10 µL		
HBSS	775 µL		

Unfortunately, as the research in this thesis was undertaken as part of an international consortium, there were some limitations (*e.g.* cost and time restrictions) on this work and so whilst, a suitable lung simulant fluid was selected and an SOP was devised, the impact of inhalation-simulant fluids on ENM transformation was not evaluated and will be the focus of future work. Instead, for Publication IV the focus became heavily directed towards simulating the oral, ENM ingestion exposure route instead, using a tried and tested protocol for oral simulants previously devised by the Leibniz Research Institute for Environmental Medicine (IUF).

5.2.2 Oral Ingestion Simulant Fluids

For the oral, ingestion simulant fluids, the IUF gastrointestinal (GIT) simulant fluids were utilised, as these simulants had been previously used to successfully assess the effects of ENMs upon advanced GIT models *in vitro* (28). These oral simulants are devised to mimic the passage of ENMs from oral ingestion, to the stomach and then

onto the intestine. The protocol involves two, 30 minute incubations with two different simulant fluids; a gastric (pH 2.7) and intestinal (pH 9.5) fluid. Table 3 displays the composition of these simulant fluids and highlights that they are simple, cost-effective and easily reproducible fluids. Whilst, the GIT simulants are limited by the lack of some the important digestive enzymes (*e.g.* amylase, maltase, lactase, lipase and proteases, like pepsin) and resident gut microbes that would provide precise physiological relevance, they do offer the dynamic pH changes and harsh transition from acidic to alkaline conditions experienced during digestion.

Table 3: Composition of the gastric and intestinal simulant fluids used in the pre-treatment of the ENMs used in publication IV. Both simulant fluids were designed and published by Kämpfer et al., 2020 (28).

Gastric Solution (34mM NaCl/HCl)	
pH 2.7	
Ingredient	Concentration in 1.0L of ddH₂O
Sodium Chloride	1.98 g/L
Hydrochloric Acid	For pH Adjustment
Intestinal Solution (50mM Carbonate/Bicarbonate Buffer)	
pH 9.5	
Ingredient	Concentration in 1.0L of ddH₂O
Sodium Carbonate	0.84 g/L
Sodium Bicarbonate	3.58 g/L
Sodium Chloride	2.00 g/L

Following incubation with the GIT simulant fluids, it was important to mimic the final transition from the GIT to the liver; transport *via* the circulatory system. To emulate this, the ENMs pre-treated with GIT simulant fluids underwent a further incubation in 55% human blood plasma (pH 7.4) for one hour. A ratio of 11 parts human blood plasma to 9 parts ENM solution was devised in order to represent the physiologically relevant composition of plasma in human blood (29). Using these pre-treated ENMs, both acute (24 h) and longer-term (120 h) exposures were conducted using the 3D HepG2 model developed in publications II and III. Two ENMs, Titanium Dioxide (TiO₂) and Silver (Ag) were selected to evaluate if pre-treating these materials with

ingestion simulant fluids would induce a significantly different genotoxicological outcome in the liver spheroids. Both TiO₂ and Ag were selected, as they are often found incorporated in applications where there is a high possibility of human ingestion, from food packaging, food additives (*e.g.* nano-sized E171, E174), dental implants / dentures, toothpaste and mouthwash to drinking water purification and fertilizers / pesticides (30–34). Based on the low-dose concentration range used throughout this thesis, the top dose of 10.0 µg/mL was selected to evaluate if pre-treating ENMs was a necessary step to more predictive *in vitro* ENM hazard assessment. Whilst two exposure durations and two materials were investigated in this study, for publication VI, only the acute exposure data for Ag ENMs was taken forward for publication. The reason behind this was that the collaborating institutions contributing to this publication only addressed 24 h ENM exposures with and without pre-treatment schemes for Ag and Silica ENMs alone. Thus, for uniformity in the manuscript, the data generated on TiO₂ was not included.

Whilst, the TiO₂ data has not been published, it has been included here alongside the Ag ENM data, as it was found to generate similar results to that seen with the Ag ENMs and further supports the conclusions of publication IV (Fig. 3). In addition, the prolonged exposure data with pre-treated ENMs was not published in publication IV, but is displayed below (Fig. 3). Alongside the albumin and urea liver function assays described in publication II and III, two toxicological endpoints were assessed; (pro-)inflammatory response and genotoxicity. Both interleukin 8 (IL-8) and tumour necrosis factor alpha (TNF- α) are indicators of an acute inflammatory response and so, (pro-)inflammatory mediator release was compared following exposure of the 3D HepG2 liver spheroids to pristine ENM versus those same materials pre-treated with the oral simulant fluids. IL-8 release was selected as it is indicative of an early, localised (pro-)inflammatory response and can be secreted by any cells with the presence of toll-like receptors (TLRs) that are involved in innate immune response. Whilst IL-8 is a chemoattractant cytokine responsible for neutrophil recruitment and degranulation, TNF- α is a cytokine released primarily by localised immune cells, like neutrophils, leukocytes and macrophages (35). TNF- α is a cytokine in the systemic circulation and forms part of the acute phase reaction alongside IL-6 (36). IL-6 was also investigated, but all the results were found to be below detectable limits and so this cytokine was not considered further (data not shown).

Both pre-treated (PT) TiO₂ and Ag ENMs were shown to induce an elevated IL-8 and TNF- α response compared to their pristine counterparts; with PT TiO₂ and Ag

inducing a significant increase in IL-8 (Fig. 3A) and TNF- α (Fig. 3C) respectively, following acute 24 h exposure. Yet, following long-term exposures, this effect was no longer observed (Fig. 3B & D). It is important to note that the IL-8 and TNF- α release observed after ENM exposure was not significantly greater than that seen in the untreated, negative control. The overall increase in the release of IL-8 between the acute and longer-term ENM exposure (Fig 3A & B), is thought to arise as a result of reduced oxygen diffusion towards the centre of the spheroid leading to a larger number of hepatocytes experiencing hypoxic conditions, which has been shown to increase IL-8 production (37–39). Conversely, TNF- α release is shown to decrease after the 120 h exposure, which could be attributable to the fact that TNF- α is an acute phase inflammatory chemokine and is often released immediately after an toxicological insult, like a single, bolus exposure to ENM. Consequently, the elevated TNF- α released immediately after 24 h exposure to ENM may have subsided over the 120 h after the original insult. With the exception of the TNF- α release associated with longer-term ENM exposures, PT TiO₂ and Ag ENMs induced a higher release of (pro-)inflammatory mediators compared to the pristine material. This suggests that ENM transformation, as a result of the GIT and human blood plasma pre-treatment scheme, could have an effect on the biological interaction of both TiO₂ and Ag ENMs and may be influential in mediating a (pro-)inflammatory response in HepG2 liver spheroids. For example, over a 24 h period in DMEM media alone, pristine TiO₂ ENMs were found to exhibit high oxygen reactivity, which could be further exacerbated by exposure to the extreme changes in pH induced with sequential incubation in the GIT pre-treatment simulants. This increase in REDOX reactivity and the release of free radicals, like ROS, may be responsible for the elevated (pro-)inflammatory response observed following acute exposure to pre-treated TiO₂ ENMs. However, pre-treating TiO₂ and Ag ENMs did not significantly impede liver functionality nor induce elevated cytotoxicity or genotoxicity (Fig 4.) over the pristine ENM exposures in HepG2 liver spheroids.

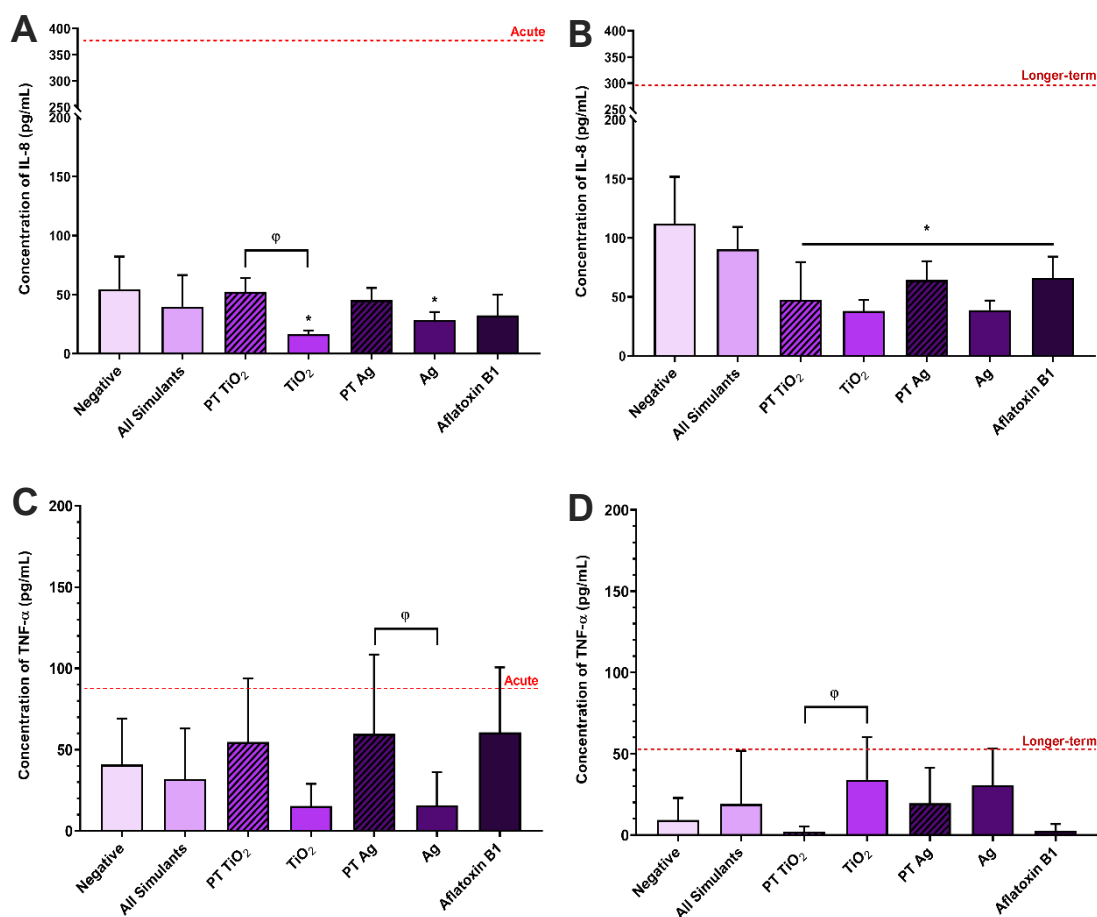


Figure 3: Comparison of IL-8 (A & B) and TNF- α (C & D) pro-inflammatory response in HepG2 spheroids post-acute (24 h) and longer-term (120 h) exposure to both pristine TiO₂ and Ag ENMs, and TiO₂ and Ag ENMs pre-treated (PT) with GIT simulant fluids. Mean data of three biological replicates, analysed in triplicate (n=9) presented \pm SD. Red dotted line represents the mean positive control response induced by 50 μ g/mL of TNF- α protein (NBP2-35076-50 μ g, Biotechne, UK). Significance indicated in relation to the negative control: * = $p \leq 0.05$ with significance between groups indicated as: $\phi = p \leq 0.05$.

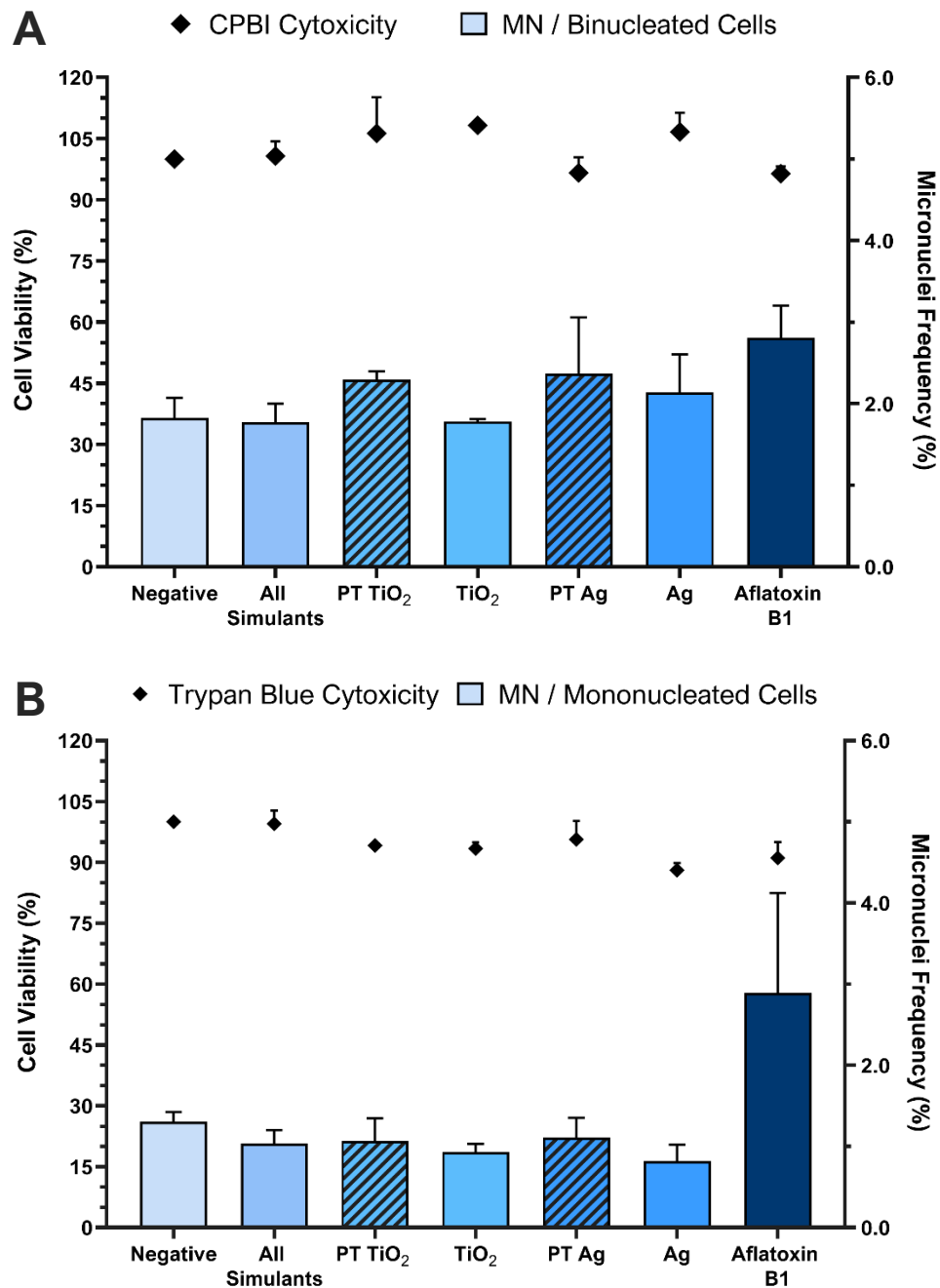


Figure 4: Cytotoxicity (cell viability) and genotoxicity (micronucleus frequency) response in HepG2 spheroids following acute (24 h) (A) and longer-term (120 h) (B) exposure to both pristine and pre-treated (PT) TiO₂ and Ag ENMs using the micronucleus (MN) assay. For acute exposures, 1000 binucleated cells were scored per dose per replicate using the cytokinesis-block version of the MN assay (3000 binucleate cells scored in total); whilst 2000 mononucleated cells per dose per replicate were scored using the mononuclear version of the assay (6000 mononucleated cells scored in total). Mean data of three biological replicates (n=3) presented ± SD.

Whilst neither the longer-term ENM exposures nor the TiO₂ ENM exposures were included in publication IV, acute exposure to both pristine and pre-treated TiO₂ did demonstrate a similar response to that observed with Ag ENMs and further supports the main outcomes of this publication. This publication was beneficial to the wider research community, as it provided an SOP to simulate both inhalation and ingestion ENM exposure for secondary sites of deposition, namely the liver. In addition, this publication highlighted that a tiered approach to assess the physico-chemical transformation of the ENMs in biological simulant fluids should be determined prior to exposure upon *in vitro* cultures. This way any ENMs shown to undergo considerable biotransformation under these simulated conditions are more likely to induce a significantly differently biological response and should be assessed for hazard induction *in vitro* using the pre-treatment schemes described in publication IV.

5.3 ENM Exposure Regimes

The natural progression for this research was to continue with the acute (24 h) versus longer-term (120 h) ENM exposure approach to evaluate if the toxicological effects observed with a wider range of five different ENMs (TiO₂, Zinc Oxide [ZnO], Ag, Barium Sulfate [BaSO₄] and Cerium Dioxide [CeO₂]) following 24 h exposure were still apparent after 120 h. These five materials were selected from different physico-chemical groupings (*e.g.* insoluble, soluble and passive) with the aim to evaluate a range of ENMs with diverse intrinsic properties which may be reflected in their behaviours within a biological environment and ascertain the predictive capabilities of the 3D liver model. Both ZnO and Ag were categorised as soluble, non-biopersistent materials; TiO₂ and CeO₂ were categorised as insoluble, highly agglomerated materials; and, BaSO₄ was selected as a passive, biopersistent material. These five materials are also used extensively in the manufacturing industry (*e.g.* automotive, energy generation, electrical products) as well as a range of consumer applications (*e.g.* food packaging, cosmetics, textiles) and are therefore likely to be exposed to in a repeated manner, over longer periods of time. Prolonged exposure to ENMs may induce repetitive hepatic injury leading to chronic liver disease (*e.g.* cirrhosis, hepatocellular carcinoma), whereby the regenerative capabilities are impaired, and the hepatocytes begin to undergo cell death as a result of inflammation (40,41). Consequently, it is important to consider the effects

associated with ENM exposure not only over an acute exposure, but a prolonged exposure too.

To mimic this more physiologically relevant exposure scenario more closely, a 120 h (five day) exposure regime was selected as it offered a prolonged exposure duration whilst allowing for 75.0 – 80.0% HepG2 cell viability to be maintained. In the first prolonged exposure regime, a single, bolus dose of the final ENM concentration was administered on the first day with a further four-day incubation before harvesting. In theory, this extended, single exposure regime should provide a chance for the hepatocytes to alleviate the immediate insult, recover and ameliorate any adverse effects induced by the materials, similar to what might happen within the human body. Unlike any other organ, the liver has the ability to repair and regenerate following toxicological insult, with only 51% of the original liver mass required for the organ to regenerate back to its full size (42). However, if this exposure were to be a regular event, the potential for ENM bioaccumulation and a prolonged or exaggerated biological response, could have a different adverse effect upon the liver spheroids in the long run. Therefore, the second prolonged exposure regime analysed in this publication was a daily, repeated exposure of the final ENM concentration fractionated into five equal parts. This fractionated dosing regime was devised to simulate the potential repeated ENM exposure humans are more likely to experience naturally and allows for a direct comparison between the individual and recurring exposure regimes to be assessed. It was important to consider the potential variation in toxicological outcome that could arise as a result of the repeated, chronic-like exposure scenario in comparison to the single, bolus dose, as a significant difference in hazard endpoints could dictate how future *in vitro* ENM exposure approaches are conducted.

For the repeated, fractionated ENM exposure, only two materials (TiO₂ and ZnO) were taken forward in the initial assessment and if a significant difference in the toxicological outcome was observed in the HepG2 liver spheroids between the two prolonged exposure regimes, the remaining materials would be further tested using a repeated ENM regime. TiO₂ and ZnO were selected as both were found to have a highly genotoxic nature in HepG2 liver spheroids following acute, 24 h ENM exposure, but only ZnO was found to elicit this genotoxic affect following prolonged, 120 h ENM exposure. With TiO₂ and ZnO inducing a negative and positive genotoxic response respectively, it was important to determine if a similar genotoxic effect was also observed following a prolonged, repeated exposure scenario, thus supporting the

previous classification identified by the single, bolus exposure regime. Instead of assessing the full ENM concentration range, a lower (0.5 µg/mL) and higher dose (5.0 µg/mL) from the original concentration range of 0.2 – 10.0 µg/mL were selected. Interestingly, across all doses, a similar genotoxic response was observed between the two distinct ENM exposure regimes with both TiO₂ and ZnO. Whereby, there was no significant difference in the fixed DNA damage detected following either a single, bolus or repeat, fractionated, prolonged low-dose ENM exposure in HepG2 liver spheroids. This experiment deems both exposure regimes interchangeable and negates the need for a more complex exposure regime for *in vitro* ENM hazard assessment in HepG2 liver spheroids.

Publication V illustrated that all five materials induced a diverse toxicological response in HepG2 liver spheroids, with a significant difference (*e.g.* IL-8 (pro-)inflammatory response and fixed DNA damage) observed following the acute (24 h) and prolonged (120 h) ENM exposures. This further highlights the importance of evaluating longer-term exposures to fully understand the prolonged effects of acute ENM exposures and the accumulated effects were the exposure to be a recurring event. One major outcome of this research, was even with the low doses of ENM applied in this study, all five of the materials tested were shown to induce fixed DNA damage in 3D HepG2 spheroids following acute exposure, leading to the following genotoxicity potency ranking: ZnO > TiO₂ > BaSO₄ = CeO₂ > Ag. This elevated level of genotoxicity was no longer present following prolonged ENM exposure, for reasons such as ENM agglomeration, dissolution rates and oxygen reactivity, discussed in the publication V. However, this did raise the question whether the genotoxicity outcome observed would still be evident if secondary genotoxicity mechanisms (*e.g.* inflammatory-driven oxidative DNA damage) were also at play.

5.4 Secondary Genotoxicity and *In Vitro* 3D Liver Coculture Model

Development

Following publication V, it was important to include the evaluation of secondary genotoxicity. Secondary genotoxicity has been identified as the main genotoxic mechanism *in vivo* and arises as a result of DNA damaged induced by chronic inflammation, initiated *via* a cytokine storm and the activation/recruitment of immune cells, such as macrophages and/or neutrophils releasing excessive levels of genotoxic

ROS (15,43). With the elevated (pro-)inflammatory response, high oxygen reactivity and dissolution associated with some of the ENMs investigated, it is important to consider the effect these materials may have upon secondary genotoxicity in the HepG2 liver model. In order to investigate this, additional cell types were essential and so a co-culture with the liver resident macrophages, Kupffer cells, was developed. Kupffer cells are active members of the mononuclear phagocytic system and serve a vital role in host defence through the mediation of the innate immune response, hepatotoxicity, regeneration and prevention of liver disease (44). The mediation of hepatic inflammatory response and subsequent oxidative stress, deems the Kupffer cells a suitable addition in the HepG2 liver model for assessing potential secondary genotoxicity associated with ENM exposure. As part of the non-parenchymal cell population, Kupffer cells contribute to 15% of the total hepatic cell population resulting in a 1 to 4 ratio of Kupffer cells to hepatocytes (45). With this physiology in mind, the existing 3D HepG2 liver model described in publication II and III was adapted to include the addition of human Kupffer cells seeded in a ratio of 1:4 HepG2 cells. The Kupffer cells were seeded into the droplets alongside the hepatocytes and incubated for three days to allow the spheroids to form. The SOP devised for the co-culture model follows an almost identical approach to the one described in publication III, with the exception of human Kupffer cells being added straight from cryopreservation and into the seeding process. The human Kupffer cells used in this co-culture were fully differentiated cells, which do not actively divide; they cannot be sub-cultured and so were added into the culture immediately after thawing (46). As a result, the Kupffer cells were thawed on the day of seeding, a Trypan Blue viability test was conducted and the cells re-suspended into the exact concentration (4.0×10^4 cells/mL) required for seeding 4000 cells per spheroid. Due to the highly adhesive nature of the Kupffer cells, the seeding process is done promptly and with the Kupffer cells kept in cold (4°C) co-culture medium until the last possible moment prior to seeding. As the epithelial cells and macrophages have different recommended culture mediums, initial optimisation work began with the development of an appropriate culture medium that would support both cell types effectively for 10 - 14 days of culture. Culture medium compositions were developed on the premise that each cell line would function appropriately if they had a representative proportion of their respective culture medium present; with this in mind, the following medium compositions were initially evaluated:

- A. 100% HepG2 Medium (1X Dulbecco's Modified Eagle Medium (DMEM) with 4.5g/L D-Glucose and L-Glutamine (41965-039, GIBCO®, Paisley, UK) with 10% foetal bovine serum and 1% penicillin/streptomycin)
- B. 100% Human Kupffer Cell Medium (Human Hepatic KC Maintenance Medium (Cat#. KC-2, ZenBio, UK))
- C. 25% HepG2: 75% Kupffer Medium
- D. 50% HepG2: 50% Kupffer Medium
- E. 75% HepG2: 25% Kupffer Medium

For initial optimisation, the HepG2/Kupffer cell co-culture spheroids were cultured over a 10 day period, with supernatants harvested on days 1, 4, 7, and 10 post-seeding in the hanging drop format. With the supernatants harvested, the Bromocresol Green Albumin Assay Kit (MAK124, Sigma Aldrich, UK (Fig. 5) and a TNF- α ELISA for (pro-)inflammatory response (Fig. 6) were analysed across two biological replicates to determine baseline liver-like functionality and macrophage activity in the co-culture spheroid across varying cell culture medium compositions. There was no significant difference in the concentration of albumin produced (Fig. 5) or the TNF- α released (Fig. 6) from each co-culture spheroid in relation to the cell culture medium composition used. Composition C was shown to yield the highest level of albumin over the first 7 days of culture, which could suggest this may be the most beneficial media composition for the co-culture. However, media composition E illustrates the greatest consistency over the 10 days in culture, with minimal fluctuation in albumin production. In addition, composition E, only slightly behind that of composition C, showed the greatest TNF- α cytokine release and inferred Kupffer cell activity. With no significant differences between culture medium C and E, medium composition E (75% HepG2: 25% Kupffer Medium) was selected as the co-culture medium to proceed with for all HepG2/Kupffer cell co-culture spheroid experiments, as this media composition is a true reflection of the HepG2:Kupffer cell ratio used.

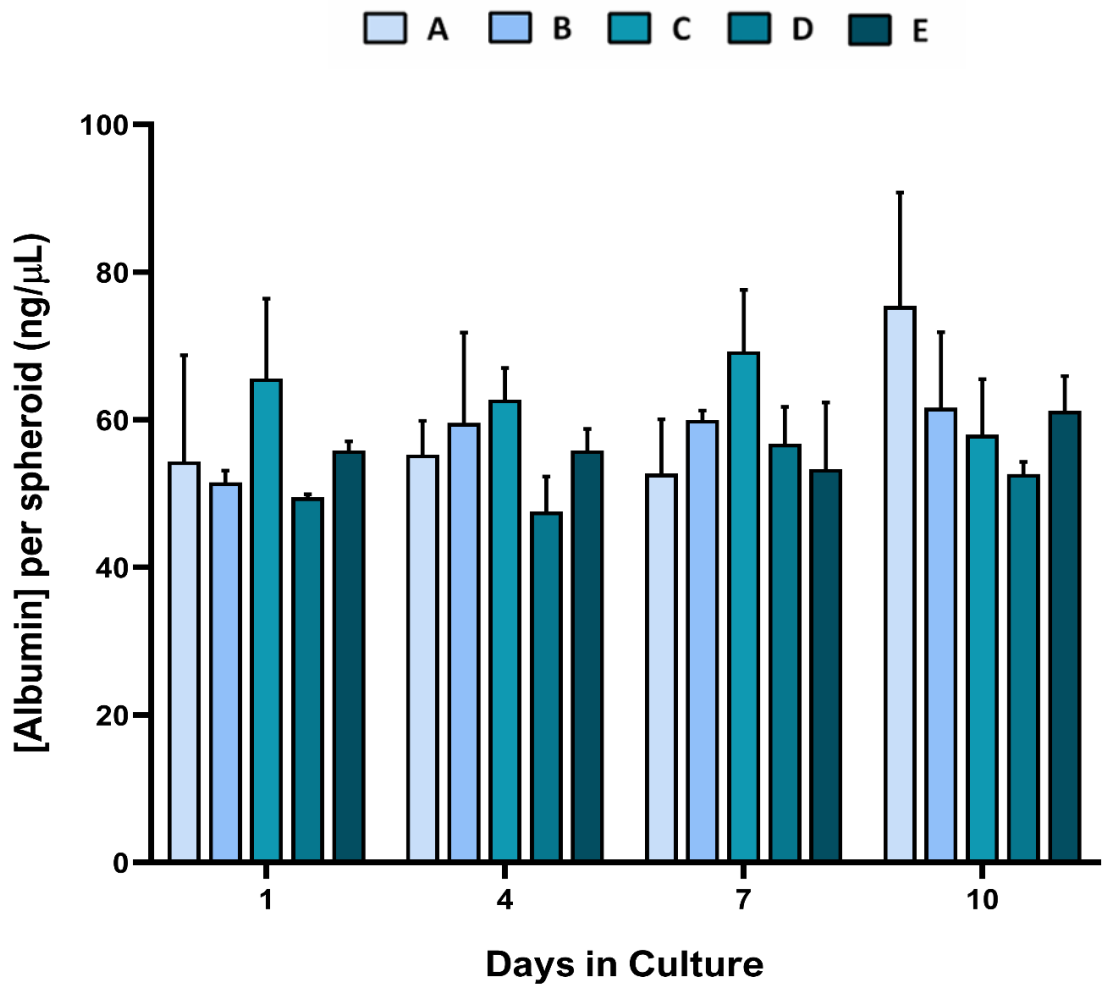


Figure 5: Albumin expression in HepG2 and Kupffer cell (KC) co-culture liver spheroids (5000 cells/spheroid) cultured in the hanging drop model, with varying culture medium compositions, over a 10 day period. (A) 100% HepG2 Medium, (B) 100% Human Kupffer Cell Medium, (C) 25% HepG2: 75% KC Medium, (D) 50% HepG2: 50% KC Medium and (E) 75% HepG2: 25% KC Medium. Mean data of two biological replicates, analysed in triplicate (n=6) presented \pm SEM. No statistically significant results were identified due to large standard deviation.

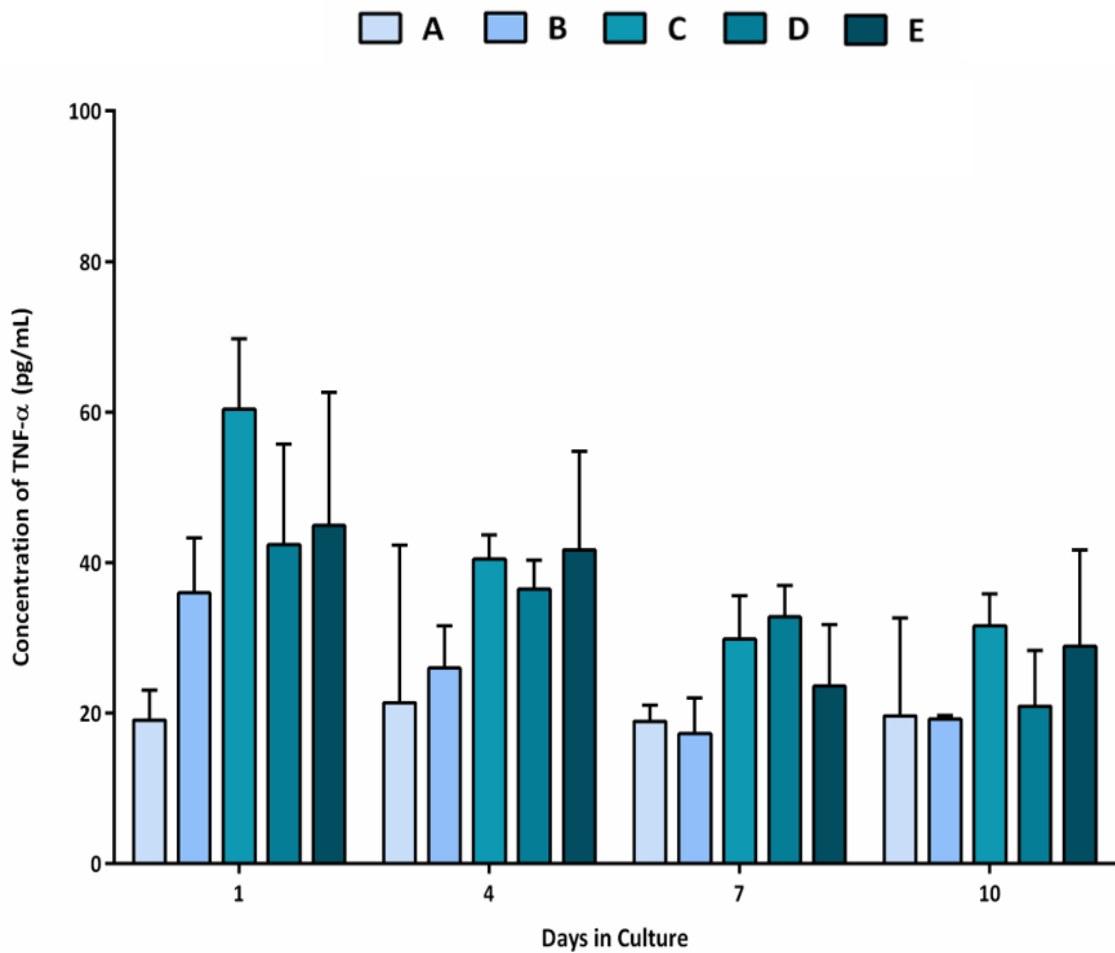


Figure 6: Concentration of TNF- α in HepG2 and Kupffer cell (KC) co-culture liver spheroids (5000 cells/spheroid) cultured in the hanging drop model, with varying culture medium compositions, over a 10 day period. (A) 100% HepG2 Medium, (B) 100% Human Kupffer Cell Medium, (C) 25% HepG2: 75% KC Medium, (D) 50% HepG2: 50% KC Medium and (E) 75% HepG2: 25% KC Medium. Mean data of two biological replicates, analysed in triplicate (n=6) presented \pm SEM. No statistically significant results were identified due to large standard deviation.

Alongside the supernatant, the spheroids themselves were also harvested for CD68 (ab222914, Abcam, UK) fluorescence imaging to assess the Kupffer cell integration within the co-culture spheroid (Fig. 7; Fig 8). Kupffer cell integration into the 3D liver spheroid was assessed to determine if the macrophages were integrated evenly throughout the spheroid and weren't found to remain on the surface. Combining the Kupffer cells with the HepG2 cells in a single cell suspension prior to seeding aided macrophage integration from the outset, as it allows for both cell types to coalesce

simultaneously and form a compact 3D structure similar to that of the monoculture. Fig. 7 demonstrates the full and even integration of Kupffer cells (green) into the 3D hepatic spheroid with HepG2 (blue) cells. Whilst the presence of Kupffer cells is limited, that is to be expected with only 400 macrophages seeded alongside 1600 HepG2s per spheroid; a physiologically relevant ratio for an un-inflamed human liver. Fig. 8 further highlights the integration of the Kupffer cells is present throughout the 3D spheroid and not just on the surface of the spheroid.

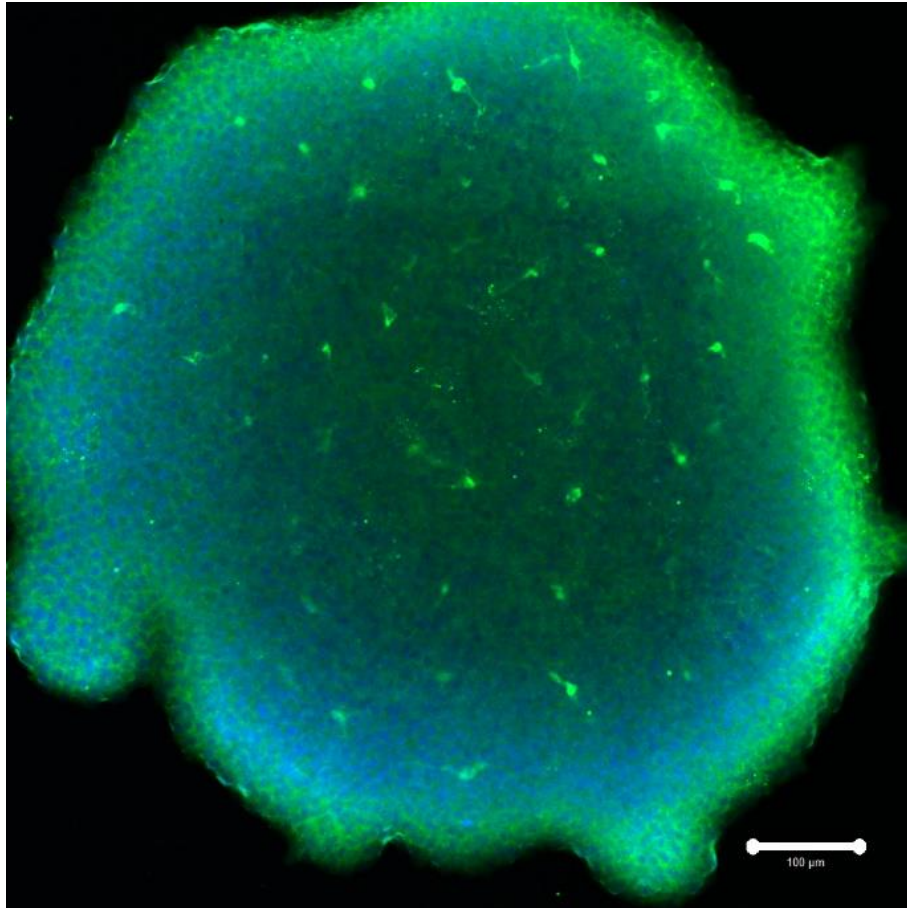


Figure 7: Confocal microscopy image of a HepG2/Kupffer cell co-culture spheroid on Day 1, *i.e.* 24 h after agarose transfer and 4 days after seeding. Green fluorescence represents the CD68 (ab222914, Abcam, UK) positive staining for the KCs, whilst the blue fluorescence signifies the DAPI nuclear staining. Scale bar represents 100μM.

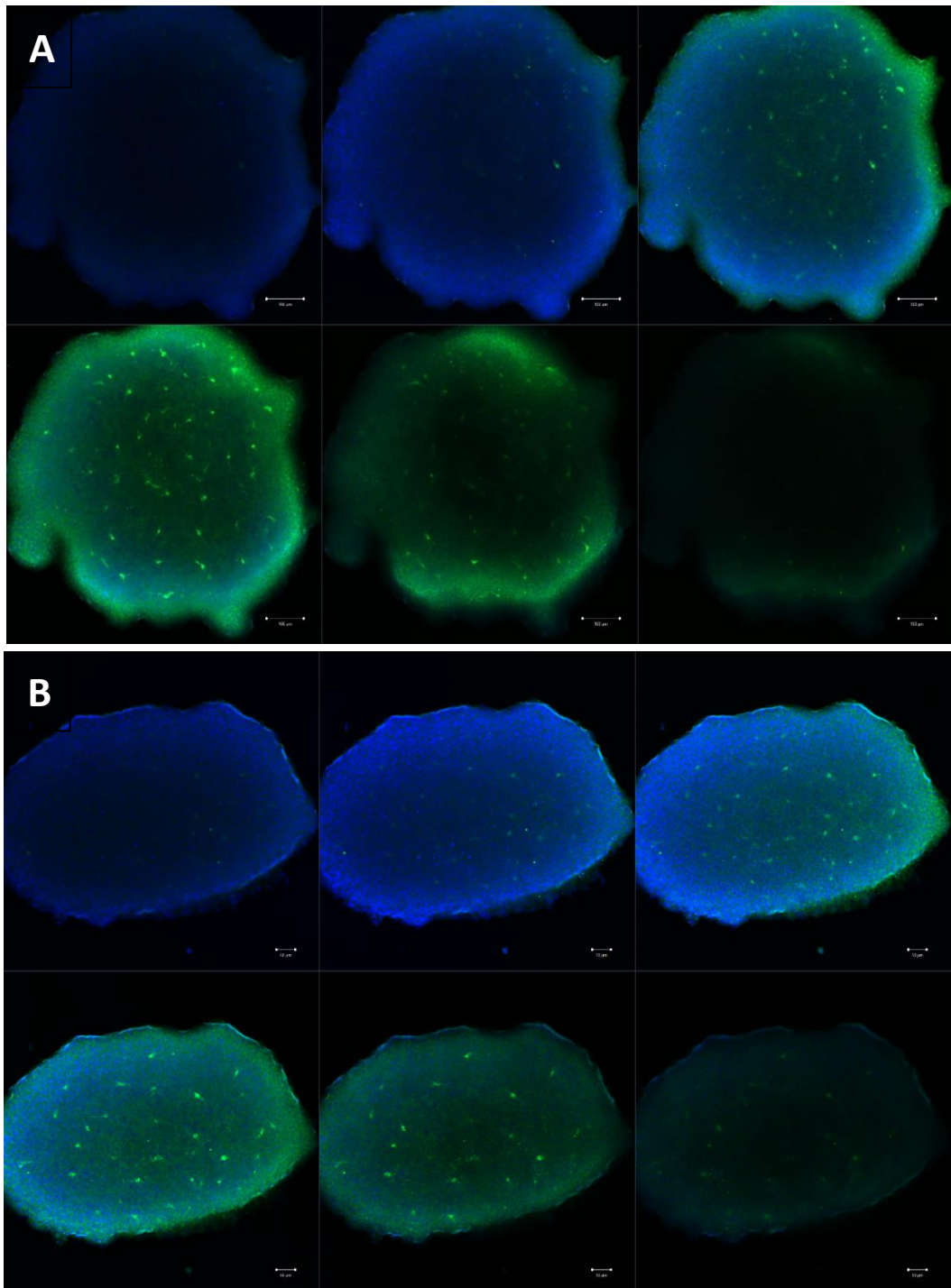


Figure 8: Confocal microscopy Z-stack image of two (A & B) different HepG2/Kupffer cell co-culture spheroids on Day 1, *i.e.* 24 h after agarose transfer and 4 days after seeding. Green fluorescence represents the CD68 (ab222914, Abcam, UK) positive staining for the Kupffer cells, whilst the blue fluorescence signifies the DAPI nuclear staining. Scale bar represents 100μM.

5.4.1 *In Vitro* 3D Liver Coculture Model Characterisation

Once optimised, the HepG2/Kupffer cell model was fully characterised for cell viability over time, liver functionality and CYP450 metabolic activity. The model was also exposed to a known hepatic chemical carcinogen, Aflatoxin B1 (AFB1), and two ENMs (TiO₂ and Ag) for an acute (24 h) and prolonged (120 h) exposure regime as conducted for the HepG2 monoculture spheroid described in publication III (47).

To establish if the co-culture of HepG2 and Kupffer cells not only enhanced the physiological relevance of the model, but the longevity and liver-like functionality, both the cells and supernatant were harvested simultaneously on 1, 4, 7, 10 and 14 days after transfer to the base of the 96-well plates. A viability count to determine the proportion of live and dead cells was taken using the Trypan Blue Exclusion Assay, whilst liver-like functionality was determined by the quantification of albumin and urea present in the supernatant using a BCG Albumin Assay Kit (MAK124, Sigma Aldrich, UK) and Urea Assay Kit (MAK006, Sigma Aldrich, UK). Fig. 9A shows that the viability of the co-culture declines at a greater rate than the monoculture, however, it appears to plateau at 65% viability between 7 - 10 days in culture before the viability begins to improve again. This pattern supports observations that the coculture takes longer to stabilise and coalesce to form compact 3D structures. Fig. 9A demonstrates that although the viability of the coculture model does not drop below 65%, 10% higher than that of the monoculture, the average percentage viability for both the monoculture and coculture models over the 14 day culture period was 75.46% and 75.12%, respectively. Fig. 9B illustrates a similar trend to the cell viability, in that the albumin production in the coculture spheroid decreases initially from days 1 to 4 before it begins to increase of which, there is a significant increase in albumin concentration by days 10 and 14. However, even with this increase, the level of albumin produced by the coculture spheroid does not exceed that of the monoculture. Conversely, the concentration of urea produced by both spheroid models was very similar, with the coculture reaching a higher (+0.224 ng/μL) urea production level than that of the monoculture. The concentration of urea in the coculture model, does not follow a similar trend to Fig 9. A & B, in that there is a time-dependent increase in urea over the duration of the 14 days, with a significant increase in urea present after 7 days in culture. One observation between the characterisation profiles of the two spheroid models is that the coculture seems to require more time to form a compact, spherical spheroid, whereby the viability and liver-like functionality appears to

increase later on in the culture period. This could suggest this coculture model may be viable for longer than the 14 day period studied.

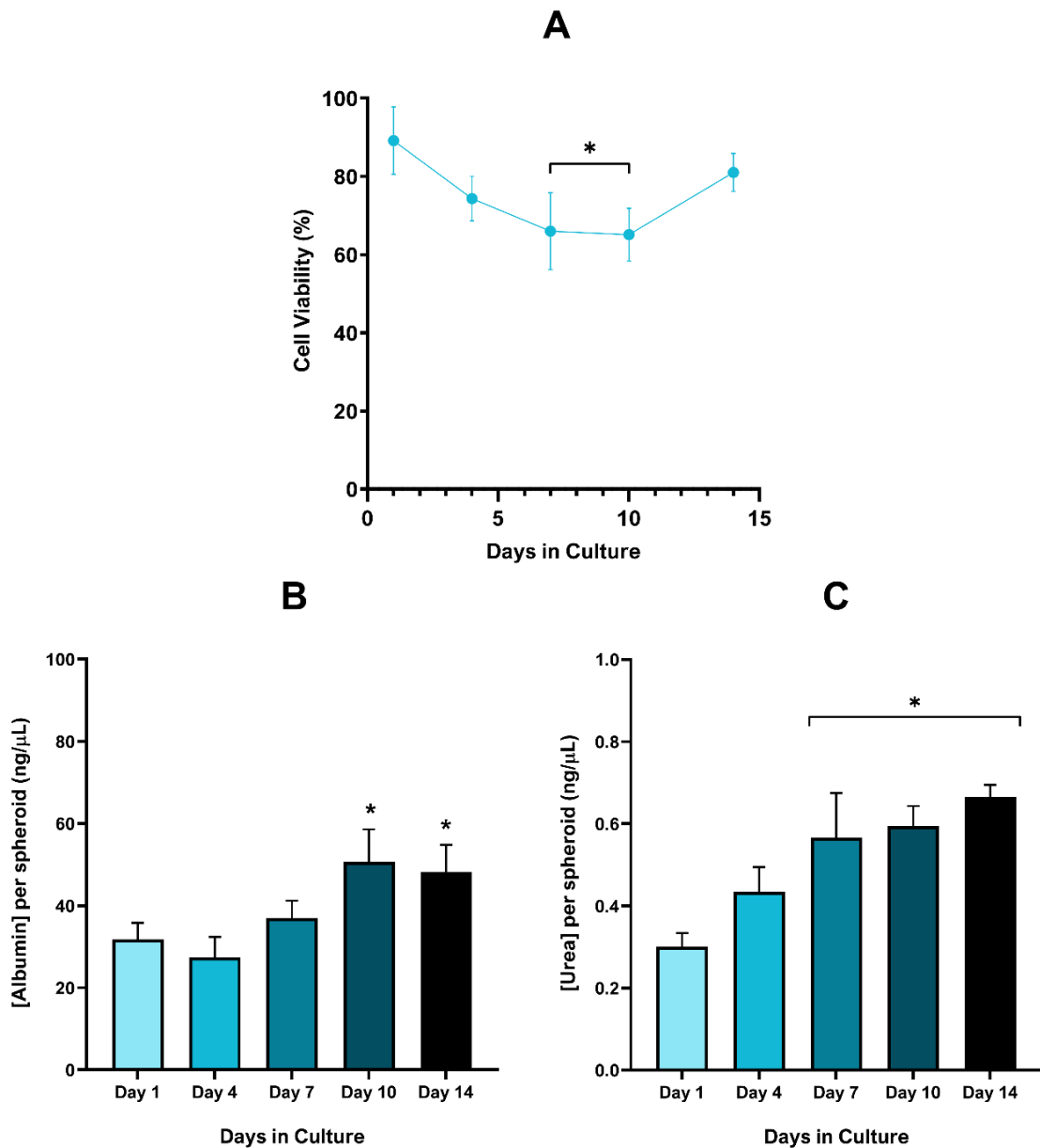


Figure 9: Average cell viability (%) (A), concentration of albumin (B) and urea (C) per HepG2/Kupffer cell coculture spheroid during 14 days in culture post agarose transfer. Error bars represent mean \pm SD, $n=3$. Significance indicated in relation to Day 1: * = $p \leq 0.05$.

To assess the background inflammatory levels in the HepG2/Kupffer cell spheroids, IL-8 release was assessed over the 14 day culture period (Fig. 10). IL-8 is a chemoattractant cytokine released by both hepatocytes and Kupffer cells, and is responsible for neutrophil recruitment and the activation of phagocytosis, so is important in maintaining the homeostatic balance in the cell (48). In the HepG2 monoculture, the untreated control on Day 1 is normally below 50 pg/mL, which illustrates the coculture is functioning in a similar manner with only a slightly greater (~ 15 pg/mL) release in IL-8, which can be explained by the addition of the macrophage cell line. Interestingly, the IL-8 data (Fig. 10) shows that as the time in culture increases, the level of inflammation in the culture also increases with a significant increase ($p \leq 0.02$) in IL-8 release observed following 7 days in culture. This time-dependent increase in IL-8, as described in publication V, has been previously linked to the elevated hypoxia experienced towards the centre of the spheroids, due to the reduced diffusion of oxygen through the ever proliferating spheroid. To ensure the Kupffer cells would respond to an inflammatory agent, the coculture was exposed to a positive assay control of 0.25 $\mu\text{g/mL}$ of TNF- α protein for 24 h, which induced 310 pg/mL of IL-8; a similar response to that observed with the monoculture.

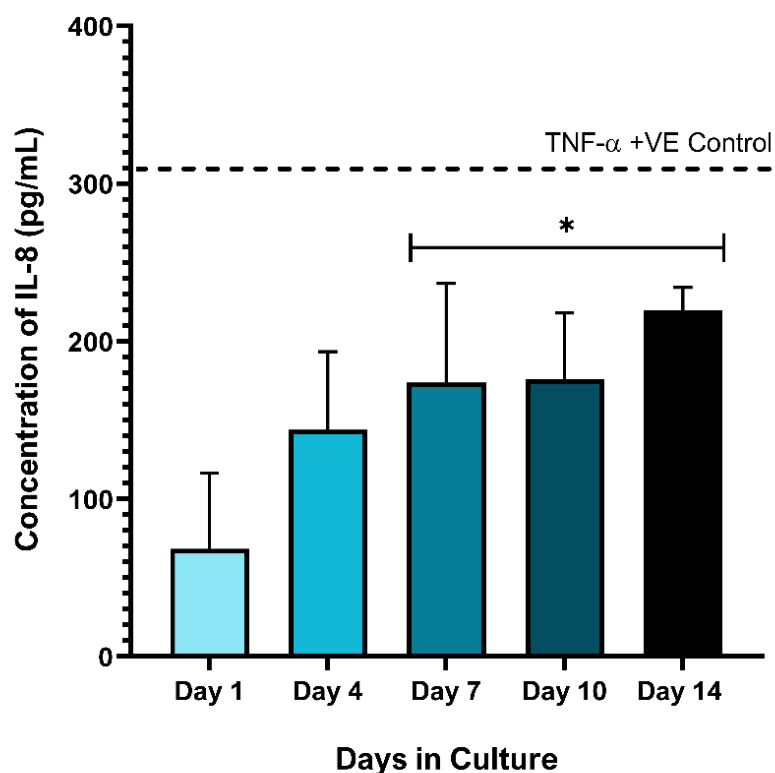


Figure 10: Baseline concentration of IL-8 (pro-)inflammatory mediator release from 80 pooled HepG2/Kupffer cell coculture spheroids over 14 days in culture. IL-8 analysis was determined using the Human IL-8/CXCL8 DuoSet ELISA DY208-05 (R&D Systems, UK). Mean data of three biological replicates, analysed in triplicate (n=9) is presented \pm SD. Dotted line represents the mean positive assay control response induced by 0.25 μ g/mL of TNF- α protein (NBP2-35076-50 μ g, Biotechne, UK). Significance is indicated in relation to Day 1 as follows: * = $p < 0.05$.

5.4.2 *In Vitro* 3D Liver Coculture Model ENM Exposures

With the HepG2/Kupffer cell coculture model optimised and functioning over the 14 day culture period, the coculture spheroids were then exposed to two different ENMs; TiO₂ and Ag. These two materials were selected as they are in keeping with the other investigations (*i.e.* publication IV) conducted into enhancing the physiological relevance of the HepG2 spheroid model for ENM hazard assessment. Three increasing concentrations, 0.5 μ g/mL, 1.0 μ g/mL and 5.0 μ g/mL, were analysed for liver-like functionality, inflammatory cytokine release, cytotoxicity and genotoxicity, following both acute (24 h) and prolonged (120 h) ENM exposure. Following either acute or prolonged ENM exposures, there was no significant reduction in albumin or urea

production (Fig 11A & B), highlighting there was no adverse effect to the fidelity of the coculture spheroids during these exposures.

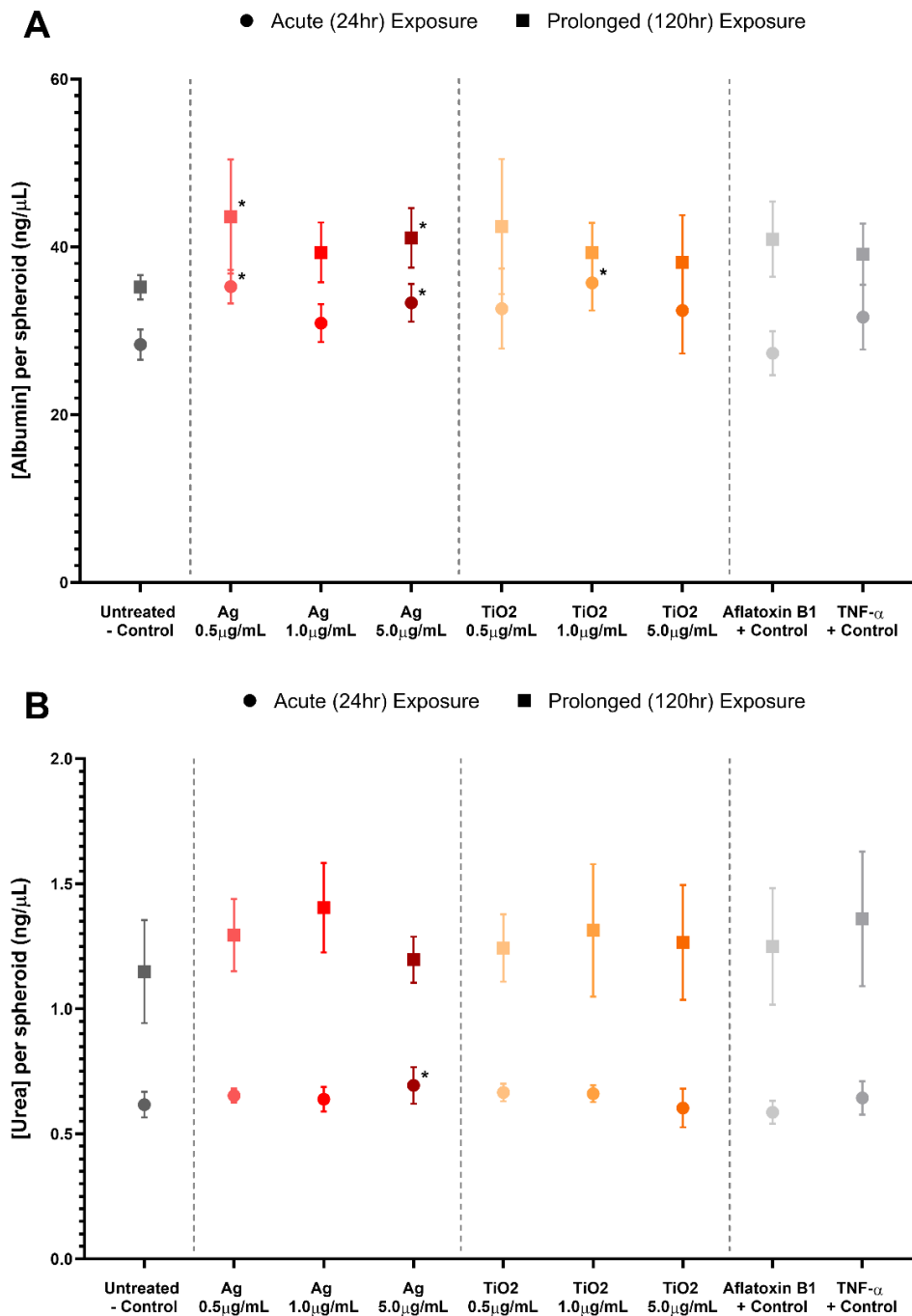


Figure 11: Average concentration of (A) albumin and (B) urea produced by HepG2/KC coculture spheroids following acute (24 h; circle symbols), and prolonged (120 h; square symbols), exposure to Ag and TiO₂ at 0.5 µg/mL, 1.0 µg/mL and 5.0 µg/mL. Mean data from three biological replicates, analysed in triplicates ± SD are presented, n = 9. Significance indicated as follows: * = $p < 0.05$.

The release of inflammatory cytokines IL-8 and TNF- α were assessed to ascertain if acute or prolonged exposure to either TiO₂ or Ag ENMs would induce an elevated state of inflammation in the coculture model, and if the presence of macrophages would prolong this inflammatory insult over the extended 120 h exposure. Once again, neither ENM regardless of the concentration or exposure duration induced a detectable response in TNF- α levels. Whilst the positive assay control (0.25 μ g/mL of TNF- α protein) induced a positive response within the expected historical range in both IL-8 and TNF- α ELISAs, all the other exposures fell below detectable limits in the TNF- α assay (data not shown). Instead, there was an IL-8 response, with the background IL-8 release in the untreated, negative control following acute exposure, almost 3-fold higher than that in the monoculture models, but this data does align with IL-8 present on days 1 and 4 of the 14 day coculture characterisation above (Fig. 10). In contrast to the monoculture data published in publication V, acute exposure to increasing concentrations of Ag ENMs induced an insignificant, yet slightly increased IL-8 response (Fig. 12A), whilst in the monoculture the opposite occurred. Cellular uptake in epithelial-like HepG2 cells can be restricted by the size of the particle or agglomerate, so higher levels of ENM agglomeration may reduce the number of particles entering the hepatocytes and potentially lessen the adverse effects of ENM exposure. However, with macrophages able to engulf particles up to three times greater than their own volume (49), this repressed cellular uptake may no longer be present in the co-culture spheroids. Further to this, the higher concentrations of ENMs may result in greater phagocytosis, specifically by the macrophage population, which in turn could induce greater ROS release *via* “oxidative respiratory bursts” triggering further release of inflammatory cytokines and subsequent inflammation (50,51). After prolonged Ag and TiO₂ ENM exposure, however (Fig. 12B), the IL-8 release remained consistent across all three concentrations of each material, a trend similar to that of the Ag exposures in the monoculture spheroids. Interestingly, for acute TiO₂ exposures, 1.0 μ g/mL induced the greatest IL-8 release with 265.34 pg/mL present, whilst in the monoculture, 0.5 μ g/mL of TiO₂ induced the only significant increase in IL-8 release. Between 0.5 μ g/mL and 1.0 μ g/mL, publication V illustrated there was no significant difference in agglomeration, +4 nm in average diameter between the two, whilst the average size of the agglomerated material almost doubled at the highest concentration of 5.0 μ g/mL. This suggests that at the higher concentrations of ENM, a reduced inflammatory response may be attributable to impeded ENM penetration into the spheroid due to the large agglomerate size.

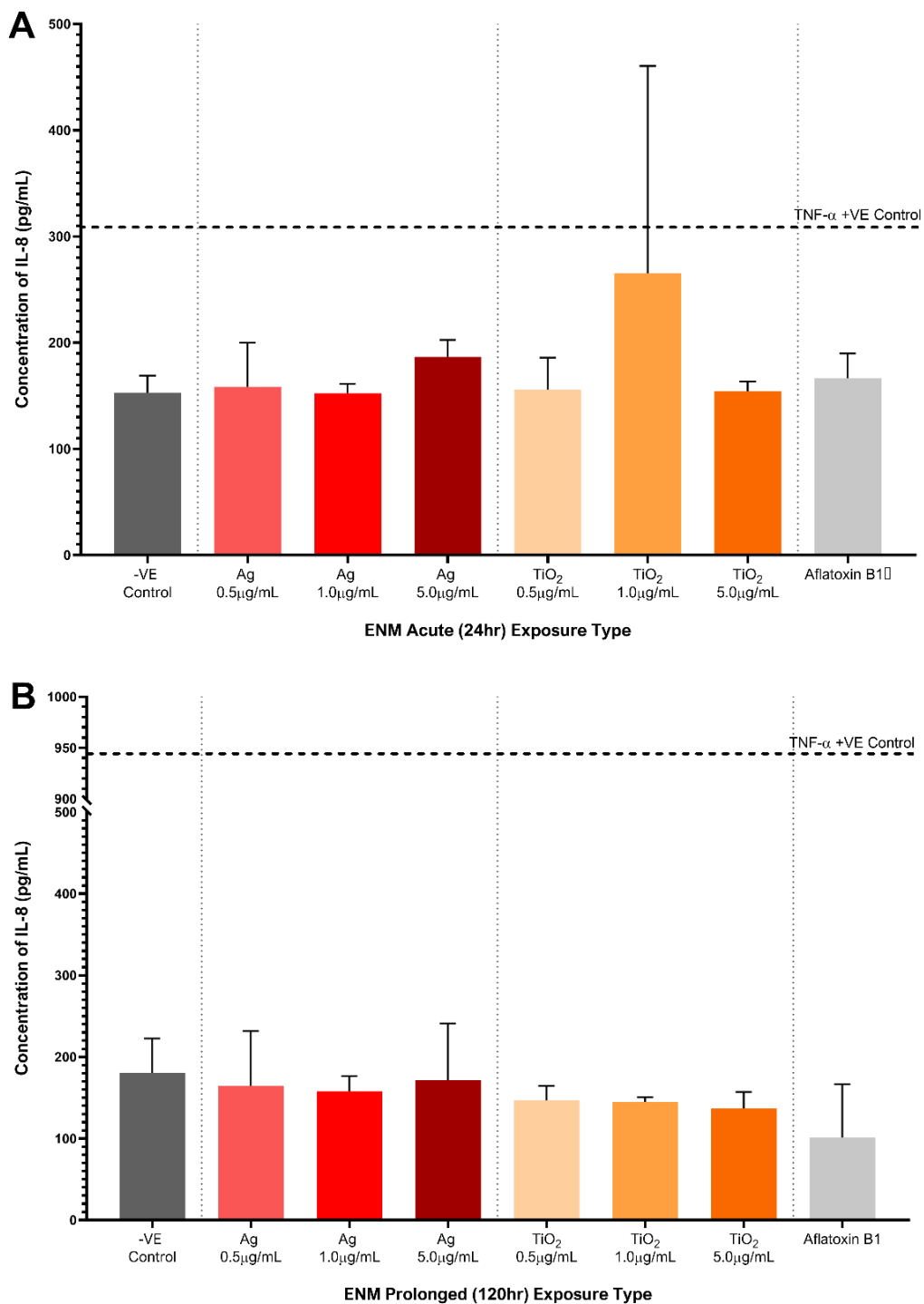


Figure 12: Baseline concentration of IL-8 (pro-)inflammatory mediator release from HepG2/KC coculture spheroids following (A) acute (24 h) and (B) prolonged (120 h) exposure to Ag and TiO₂ ENMs at 0.5 μg/mL, 1.0 μg/mL and 5.0 μg/mL. Mean data from three biological replicates, analysed in triplicates ± SD are presented, n = 9. Significance indicated as follows: * = $p < 0.05$.

Alongside genotoxicity, cytotoxicity was assessed and no significant cytotoxicity was observed in the coculture spheroids irrespective of the ENM, exposure concentration or duration, confirming DNA damage was evaluated with an appropriate dose range. Whilst the background micronucleus frequency, as highlighted by the untreated negative control in Fig. 13A and B, was slightly higher (~0.5%) than that observed in the monoculture, no significant micronuclei induction was observed regardless of the material, concentration applied or exposure duration. However, it is worth noting that acute exposure to 0.5 µg/mL and 5.0 µg/mL of Ag ENMs induced a 2-fold increase in MN frequency in the HepG2/KC coculture spheroids compared to that found in the HepG2 monoculture spheroids. Furthermore, acute exposure to 0.5 µg/mL, 1.0 µg/mL and 5.0 µg/mL of TiO₂ induced a 3.25-, 2.03- and 1.59-fold increase in MN induction, compared to the monoculture, with a frequency of 3.9%, 3.65% and 4.77%, respectively. Although there are notable differences between the monoculture and coculture in the genotoxicity observed post-acute ENM exposure, this elevated response was not seen following prolonged exposure to Ag and TiO₂ ENMs. In fact, the prolonged ENM exposures induced a similar MN induction to those observed previously in the monoculture spheroids and again displayed no significant genotoxicity regardless of material or applied concentration (Fig. 13B).

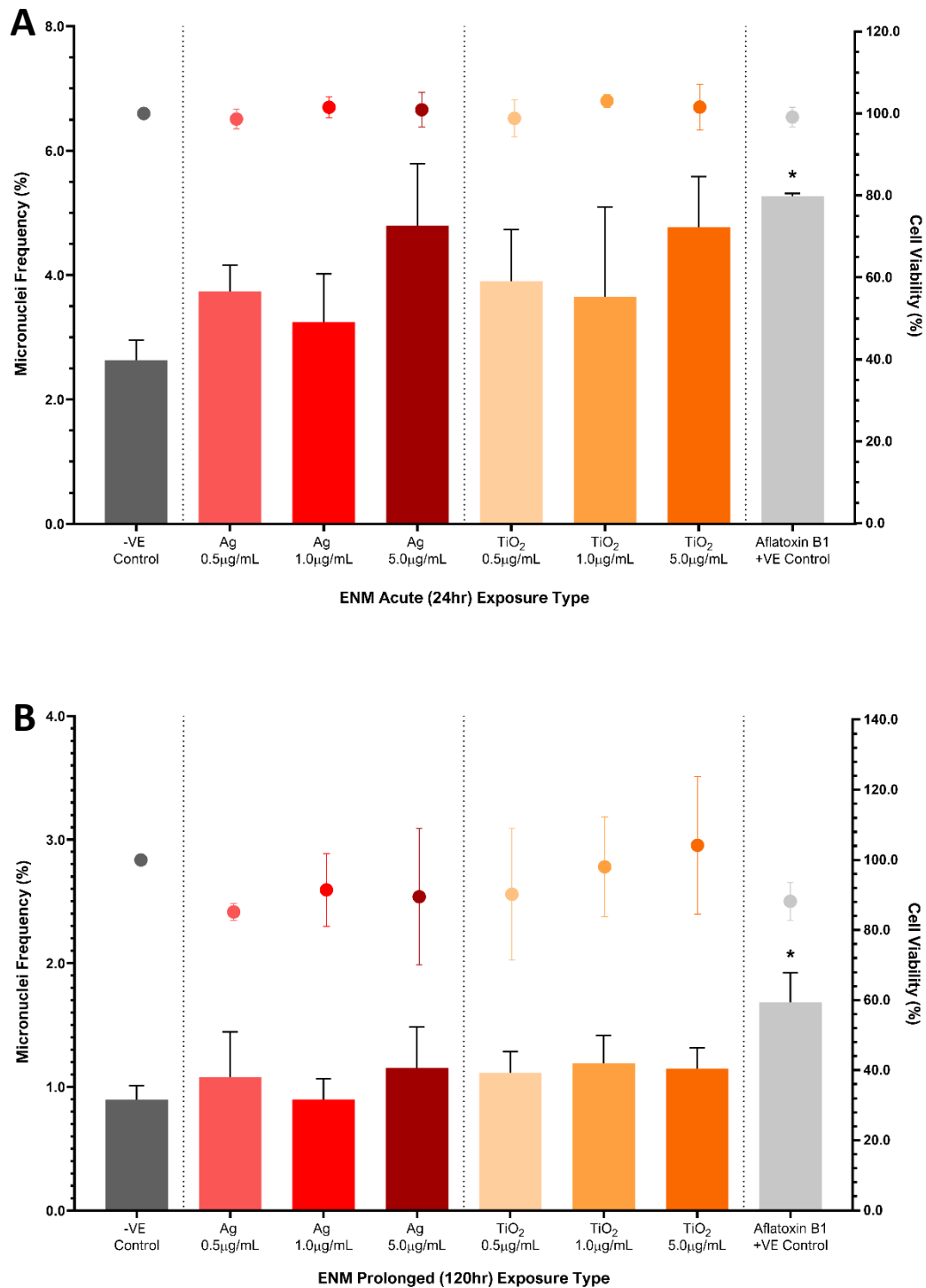


Figure 13: Cytokinesis-Block Proliferation Index (CBPI) and Micronuclei (MN) Frequency (%) induced in HepG2/KC coculture spheroids following (A) acute (24 h) and (B) prolonged (120 h) exposure to Ag and TiO₂ Exposures at 0.5 µg/mL, 1.0 µg/mL and 5.0 µg/mL. CBPI is represented by the points, whilst the MN frequency is represented by the bars. Mean data of 3000 binucleated cells scored \pm SD presented, $n = 3$. Significance indicated as follows: * = $p < 0.05$.

In conclusion, while the addition of primary macrophages to the spheroid model enhances the physiological relevance and liver-like functionality of the model, it does not appear to increase the sensitivity of the model to ENM insult. However, the true sensitivity of this model may be masked by the variation observed amongst biological replicates; a common limitation when working with primary cells. For example, with reduced variation amongst replicates or more than three biological replicates assessed, the enhanced genotoxicity observed in response to acute ENM exposure may then have been significant. Although insignificant, it may be worth noting that the varying pattern of IL-8 inflammation induced by the different concentrations of Ag ENM exposure in both acute and prolonged exposures mirrors that seen in the micronuclei induction and thus, could be indicative of potential inflammation-associated secondary genotoxicity. TiO₂ on the other hand was shown to be significantly genotoxic following acute 24 h exposure to doses as low as 1.0 µg/mL in the monoculture model, yet in the coculture model no significant genotoxicity was observed. This could be linked to the presence of the macrophages phagocytosing and clearing the material and thus reducing the number of ENMs coming into contact with, the surrounding hepatocytes.

In summary, there is a distinct lack of suitable 3D *in vitro* liver models that have the capability to emulate secondary genotoxicity and so, the full spectrum of ENM-associated genotoxicity mechanisms remain to be fully understood (43). The aim of this research was to develop an advanced 3D *in vitro* hepatic coculture model capable of reliably evaluating a variety of hazard endpoints in conjunction with detecting secondary genotoxicity following acute, prolonged and repeated ENM exposures in a routine and easily accessible manner. With further optimisation this advanced HepG2/KC coculture model could provide a more reliable insight into whether the elevated (pro-)inflammatory response and oxygen reactivity seen with some of the ENMs could further perpetuate the genotoxicity observed *via* secondary genotoxicity mechanisms. Unfortunately, as it currently stands, the variation amongst replicates, the expensive nature of the model and added complexity of culturing primary KCs with limited additional predictive capabilities deems the coculture model unsuitable for robust, high through-put ENM hazard assessment *in vitro*.

5.5 Future Outlooks

This research has substantial potential to provide a novel model and approach that expands the scope of *in vitro* hazard characterisation tools for ENM evaluation. For the monoculture HepG2 spheroid model established, it is important to assess the transferability and reproducibility of this model in both academic and industrial laboratories alike. A pre-validation experimental investigation has demonstrated that the HepG2 spheroid model described in this thesis is robust and successfully transferable across three laboratories, one industrial and two academic laboratories alike, with great concordance in hazard endpoints covering both pro-inflammatory cytokine evaluation and genotoxicity testing. This 3D liver model with accompanying SOPs now needs to be tested in a large scale interlaboratory trial for further validation to support and encourage use in a regulatory risk assessment setting.

With respect to the HepG2/KC coculture model, proof-of-principle was demonstrated in this thesis, but future work should be focussed towards further optimisation of the model to ascertain its full potential as an alternative *in vitro* test system for assessing secondary genotoxicity. With ENMs reciprocally linked to liver inflammation, the ratio of Kupffer cells to hepatocytes could be increased respectively from 1:4 to 1:2 in order to better mimic an inflamed state, whereby there would be a greater recruitment of macrophages and secondary genotoxicity mechanisms may be more prevalent (52). This co-culture model could also be progressed further to include other additional cell types (*e.g.* stellate cells, liver sinusoidal endothelial cells), to enhance aspects of human physiology critical to the development of certain liver diseases. For example, AOPs for liver fibrosis have identified liver necrosis, stellate cell activation and TGF- β signalling as key events in the progression of the disease, which could be targeted and assessed with the addition of hepatic stellate cells in an *in vitro* test system (41,53,54). Alongside the model, it is important to consider the AOP framework discussed in publication I, as hepatic AOPs could be the key to unlocking the next set of early-detection biomarker endpoints to target for liver disease. For example, the identification of critical events (*e.g.* chronic inflammation, oxidative stress, NF- κ B activation, p53 and β -catenin gene expression) and mechanisms (*e.g.* mutagenic or non-mutagenic modes of action) behind ENM associated hepatotoxicity allows for the targeted development of more predictive endpoints for liver disease progression.

Furthermore, it will also be important to understand the significance of an oxygen rich environment, normally used to maintain hepatic cultures, upon hepatotoxicity and whether more biologically relevant oxygen concentrations should be utilised for future *in vitro* hazard assessment. For example, physioxia in the liver forms a gradient between 3.0 – 11.0% oxygen from the perivenous to the periportal region, as opposed to the 21.0% atmospheric oxygen concentrations used in standard cell culture practice (55). Previous research has found lower oxygen tensions to induce global transcriptional reprogramming, resulting in changes to cell proliferation and viability, mitochondrial metabolic activity, drug tolerance, anti-oxidant levels, DNA strand breaks and oxidative DNA damage (38,56,57). Therefore, it is important to acknowledge that these adaptations could dramatically affect the toxicological outcome following ENM exposure. DiProspero *et al.*, found HepG2 drug (*e.g.* acetaminophen, cyclophosphamide and AFB1) response was oxygen tension-dependent with both acetaminophen and AFB1 displaying a significant increase in potency at physiologically relevant oxygen tensions, with the AFB1 EC₅₀ value decreasing from 21.1 nM at 20.0% O₂ to 1.9 nM at 3% O₂ (58). It was hypothesised that the oxygen-dependent decreases in chemical potency and overall toxicity suggests the HepG2 cells could be accessing different metabolic pathways to metabolise the drugs. AFB1 has previously displayed mechanisms of action linked to CYP3A4 and CYP1A2 in order to synthesise the carcinogenic metabolite, and interestingly, an increase in CYP1A2 transcripts was observed at both 8.0% and 3.0% O₂ tensions indicating the increase in AFB1 toxicity could be due to increased CYP1A2 activity (58). This research highlights oxygen-induced changes in drug potency and overall toxicity, and offers an insight into the potential liver-induced injuries or drug-drug interactions, which may have been overlooked under standard culture practice. Based on these results and others alike, it would be invaluable to assess ENM toxicity in the HepG2 spheroid models at physiologically relevant O₂ concentrations as the toxicity profile could change dramatically. The ongoing advancement and enhanced predictability of the 3D liver models alongside the development of novel, biomarker panels could provide an effective, prognostic *in vivo* alternative test system for both chemical and ENM associated hepatic toxicology.

5.6 Conclusion

In conclusion, this research illustrates the successful development of a versatile, cell-line based 3D *in vitro* hepatic spheroid model that can be adapted to support different aspects of human physiology (*e.g.* a co-culture model, physioxia and biological fluid simulants) and is capable of evaluating more realistic, prolonged and repeated, ENM exposures. One unique feature of this 3D HepG2 spheroid model is that it retains the ability to proliferate, and thus is able to support fixed DNA damage assessment *via* the *in vitro* MN Assay. During this development process, a number of transferable SOPs for the construction of this model, coupled to more physiologically relevant ENM exposure regimes and endpoint analysis were developed following the ‘Good *In Vitro* Methods Practice’ (GIVMP), OECD guidelines, to ensure the SOPs had potential to be adopted into standard regulatory practice upon full validation. In particular, the OECD ‘gold standard’ *in vitro* MN assay, originally designed for assessing chemical associated chromosomal damage in 2D cultures, has been adapted to support genotoxicity assessment following both acute and prolonged or repeated ENM exposure in 3D HepG2 spheroids. Another of the SOPs provides a tiered testing strategy to better predict which ENM is susceptible to biotransformation allowing for the necessary use of ENM pre-treatment schemes when assessing the human health hazards associated with both ENM inhalation and ingestion exposure. Lastly, this project has recapitulated the benefits of an AOP targeted approach for the identification and development of novel, early-detection biomarkers of liver disease and illustrated the successful application of a variety of ENM hazard endpoints (*e.g.* liver functionality, cytotoxicity, (pro-)inflammatory response and genotoxicity) with this 3D HepG2 liver model. Furthermore, a genotoxicity potency ranking of five ENMs tested at low concentrations, relevant to the liver was established. All five of the materials tested were shown to induce fixed DNA damage in 3D HepG2 spheroids following acute exposure, leading to the following genotoxicity potency ranking: ZnO > TiO₂ > BaSO₄ = CeO₂ > Ag. In conclusion, the 3D *in vitro* hepatic spheroid model and supporting SOPs developed within this project have the capacity to be utilised for evaluating more realistic ENM exposures, thereby providing a future *in vitro* approach to better support ENM hazard assessment in a routine and easily accessible manner.

6.0 References

1. Hardy A, Benford D, Thorhallur H, Jeger MJ, Knutsen HK, More S, et al. Guidance on risk assessment of the application of nanoscience and nanotechnologies in the food and feed chain: Part 1, human and animal health. *EFSA Journal*. 2018;16(7):5327.
2. Oberdörster G, Stone V, Donaldson K. Toxicology of nanoparticles: A historical perspective. *Nanotoxicology*. 2007;1(1):2–25.
3. Research and Markets 2018. Global Nanotechnology Market (by Component and Applications), Funding & Investment, Patent Analysis and 27 Companies Profile & Recent Developments - Forecast to 2024.
4. Russell WMS, Burch RL. *The Principles of Humane Experimental Technique*. 1959.
5. Monopoli MP, Walczyk D, Campbell A, Elia G, Lynch I, Baldelli Bombelli F, et al. Physical–Chemical Aspects of Protein Corona: Relevance to *in Vitro* and *in Vivo* Biological Impacts of Nanoparticles. *Journal of the American Chemical Society*. 2011;133(8):2525–34.
6. Rampado R, Crotti S, Caliceti P, Pucciarelli S, Agostini M. Recent Advances in Understanding the Protein Corona of Nanoparticles and in the Formulation of “Stealthy” Nanomaterials. *Frontiers in Bioengineering and Biotechnology*. 2020;(8):166.
7. Tenzer S, Docter D, Kuharev J, Musyanovych A, Fetz V, Hecht R, et al. Rapid formation of plasma protein corona critically affects nanoparticle pathophysiology. *Nature Nanotechnology*. 2013;8(10):772–81.
8. Modrzynska J, Berthing T, Ravn-Haren G, Kling K, Mortensen A, Rasmussen RR, et al. In vivo-induced size transformation of cerium oxide nanoparticles in both lung and liver does not affect long-term hepatic accumulation following pulmonary exposure. *PLoS ONE*. 2018;13(8).
9. Kermanizadeh A, Løhr M, Roursgaard M, Messner S, Gunness P, Kelm JM, et al. Hepatic toxicology following single and multiple exposure of engineered nanomaterials utilising a novel primary human 3D liver microtissue model. *Particle and Fibre Toxicology*. 2014;11(1):56.

10. Kermanizadeh A, Berthing T, Guzniczak E, Wheeldon M, Whyte G, Vogel U, et al. Assessment of nanomaterial-induced hepatotoxicity using a 3D human primary multi-cellular microtissue exposed repeatedly over 21 days - The suitability of the in vitro system as an in vivo surrogate. *Particle and Fibre Toxicology*. 2019;16(1):42.
11. Kermanizadeh A, Powell LG, Stone V. A review of hepatic nanotoxicology—summation of recent findings and considerations for the next generation of study designs. *Journal of Toxicology and Environmental Health - Part B: Critical Reviews*. 2020;(23):137–76.
12. Lauschke VM, Shafagh RZ, Hendriks DFG, Ingelman-Sundberg M. 3D Primary Hepatocyte Culture Systems for Analyses of Liver Diseases, Drug Metabolism, and Toxicity: Emerging Culture Paradigms and Applications. *Biotechnology Journal*. 2019;14(7):1800347.
13. Moradi E, Jalili-Firoozinezhad S, Solati-Hashjin M. Microfluidic organ-on-a-chip models of human liver tissue. *Acta Biomaterialia*. 2020;(116):67–83.
14. Sacchi M, Bansal R, Rouwkema J. Bioengineered 3D Models to Recapitulate Tissue Fibrosis. *Trends in Biotechnology*. 2020;(38):623–36.
15. Llewellyn SV, Niemeijer M, Nymark P, Moné MJ, Water B, Conway GE, et al. In Vitro Three-Dimensional Liver Models for Nanomaterial DNA Damage Assessment. *Small*. 2021;2006055.
16. Papp T, Schiffmann D, Weiss D, Castranova V, Vallyathan V, Rahman Q. Human health implications of nanomaterial exposure. *Nanotoxicology*. 2008;2(1):9–27.
17. Pietroiusti A, Stockmann-Juvala H, Lucaroni F, Savolainen K. Nanomaterial exposure, toxicity, and impact on human health. *Wiley Interdisciplinary Reviews: Nanomedicine and Nanobiotechnology*. 2018;10(5):e1513.
18. Elespuru R, Pfuhler S, Aardema MJ, Chen T, Doak SH, Doherty A, et al. Genotoxicity assessment of nanomaterials: Recommendations on best practices, assays, and methods. *Toxicological Sciences*. 2018;164(2):391–416.
19. Doak SH, Manshian B, Jenkins GJS, Singh N. In vitro genotoxicity testing strategy for nanomaterials and the adaptation of current OECD guidelines.

- Mutation Research - Genetic Toxicology and Environmental Mutagenesis. 2012;745(1–2):104–11.
20. Shah U-K, Mallia J de O, Singh N, Chapman KE, Doak SH, Jenkins GJS. A three-dimensional in vitro HepG2 cells liver spheroid model for genotoxicity studies. *Mutation Research/Genetic Toxicology and Environmental Mutagenesis*. 2018;825:51–8.
 21. Gunness P, Mueller D, Shevchenko V, Heinzle E, Ingelman-Sundberg M, Noor F. 3D organotypic cultures of human heparc cells: A tool for in vitro toxicity studies. *Toxicological Sciences*. 2013;133(1):67–78.
 22. Marion MJ, Hantz O, Durantel D. The HepaRG cell line: biological properties and relevance as a tool for cell biology, drug metabolism, and virology studies. *Methods in molecular biology*. 2010;640:261–72.
 23. Guillouzo A, Corlu A, Aninat C, Glaise D, Morel F, Guguen-Guillouzo C. The human hepatoma HepaRG cells: A highly differentiated model for studies of liver metabolism and toxicity of xenobiotics. *Chemico-Biological Interactions*. 2007;168(1):66–73.
 24. Llewellyn SV, Kämpfer A, Keller JG, Vilsmeier K, Büttner V, Ag Seleci D, et al. Simulating Nanomaterial Transformation in Cascaded Biological Compartments to Enhance the Physiological Relevance of In Vitro Dosing Regimes: Optional or Required? *Small*. 2021;202004630.
 25. Bustamante-Marin XM, Ostrowski LE. Cilia and Mucociliary Clearance. *Cold Spring Harbor Perspectives in Biology*. 2017;9(4).
 26. Moss, R O. Simulants of lung interstitial fluid. *Health Phys*. 1979;36:3.
 27. Hassoun M, Royall PG, Parry M, Harvey RD, Forbes B. Design and development of a biorelevant simulated human lung fluid. *Journal of Drug Delivery Science and Technology*. 2018;47:485–91.
 28. Kämpfer AAM, Busch M, Schins RPF. Advanced in vitro testing strategies and models of the intestine for nanosafety research. *Chemical Research in Toxicology*. 2020;(33):1163–78.
 29. Mathew J, Bhimji SS. Physiology, Blood Plasma. *StatPearls*. 2018. Available from: <http://www.ncbi.nlm.nih.gov/pubmed/30285399>.

30. Baranowska-Wójcik E, Sz wajgier D, Oleszczuk P, Winiarska-Mieczan A. Effects of Titanium Dioxide Nanoparticles Exposure on Human Health—a Review. *Biological Trace Element Research*. 2020;(193):118–29.
31. Ziental D, Czarczynska-Goslinska B, Mlynarczyk DT, Glowacka-Sobotta A, Stanis z B, Goslinski T, et al. Titanium dioxide nanoparticles: Prospects and applications in medicine. *Nanomaterials*. 2020;(10):387.
32. Musial J, Krakowiak R, Mlynarczyk DT, Goslinski T, Stanis z BJ. Titanium dioxide nanoparticles in food and personal care products—what do we know about their safety? *Nanomaterials*. 2020;(10):1–23.
33. Talapko J, Matije vić T, Juzbašić M, Antolović-Požgain A, Škrlec I. Antibacterial activity of silver and its application in dentistry, cardiology and dermatology. *Microorganisms*. 2020;(8):1–13.
34. Pulit-Prociak J, Banach M. Silver nanoparticles - A material of the future...? *Open Chemistry*. 2016;14(1):76–91.
35. Elsabahy M, Wooley KL. Cytokines as biomarkers of nanoparticle immunotoxicity. *Chemical Society Reviews*. 2013;42(12):5552–76.
36. Moshage H. Cytokines and the hepatic acute-phase response. *The Journal of Pathology*. 1997;181(3):257–66.
37. Desbaillets I, Diserens AC, de Tribolet N, Hamou MF, van Meir EG. Upregulation of interleukin 8 by oxygen-deprived cells in glioblastoma suggests a role in leukocyte activation, chemotaxis, and angiogenesis. *Journal of Experimental Medicine*. 1997;186(8):1201–12.
38. Sonna LA, Cullivan ML, Sheldon HK, Pratt RE, Lilly CM. Effect of hypoxia on gene expression by human hepatocytes (HepG2). *Physiological Genomics*. 2003;12:195–207.
39. Li XP, Yang XY, Biskup E, Zhou J, Li HL, Wu YF, et al. Co-expression of CXCL8 and HIF-1 α is associated with metastasis and poor prognosis in hepatocellular carcinoma. *Oncotarget*. 2015;6(26):22880–9.
40. Lauschke VM, Hendriks DFG, Bell CC, Andersson TB, Ingelman-Sundberg M. Novel 3D Culture Systems for Studies of Human Liver Function and

- Assessments of the Hepatotoxicity of Drugs and Drug Candidates. *Chemical Research in Toxicology*. 2016;29(12):1936–55.
41. van Grunsven LA. 3D in vitro models of liver fibrosis. *Advanced Drug Delivery Reviews*. 2017;121:133–46.
 42. Michalopoulos GK. Liver regeneration. *Journal of Cellular Physiology*. 2007;(213):286–300.
 43. Evans SJ, Clift MJD, Singh N, de Oliveira Mallia J, Burgum M, Wills JW, et al. Critical review of the current and future challenges associated with advanced in vitro systems towards the study of nanoparticle (secondary) genotoxicity. *Mutagenesis*. 2017;32(1):233–41.
 44. Dixon LJ, Barnes M, Tang H, Pritchard MT, Nagy LE. Kupffer cells in the liver. *Comprehensive Physiology*. 2013;3(2):785–97.
 45. Crawford JM, Bioulac-Sage P, Hytioglou P. Structure, Function, and Responses to Injury. *MacSween's Pathology of the Liver*. 2018:1–87.
 46. Li F, Cao L, Parikh S, Zuo R. Three-Dimensional Spheroids With Primary Human Liver Cells and Differential Roles of Kupffer Cells in Drug-Induced Liver Injury. *Journal of Pharmaceutical Sciences*. 2020;109(6):1912–23.
 47. Llewellyn SV, Conway GE, Shah U-K, Evans SJ, Jenkins GJS, Clift MJD, et al. Advanced 3D liver models for in vitro genotoxicity testing following long-term nanomaterial exposure. *Journal of Visualized Experiments*. 2020;(160).
 48. Bickel M. The role of interleukin-8 in inflammation and mechanisms of regulation. *Journal of periodontology*. 1993;64(5 Suppl):456–60.
 49. Lavoie PM, Levy O. Mononuclear Phagocyte System. *Fetal and Neonatal Physiology*. 2017:1208-1216.e3.
 50. Singh AK. Mechanisms of Nanoparticle Toxicity. *Engineered Nanoparticles*. 2016:295–341.
 51. Vida C, de Toda IM, Cruces J, Garrido A, Gonzalez-Sanchez M, de la Fuente M. Role of macrophages in age-related oxidative stress and lipofuscin accumulation in mice. *Redox Biology*. 2017;12:423–37.

52. Rose KA, Holman NS, Green AM, Andersen ME, Lecluyse EL. Co-culture of Hepatocytes and Kupffer Cells as an in Vitro Model of Inflammation and Drug-Induced Hepatotoxicity. *Journal of Pharmaceutical Sciences*. 2016;105(2):950–64.
53. Prestigiacomo V, Weston A, Messner S, Lampart F, Suter-Dick L. Pro-fibrotic compounds induce stellate cell activation, ECM-remodelling and Nrf2 activation in a human 3D-multicellular model of liver fibrosis. *PLoS ONE*. 2017;12(6).
54. Messner CJ, Babrak L, Titolo G, Caj M, Miho E, Suter-Dick L. Single cell gene expression analysis in a 3d microtissue liver model reveals cell type-specific responses to pro-fibrotic $\text{tgf-}\beta\text{1}$ stimulation. *International Journal of Molecular Sciences*. 2021;22(9):4372.
55. Kietzmann T. Metabolic zonation of the liver: The oxygen gradient revisited. *Redox Biology*. 2017;(11):622–30.
56. Dubbelboer IR, Pavlovic N, Heindryckx F, Sjögren E, Lennernäs H. Liver cancer cell lines treated with doxorubicin under normoxia and hypoxia: Cell viability and oncologic protein profile. *Cancers*. 2019;11(7).
57. Timpano S, Guild BD, Specker EJ, Melanson G, Medeiros PJ, Sproul SLJ, et al. Physioxic human cell culture improves viability, metabolism, and mitochondrial morphology while reducing DNA damage. *FASEB Journal*. 2019;33(4):5716–28.
58. DiProspero TJ, Dalrymple E, Lockett MR. Physiologically relevant oxygen tensions differentially regulate hepatotoxic responses in HepG2 cells. *Toxicology in Vitro*. 2021;74:105156.

7.0 Evidence of Publication

I. *In Vitro* Three-Dimensional Liver Models for Nanomaterial DNA Damage Assessment

Llewellyn, S.V., Niemeijer, M., Nymark, P., Moné, M.J., van de Water, B., Conway, G.E., Jenkins, G.J.S. and Doak, S.H. (2021). *In Vitro* Three-Dimensional Liver Models for Nanomaterial DNA Damage Assessment. *Small*, 2006055. doi: 10.1002/sml.202006055

Submitted: Small Journal, 28th September 2020

Published: 15th January 2021

The screenshot shows the Wiley Online Library interface. At the top, there is a search bar and a 'Login / Register' link. The main content area features the journal logo 'small' with 'NANO · MICRO' above it. The article title 'In Vitro Three-Dimensional Liver Models for Nanomaterial DNA Damage Assessment' is prominently displayed. Below the title, the authors' names are listed: Samantha V. Llewellyn, Marije Niemeijer, Penny Nymark, Martijn J. Moné, Bob van de Water, Gillian E. Conway, Gareth J. S. Jenkins, and Shareen H. Doak. The publication date is 'First published: 15 January 2021' and the DOI is 'https://doi.org/10.1002/sml.202006055'. On the right side, there is a 'Metrics' section showing an Altmetric score of 4. There are also links for 'Figures', 'References', 'Related', and 'Information'.

II. Advanced 3D Liver Models for Genotoxicity Testing *In Vitro* Following Long-Term Nanomaterial Exposure.

Llewellyn, S. V., Conway, G. E., Shah, U. K., Evans, S. J., Jenkins, G. J. S., Clift, M. J. D., Doak, S. H. Advanced 3D Liver Models for *In vitro* Genotoxicity Testing Following Long-Term Nanomaterial Exposure. *J. Vis. Exp.* (160), e61141, doi:10.3791/61141.

Submitted: JoVE Journal, 20th December 2019

Published: 6th May 2020

The screenshot shows the JoVE Journal interface. At the top, there is a search bar and navigation links for 'Faculty Resource Center', 'COVID-19', 'Research', 'Education', 'Authors', 'Librarians', 'About', 'Sign In', and 'Contact Us'. The main content area features the article title 'Advanced 3D Liver Models for In vitro Genotoxicity Testing Following Long-Term Nanomaterial Exposure' under the 'Bioengineering' category. Below the title, the authors' names are listed: Samantha V. Llewellyn¹, Gillian E. Conway¹, Ume-Kulsoom Shah¹, Stephen J. Evans¹, Gareth J.S. Jenkins¹, Martin J.D. Clift¹, and Shareen H. Doak¹. The publication date is 'Published: June 5, 2020'. On the right side, there is a video player with a 'Play Video' button. Below the video player, there are social media icons for Twitter, Facebook, LinkedIn, and YouTube, along with a 'PDF' button and a 'DOI' link.

III. Adaptation of the *in vitro* micronucleus assay for genotoxicity testing using 3D liver models supporting longer-term exposure durations.

Conway, G.E., Shah, U.-K., Llewellyn, S., Cervena, T., Evans, S.J., Al Ali, A.S., Jenkins, G.J., Clift, M.J.D., and Doak, S.H. (2020) Adaptation of the *in vitro* micronucleus assay for genotoxicity testing using 3D liver models supporting longer-term exposure durations. *Mutagenesis*, 35(4), Pages 319–330. doi: 10.1093/mutage/geaa018

Submitted: *Mutagenesis* Journal, 15th May 2020

Published: 1st July 2020



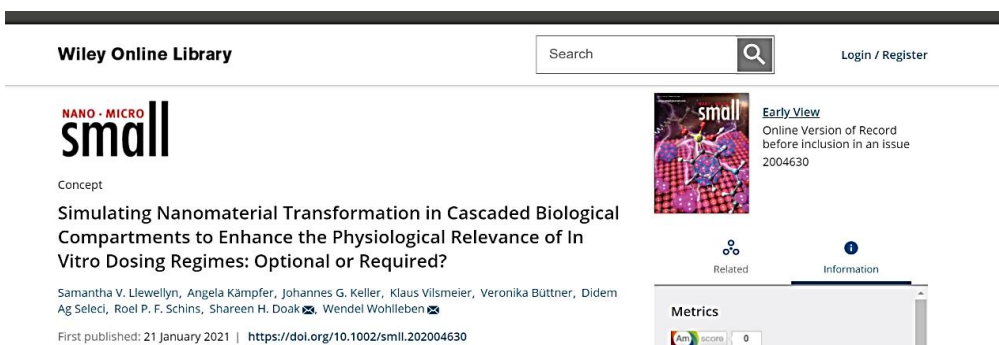
The screenshot shows the article page for 'Adaptation of the *in vitro* micronucleus assay for genotoxicity testing using 3D liver models supporting longer-term exposure durations' in the journal *Mutagenesis*. The page features the journal's logo, navigation menus, and a 'View Metrics' button. The article title is prominently displayed, along with the authors' names: Gillian E Conway, Ume-Kulsoom Shah, Samantha Llewellyn, Tereza Cervena, Stephen J Evans, Abdullah S Al Ali, Gareth J Jenkins, Martin J D Clift, and Shareen H Doak. There is also an 'Email alerts' button and a 'PDF' icon.

IV. Simulating Nanomaterial Transformation in Cascaded Biological Compartments to enhance the Physiological Relevance of *In Vitro* Dosing Regimes: Optional or Required?

Llewellyn, S.V., Kämpfer, A., Keller, J.G., Vilsmeier, K., Büttner, V., Ag Seleci, D., Schins, R.P.F., Doak, S.H. and Wohlleben, W. (2021). Simulating Nanomaterial Transformation in Cascaded Biological Compartments to Enhance the Physiological Relevance of *In Vitro* Dosing Regimes: Optional or Required? *Small*, 2004630. doi: 10.1002/smll.202004630.

Submitted: *Small* Journal, 30th July 2020

Published: 21st January 2021



The screenshot shows the article page for 'Simulating Nanomaterial Transformation in Cascaded Biological Compartments to Enhance the Physiological Relevance of *In Vitro* Dosing Regimes: Optional or Required?' in the journal *Small*. The page features the journal's logo, a search bar, and a 'Login / Register' button. The article title is prominently displayed, along with the authors' names: Samantha V. Llewellyn, Angela Kämpfer, Johannes G. Keller, Klaus Vilsmeier, Veronika Büttner, Didem Ag Seleci, Roel P. F. Schins, Shareen H. Doak, and Wendel Wohlleben. There is also an 'Early View' button and a 'Metrics' section.

V. **Understanding the Impact of More Realistic Low-dose, Prolonged Engineered Nanomaterial Exposure on Genotoxicity using 3D Models of the Human Liver.**

Llewellyn, S.V., Conway, C.E., Zanoni, I., Jørgensen, A.K., Shah, U-K., Ag Seleci, D., Keller, J.G., Kim, J.W., Wohlleben, W., Jensen, K.A., Costa, A., Jenkins, G.J.S., Clift, M.J.D., and Doak, S.H. (2021). Understanding the Impact of More Realistic Low-dose, Prolonged Engineered Nanomaterial Exposure on Genotoxicity using 3D Models of the Human Liver. *J. Nanobiotechnol*, 19(193). doi: 10.1186/s12951-021-00938-w

Submitted: Journal of Nanobiotechnology, 22nd March 2021

Published: 28th June 2021

The screenshot shows the article page on the BMC website. At the top, the BMC logo and 'Part of Springer Nature' are visible. The journal title 'Journal of Nanobiotechnology' is prominently displayed. Below the journal title, there are navigation links for 'Home', 'About', 'Articles', and 'Submission Guidelines'. The article title is 'Understanding the impact of more realistic low-dose, prolonged engineered nanomaterial exposure on genotoxicity using 3D models of the human liver'. The authors listed are Samantha V. Llewellyn, Gillian E. Conway, Ilaria Zanoni, Amalie Kofoed Jørgensen, Ume-Kulsoom Shah, Didem Ag Seleci, Johannes G. Keller, Jeong Won Kim, Wendel Wohlleben, Keld Alstrup Jensen, Anna Costa, Gareth J. S. Jenkins, Martin J. D. Clift & Shareen H. Doak. The article is published in the *Journal of Nanobiotechnology*, volume 19, article number 193, in 2021. A 'Download PDF' button is available. On the right side, there is a 'Sections' menu with options for 'Abstract', 'Background', 'Results', 'Discussion', and 'Conclusion'. The 'References' tab is also visible.

8.0 Appendices

Appendix I

JoVE Journal Visualized Experiments Video (MP4 File) published alongside
Publication II: Advanced 3D Liver Models for Genotoxicity Testing *In Vitro*
Following Long-Term Nanomaterial Exposure.